



HAL
open science

Biodiesel: combustion des esters éthyliques d'huiles végétales comme additifs au pétrodiesel

Hayat Bennadji

► **To cite this version:**

Hayat Bennadji. Biodiesel: combustion des esters éthyliques d'huiles végétales comme additifs au pétrodiesel. Autre. Institut National Polytechnique de Lorraine, 2010. Français. NNT: 2010INPL044N . tel-01748803

HAL Id: tel-01748803

<https://hal.univ-lorraine.fr/tel-01748803v1>

Submitted on 29 Mar 2018

HAL is a multi-disciplinary open access archive for the deposit and dissemination of scientific research documents, whether they are published or not. The documents may come from teaching and research institutions in France or abroad, or from public or private research centers.

L'archive ouverte pluridisciplinaire **HAL**, est destinée au dépôt et à la diffusion de documents scientifiques de niveau recherche, publiés ou non, émanant des établissements d'enseignement et de recherche français ou étrangers, des laboratoires publics ou privés.



AVERTISSEMENT

Ce document est le fruit d'un long travail approuvé par le jury de soutenance et mis à disposition de l'ensemble de la communauté universitaire élargie.

Il est soumis à la propriété intellectuelle de l'auteur. Ceci implique une obligation de citation et de référencement lors de l'utilisation de ce document.

D'autre part, toute contrefaçon, plagiat, reproduction illicite encourt une poursuite pénale.

Contact : ddoc-theses-contact@univ-lorraine.fr

LIENS

Code de la Propriété Intellectuelle. articles L 122. 4

Code de la Propriété Intellectuelle. articles L 335.2- L 335.10

http://www.cfcopies.com/V2/leg/leg_droi.php

<http://www.culture.gouv.fr/culture/infos-pratiques/droits/protection.htm>

INSTITUT NATIONAL POLYTECHNIQUE DE LORRAINE

ÉCOLE DOCTORALE : RP2E
Laboratoire Réactions et Génie des Procédés (LRGP)

THÈSE

Présentée et soutenue publiquement le 07/10/2010
Pour l'obtention du grade de Docteur de l'INPL
(Spécialité : Génie des Procédés et des Produits)

Par

Hayet BENNADJI

Biodiesel: Combustion des esters éthyliques d'huiles
végétales comme additifs au pétrodiesel

Biodiesel: Combustion of fatty acid ethyl esters as
additives to petrodiesel

Directeur de thèse :	Francis BILLAUD	DR CNRS (Nancy)
Co-directeur de thèse :	Lucie CONIGLIO-JAUBERT	MdC (Nancy)

Composition du jury :

<i>Président du jury :</i>	Valérie TSCHAMBER	Professeur (Mulhouse)
<i>Rapporteurs :</i>	Nabiha CHAUMEIX	DR CNRS (Orléans)
	Edward BLUROCK	Associate Professor (Lund, Suede)
<i>Examineur :</i>	Pierre-Alexandre GLAUDE	CR CNRS (Nancy)
<i>Membre invité :</i>	Guillaume DAYMA	MdC (Orléans)

Remerciements

Ce travail de thèse a été réalisé à l'ex-Département de Chimie physique des Réactions (DCPR), nommé maintenant Laboratoire de Réactions et Génie des Procédés (LRGP) après la fusion avec les autres laboratoires de l'Ecole Nationale Supérieure des Industries Chimiques (ENSIC).

Je tiens à remercier en premier lieu Monsieur Gabriel WILD, directeur du LRGP, pour m'avoir accueilli au sein de son équipe et pour avoir mis à ma disposition tous les moyens techniques du laboratoire.

Mes sincères remerciements vont également à Madame Lucie CONIGLIO et à Monsieur Francis BILLAUD, pour leur encadrement, pour la confiance qu'ils m'ont accordée et pour la formation scientifique qu'ils m'ont permis d'acquérir.

J'exprime mes sincères remerciements à Madame Nabiha SHOUMEIX et à Monsieur Edward BLUROKS d'avoir accepté de faire la relecture de ce rapport. Je leur suis reconnaissante pour le temps qu'ils ont consacré à ce travail.

J'adresse mes remerciements à Madame Frédérique BATTIN-LECLERC qui a gracieusement mis à ma disposition le matériel nécessaire durant mes trois ans de thèse et à Monsieur Pierre-Alexandre GLAUDE pour son savoir faire, ses précieux conseils prodigués lors de l'étude théorique de la cinétique de combustion et l'étude expérimentale en tube à onde choc, je lui suis reconnaissante de faire partie du jury.

Je remercie également Madame Valérie TSCHAMBER, Monsieur Guillaume DAYMA d'avoir participé à mon jury de soutenance et l'intérêt porté à mon travail.

Je n'oublie pas adresser mes remerciements aux membres de l'ex-DCPR et du laboratoire de Gestion des Risques et Environnement de Mulhouse: enseignants-chercheurs, personnel technique, personnel administratif, et doctorants.

Je dédie cette thèse à toute ma famille, qui m'a toujours encouragé:
Ma très chère maman, mon très cher papa et mes chers sœurs et frères

It suddenly struck me that that tiny pea, pretty and blue, was the Earth. I put up my thumb and shut one eye, and my thumb blotted out the planet Earth. I didn't feel like a giant. I felt very, very small.

Neil Armstrong

This English dissertation is preceded by a summarization in French which brings together the mainly work accomplished during this thesis.

Ce rapport est écrit en anglais et précédé par un résumé en français qui regroupe essentiellement les travaux accomplis durant cette thèse.

Résumé

BIODIESEL: COMBUSTION DES ESTERS ETHYLIQUES D'HUILES VEGETALES COMME ADDITIFS AU PETRODIESEL

Table des matières

Introduction générale	1
1. Les ressources alternatives au pétrodiesel	1
2. Etudes actuelles sur les moteurs thermiques	2
3. Maîtrise de l'émission des polluants	3
I. Etude bibliographique	7
I.1 Les matières premières	7
I.1.1 Les huiles végétales	7
I.1.2 Les autres sources lipidiques	9
I.1.3 Les alcools	9
I.1.3.1 Le méthanol et le biométhanol	9
I.1.3.2 L'éthanol	10
I.2 Les biocarburants pour le secteur du transport	11
I.3 Généralités sur les moteurs thermiques	13
I.3.1 Moteurs à combustion externe	13
I.3.2 Moteurs à combustion interne	13
I.3.3 Evolution de la législation sur les émissions polluantes	14
I.3.4 Techniques de réduction de la consommation de carburant et des émissions polluantes des moteurs alternatifs	15
I.4 Utilisation du biodiesel dans les moteurs	17
I.4.1 Utilisation directe des huiles végétales	17
I.4.2 Performances des Esters d'Huiles Végétales (EHV) en tant que carburant	18
I.4.3 Impacts des Esters d'Huiles Végétales sur les émissions	19
II. Dispositifs expérimentaux	23
II.1 Chimie de la combustion	23
II.2 Dispositif expérimental du réacteur tubulaire	26
II.2.1 Descriptif général	26
II.2.1.1 Section alimentation du réacteur	29

II.2.1.2	Section de mélange et de préchauffage de la charge du réacteur	31
II.2.1.3	Section réaction	32
II.2.1.4	Section de séparation et analyse	33
II.2.2	Bilan de matière	36
II.2.3	Etude paramétrique	36
II.2.4	Mesure du profil de température du réacteur	37
II.2.5	Techniques d'analyses et de mesures	38
II.2.5.1	Etalonnages des régulateurs de débit massique (RDM)	38
II.2.5.2	Etalonnage de l'analyseur IR COSMA-CRISTAL 300	39
II.2.5.3	Etalonnage des chromatographes	39
II.3	Dispositif expérimental du tube à onde choc	45
II.3.1	Principe du tube à onde de choc	46
II.3.2	Description du tube à choc du LRGP (ENSIC-Nancy)	48
II.3.3	Mise en œuvre du tube à onde de choc	49
II.3.4	Etudes paramétriques	51
III.	Description du système EXGAS-ESTERS	54
III.1	Description générale du système EXGAS-ESTERS	54
III.1.1	Base C ₀ -C ₂	54
III.1.2	Générateur de mécanismes primaires détaillés de consommation des réactifs	55
III.1.3	Générateur de mécanismes secondaires de consommation des produits primaires	56
III.2	Mécanisme d'oxydation de butanoate d'éthyle à haute température	56
III.3	Mécanismes d'oxydation des esters insaturés à haute température	56
III.4	Conclusion	57
IV.	Etude expérimentale et simulation de l'oxydation des esters méthyliques et éthyliques	58
IV.1	Etude en tube à onde de choc	58
IV.1.1	Conditions expérimentales	58
IV.1.2	Etude paramétrique	59

IV.1.3	Approche Statistique	60
IV.1.4	Modélisation et simulation des résultats obtenus en tube à choc	60
IV.1.4.1	Comparaison des simulations et des expériences	60
IV.1.4.2	Analyse de flux	61
IV.1.4.3	Analyse de sensibilité	62
IV.2	Etude en réacteur tubulaire à écoulement piston	62
IV.2.1	Conditions opératoires	63
IV.2.2	Identification des produits analysés	63
IV.2.3	Bilan de matière	64
IV.2.4	Reproductibilité des résultats	64
IV.2.5	Etude paramétrique	64
IV.2.6	Modélisation et simulation des résultats obtenus en tube à choc	65
IV.2.6.1	Comparaison simulation et expérience	65
IV.2.6.2	Analyse de flux	66
IV.2.6.3	Analyse de sensibilité	66
IV.3	Conclusion	67
	Conclusion & perspectives	68
	Publications et communications issues de ce travail de thèse	70
	Références bibliographiques	72
	Annexes	78
	A. Bilan de matière élémentaire et global	
	B. Calcul du réacteur piston (Plug flow reactor)	
	C. Mesure des profils de température	
	D. Courbes d'étalonnage des RDM	
	E. Description de la méthode d'étalon interne	
	F. Conditions d'analyse des chromatographes et temps de rétention des produits	
	G. Calcul du temps de passage	
	H. Calcul de l'état des gaz après l'onde de choc	

Introduction générale

1. Les ressources alternatives au pétrodiesel

Issus de programmes lancés à la fin des années 70 pour relâcher la contrainte pétrolière, les biocarburants ont plus de 20 ans de développement industriel. Ils suscitent aujourd'hui un regain d'intérêt fort car ils pourraient permettre, dans le secteur des transports, une réduction de la consommation de pétrole et une diminution des rejets de gaz à effet de serre. Ce regain d'intérêt est particulièrement visible en Europe où les directives adoptées au début de la décennie fixent des objectifs ambitieux d'incorporation de biodiesel dans le pétrodiesel (5.75 % volumique en 2010 et 8 % en 2015) et obligent les États membres à développer les filières biocarburants. En effet, le biodiesel, est une énergie renouvelable considérée comme une sérieuse alternative au pétrole et peut être produit à partir de sources naturelles telles les graisses animales et tout particulièrement les matières et huiles végétales comme le colza. Les huiles végétales renferment majoritairement des triglycérides (triesters du glycérol et d'acides gras : acides carboxyliques à longue chaîne carbonée, saturés ou portant une, voire deux, liaisons éthyléniques) et, en moindres proportions, des acides gras sous forme libre, des phospholipides, des stérols, de l'eau et d'autres impuretés. Elles ne peuvent pas être utilisées directement dans les moteurs Diesel classiques (viscosités élevées, risques de dépôts, indices de cétane faible, mauvaises caractéristiques à froid, ...) (Ballerini, 2006). C'est la raison pour laquelle les huiles végétales doivent être préalablement transformées en esters via une transestérification par addition d'un alcool pour produire le biodiesel qui est donc typiquement un mélange d'esters d'acides gras. Actuellement, le méthanol est l'alcool majoritairement utilisé et conduit au biodiesel composé d'esters méthyliques d'huiles végétales (EMHV); leur mélange à raison de 5% en volume au diesel est distribué de façon banalisée. Néanmoins, la possibilité de produire des esters éthyliques d'huiles végétales (EEHV), en remplaçant le méthanol par l'éthanol, est en cours de développement (Ballerini, 2006). En effet, l'éthanol obtenu à partir de la biomasse, conduit à la filière EEHV qui offre l'opportunité de produire un biodiesel issu exclusivement du végétal. En outre, les carburants EMHV et EEHV présentent des caractéristiques motrices équivalentes.

Des recherches ont montré que, comparativement à l'utilisation du gazole (pétrodiesel pur) comme carburant, l'addition d'EMHV et d'EEHV dans les moteurs Diesel conduit à une diminution des émissions de monoxyde de carbone (CO), d'hydrocarbures imbrûlés et de particules, ainsi qu'à

un bilan global positif en dioxyde de carbone. En outre, les EMHV et les EEHV présentent une biodégradabilité totale. Makarevicienne et Janulis (2003) ont montré que les émissions d'oxydes d'azote (NOx), de monoxyde de carbone (CO) et de particules sont significativement plus faibles en utilisant comme biodiesel les esters éthyliques par rapport aux esters méthyliques. De plus, les EEHV sont plus rapidement biodégradables que les EMHV.

2. Etudes actuelles sur les moteurs thermiques

L'énergie nécessaire à la propulsion et au fonctionnement de la majorité des véhicules routiers continuera encore des décennies à être fournie par des moteurs thermiques. Dans le but de réduire la dépendance énergétique et d'abaisser les niveaux d'émissions de gaz à effet de serre et des polluants locaux, les travaux de recherche s'intéressent à reformuler le carburant et à améliorer le fonctionnement des moteurs pour les rendre plus propres et plus économes.

La réduction de la consommation du carburant a été recherchée sur les moteurs à allumage commandé (dits « à essence ») comme sur les moteurs Diesel (dits par analogie « à allumage par compression »). Différentes voies ont été explorées :

- Réduction des frottements par optimisation de la lubrification,
- Optimisation de l'injection du carburant dans les cylindres, notamment en exploitant les techniques de modélisation et de simulation,
- Etude des phénomènes de combustion, détermination des températures optimales qui permettraient de réduire des émissions des polluants locaux,
- Etudes des potentialités du taux de compression variable et de la réduction de cylindrée («downsizing»),
- Optimisation de la composition des carburants pour améliorer les performances du moteur et pour réduire les émissions,
- Etude des potentialités des moteurs de nouvelle conception : combustion homogène dans un moteur Diesel dite «HCCI» (Homogeneous Charge Compression Ignition) et combustion essence par Auto-Inflammation contrôlée dite «CAI».

3. Maîtrise de l'émission des polluants

La combustion du gazole dans un moteur Diesel génère un certain nombre de résidus. Ceux-ci découlent des réactions radicalaires complexes de la combustion et dépendent essentiellement :

- Du carburant utilisé,
- De la température de fonctionnement du moteur,
- De la conception de la chambre de combustion,
- Du système d'injection.

Une combustion menée de façon la plus complète possible contribue à une production minimale de résidus. Une adéquation parfaite entre les quantités maximales de carburant et d'air contenu dans la chambre de combustion, ainsi qu'un brassage optimal, limitent la production de polluants. Ceux-ci sont généralement l'eau (H_2O), le dioxyde de carbone (CO_2), tous deux considérés comme non polluants et, dans de faibles proportions, une série de composés indésirables :

- le monoxyde de carbone (CO),
- des hydrocarbures imbrûlés (HC),
- les oxydes d'azote (NO_x),
- les particules de suie.

Les solutions proposées pour réduire la production de polluants passent par la mise en œuvre:

- d'un système d'injection performant,
- d'un catalyseur d'oxydation,
- d'un système de recyclage des gaz d'échappement, et
- d'un filtre à particules.

Les normes sur les émissions polluantes devenant de plus en plus sévères, il est à présent indispensable d'optimiser aux mieux les systèmes de combustion.

L'optimisation de la combustion dans le cylindre a consisté à rechercher les conditions optimales de température, de pression, d'homogénéité du mélange air/carburant. En particulier, l'amélioration de la qualité de l'auto-inflammation de mélanges homogènes devrait conduire à d'importants progrès sur la détermination des configurations optimales qui permettent de minimiser la formation de polluants ainsi que le bruit du moteur. Cette étape d'optimisation des phénomènes liés à la combustion peut se faire soit à partir d'observables (expériences), soit par le

biais de calculs prévisionnels (simulation) impliquant préalablement la mise en œuvre de modèles (modélisation) capables de reproduire une base d'informations expérimentales déjà disponible. Ainsi, la modélisation est un moyen intéressant permettant de limiter le nombre d'expériences nécessaires pour l'optimisation des phénomènes de combustion. Néanmoins, les modèles physico-chimiques ne sont pas encore pleinement satisfaisants, particulièrement dans le cas de la combustion homogène dite HCCI. Il existe encore peu d'éléments permettant d'avoir une connaissance précise de la nature des phénomènes mis en œuvre lors de la combustion et des moyens permettant de la contrôler. Deux types de modélisation ont été réalisées dans la littérature l'une avec un schéma cinétique détaillé (Battin-Leclerc, 2008) obtenu grâce à l'utilisation de logiciels de génération automatique (Ranzi et al., 1995 ; Warth et al., 2000), l'autre avec un schéma cinétique réduit généré manuellement (Griffiths, 1995). Par ces recherches, d'importants paramètres influençant la combustion ont pu être identifiés et ouvre la voie à une amélioration du fonctionnement des moteurs en termes de performances et d'émissions.

Concernant le post-traitement, deux familles de systèmes (et parfois leur combinaison) ont fait l'objet de travaux conséquents : les systèmes dits « DeNOx » de traitement des oxydes d'azote et les filtres à particules (ainsi que leur régénération).

L'efficacité de la combustion du mélange air/carburant à l'intérieur du cylindre du moteur peut être améliorée de façon conséquente. Les progrès de la modélisation et de la simulation numérique ont permis des avancées notables dans la compréhension et la maîtrise des phénomènes de mécanique des fluides, d'aérothermique et de combustion. L'application de ces connaissances et des techniques nouvelles devraient faire progresser le rendement des moteurs en facilitant l'optimisation de l'injection (forme, moment, position...) et des paramètres tels la température ou la pression. La récupération de l'énergie véhiculée par les gaz d'échappement est aussi une idée qui suscite de l'intérêt.

En outre, les progrès en chimie devraient aussi être un apport intéressant à deux niveaux :

- Une meilleure compréhension et donc une plus grande maîtrise de la chimie de la combustion dans les cylindres des moteurs (y compris la formation des polluants),
- Une optimisation des méthodes de post-traitement et de régénération des filtres.

Les recherches en cinétique de combustion et en catalyse s'avèrent primordiales pour avoir une meilleure connaissance des émissions de polluants, augmenter le rendement des procédés d'élimination des polluants et trouver des alternatives aux métaux nobles.

Afin de réduire les émissions de polluants ainsi que la dépendance de l'Europe et du monde en général vis à vis des pays producteurs de pétrole, les chercheurs scientifiques ont concentré leur attention sur l'utilisation du biodiesel comme biocarburant. Concernant la production de biodiesel, la plupart des usines utilisent actuellement le méthanol comme alcool lors de la transestérification; or, le méthanol étant issu traditionnellement de produits dérivés du pétrole et le biodiesel ainsi obtenu (composé d'esters méthyliques) n'est renouvelable qu'à 90% en masse. En revanche, l'utilisation du bioéthanol comme alcool conduit à un biodiesel (composé d'esters éthyliques) qui est entièrement renouvelable ; i.e. réduit encore davantage les émissions de gaz à effet de serre (Lapuerta et al., 2008). Le biodiesel commercialisé en France, c'est-à-dire les esters méthyliques d'huiles de colza (RME), renferment des molécules ayant entre 14 à 22 atomes de carbone. Certaines entreprises françaises ont planifié, pour 2008, de doubler leur production de biodiesel en ouvrant une nouvelle chaîne de production parallèle d'esters éthyliques d'huiles de colza (REE).

Dans cette optique, l'objectif majeur de ce travail de thèse est de comprendre la cinétique d'oxydation des molécules modèles d'esters éthyliques et de comparer aussi leur réactivité avec celle des esters méthyliques.

Après une introduction sur les objectifs de la thèse, une première partie synthétise les principales données bibliographiques et les travaux antérieurs les plus marquants.

Une deuxième partie est consacrée à la description des dispositifs expérimentaux utilisés pour générer les informations nécessaires à la mise au point de modèles cinétiques basses et hautes températures. Le premier dispositif correspond à un réacteur tubulaire à écoulement piston, utilisé auparavant pour la pyrolyse d'huiles végétales. Son adaptation à l'oxydation des esters éthyliques, ainsi que les techniques d'analyse utilisées au cours des travaux réalisés sur ce pilote expérimental sont également évoquées. Le deuxième dispositif est un tube à onde de choc déjà éprouvés au cours de nombreux travaux développés au sein du Laboratoire Réactions et Génie des Procédés (LRGP-Nancy) (Fournet et al., 1999 ; Belmekki et al., 2002 ; Dayma et al., 2003 ; Hakka et al., 2010).

La troisième partie présente les principales caractéristiques de la nouvelle version du logiciel EXGAS-ESTERS et des modèles d'oxydation à haute température de l'acrylate d'éthyle, de l'acrylate de méthyle, de crotonate d'éthyle, de crotonate de méthyle et de butanoate d'éthyle.

La quatrième est consacrée à une présentation des résultats expérimentaux et théoriques concernant l'oxydation des esters étudiés dans les domaines relatifs aux basses et hautes températures.

Nous renfermerons enfin ce travail par une conclusion et les perspectives.

I. Etude bibliographique

L'Union Européenne a comme but le développement des biocarburants, notamment pour la lutte contre le changement climatique et la diminution de la dépendance énergétique. En France, le secteur de transports est le premier émetteur de gaz à effet de serre et dépend à 97% du pétrole (Ballerini, 2007). Les biocarburants apportent de manière complémentaire une voie de réduction à court terme des émissions de gaz à effet de serre et représentent la première alternative aux produits pétroliers dans ce secteur. Le biodiesel est un carburant employé dans les moteurs diesel en remplacement ou en en mélange avec le gazole. C'est actuellement le deuxième biocarburant le plus utilisé dans le monde après l'éthanol et le biodiesel substitue à plus de 2.5% le gazole (Ballerini, 2007). Dans un tel contexte, il devient urgent de développer de nouvelles filières, impliquant d'autres ressources végétales et d'autres technologies.

I.1 Les matières premières

I.1.1 Les huiles végétales

La production mondiale d'huiles végétales est évaluée à 101 Mt en 2003, 123 Mt pour 2006. Les estimations pour 2010 se situent autour de 130 Mt. Les huiles de palme et de soja représentent à elles seules 58 % du marché. Viennent ensuite les huiles de colza et de tournesol avec respectivement 14 % et 9 % des volumes produits. L'huile de coton, avec 4 %, se situe au cinquième rang devant l'huile de palmiste et l'huile d'arachide.

L'Indonésie et la Malaisie avec une production de plus de 17 millions de tonnes sont les premiers producteurs et les premiers exportateurs mondiaux d'huiles végétales. Avec la production chinoise, ces trois pays assurent à eux seuls plus de 40 % de la production mondiale. Avec une production de l'ordre de 12 millions de tonnes chacun, l'Union Européenne et les États Unis figurent ensuite parmi les principaux pays producteurs.

En Europe, la production de graines de colza est prépondérante devant celle de tournesol, celle du soja étant très marginale. Le tableau I.1 illustre des données relatives à la production européenne de ces trois huiles végétales.

Par ailleurs, les huiles sont essentiellement constituées de triglycérides, à hauteur de 95-98 %. Les constituants mineurs sont des acides gras libres, des mono et diglycérides, des phospholipides, des tocophérols, des stérols, des colorants et odorants naturels. Les triglycérides sont constitués d'une molécule de glycérol estérifiée avec trois molécules d'acides gras. Le tableau

I.2 présente la composition en acides gras d'huiles végétales courantes. Cette composition varie suivant les pays et les saisons.

Tableau I.1 : Production européenne d'huiles végétales (Ballerini, 2006)

(Commission Européenne, Direction Générale de l'Agriculture, 1999-2002 ; COPA/COGECA, 2003).

Huile	Pays	Surface cultivée (10 ³ ha)			Rendement (t/ha)			Production (10 ³ t)		
		1999	2002	2003	1999	2002	2003	1999	2002	2003
Colza	Allemagne	1207	1285	1269	3.29	3.33	2.87	3970	4275	3644
	France	1369	1061	1077	3.27	3.23	3.08	4472	3430	3321
	GB	537	432	542	3.23	3.33	3.27	1732	1437	1771
	EU-15	3589	3070	3216	3.17	3.1	2.82	11369	9522	9080
	Tchéquie	349	313	250	2.67	2.3	1.56	931	722	390
	Pologne	545	439	426	2.08	2.27	1.77	1132	985	754
Tournesol	Espagne	850	754	787	0.68	1	0.91	579	757	716
	France	799	616	686	2.29	2.43	2.08	1829	1497	1424
	Italie	235	167	129	3.08	2.1	1.47	724	351	190
	EU-15	1997	1627	1712	1.66	1.7	1.45	3323	2758	2482
	Hongrie	521	418	505	1.52	1.86	1.92	793	77	970
Soja	France	102	92	81	2.89	2.89	1.89	295	266	153
	Italie	231	128	140	4.63	3.9	3.21	1070	499	450
	EU-15	356	235	236	4	3.42	2.69	1425	804	635

Tableau I.2 : Composition en acides gras d'huiles végétales

(Hennico et al., 1995 ; Ballerini., 2006 ; Lotero et al., 2005).

	Mystérique	Palmitique	Palmitoléique	Stéarique	Oléique	Linoléique	Linoléique	Arachidique	Gadoléique	Béhnéique	Erucique	
	C14:0	C16:0	C16:1	C18:0	C18:1	C18:2	C18:3	C20:0	C20:1	C22:0	C22:1	Indice d'iode
^a Colza		5		2	59	21	9	< 0.5	1	< 0.5	< 1	
^a Soja		10		4	23	53	8	< 0.5	< 0.5	< 0.5	-	
^a Tournesol		7		4	22	65	< 0.5	< 0.5	< 0.5	< 0.5	-	
^b Colza		5		2.5	59	21	9	< 0.5	1	< 0.5	1	111
^b Tournesol		6		5	18	69	< 0.5	< 0.5	< 0.5	1		135
^b Tournesol Oléique		4		4	80	10	< 0.5	1	< 0.5	1		87
^b Soja		10		4	23	53	8	< 0.5	< 0.5	< 0.5		133
^b Palme	1	44		6	38	10	< 0.8	< 0.5				50
^b Lin		6		3	19	17	54		< 0.5	< 0.5		187
^c Colza		3.5		0.9	64.4	22.2	8.2					
^c Olive vierge		9.2	0.8	3.4	80.4	4.5	0.6					
^c Tournesol		6		4.2	18.7	69.3						
^c Soja	0.1	10.6		4.8	22.5	52.3	8.2					
^c Palme	1.2	47.9		4.2	37	9.1	0.3					

^a (Hennico et al., 1995); ^b (Ballerini., 2006) ; ^c (Lotero et al., 2005).

C x:y : symbole désignant les acides gras; où x représente le nombre d'atomes de carbone et y le nombre de doubles liaisons éthyléniques, celles-ci étant toujours séparées par un groupement méthylène CH₂ lorsqu'il y en a plusieurs.

I.1.2 Les autres sources lipidiques

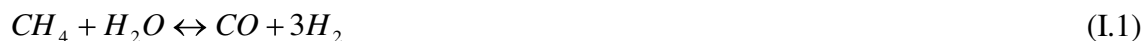
En France, la production annuelle d'huiles alimentaires usagées est d'environ 65000 à 150 000 tonnes. Seules environ 26 000 tonnes sont collectées et valorisées. Une partie est souvent rejetée dans le réseau d'assainissement. Le code de l'environnement impose aux restaurateurs d'assurer l'élimination et la valorisation de ces huiles usagées. L'emploi d'huiles de fritures recyclées réduit le coût des matières premières mais augmente le coût du traitement. Elles ont un indice d'acide élevé qui constitue un handicap en transestérification par catalyse homogène basique. La distillation sous vide des esters obtenus à partir de ces huiles est nécessaire. Les graisses animales constituent aussi une autre source lipidique pour produire le biodiesel. Il existe 5 grandes variétés de graisses animales : le saindoux (porc), le suif (bovins et ovins), les graisses d'os, les graisses de volailles souvent en mélanges (poulet, canard, oie, dinde) et les huiles de poisson. Ce pendant, les huiles de poisson, de par leur indice d'iode très élevé (>150), et une forte insaturation ne peuvent pas être utilisées comme carburant, du fait de risques importants d'oxydation et de polymérisation. La forte acidité contenue dans des graisses ne leur permet pas d'être utilisées directement dans les unités de production de biodiesel. Un prétraitement consisterait à diminuer l'acidité de ces graisses par estérification en catalyse acide.

I.1.3 Les alcools

I.1.3.1 Le méthanol et le biométhanol

Le méthanol est un des produits de la chimie organique les plus fabriqués au monde, avec une production d'environ 21 Mt/an, dont 5.1 Mt aux Etats-Unis, 2.3 Mt au Canada, 2.2 Mt en Arabie Saoudite et 1.6 Mt en Allemagne.

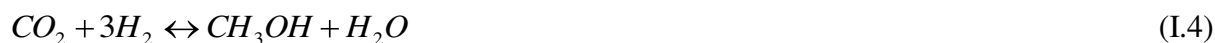
Autrefois obtenue par distillation du bois, la fabrication du méthanol se fait aujourd'hui essentiellement à partir du gaz de synthèse ($CO + H_2$), lui-même obtenu par oxydation partielle du méthane, par gazéification des hydrocarbures plus lourds, ou principalement par reformage à la vapeur du méthane ou du naphta. Les réactions mises en jeu sont :



La synthèse du méthanol repose ensuite sur la mise en œuvre de la réaction suivante, menée à 250 °C, sous 50 bars et en présence d'oxyde de zinc jouant le rôle de catalyseur :



et dans une moindre mesure, sur la transformation du gaz carbonique:



Le méthanol, via son obtention à partir de gaz de synthèse résultant de dérivés d'origine pétrolière, donc non renouvelable (méthane, hydrocarbures lourds ou naphtha), est amené à être remplacé dans les utilisations biocarburant par de l'éthanol, ce dernier étant d'origine végétale. C'est la raison pour laquelle une autre alternative de production du gaz de synthèse par gazéification de matières lignocellulosiques (bois, herbe) est en cours d'étude, permettant de conduire au biométhanol. Toutefois, si le gaz de synthèse ainsi obtenu à partir d'une source végétale renouvelable mérite le nom de biogaz de synthèse, le biométhanol reste produit par synthèse catalytique.

I.1.3.2 L'éthanol

S'il existe encore une production industrielle d'éthanol à partir d'éthylène d'origine pétrolière, pour l'essentiel en Arabie Saoudite, la majeure partie de l'éthanol produit est fabriqué par fermentation de matières premières d'origine végétale. Les principales matières premières sont :

- Les plantes sucrières (betterave, canne à sucre, sorgo sucrier) qui renferment des sucres quasiment fermentescibles en éthanol,
- Les plantes céréalières (maïs, blé, orge, tubercules) dans lesquelles les sucres sont sous forme d'amidon, qui doit être hydrolysé en monomères sucrés pour pouvoir être transformés en éthanol,
- Les plantes lignocellulosiques telles que des résidus agricoles ou forestiers.

En France, l'éthanol est principalement issu de la betterave et du blé. Aux Etats-Unis, la source principale est le maïs. Le tableau I.3 présente la production française d'éthanol à partir de betterave et de blé en 2003 et les prévisions pour 2010.

Tableau I.3 : Production française d'éthanol (IFP, 2005)

	2003		Prévisions 2010	
	Surface cultivée (ha)	Quantité produite (t)	Surface cultivée (ha)	Quantité produite (t)
Betterave	12 000	60 000	53 600	300 000
Blé	14 400	36 000	270 000	700 000

La consommation d'énergie primaire liée à la production d'éthanol à partir de jus de betteraves peut représenter 30 à 40 % du contenu énergétique de l'éthanol. Néanmoins,

l'amélioration des techniques de production d'éthanol et la réduction des coûts de production est nécessaire au développement de la production de biodiesel. Cette production ne doit cependant pas se faire avec des engrais polluants ou d'origine fossile.

Par ailleurs, la production d'éthanol pour la filière biodiesel peut entrer en compétition avec la production d'éthanol comme biocarburant dans les moteurs essences. Dans les deux cas, l'augmentation des surfaces agricoles dédiées à la production d'éthanol entrera en compétition avec celles dédiées aux ressources alimentaires.

I.2 Les biocarburants pour le secteur du transport

Les deux principaux secteurs consommateurs de carburants sont le transport et l'agriculture. Ceux-ci contribuent majoritairement à la pollution de l'environnement qui peut être réduite en remplaçant le carburant d'origine fossile par un biocarburant d'origine renouvelable. Les principaux biocarburants sont le biodiesel et le bioéthanol. Comme présenté dans les paragraphes précédents, le bioéthanol est produit à partir de la fermentation de la cellulose, du sucre de canne, de maïs et du sucre de betterave. Les deux derniers sont les principales sources d'éthanol en Europe. En revanche, le biodiesel est un carburant qui est produit à partir des huiles végétales ou des graisses animales. Pour le secteur du transport, les pays européens utilisent du biodiesel ou d'autres carburants renouvelables qui peuvent remplacer le pétrodiesel ou l'essence d'origine pétrolière. Plusieurs facteurs doivent être pris en compte avant de recommander l'utilisation à différentes échelles d'un nouveau carburant alternatif. Une liste non exhaustive est citée ci-après.

- Le carburant doit répondre à la technologie actuelle des moteurs car une modification importante de la technologie nécessite un capital énorme,
- Les coûts d'investissement doivent être raisonnables pour faciliter le développement des procédés de fabrication des biocarburants,
- La compatibilité environnementale comparée au carburant conventionnel doit être évidente. Il serait inacceptable que le nouveau biocarburant soit plus polluant,
- Les coûts additionnels pour l'utilisateur en termes d'entretien, d'usure d'équipement et de durée de vie de l'huile de lubrification doivent être moindres. Des coûts additionnels trop élevés auront un effet négatif sur l'acceptation de ce biocarburant (Ballerini, 2007).

En France, les Esters Méthyliques d'Huiles de Colza (EMC) sont commercialisés sous la marque DIESTER (Diesel ESTER) qui est une marque déposée par Sofiproteol. Actuellement, 100 % des véhicules diesel roulent déjà avec du Diester (en mélange banalisé jusqu'à 5 % dans le

gazole). Passer à une proportion de 5% n'aurait pas de conséquence sur le fonctionnement des moteurs actuels. Le gouvernement français a indiqué en 2005 que le pourcentage en diester devrait atteindre 5.75% en 2008, 7% en 2010 et 10% en 2015.

Le tableau I.4 récapitule la capacité de production du Diester de quelques sites industriels en France.

Tableau I.4 : Capacités de production du Diester des différents sites de production français

(Ballerini, 2007)

Unité de production	Capacité (Tonnes)
Bordeaux	200 000
Boussens	40 000
Compiègne	200 000
Coudekerque	200 000
Grand-Couronne	500 000
La pallice	10 000
Le Mériot	250 000
Montoir	250 000
Sète	200 000

Dans le contexte d'une forte croissance d'activité et dans une logique de développement durable qui fait partie des axes stratégiques du groupe sofiprotéol, les développements industriels envisagés sont pensés pour l'avenir en termes d'écologie industrielle. L'objectif est toujours de chercher à améliorer le bilan énergétique du Diester au travers des plans de développements industriels et de l'amélioration des procédés de production. Aussi, diverses mesures ont été prises en ce sens, parmi lesquelles :

- L'introduction d'une unité de cogénération produisant de l'électricité et de la vapeur d'eau issue de la biomasse,
- La substitution du méthanol par l'éthanol d'origine végétale (bioéthanol) dans la réaction de transestérification,
- L'amélioration des procédés pour limiter la consommation d'eau,
- La mise en place de chartes environnementales pour la production du colza et du tournesol Diester.

L'organisation de la filière industrielle oléagineuse permet en outre à la logistique d'être optimisée puisque les activités de trituration, raffinage et production de diester sont souvent intégrées dans un même site, ce qui limite les coûts de transports (www.prolea.com).

I.3 Généralités sur les moteurs thermiques

Les moteurs thermiques ont pour rôle de transformer l'énergie thermique en énergie mécanique. Encore appelés, moteurs à combustion, ils sont généralement distingués en deux catégories : les moteurs à combustion externe et ceux à combustion interne (Sovanna et al., 2005).

I.3.1 Moteurs à combustion externe

Ce type de moteur a été inventé par Robert Stirling en 1816. La chaleur est produite dans une chambre de combustion (chaudière) séparée de la chambre de détente. Cette chaleur est utilisée pour vaporiser de l'eau. La vapeur d'eau sous pression obtenue par cette vaporisation est alors envoyée dans la chambre de détente où elle actionne un piston. Un système de bielle-manivelle permet ensuite de récupérer l'énergie mécanique ainsi produite en l'adaptant aux besoins.

I.3.2 Moteurs à combustion interne

Les moteurs thermiques automobiles (dits «moteurs à combustion interne») transforment l'énergie chimique contenue dans les molécules du carburant en énergie thermique puis mécanique, nécessaire à assurer le mouvement du véhicule. La présence d'un comburant dans la chambre de combustion (21% d'oxygène contenu dans l'air) est nécessaire pour que la combustion du carburant, produisant l'énergie thermique, ait lieu. L'augmentation de pression, due à la combustion, crée une force s'exerçant sur un piston et transformant le mouvement de translation de celui-ci en un mouvement de rotation du vilebrequin.

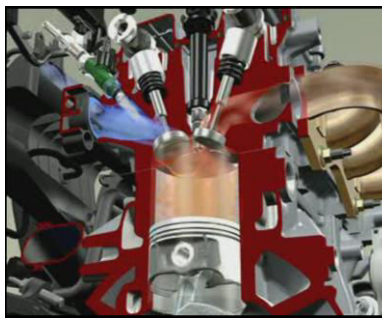


Figure I.1 : Chambre de combustion d'un moteur alternatif

(http://fr.wikipedia.org/wiki/Moteur_à_explosion)

Les moteurs à combustion interne sont classés en deux catégories suivant la technique d'inflammation du mélange gazeux carburant/air : les moteurs à allumage commandé (moteur à essence) et ceux à allumage par compression. (Sovanna et al., 2005).

- Dans les moteurs à allumage commandé (moteur essence), un mélange essence/air dans les proportions adéquates est admis dans la chambre de combustion du cylindre où l'inflammation est produite par une étincelle.
- Dans les moteurs à allumage par compression (moteur Diesel), le gazole est injecté sous pression dans la chambre de combustion contenant de l'air, préalablement comprimé et chaud, au contact duquel il s'enflamme spontanément.

I.3.3 Evolution de la législation sur les émissions polluantes

Un gaz d'échappement de moteur Diesel est un mélange relativement complexe dont les constituants peuvent être répartis en trois catégories (Degobert, 1995).

- Des composés chimiques oxydants : l'oxygène (0.2 à 2 % en volume) et des oxydes d'azote : NO (0.01 à 0.4 %), NO₂ (< 100 ppm),
- Des composés chimiques réducteurs : le monoxyde de carbone (0.1 à 6 %), l'hydrogène (0.5 à 2 %) et les hydrocarbures imbrûlés (0.5 à 1 %), catégorie incorporant les hydrocarbures proprement dits et leurs produits d'oxydation partielle (aldéhydes, etc.),
- D'autres composés : l'azote (70 à 75 %), la vapeur d'eau (7 à 12 %), le dioxyde de carbone (10 à 19.5 %), le dioxyde de soufre (15 à 60 ppm) et des traces de métaux, en général des additifs incorporés dans les carburants et les lubrifiants (plomb, phosphore, zinc, etc.). Il convient aussi de préciser que moins de 1% des gaz d'échappement rejetés par le moteur sont nocifs.

L'utilisation intensive des combustibles fossiles a conduit à la modification globale de l'environnement tels que : l'effet de serre, les pluies acides, l'atténuation de l'ozone dans la couche stratosphère, les changements climatiques, etc. L'emploi des carburants d'origine fossiles a augmenté le taux de CO₂ de 280 ppm durant la pré-industrialisation à 350 ppm de nos jours.

Les polluants émis par la combustion des différents carburants sont classés en deux catégories définies ci-après. Les émissions de ces polluants ont divers effets néfastes sur la santé humaine, à courts et à longs termes. (Guo et al., 2006)

- Les polluants réglementés. Leur émission est limitée par les législations environnementales (U.S.EPA et EURO). Ces polluants sont en général les oxydes d'azote (NO_x), le monoxyde de carbone (CO), les hydrocarbures imbrûlés et les fines particules.

- Les polluants non réglementés. Pour ce type de polluants, aucune limite législative n'a été prescrite. Ils sont en particulier : les aldéhydes (formaldéhyde), le benzène, le toluène, le xylène (BTX), le dioxyde de soufre (SO₂), le dioxyde de carbone (CO₂), le méthane.

Cependant, depuis 1990, le taux de rejets de gaz d'échappement dans l'atmosphère est limité par la normalisation européenne (normes Euro). Le tableau I.5 rend compte des différentes normes Euro en fonction des polluants réglementés.

Tableau I.5: Normes euros (Panorama 2008 - IFP)

Normes	Année	HC ^a +NO _x mg.km ⁻¹	NO _x mg.km ⁻¹	CO mg.km ⁻¹	PM ^a mg.km ⁻¹
Euro I	1992	970	-	2720	140
Euro II	1996	700	-	1000	80
Euro III	2000	560	500	640	50
Euro IV	2005	300	250	500	25
Euro V	2009	230	180	500	5
Euro VI	2014	170	80	500	4.5

^a hydrocarbures (HC), particules (PM)

I.3.4 Techniques de réduction de la consommation de carburant et des émissions polluantes des moteurs alternatifs

Les constructeurs ont réussi à développer des moteurs Diesel possédant un rendement thermique élevé et capables de délivrer une puissance importante. Au cours de ces dernières années, des changements significatifs ont été réalisés pour le développement de moteurs Diesel plus « propres » grâce à l'utilisation de systèmes de commande d'injection de carburant particuliers. Ces systèmes comprennent une injection à plusieurs étages, des turbocompresseurs et un recyclage des gaz d'échappement (RGE). Toutefois, un des principaux problèmes persistants, en rapport avec le principe de base du moteur thermique, est la nature des produits issus de la combustion et rejetés dans le milieu ambiant. On y trouve de fortes quantités de dioxyde de carbone (CO₂) qui résulte de la réaction des atomes de carbone des molécules d'hydrocarbures avec l'oxygène. Ce dégagement de CO₂ est inhérent au principe même du moteur à explosion fonctionnant avec des hydrocarbures, un « gaz à effet de serre » dont les répercussions sur le climat sont à présent clairement identifiés. Hormis le CO₂, d'autres composés sont émis lors des réactions qui ont lieu dans le cylindre du moteur : le monoxyde de carbone, le monoxyde et dioxyde d'azote (en raison de l'azote de l'air présent dans le cylindre), les hydrocarbures imbrûlés, les composés dits « aromatiques » (hydrocarbures comportant un ou plusieurs cycles benzéniques), carbone

(particules), etc.... Ces produits constituent ce qu'il est appelé par convention les «polluants locaux».

Dans la mesure où le dégagement de CO₂ est lié au principe même du moteur thermique fonctionnant avec des hydrocarbures, il est impossible de s'en affranchir. Trois solutions sont envisageables pour en réduire les émissions :

- Augmenter le rendement des moteurs, c'est-à-dire mieux récupérer l'énergie contenue dans la molécule d'hydrocarbure et donc consommer moins de carburant, tout en délivrant la même quantité d'énergie mécanique. Une consommation moindre en carbone se traduira par un rejet moindre de CO₂ dans l'atmosphère. Cette optimisation du rendement permet aussi de réduire la dépendance énergétique.
- Utiliser plus souvent le moteur sur les points de fonctionnement présentant les meilleurs rendements, soit par la boîte de vitesse (à variation continue), soit par l'architecture (moteur à taux de compression variable), soit par l'utilisation d'une source d'énergie auxiliaire (alternateur-démarrateur, hybridation).
- Utiliser des carburants dont la molécule contient un nombre d'atomes de carbone relativement faible par rapport au nombre d'atomes d'hydrogène (rapport C/H plus faible) à condition que l'utilisation de ces carburants n'entraîne pas une dégradation du rendement thermodynamique de combustion. Ce raisonnement conduirait à privilégier l'utilisation du gaz naturel pour véhicule (GNV, constitué majoritairement de méthane caractérisé par un rapport C/H proche de 0.25, à comparer aux rapports C/H de l'ordre de 0.53 pour l'essence et le gazole). Le méthane pose néanmoins d'autres problèmes à savoir; la limitation d'autonomie des véhicules, le réseau d'approvisionnement, les émissions d'imbrûlés possédant un impact (gaz à effet de serre).

Concernant les polluants locaux émis par les moteurs à combustion interne, leur présence dans les gaz d'échappement peut, à priori, être réduite à deux niveaux :

- En optimisant la combustion du mélange hydrocarbures/air dans le cylindre et (ou) en traitant les produits issus de la combustion entre leur échappement du cylindre et leur rejet dans l'atmosphère (post-traitement).
- En optimisant le rendement des moteurs thermiques et en réalisant un «post-traitement» des gaz d'échappement.

I.4 Utilisation du biodiesel dans les moteurs

Le biodiesel est le carburant composé d'Esters Méthyliques d'Huiles Végétales (EMHV) ou d'Esters Ethyliques d'Huiles Végétales (EEHV), par opposition au traditionnel diesel (pétrodiesel). Les EMVH ont des propriétés proches de celles du gazole, ce qui n'est pas le cas des huiles végétales. L'intervalle de distillation des EMHV est compris entre 320°C et 350°C, les situant au niveau des fractions les plus lourdes de la coupe gazole.

Le tableau I.6 compare les principales caractéristiques physico-chimiques, utiles pour un carburant, du gazole, de l'huile colza et des esters méthyliques d'huile de colza.

Tableau I.6 : Caractéristiques physico-chimiques utiles pour un carburant, du gazole, de l'huile de colza et des EMVH (Ballerini, 2006)

Caractéristiques	Gazole	Huile de colza	EMHV
Densité à 15°C	0.82-0.86	0.92	0.8
^a Indice de cétane	> 49	35	51
^b Point d'éclair °C	> 55	-	185
^c PCI (MJ/l)	35.3 - 36.3	34.3	33.2
Viscosité à 40°C (mm ² /s)	2 - 4.5	30.2	4.5

^a Indice de cétane : caractérise le délai d'auto inflammation ; minimum légal : 48 pour les véhicules, ^b Point éclair : température à partir de laquelle les vapeurs dégagées sont inflammables, ^c PCI : Pouvoir Calorifique Inférieur.

En France deux mélanges d'esters méthyliques sont utilisés avec le diesel conventionnel :

- un mélange à 5 % volumique pour le grand public, l'EMHV 5,
- un mélange à 30-50 % volumique pour les flottes captives, l'EMHV 30.

Les esters alcooliques d'huiles végétales sont biodégradables, faiblement toxiques vis-à-vis des espèces animales et des micro-organismes et présentent peu ou pas de risques vis-à-vis de l'environnement en cas de déversement accidentel dans la nature. Leurs autres avantages sont : l'absence du soufre et des composés aromatiques, leur pouvoir lubrifiant, la diminution des émissions d'hydrocarbures et de particules et un bilan CO₂ positif.

I.4.1 Utilisation directe des huiles végétales

Rudolf Diesel, à l'origine, a développé le moteur qui porte son nom en utilisant de l'huile d'arachide. Toutefois la filière huile en tant que telle n'est pas viable pour les moteurs Diesel modernes, essentiellement à injection directe (forte viscosité, risque de dépôts, indice de cétane faible, mauvaises caractéristiques à froid, etc). Des utilisations en mélange ont été expérimentées.

Celles-ci ont fait apparaître à long terme des baisses de performances du moteur en raison de dépôts sur les injecteurs et sur le piston et du gommage des segments.

Pour un moteur Diesel moderne, l'utilisation directe d'huile de colza pure conduit aux constats suivants (rejets par rapport au diesel classique):

- Doublement des niveaux de CO,
- Quadruplement des émissions d'hydrocarbures,
- Réduction des rejets de NO_x de 25 % (combustion à des températures moins élevées),
- Augmentation des émissions de particules de 90 à 140 %, des aldéhydes et cétones de 30 à 330 %.

Cependant, l'utilisation d'une préchambre permet d'améliorer les performances du moteur et de réduire les rejets. Le développement de nouveaux moteurs spécifiques permettrait une utilisation directe plus performante des huiles végétales.

I.4.2 Performances des Esters d'Huiles Végétales (EHV) en tant que carburant

L'incorporation d'EMHV permet d'augmenter significativement le pouvoir lubrifiant des gazoles, notamment ceux à basse teneur en soufre. Des tests d'usure ont montré que l'addition d'esters méthyliques de colza à des teneurs comprises entre 2 et 5 % volumique réduit l'usure des pièces métalliques en contact avec le carburant. Les caractéristiques à froid des esters d'huiles végétales sont très voisines de celles des gazoles mais restent en deçà de celles des gazoles en hivers et plus encore des gazoles grands froids. Les EMHV ont un Pouvoir Calorifique Inférieur (PCI) massique plus faible de 11 % que celui des gazoles et un PCI volumique plus faible de 7%. De ce fait, la consommation (en l/100 km parcourus) est plus importante d'environ 7 %.

Des essais sur banc moteur et kilométrages expérimentés par l'IFP ont montré que l'emploi de l'EMHV5 n'avait aucune incidence sur les caractéristiques de combustion et d'injection, ni sur le comportement en endurance, ni sur le fonctionnement des systèmes post-traitement. Une bonne compatibilité des matériaux a été constatée. Une très légère augmentation de la consommation de carburant, de l'ordre de 0.3 %, a toutefois été observée. Les mélanges EMHV30 sont utilisés avec succès dans des moteurs adaptés.

I.4.3 Impacts des Esters d'Huiles Végétales sur les émissions

Les EMHV offrent un bilan environnemental positif. Leur utilisation permet de réduire les émissions en CO, hydrocarbures et particules. En revanche leur température de combustion plus élevée induit une augmentation des rejets en NO_x. Des gains très appréciables sont observés en terme de rejets de gaz à effet de serre, comme le montre la figure I.2.

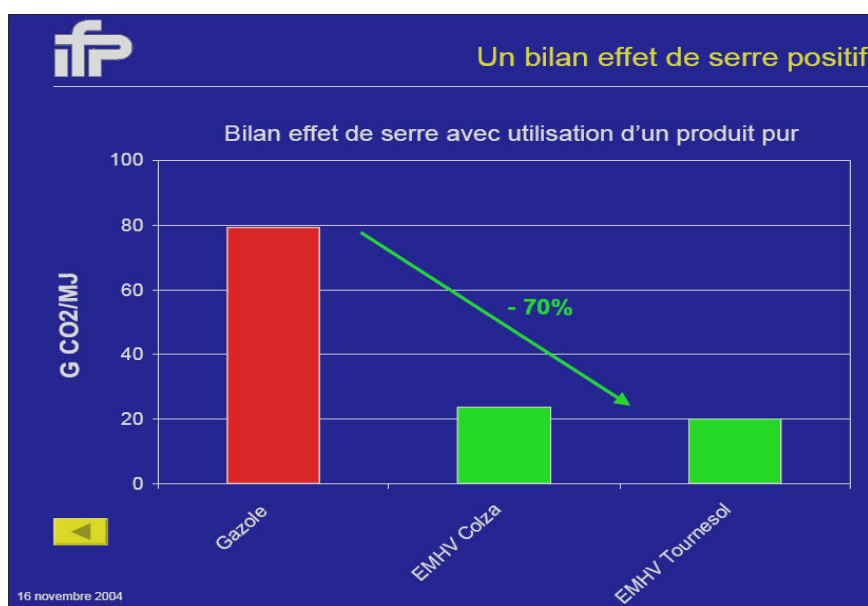


Figure I.2 : Bilan effet de serre des EMHV (IFP)

Le tableau I.7 présente les émissions de deux mélanges de biodiesel, le B100 (100 % de biodiesel) et le B20 (20% de biodiesel avec le gazole) comparative au diesel pur.

Tableau I.7: Emissions de mélanges de biodiesel (Ballerini, 2006)

Emissions	B100	B20
CO ₂	- 48	- 12
HC imbrulés	- 67	- 20
Particules	- 47	- 12
NO _x	+ 10	+ 2
Sulfates	- 100	- 20
Toxiques	- 60 à - 90	-12 à - 20
Mutagènes	- 80 à - 90	- 20

Par ailleurs, des essais sur moteurs réels (Audi 80 Diesel, 4 cylindres à injection directe) ont montré que sur la base des émissions en NO_x, CO, hydrocarbures et particules, ainsi qu'en termes de biodégradabilité dans l'eau, les EEHV avaient un effet négatif moindre sur l'environnement que les EMHV. Un mélange diesel (50 %) et EEHV (50 %) a montré, comparativement au diesel pur,

une réduction des émissions de l'ordre de 1.2 % pour les NO_x, de 1.8 % pour le CO, de 18 % pour les hydrocarbures et 45 % pour les particules (Makarevicienne et Janulis, 2003).

I.5 Etude cinétique de l'oxydation des esters méthyliques et éthyliques

Comme il a été illustré dans les paragraphes précédents, les biodiesels sont des mélanges d'esters alkylés saturés ou non-saturés (mélanges de méthyle esters pour le biodiesel commercial, mélanges d'éthyle esters au stade recherche) qui contiennent des chaînes carbonées comportant entre 12 à 22 atomes de carbone. Ces alkyles esters peuvent renfermer jusqu'à 3 liaisons éthyléniques, séparées par un groupement méthyle. L'ester majoritaire d'un biodiesel issu d'une huile de colza est l'ester de l'acide oléique, possédant une longue chaîne à 18 atomes de carbone avec une seule liaison éthylénique.

Bien que le butanoate de méthyle (C₅H₁₀O₂), le propanoate d'éthyle (C₅H₁₀O₂), le butanoate d'éthyle (C₆H₁₂O₂) ou encore le crotonate de méthyle (C₅H₈O₂) ne soient pas réellement présents dans le biodiesel, ils présentent la même structure chimique R₁C(=O)OR₂, avec R₁ une chaîne alkyle saturée ou non-saturée et R₂ le groupement méthyle ou éthyle. L'avantage d'étudier l'oxydation de ces molécules modèles est que les mécanismes impliqués sont plus simples et plus faciles à déterminer que s'il s'agissait de réels esters d'acides gras avec de longues chaînes alkyles R₁.

Gaïl et al. (2007) ont réalisé une étude expérimentale et théorique de la combustion du butanoate de méthyle. Les expériences ont été menées en réacteur parfaitement agité de 800 à 1350 K, en réacteur à écoulement à pression variable de 500 à 900 K et en flamme de diffusion à contre-courant. Concernant l'étude théorique, Gaïl et al. (2007) ont proposé un modèle cinétique basé sur la version de Fisher et al. (2000), dont ils ont apporté des modifications afin de reproduire les résultats expérimentaux.

Sarathy et al. (2007) ont réalisé une étude comparative de la réactivité de deux esters ayant le même nombre d'atomes de carbone. Ces deux esters sont respectivement le butanoate de méthyle et le crotonate de méthyle, ce dernier est un intermédiaire de l'oxydation du butanoate de méthyle (Gaïl et al., 2007). Leur combustion a été étudiée dans un réacteur parfaitement agité et dans une flamme de diffusion à contre-courant, en reproduisant les mêmes conditions expérimentales pour les deux composés. Les fractions molaires de différents produits ont été obtenues. Les deux esters méthyliques présentent les réactivités similaires. Les résultats expérimentaux obtenus montrent que la combustion du crotonate de méthyle conduit à de plus grandes proportions d'acétylène, de

1-propyne, de 1-butène et de 1,3-butadiène que le butanoate de méthyle, molécules précurseurs de formation de suie.

Metcalfé et al. (2007) ont réalisé une étude de l'auto-inflammation du butanoate de méthyle et du propanoate d'éthyle en tube à onde choc, de 1100 à 1670 K et des pressions de 1 atm et 4 atm. Les auteurs ont également proposé un mécanisme réactionnel pour reproduire leurs résultats expérimentaux, en utilisant des calculs théoriques pour la détermination des données thermodynamiques et cinétiques (El-Nahas et al., 2007). Leur modèle a été légèrement modifié pour simuler des résultats expérimentaux de l'oxydation du propanoate d'éthyle dans réacteur auto-agité par jets gazeux entre 750 et 1100 K, à une dilution de 0.1 %, des richesses de 0.3, 0.6, 1 et 2, et un temps de passage de 0.7 s (Metcalfé et al., 2009).

Dooley et al. (2008) ont mesuré les délais d'auto-inflammation du butanoate de méthyle en tube à choc de 1250 à 1760 K et des pressions de 1 et 4 atm, ainsi qu'en machine à compression rapide entre 640 et 949 K, à 10, 20 et 40 atm. Leurs résultats, ainsi que d'autres issus de la littérature (Gail et al., 2007), ont été utilisés pour valider un nouveau modèle proposé pour l'oxydation du butanoate de méthyle.

Walton et al. (2009) ont publié une étude menée sur l'auto-inflammation du butanoate de méthyle et de propanoate d'éthyle à des températures de 935 à 1117 K et des pressions de 4.7 et 19.6 atm en machine à compression rapide, a été réalisée. Des modèles cinétiques détaillés d'oxydation du butanoate de méthyle et de propanoate d'éthyle ont été proposés par les auteurs.

Ces différentes études ont montré que ces molécules à courte chaîne carbonée (butanoate de méthyle, crotonate de méthyle et propanoate d'éthyle) ne sont pas des molécules modèles adéquates pour représenter la combustion du biodiesel carburant. Pour cela, d'autres auteurs ont orienté leur recherche vers les esters à longue chaîne carbonée.

Dagaut et al. (2007) ont publié une étude expérimentale sur l'oxydation d'esters méthyliques d'huile de colza (RME) en réacteur auto-agité par jets gazeux à des températures allant de 800 à 1400 K et des pressions de 1 et 10 atm. Une comparaison de leurs résultats avec ceux obtenus par Ristori et al., 2001 sur les alcanes ont montré une forte similarité entre la réactivité des esters méthyliques dérivés de l'huile de colza et celle des alcanes.

Szybist et al. (2007) ont mené une étude expérimentale de l'oxydation du décanoate de méthyle en moteur CFR. De nombreux produits intermédiaires stables ont été détectés par FTIR et par GC/MS y compris des esters méthyliques saturés et insaturés, des acides carboxyliques et d'autres espèces oxygénées.

Herbinet et al. (2008) ont publié un mécanisme détaillé d'oxydation à basse et à haute températures du décanoate de méthyle. Le modèle, comprenant 3036 espèces et 8555 réactions, a été testé après réduction (125 espèces et 713 réactions élémentaires) avec les résultats expérimentaux obtenus par Seshadri et al. (2009) sur l'oxydation du décanoate de méthyle en flamme laminaire non prémélangée.

HadjAli et al. (2009) ont mesuré l'auto-inflammation d'une série d'esters méthyliques allant du butanoate de méthyle à l'heptanoate de méthyle à basse température de 650 à 850 K et à des pressions comprises entre 4 et 20 bar. Différents éthers cycliques ont pu être identifiés par les auteurs.

Schönborn et al. (2009) ont étudié dans un moteur Diesel monocylindrique l'effet de la structure moléculaire des esters (laurate de méthyle, myristate de méthyle, palmitate de méthyle, stéarate de méthyle, oléate de méthyle, linoléate de méthyle, béhénate de méthyle et oléate d'éthyle) sur la combustion de carburants biodiesel. Il a été observé que le délai d'auto-inflammation diminue avec l'augmentation de la longueur de chaîne et le nombre d'insaturation des esters méthyliques. L'émission des particules de suies est aussi fortement corrélée avec le nombre d'insaturation des esters méthyliques.

I.6 Conclusion

Cette partie a présenté les principales sources de production de biodiesel, des généralités sur la combustion, l'oxydation des esters méthyliques et éthyliques dans les moteurs et la formation des polluants (travaux expérimentaux et des modèles cinétiques proposés dans la littérature). Des informations complémentaires concernant les études expérimentales, la modélisation des molécules modèles ou réelles à longues chaînes sont fournies dans le chapitre I de la thèse « Combustion kinetics of biodiesel (methyl and ethyl esters) - A review ».

II. Dispositifs expérimentaux

Durant ce travail de thèse, deux techniques expérimentales ont été utilisées afin d'étudier la cinétique d'oxydation des cinq esters suivants : le butanoate d'éthyle, le crotonate d'éthyle, l'acrylate d'éthyle, le crotonate de méthyle et l'acrylate de méthyle. L'auto-inflammation de tous ces composés oxygénés a été étudiée dans un tube à onde de choc. Seule l'oxydation à pression atmosphérique et dans les domaines à basse et à haute température du butanoate d'éthyle a été réalisée dans un réacteur tubulaire à écoulement piston. Cette partie présente les généralités relatives aux dispositifs expérimentaux utilisés au laboratoire pour l'étude de la cinétique chimique de combustion. Il détaille les montages expérimentaux utilisés et leurs modes opératoires :

- tube à onde de choc pour la détermination des délais d'auto-inflammation des cinq esters à haute température (1000-1500 K) et à haute pression (7-9 atm),
- réacteur tubulaire à écoulement piston afin de suivre l'oxydation butanoate d'éthyle à basse température (550-1150 K) et à pression atmosphérique. Le Montage expérimental a été développé et amélioré au cours de cette thèse, ainsi que les techniques d'analyse employées et la mise en œuvre expérimentale. Néanmoins, il est important de noter que ce montage n'a pu être totalement réalisé qu'à la fin de cette thèse. Des améliorations supplémentaires devront être réalisées dans le futur.

II.1 Chimie de la combustion

La maîtrise des modes de combustion dans le moteur, l'optimisation énergétique, la maîtrise des polluants en sortie de la chambre de combustion rendent indispensable une représentation détaillée des mécanismes d'oxydation des carburants. Pour connaître les voies réactionnelles liées à la formation des différentes espèces chimiques obtenues lors du processus de combustion, des études cinétiques sont effectuées par différentes approches expérimentales. Ces dispositifs expérimentaux permettent de déterminer la vitesse à laquelle se déroulent les réactions chimiques et les espèces intermédiaires qui se forment au cours de l'oxydation. Trois types de dispositifs sont principalement utilisés:

❖ **Les réacteurs idéaux** : réacteur fermé (RF), réacteur parfaitement agité (RPA) et réacteur à écoulement piston (RP):

- **Réacteur fermé (RF)** est un réacteur à volume constant dans lequel est introduit le mélange carburant et comburant. Il permet de suivre les variations de pression et de température en fonction du temps et d'effectuer des prélèvements gazeux. Les

phénomènes trop rapides ne peuvent pas être étudiés dans ce type réacteur car le temps de réaction doit être au minimum de quelques dizaines de secondes. De plus, le mélange peut mettre un certain temps avant d'atteindre une homogénéité en pression et température. Cette technique a donc une certaine limitation d'utilisation et est surtout applicable aux phénomènes lents (plusieurs dizaines de secondes) et à basse température.

➤ **Réacteur parfaitement agité (RPA)** est un réacteur couramment utilisé. Il est en général utilisé en milieu très dilué et dans des gammes de températures qui peuvent varier de 550 à 1300 K et de 1 à 40 atm pour la pression. Dans tout le volume du réacteur, la pression et la température sont constantes et les concentrations sont uniformes. Le mélange « carburant et oxydant » est considéré comme instantané. Pour obtenir cette homogénéité, différentes méthodes sont utilisées :

- à l'aide d'un agitateur (en milieu dilué) ;
- par agitation au moyen de jets gazeux (turbulents). Certaines règles de construction de ce réacteur doivent être appliquées comme le rapport entre le diamètre de l'injecteur et celui du réacteur. Le temps de séjour peut varier de quelques millisecondes à quelques secondes. L'optimum est obtenu pour un rayon du réacteur de 2 cm, avec un temps de séjour de l'ordre de 20 millisecondes. Il permet principalement d'obtenir par prélèvement (sonde) ou refroidissement (piégeage) les produits intermédiaires stables de la combustion. Il est facile à mettre en œuvre et à modéliser.

➤ **Réacteur piston (RP)** comme le RPA est employé en milieu très dilué et dans de larges gammes de température et de pression. Le mélange gazeux peut être chauffé à l'aide d'un four lors de son passage dans le réacteur. Le volume et la pression sont constants. La température et les concentrations sont uniformes sur une section du réacteur, mais varient axialement entre l'entrée et la sortie. Pour une cinétique d'ordre n positif, et une conversion de sortie donnée, le temps de passage (τ) d'un RP est inférieur à celui du RPA. Le RP est donc plus performant que le RPA. De tels réacteurs sont faciles à modéliser (par une cascade de réacteurs parfaitement agités) pour les conditions d'écoulement idéales. Dans le cas contraire, pour le réacteur tubulaire à écoulement laminaire, il faut tenir compte du profil de vitesse et de la diffusion. La réalisation de ce type de réacteur n'est pas simple et différents paramètres doivent être pris en compte :

- la température des gaz dans le réacteur doit être uniforme. Le carburant et le comburant sont préchauffés séparément pour obtenir la température définie dès le début de la réaction ;
- le temps de mélange des gaz doit être instantané. Or, quand les réactifs sont introduits séparément dans le réacteur, le temps pour obtenir un mélange homogène est assez long (quelques millisecondes). La turbulence est donc nécessaire pour éviter que la réaction ne soit plus avancée à certains points que d'autres dans le réacteur ;
- l'écoulement des gaz à l'intérieur du réacteur tubulaire doit être uniforme pour éviter un gradient radial de concentration. Dans ce cas, le régime de vitesse des gaz doit également être turbulent et non laminaire.

❖ **Les systèmes à compression** avec la machine à compression rapide (MCR) et le tube à onde de choc (TC) : ils sont souvent utilisés en milieu dilué et sont en général modélisés comme des réacteurs fermés adiabatiques. Ces deux systèmes permettent de mesurer des délais d'auto-inflammation d'un mélange gazeux combustible amené dans des conditions d'auto-inflammation à une pression et à une température données. En MCR, la gamme (T, P) balayée peut recouvrir des basses températures et des pressions élevées. Cela permet ainsi de couvrir entièrement la zone du coefficient négatif de température (zone où l'on observe une baisse de réactivité des carburants avec l'augmentation de la température). C'est le dispositif qui se rapproche le plus des conditions d'auto-inflammation dans un moteur. Quant au tube à onde de choc, il est le seul dispositif permettant d'étudier les réactions à haute température de manière précise et contrôlée. De plus, il peut être couplé facilement à des techniques de détection, la gamme (T, P) balayée peut recouvrir de plus hautes températures et de plus hautes pressions ($1 < P < 600$ atm) que pour la MCR.

❖ **Les brûleurs à flamme de pré-mélange ou à flamme de diffusion :**

La flamme plate laminaire de pré-mélange est beaucoup plus facile à modéliser (réacteur piston à diffusion axiale) que la flamme de diffusion. Elle permet une étude plus simple de la combustion puisque cette flamme unidimensionnelle ne présente que des gradients de concentration et de température suivant un seul axe, celui du brûleur. Elle permet d'obtenir par prélèvement (sonde) à différentes hauteurs du brûleur les produits intermédiaires stables ou radicalaires de la combustion. Les études en flamme permettent des études à haute température ($800 < T < 2000$ K) et principalement à basse pression (< 1 atm) mais aussi à pression atmosphérique.

Les résultats obtenus dans ces différents dispositifs servent de base à l'élaboration de modèles cinétiques qui regroupent toutes les réactions ayant lieu pendant la combustion. Ces modèles doivent permettre de simuler les résultats expérimentaux disponibles pour plusieurs types de réacteurs et dans une vaste gamme de conditions expérimentales. En comparant les résultats simulés avec ceux obtenus expérimentalement. Un mécanisme validé, capable de reproduire les délais d'inflammation et les profils d'espèces de tous les intermédiaires observés dans le plus grand nombre de ces dispositifs est un mécanisme qui sera considéré comme suffisamment fiable pour être utilisé dans d'autres conditions opératoires. Il pourra alors être employé dans des calculs appliqués à l'optimisation et au dimensionnement des systèmes de combustion (moteur, four ...) pour réduire la pollution et augmenter le rendement et ainsi prédire les concentrations de polluants et les vitesses de réaction.

II.2 Dispositif expérimental du réacteur tubulaire

II.2.1 Descriptif général

Le dispositif expérimental utilisé au cours de cette thèse a été spécialement réalisé pour les études cinétiques en phase gazeuse. Le pilote est constitué principalement d'un réacteur tubulaire à écoulement piston qui a déjà été utilisé pour l'étude des réactions de pyrolyse des huiles végétales usagées et les acides carboxyliques (thèse de J. Gornay (2006)). Toutefois, une étude préliminaire du butanoate de méthyle a permis de montrer que le pilote initial (Gornay, 2006) n'était plus adapté à l'étude de l'oxydation des hydrocarbures. Certains problèmes ont compliqué le protocole expérimental de l'oxydation, citons :

- Le butanoate de méthyle a provoqué une dégradation du filtre de l'analyseur IR.
- L'étude du butanoate de méthyle a permis de vérifier que le contacteur gaz/liquide, utilisé en amont du réacteur pour son alimentation, fonctionne comme un simple évaporateur et non un saturateur.
- La présence du thermocouple au sein du réacteur au cours de la réaction a montré un effet catalytique.

D'autres problèmes sont survenus avec les anciens appareils chromatographiques, ce qui a nécessité de changer tous les chromatographes du pilote initial.

Durant cette thèse, le dispositif a été modifié afin de permettre l'étude de l'oxydation des hydrocarbures liquides et spécialement des biocarburants:

- Une ligne d'oxygène a été placée pour l'alimentation du réacteur en comburant dont le débit est régulé à l'aide d'un régulateur de débit massique RDM.

- Un évaporateur garni en anneaux Raschig et son système de chauffage a été remplacé par une chambre de mélange et d'évaporation d'ester (CEM) de type Bonkhorst (HIGH-TECH B.V).
- Deux vannes avec anti-retour ont été installées pour isoler les deux circuits relatifs au régime permanent et au régime transitoire.
- Deux cartouches remplies de coton ont été placées en série afin de casser les éventuels aérosols formés pendant les réactions d'oxydation.
- Deux nouveaux chromatographes ont été installés pour une analyse en ligne des gaz issus de la combustion du carburant.
- Un nouveau chromatographe muni d'une colonne capillaire a permis de séparer d'une façon satisfaisante les hydrocarbures oxygénés en particuliers les acides carboxyliques à longue chaîne carbonée.

La figure (II.1) présente le schéma du dispositif expérimental de l'oxydation des esters dans un réacteur tubulaire à écoulement piston. Ce dispositif est principalement constitué de quatre zones.

Zone 1 : Alimentation du réacteur,

Zone 2 : Section de mélange et de préchauffage de la charge du réacteur,

Zone 3 : Section réaction, avec un réacteur tubulaire placé dans un four,

Zone 4 : Section de séparation et analyse des produits.

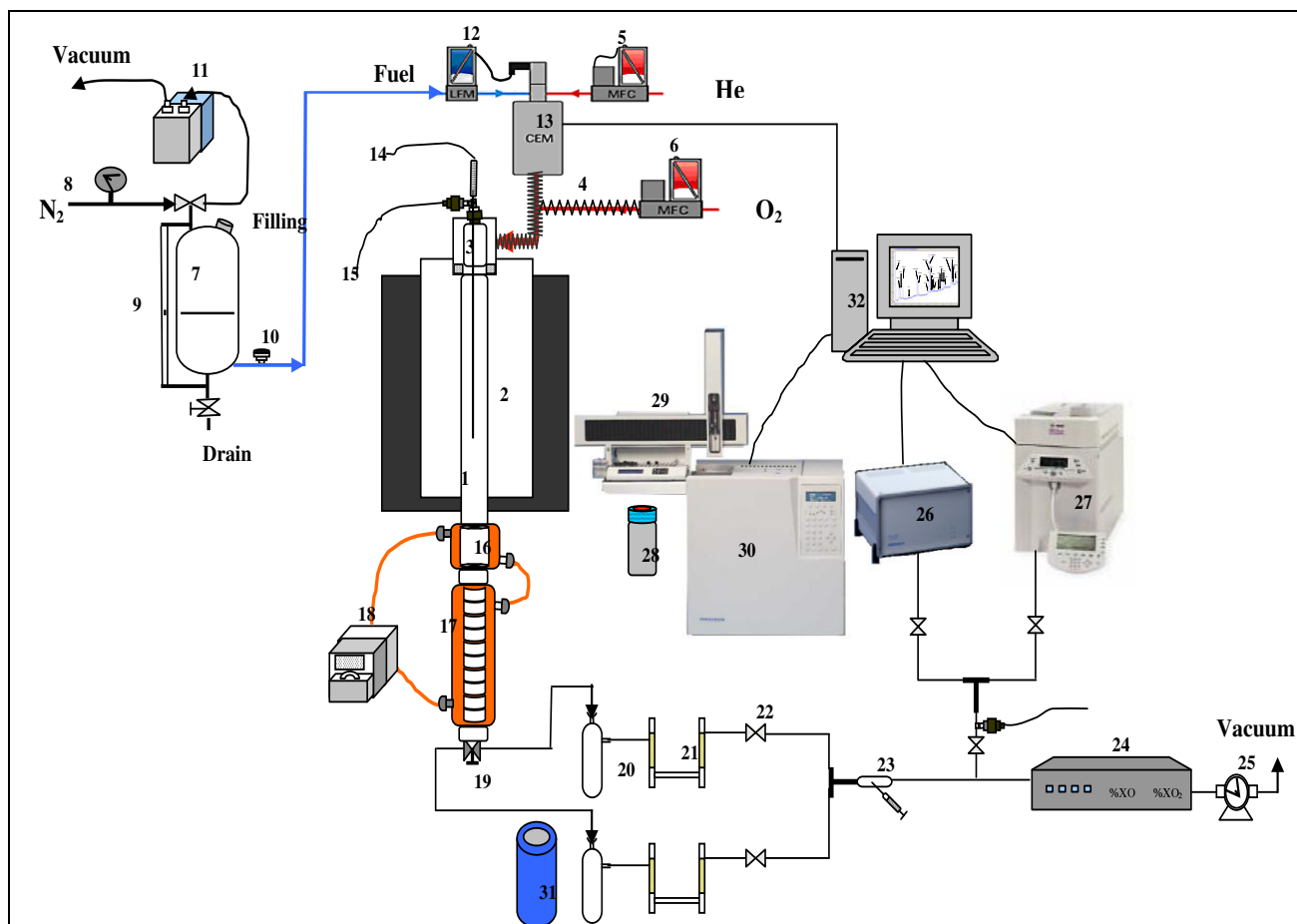


Figure II.1 : Schéma du dispositif expérimental de l'oxydation du biodiesel.

- | | |
|---|--|
| 1. Réacteur piston en quartz | 17. Colonne de séparation |
| 2. Four (Thermolyne) | 18. Cryostat |
| 3. Zone de préchauffage | 19. Vanne trois voies |
| 4. Résistance chauffante (Thermocoax) | 20. Piège liquide |
| 5. Régulateur de débit massique (He) | 21. Cartouche + coton |
| 6. Régulateur de débit massique (O ₂) | 22. Vanne |
| 7. Réservoir d'hydrocarbure (HC) | 23. Ampoule + Seringue (analyse GC/MS) |
| 8. Manomètre | 24. Analyseur IR (analyse %CO, %CO ₂) |
| 9. Jauge du réservoir | 25. Compteur à gaz |
| 10. Vanne d'alimentation en HC | 26. CPG-Catharomètre-TCD PR 1250 (analyse O ₂) |
| 11. Pompe à vide | 27. CPG-FID Agilent 6850 (analyse des incondensables) |
| 12. Débitmètre liquide | 28. Flacon d'analyse des condensables |
| 13. Chambre de mélange et d'évaporation | 29. Passeur automatique (Type ALS 404) |
| 14. Thermocouple (type K) | 30. CPG-FID PR 2100 (analyse des condensables) |
| 15. Capteur de pression | 31. Dewar d'azote liquide |
| 16. Trempe à passage annulaire | 32. Ordinateur muni de cartes d'acquisition |

II.2.1.1 Section alimentation du réacteur

L'alimentation en réactifs permet d'acheminer les réactifs au sein du réacteur à des débits connus et contrôlés par les régulateurs de débit. Le diluant et le comburant utilisés sont respectivement l'hélium à 99.999% de pureté (Messer, qualité 5) et l'oxygène à 99.999% (Messer, qualité 5). L'hélium a été choisi plutôt que l'azote afin de pouvoir séparer les condensables sans piéger le diluant. L'alimentation des gaz est assurée par deux régulateurs de débit massique (RDM) : un RDM 280 Alphagaz et un régulateur Bronkhorst (El-Flow) pour contrôler les débits du dioxygène et de l'hélium respectivement. De plus, un RDM liquide Bronkhorst (CORI-FLOW) a assuré l'alimentation en butanoate d'éthyle (Fluka, $\geq 98\%$ de pureté).

Afin d'éviter tout risque de condensation, les lignes par lesquelles passe l'ester vaporisé sont chauffées à 383 K à l'aide d'un cordon chauffant. Elles sont en outre isolées à l'aide d'une gaine isolante à base de laine de verre recouverte par du papier d'aluminium.

❖ Dispositif de mélange et d'évaporation

Le dispositif a été conçu par la société Bronkhorst (HIGH-TECH B.V) et se compose de 3 éléments (cf. figure II.2) :

- un régulateur de débit massique liquide série CORI-FLOW; pour contrôler le débit de l'ester pour une gamme allant de 1 g/h jusqu'à 60 g/h à une pression relative de 2 bars.
- un régulateur de débit massique gaz (EL-FLOW) pour contrôler le débit du gaz inerte (He), ayant une gamme de débit de 0.06 NL/min jusqu'à 3NL/min à une pression relative de 1 bar relatif.
- une chambre de mélange et d'évaporation (Température réglable de 20°C jusqu'à 200°C max) où le mélange liquide/gaz (ester/hélium) est chauffé puis évaporé.

Ce dispositif assure l'alimentation de l'hydrocarbure liquide dans la chambre d'évaporation comme l'illustre la Figure II.3. Le combustible liquide est préalablement stocké dans un réservoir en acier d'un litre maintenu à une pression maximale de 5 bars et comprenant :

- Une vanne manuelle de laminage à 2 voies; repère VM01,
- Une vanne manuelle 3 voies à boisseau sphérique; repère VM02,

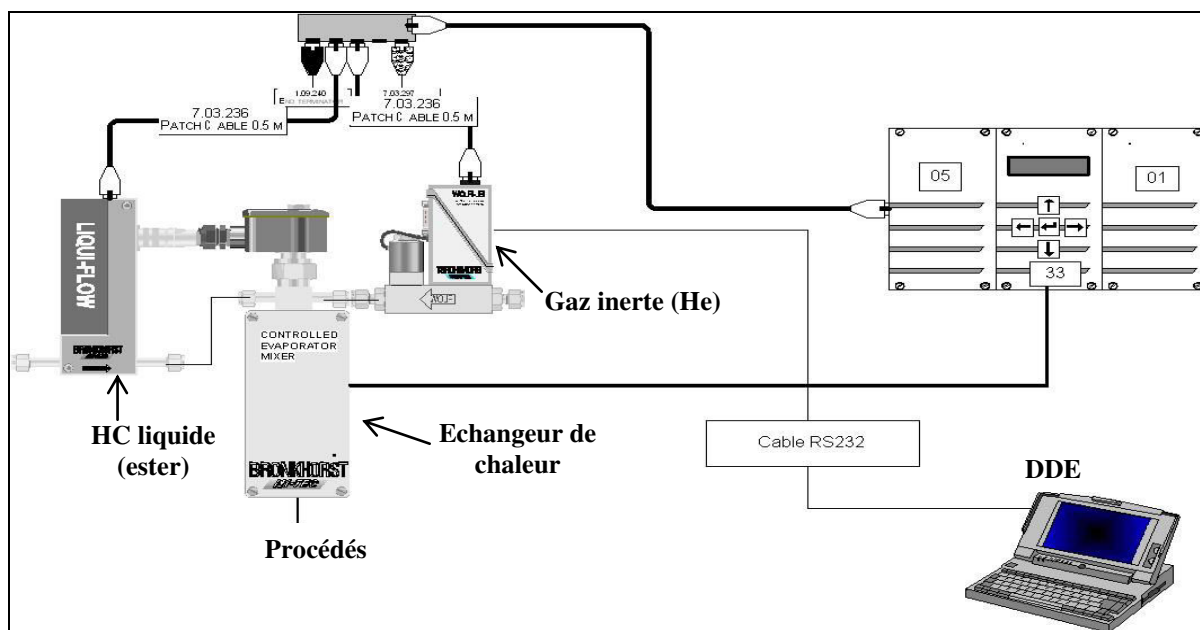


Figure II.2 : Dispositif de mélangeage et d'évaporation de l'hydrocarbure liquide.

❖ **Dispositif d'alimentation du régulateur de débit massique liquide (CORI-FLOW)**

- Une vanne manuelle 2 voies à boisseau sphérique; repère VM03,
- Un indicateur de niveau en tube PFA transparent,
- Un orifice de remplissage.

Ce réservoir est destiné à recevoir un fluide liquide destiné à être pressurisé. La mise en service du réservoir est décrite comme suit :

- On ferme les vannes VM01 (point d'utilisation du fluide sous pression) et celle de la purge VM03.
- La vanne VM02 est raccordée d'un côté sur un réseau de gaz inerte (azote) sous pression (4/5 bars), l'autre côté est raccordé à une pompe à palettes.
- On oriente le volant de la vanne VM02 vers le côté raccordé à la pompe (mise à l'air du réservoir). Ensuite, on remplit le réservoir après avoir enlevé le bouchon de l'orifice du remplissage qu'on le remet une fois l'opération terminée.
- On chasse l'air du réservoir, les gaz et l'air dégagés par cette opération sont alors aspirés par la pompe à palettes (en manœuvrant doucement la vanne VM02). Une fois la mise sous vide est effectuée, on oriente la vanne VM02 sur le côté qui est raccordé au réseau d'inerte (N_2). Le fluide est sous pression de l'azote (2 bars). Enfin, on manœuvre la vanne VM01 pour l'utilisation, sous l'effet de la poussée provoquée par la pression d'azote, le liquide monte à travers le tube pour être dirigé vers le RDM liquide (CORI-FLOW). Il est à noter que cette

opération est effectuée systématiquement à chaque remplissage du réservoir ou lors d'une mise à l'air.

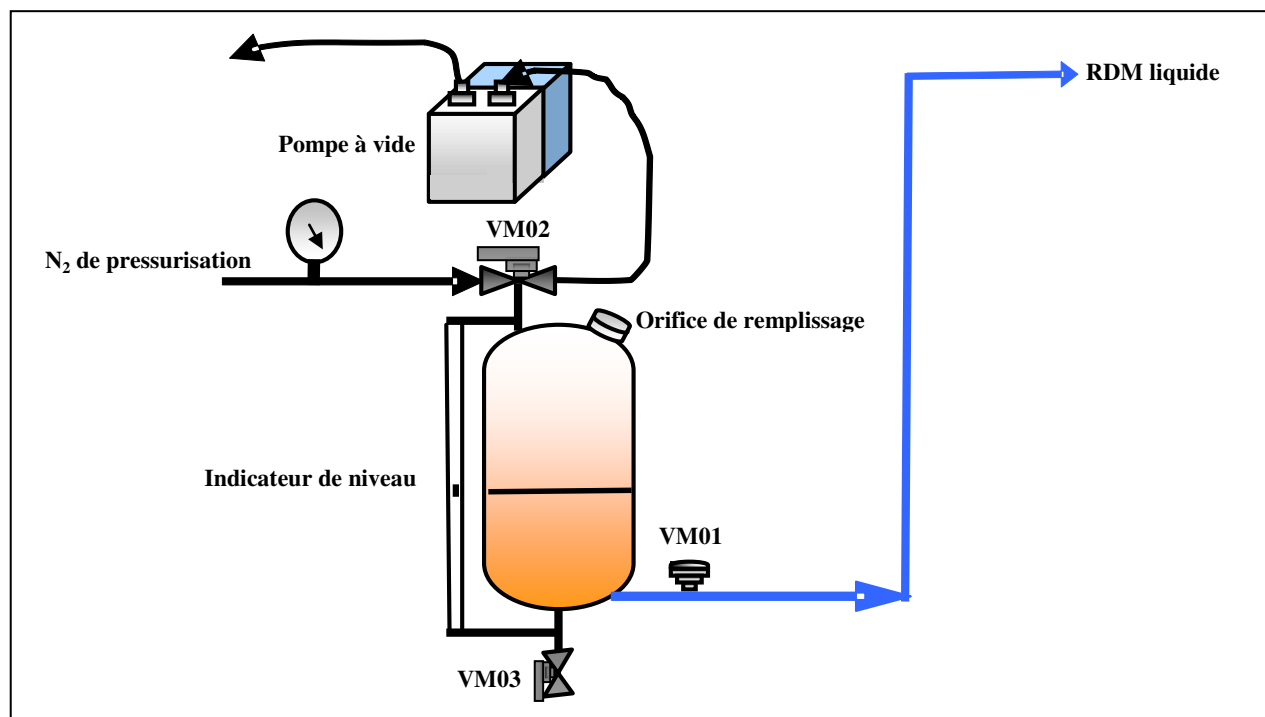


Figure II.3: Le dispositif de l'alimentation du RDM liquide par l'hydrocarbure liquide.

II.2.1.2 Section de mélange et de préchauffage de la charge du réacteur

En amont de l'entrée du réacteur, l'hélium chargé en réactif (ester) et l'oxygène sont préchauffés. Pour ce faire, les deux courants de gaz passent dans un échangeur en quartz de géométrie annulaire (assurant un transfert de chaleur efficace), muni en outre d'un garnissage sur une hauteur de 3 cm de paillettes de quartz (optimisant le mélange gaz-gaz). Le chauffage de l'échangeur est assuré par des résistances chauffantes de type "Thermocoax" thermostatées qui l'entourent. Cette zone est calorifugée grâce à de la laine de quartz elle-même entourée d'une couche de papier d'aluminium afin de limiter les pertes thermiques. La température des fils est réglée par les mesures des températures (thermocouples placés entre la paroi et le fil chauffant). Enfin, à l'entrée de la zone de mélange et de préchauffage un capteur de pression « 0-2 bar » permet de lire la pression qui règne au sein de l'ensemble du dispositif expérimental.

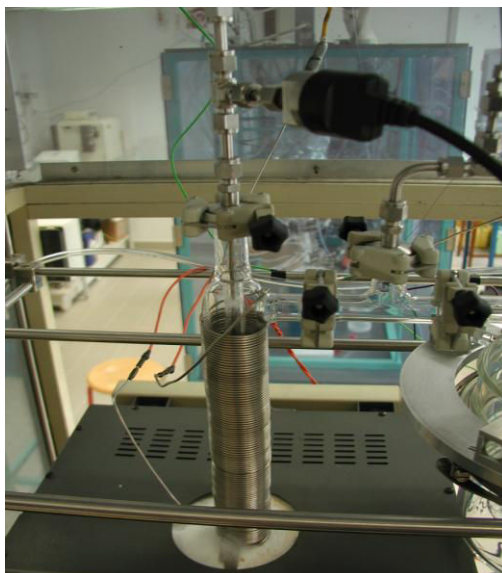


Figure II.4 : Unité de mélange et de préchauffage de l'alimentation du réacteur.

II.2.1.3 Section réaction

Le réacteur dans lequel se produit la réaction d'oxydation du mélange réactionnel (Butanoate d'éthyle + oxygène + hélium) est en quartz. Ce matériau est chimiquement inerte et il garde ses propriétés mécaniques (dimensions, étanchéité) à des températures n'excédants pas 1000°C, contrairement aux réacteurs métalliques où les parois peuvent avoir un effet catalytique (Gornay et al. 2009). Le réacteur piston est un tube de 55 cm de long, de 11 mm de diamètre externe et de 8 mm de diamètre interne. Son volume est donc 27.6 cm³; il est placé verticalement dans un four tubulaire (Thermolyne type Furnace 79300) permettant d'atteindre une température de 1200°C. Le chauffage du réacteur est assuré par effet Joule à l'aide de bobines métalliques résistives incrustées dans un matériau réfractaire. La zone chauffée a une hauteur voisine de 60 cm pour un diamètre de 15 cm. De part et d'autres de la zone chauffée sont placés deux blocs isolants ainsi que de la laine de quartz afin de limiter au maximum les pertes thermiques. La température au sein du four est mesurée à l'aide d'un thermocouple mobile de type K. Ce thermocouple (type K) permet de mesurer des températures entre -270°C et 1400°C.

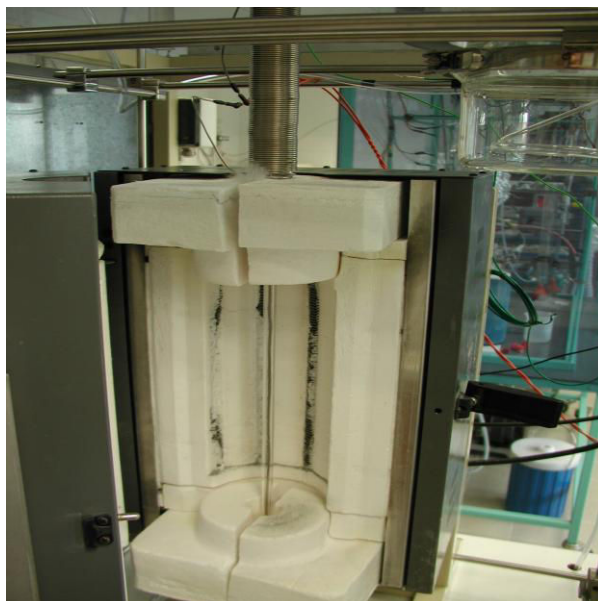


Figure II.5 : Unité réactionnelle (four et réacteur en quartz).

II.2.1.4 Section de séparation et analyse

❖ Unité de refroidissement et de séparation

À la sortie du réacteur, une trempe à espace annulaire en quartz permet le refroidissement très rapide du mélange réactionnel gazeux pour stopper la réaction dès la sortie du réacteur (figures II.6 & II.7). Cette trempe est refroidie par une enveloppe externe qui la maintient à température constante (358 K) à l'aide d'un cryostat (type Compact Julabo F30-C) faisant circuler un fluide caloporteur (Thermal H5S : 233- 393 K).



Figure II.6 : Trempe à espace annulaire.

Le tube interne en quartz a pour diamètre d_e . Le fluide caloporteur circule dans la double enveloppe de diamètre interne D_i (d_e et D_i diamètres des surfaces en contact avec le mélange gazeux).

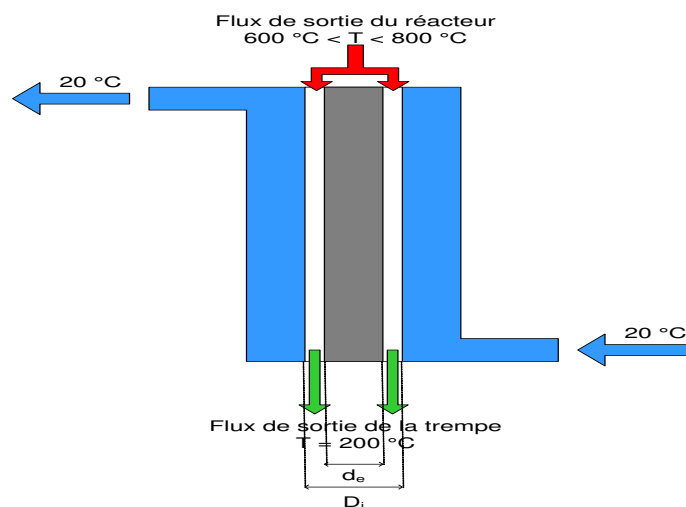


Figure II.7 : Schéma simplifié de la trempe annulaire.

- La trempe est suivie d'une colonne de séparation chauffée et maintenue à une température constante (358 K) à l'aide du même cryostat que la trempe. Cela, a pour objectif d'éviter la condensation des produits de la réaction d'oxydation.



Figure II.8: Colonne de séparation et vanne à trois voies.

Deux circuits identiques, reliés de part et d'autre par deux vannes trois voies, sont prévus soit pour le régime transitoire, soit pour le régime permanent. Le second est aussi appelé "circuit de mesures" car il sert à recueillir la phase liquide (PL) destinée à l'analyse pour identification et quantification des produits condensables de l'oxydation. Les deux circuits sont

tous équipés d'un séparateur gaz-liquide dont l'un est plongé dans un vase de Dewar rempli d'azote liquide et l'autre est introduit dans un bain d'eau glacée à basse température (0°C, voire -20°C). Le flux gazeux passe ensuite à travers une "cartouche" munie du coton pour casser les éventuels aérosols qui peuvent se former. Ainsi, les gouttelettes de la phase liquide entraînées par le diluant dès la sortie du condenseur sont piégées dans le coton. Le séparateur gaz-liquide du "circuit de mesures" est maintenu, à une température 78 K, ce qui assure la condensation des produits lourds.

Tableau II.1 : Dimensions des différents éléments du pilote d'oxydation.

Eléments	Type	Paramètre	Valeur (m)
Préchauffage de l'oxygène	Tubes en inox	L	0.55
		d_i	0.013
Mélange et préchauffage de l'alimentation du réacteur	Espace annulaire en quartz	L	0.2
		D_i	0.03
		d_e	0.01
		$h_{\text{garnissage}}$	0.03
Réacteur	Tube en quartz	L	0.55
		D_e	0.011
		d_i	0.008
Trempe	Espace annulaire en quartz	L	0.1
		D_i	0.008
		d_e	0.006

L : longueur ; d_i : diamètre interne du réacteur ; D_e : diamètre externe du réacteur ; D_i : diamètre interne du grand tube de l'espace annulaire ; d_e : diamètre externe du petit tube de l'espace annulaire ; $h_{\text{garnissage}}$: hauteur de garnissage de paillettes de quartz.

❖ Système d'analyse

Le circuit d'analyse des gaz se décompose en trois parties principales :

- 1) un analyseur infrarouge Cristal 300 de type Cosma placé en ligne sur le circuit gazeux pour la détermination des fractions molaires du monoxyde de carbone (CO) et du dioxyde de carbone (CO₂),
- 2) le circuit d'analyse de l'oxygène résiduaire par un chromatographe de type PERICHROM PR1250 muni d'un détecteur à catharomètre (TCD),
- 3) le circuit d'analyse en ligne des hydrocarbures légers (C₁-C₅) par un chromatographe Agilent 6850.

La fraction des condensables est collectée dans un piège en verre de 1 litre plongé dans un vase Dewar rempli d'azote liquide; 100µL d'octane (étalon interne, Sigma-Aldrich, ≥98%)

est ajouté à cette phase, l'ensemble est ensuite diluée dans l'acétone (Sigma-Aldrich, $\geq 99.8\%$ de pureté). L'analyse de la phase liquide est réalisée grâce à un chromatographe PERICHROM PR2100 équipé d'une colonne capillaire capable de séparer les hydrocarbures oxygénés. Par ailleurs, un chromatographe Agilent 6850 équipé d'une colonne capillaire (HP plot Q) et couplé à un spectromètre de masse permet d'identifier les espèces formées lors de la combustion de butanoate d'éthyle.

II.2.2 Bilan de matière

Des bilans de matière globaux et élémentaires (en atome de carbone) ont été calculés. Nous avons aussi vérifié que la somme des flux molaires des gaz à l'entrée du réacteur correspondant bien à ceux à la sortie. Pour le bilan élémentaire, les concentrations en atome de carbone à l'entrée et à la sortie du réacteur tubulaire ont été comparées (annexe A).

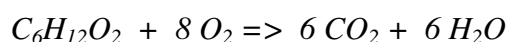
II.2.3 Etude paramétrique

Nos expériences permettent d'étudier l'influence des paramètres expérimentaux sur la cinétique de combustion d'éthyle butanoate dans un réacteur à écoulement piston. Ainsi, nous avons étudié l'effet :

- de la température du four (T) : 500-1250 K,
- du temps de passage (τ) : 0.65-1.40 s et
- de la richesse (φ) : tout en maintenant une concentration constante en ester de 1.3%.
- Les expériences d'oxydation ont été menées à une pression proche à 1 atm.
- Les résultats expérimentaux sont comparés avec ceux de la simulation réalisés avec un mécanisme cinétique détaillé généré automatiquement par EXGAS (Warth, 1999).

➤ Calcul de la richesse

Oxydation complète d'éthyle butanoate est donnée par l'équation de la réaction bilan suivante :



L'expression de la richesse φ ou rapport d'équivalence s'écrit :

$$\varphi = \frac{\left(\frac{\% \text{ Ester}}{\% \text{ Oxygène}} \right)_{\text{expérimental}}}{\left(\frac{\% \text{ Ester}}{\% \text{ Oxygène}} \right)_{\text{stoechiométrique}}} \quad (\text{II.1})$$

Dans le cas du butanoate d'éthyle (BE) on calcule la richesse selon l'expression:

$$\varphi = \frac{8}{1} \times \left(\frac{\% \text{ BE}}{\% O_2} \right)_{\text{experimental}} \quad (\text{II.2})$$

Le tableau (II.2) présente les conditions opératoires d'oxydation du butanoate d'éthyle et la composition des mélanges gazeux (pauvre, stœchiométrique et riche) pour des richesses calculées en appliquant l'équation (II.2).

Tableau II.2: Conditions opératoires appliquées pour l'oxydation du butanoate d'éthyle (EB) en réacteur piston.

	Température de four (K)	Pression (Torr)	Richesse φ	Temps de passage τ (s)	x_{ester}	x_{O_2}	x_{He}	Dilution $\frac{x_{\text{He}}}{(x_{\text{O}_2} + x_{\text{He}})}$
Temps de passage constant (τ)	450 - 1150	787-986	0.52± 0.03	0.93	0.013	0.2	0.787	79.74%
	500 - 1200	809-985	1.12± 0.03	0.93	0.013	0.0925	0.8945	90.63%
	500 - 1200	800-985	1.59 ± 0.03	0.93	0.013	0.0655	0.9215	93.36%
Richesse constante (φ)	700	845-1010	1± 0.03	0.65-1.40	0.013	0.104	0.883	89.46%
	800	800-1015	1± 0.03	0.65-1.40	0.013	0.104	0.883	89.46%
	1000	845-1025	1± 0.03	0.65-1.40	0.013	0.104	0.883	89.46%

II.2.4 Mesure du profil de température du réacteur

Le réacteur tubulaire utilisé n'a pas une température uniforme sur toute sa longueur, du fait que ce dernier est placé dans un four ayant lui-même, par construction, un profil de température. Or, pour permettre une comparaison significative entre expérience et simulation, il est indispensable de déterminer le profil de température à l'intérieur du réacteur. En simulation, le réacteur tubulaire, à écoulement piston, sera modélisé par une cascade de réacteurs parfaitement agités (RPA), la température de chaque RPA étant attribuée de façon à reproduire le profil de température du réacteur tubulaire. En outre, l'écoulement de type piston du réacteur utilisé est vérifié, en calculant le critère de Péclet pour chaque température du profil (cf. annexe B).

La température à l'intérieur du réacteur tubulaire est mesurée tous les un centimètre, depuis l'entrée jusqu'à la sortie, à l'aide d'un thermocouple coulissant. Pour des raisons de sécurité (fuites de gaz lors du déplacement du thermocouple) et pour éviter les effets catalytiques du thermocouple au cours des réactions d'oxydation, le profil de température a été mesuré en contact direct avec le gaz inerte (l'hélium) et sans réaction d'oxydation.

Les profils de température sont rassemblés dans l'annexe (C). Ces profils adoptent une forme générale semblable : une augmentation très rapide de température sur les dix premiers centimètres, puis une stabilisation autour de la valeur maximale pour environ vingt centimètres et enfin une décroissance pour les derniers vingt centimètres du réacteur. Il a été démontré que le paramètre qui influe le plus sur ces profils de température, est la température de consigne du

four. Les débits de l'hélium et d'oxygène n'ont pas d'influence notable sur les profils de température dans la gamme des débits utilisés. Comme les réactions d'oxydation sont exothermiques, il est nécessaire de travailler à dilution élevée pour laisser inchangé le profil de température, que le réacteur soit traversé par l'inerte seul, ou par le mélange réel d'oxydation.

II.2.5 Techniques d'analyses et de mesures

Nous décrirons dans cette partie les dispositifs et les méthodes de mesure et d'analyse des réactifs et des produits.

II.2.5.1 Etalonnages des régulateurs de débit massique (RDM)

❖ Etalonnage RDM gaz inerte (He) et oxygène

Pour réaliser les étalonnages des régulateurs de débits massiques, nous avons utilisé des débitmètres à bulle. Un étalonnage des régulateurs permet de déduire une relation linéaire entre la valeur affichée par le régulateur (consigne) et la valeur réelle du débit volumique calculée dans les conditions normales de température (0°C) et de pression (1atm); les courbes d'étalonnage correspondant à chaque gaz sont données dans l'annexe D.

❖ Etalonnage du RDM liquide (CORI-FLOW)

L'étude des esters éthyliques nécessite un étalonnage spécifique du RDM liquide et de l'évaporateur (Controlled Evaporator Mixer, CEM). Il est à noter que la nature du combustible, la pression, la température et le débit d'inerte sont des paramètres qui influent directement sur le régulateur de débit massique et sur l'évaporateur (cf. figure II.10). Leur utilisation s'effectuant sous une pression atmosphérique (760 torr), à des températures allant de 293 - 473 K et avec des débits d'inerte de 1-2.25 NL.min⁻¹, l'étalonnage ne pourra donc être fiable que s'il est effectué dans les mêmes conditions opératoires de l'expérience en réacteur piston. La masse réelle d'ester vaporisé est alors mesurée en fonction de la consigne du RDM. A pression atmosphérique, le RDM Liquide/Evaporateur est étalonné par pesée après condensation du butanoate d'éthyle vaporisé. Cette méthode est en outre vérifiée par CPG en utilisant un étalon interne (octane). La figure II.10 présente l'influence du débit du gaz inerte sur l'étalonnage du système RDM Liquide/CEM pour le butanoate d'éthyle à T= 373 K. Nous constatons qu'à faible débit d'inerte pour une même consigne, le RDM laisse circuler plus de combustible.

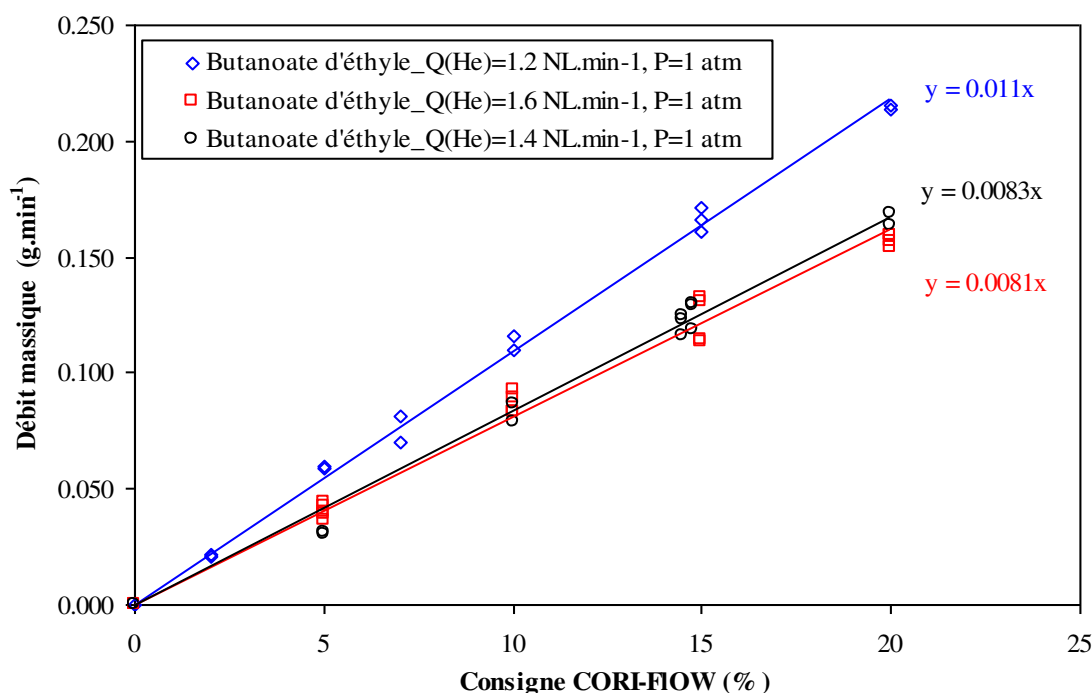


Figure II.10 : Etalonnage du RDM liquide/Evaporateur pour le butanoate d'éthyle.

II.2.5.2 Etalonnage de l'analyseur IR COSMA-CRISTAL 300

Un analyseur à absorption infrarouge non dispersive (type Cosma-Cristal 300) est utilisé en ligne pour analyser le CO et le CO₂. Cet analyseur mesure l'absorption du gaz à différentes longueurs d'onde non séparées en utilisant un faisceau large de lumière. Le détecteur est un spectromètre optico-acoustique. Il est constitué d'une cellule remplie par le gaz à analyser et d'un microphone condenseur. En traversant la cellule, une partie de la lumière est absorbée, ceci provoque une augmentation de la température qui se traduit par augmentation de la pression qui est détectée par le microphone condenseur. Pour chaque type de gaz à analyser, il faut une cellule remplie par le même gaz et un trajet optique différent. Le débit correct de gaz passant dans la cellule va de 30 L.h⁻¹ à 120 L.h⁻¹. Le réglage du zéro de l'appareil se fait à l'aide d'une bouteille d'azote à 99.995% (Messer, qualité U) munie d'un détendeur régulateur de pression réglé à environ 100 mbar. Par ailleurs, le réglage du gain est assuré par une bouteille de gaz titrés (Air liquide: 6.05 % CO + 8.37% CO₂ + 85.58% N₂) munie d'un détendeur régulateur de pression à environ 100mbar. Le choix de la gamme de mesure en CO, CO₂ de l'appareil dépend des conditions opératoires d'oxydation et du choix du réactif.

II.2.5.3 Etalonnage des chromatographes

La chromatographie est une technique d'analyse qui nous donne accès à une valeur physique (masse, pression, fraction molaire d'espèces) par un étalonnage de la réponse du détecteur aux différentes espèces. Une analyse qualitative permet d'identifier les produits

formés avec un chromatographe en phase gazeuse couplé à un spectromètre de masse (GC/MS) ou par comparaison des temps de rétention avec ceux des produits purs passés.

Le tableau (II.3) présente les caractéristiques des chromatographes utilisés

Tableau II.3 : Caractéristiques des chromatographes utilisés.

PERICHROM PR1250-Serial N°: 2704 (Analyse de O₂)			
Programme du four	Injecteur	Détecteur	Colonne
T° de sécurité du four : 85°C T° initiale : 40 °C Temps d'isotherme de T° : 10 min	Classique Température : ambiante Gaz vecteur : He Pression du gaz vecteur : 190 kPa Volume de la boucle: 3ml	TCD Température: ambiante Gain : 10 Intensité : 80 mA	Tamie moléculaire 5A°, Longueur : 2.5 m
PERICHROM PR2100 (Analyse des condensables)			
T° de sécurité du four : 250 °C T° initiale : 50°C Temps d'isotherme de T° : 20 min Rampe 1 Taux : 5°C/min T° finale : 240°C Temps d'isotherme de T° : 40 min	Split/Splitless Température : 200°C Gaz vecteur : N ₂ Pression du gaz vecteur : 30 kPa Split: 150 ml/m Passeur automatique ALS104 Seringue SGE 0.5µl Longueur de la seringue : 5cm	FID Temperature: 260°C Gain : 11 Pressions des gaz du FID Pression d'air : 50 kpa Pression de H ₂ : 50 kpa	SGE BP 21, Polyéthylène glycol polaire, capillaire Longueur : 30 m Diamètre interne : 0.53 mm Epaisseur du film : 1µm
Agilent 6850 (Analyses des légers)			
T° de sécurité du four : 255 °C T° initiale : 60°C Temps d'isotherme de T° : 10 min Rampe 1 Rate: 5°C/min T° finale : 250°C Temps d'isotherme de T° : 15 min	Split/Splitless Température: 250°C Gaz vecteur : He Pression du gaz vecteur : 103 kPa Split : 1/100 (200 ml/min) Volume de la boucle : 0.25ml T° de la boucle : 180°C	FID Temperature : 300°C Débits des gaz du FID : Air : 400 ml/min H ₂ : 30 ml/min	HP-PLOT Q, Polystyrène-divinylbenzène, apolaire, capillaire Longueur : 30 m Diamètre interne : 320 µm Epaisseur du film : 20µm
Agilent 6850 (GC/MS)			
T° de sécurité du four : 255 °C T° initiale : 60°C Temps d'isotherme de T: 10 min	Split/Splitless Température: 250°C Gaz vecteur : He Pression du gaz vecteur : 103 kPa	Spectromètre de masse Temperature: 300°C Flow rate of FID combustion gas	HP-PLOT Q, Polystyrène-divinylbenzène, apolaire, capillaire Longueur : 30 m

Rampe 1	Split : 1/100 (200 ml/min)	Air: 400 ml/min	Diamètre interne : 320 μ m Epaisseur du film : 20 μ m
Rate: 5°C/min		H ₂ : 30 ml/min	
T° finale : 250°C		Makeup flow + column	
Temps d'isotherme de T° : 15 min		flow = 25 ml/min	

Les produits légers (C₁-C₄) ont tous été étalonnés au moyen de bouteilles étalons sur le chromatographe Agilent 6850. Les droites d'étalonnage relient l'aire du pic à la pression du produit analysé selon la formule $A_j = K_j \times P_j$ (II.3)

La figure II.11 donne la réponse du détecteur FID pour une injection en ligne du méthane (CH₄).

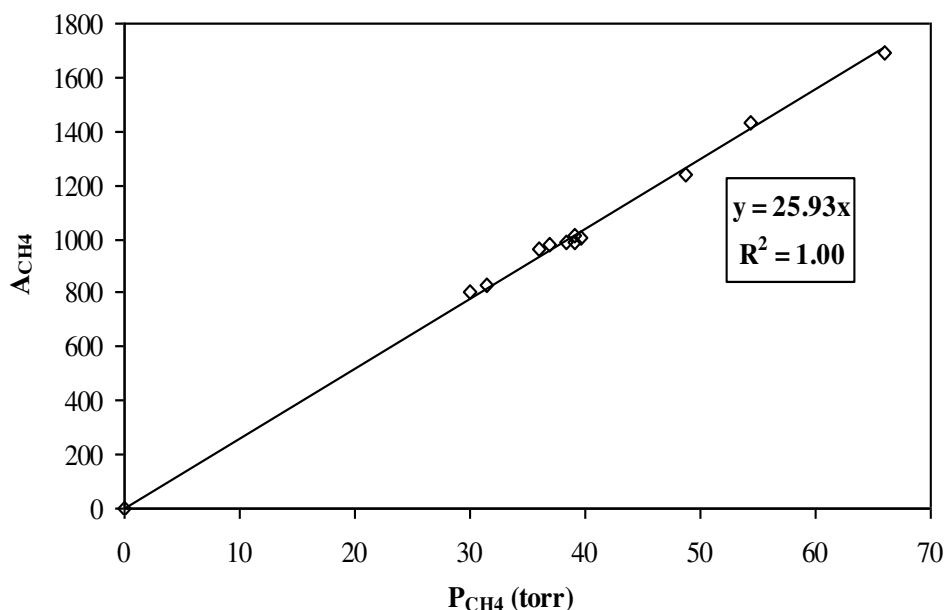


Figure II.11 : Réponse du détecteur FID (Agilent 6850) pour le méthane.

Les gaz autres que les hydrocarbures ont été étalonnés avec un CPG PR1250 muni d'un détecteur à catharomètre (TCD). Le gaz vecteur a été choisi selon la conductivité thermique entre le gaz à analyser et le gaz vecteur. Le tableau II.4 illustre les conductivités thermiques des gaz étudiés (<http://fr.wikipedia.org>)

Tableau II.4 : Conductivité thermique des gaz étudiés (wikipedia.org)

Gaz	Conductivité thermique Cal.cm ⁻¹ .s ⁻¹ (0°C)
H ₂	39.6
He	39.85
N ₂	5.68
O ₂	5.7
CH ₄	7.2

Comme l'étude de l'oxydation de butanoate d'éthyle a été effectuée sous l'hélium et que la conductivité thermique de ce gaz est proche à celle d'hydrogène; il n'a pas été possible de

séparer et mesurer l'hydrogène. La conductivité thermique de l'azote et de l'oxygène est trop proche pour pouvoir les séparer par CPG-TCD. La courbe d'étalonnage obtenue au moyen de bouteilles étalons est donnée sur la figure II.12.

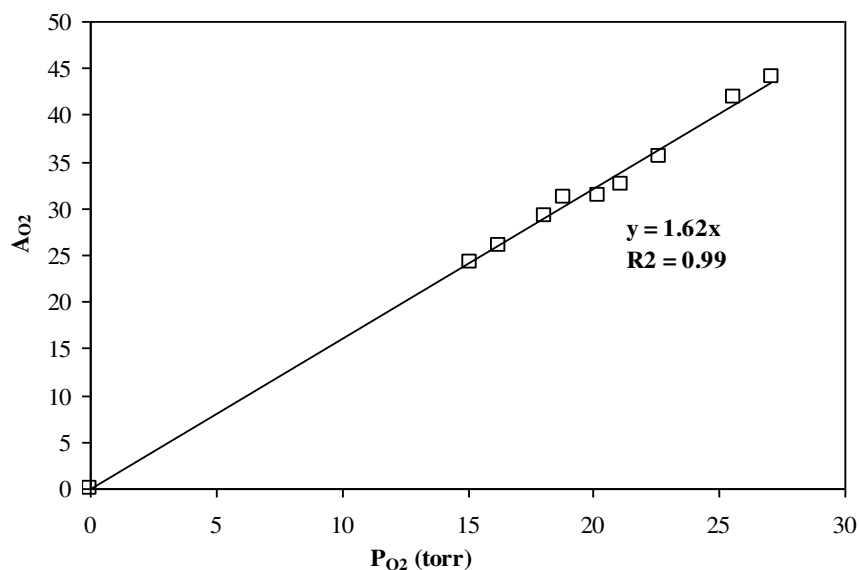


Figure II.12 : Réponse du détecteur TCD (PR1250) pour l'oxygène sous He comme gaz vecteur.

Sur le chromatographe PR2100, la plupart des composés liquides (hydrocarbures et composés oxygénés) ont été étalonnés par la méthode de l'étalon interne (décrite en détail dans l'annexe E). A titre d'illustration, La figure II.13 présente un exemple de réponse du FID (PR2100) du butanoate d'éthyle par rapport à l'octane.

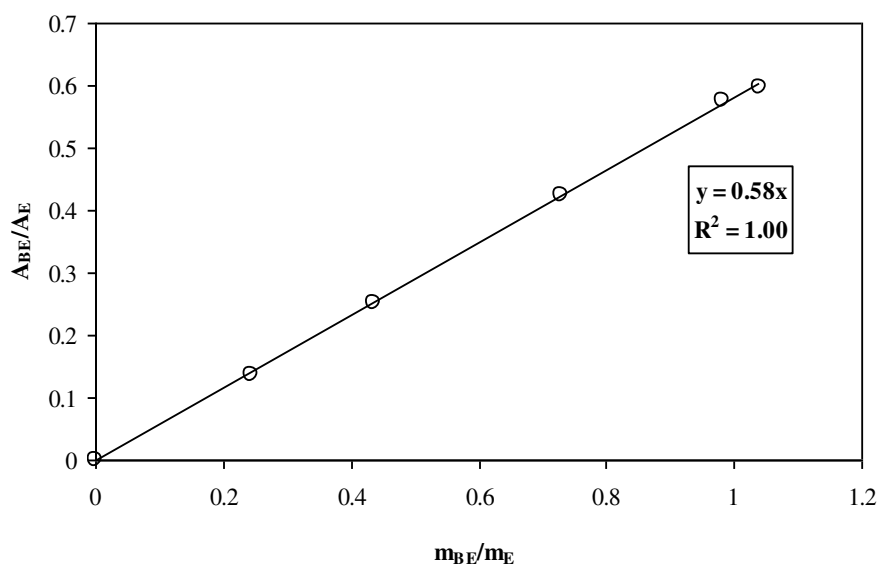


Figure II.13 : Réponse du détecteur FID (PR2100) pour le butanoate d'éthyle.

Le coefficient de réponse du butanoate d'éthyle par rapport à l'étalon interne (noté E) est la pente de la droite d'étalonnage :

$$K_{i/E}^{\text{exp}} = \frac{A_{BE} / A_E}{m_{BE} / m_E} = 0.58 \quad (\text{II.4})$$

A partir des courbes d'étalonnage, les masses des produits formés au cours de l'oxydation peuvent être déterminées à partir de l'expression (II.4) en connaissant la masse de l'étalon interne (m_E) et le rapport des aires du produit et de l'étalon interne A_i et A_E respectivement.

$$m_i = \frac{m_E}{K_{i/E}^{\text{exp}}} \times \frac{A_i}{A_E} \quad (\text{II.5})$$

Le coefficient de réponse des composés détectés par FID peut être déterminé par la méthode du nombre de carbone effectif (Effective Carbon Number, ECN) (Tranchant et al 1982). A chaque atome (carbone, oxygène) est affectée une valeur numérique qui dépend de son environnement chimique immédiat et de sa fonction (cf. tableau II-5).

Les coefficients d'étalonnage expérimentaux $K_{i/E}^{n,\text{exp}}$, sont déterminés à partir de l'expression (II.6).

$$\frac{n_i}{n_E} = K_{i/E}^{n,\text{exp}} \times \frac{A_i}{A_E} \quad (\text{II.6})$$

D'où (II.6) :

$$\frac{A_i}{A_E} = \frac{1}{K_{i/E}^{n,\text{exp}}} \times \frac{n_i}{n_E} \quad (\text{II.7})$$

Tableau II.5 : Contribution au nombre de carbone effectif des atomes d'une molécule (Tranchant et al., 1982).

Atome	Type	Contribution ECN
C	Aliphatique	1.0
C	Aromatique	1.0
C	Oléfinique	0.95
C	Acétylénique	1.3
C	Carbonyle (C=O)	0.0
C	Nitrile	0.3
O	Ether	-1
O	Alcool primaire	-0.6
O	Alcool secondaire	-0.75
O	Alcool tertiaire ou Ester	-0.25
N	Amine	Comme pour O dans le cas des alcools

n_i, n_E sont le nombre de moles du composé à analyser et de l'étalon interne respectivement.

Expérimentalement, on a déterminé le coefficient d'étalonnage par rapport aux masses du composé (i) et de l'étalon interne (E) :

$$\frac{A_i}{A_E} = K_{i/E}^{\text{exp}} \times \frac{m_i}{m_E} \quad (\text{II.8})$$

D'où (II.8)

$$\frac{A_i}{A_E} = K_{i/E}^{\text{exp}} \times \frac{n_i \cdot M_i}{n_E \cdot M_E} \quad (\text{II.9})$$

De (II.7) et (II.9) on en déduit (II.10) :

$$K_{i/E}^{n,\text{exp}} = \frac{1}{K_{i/E}^{\text{exp}}} \times \frac{M_E}{M_i} \quad (\text{II.10})$$

M_i, M_E sont les masses molaires du composé à analyser et de l'étalon interne respectivement.

Ainsi l'expression (II.7) est équivalente à l'expression (II.11) :

$$\frac{A_i}{A_E} = \frac{\text{nombre de carbones efficaces dans } i \text{ par molécule}}{\text{nombre de carbones efficaces dans } E \text{ par molécule}} \times \frac{N_a}{N_a} \times \frac{n_i}{n_E} \quad (\text{II.11})$$

N_a : est le nombre d'Avogadro: $6,0221415 \times 10^{23}$.

D'où l'expression du coefficient de réponse théorique $K_{i/E}^{n,\text{théo}}$:

$$K_{i/E}^{n,\text{théo}} = \frac{\text{nombre de carbones efficaces dans } E \text{ par molécule}}{\text{nombre de carbones efficaces dans } i \text{ par molécule}} = \frac{ECN_E}{ECN_i} \quad (\text{II.12})$$

La figure II.14 présente la réponse du FID (PR2100) pour le butanoate d'éthyle par rapport à l'octane en traçant le rapport des nombres des moles en fonction des rapports des aires.

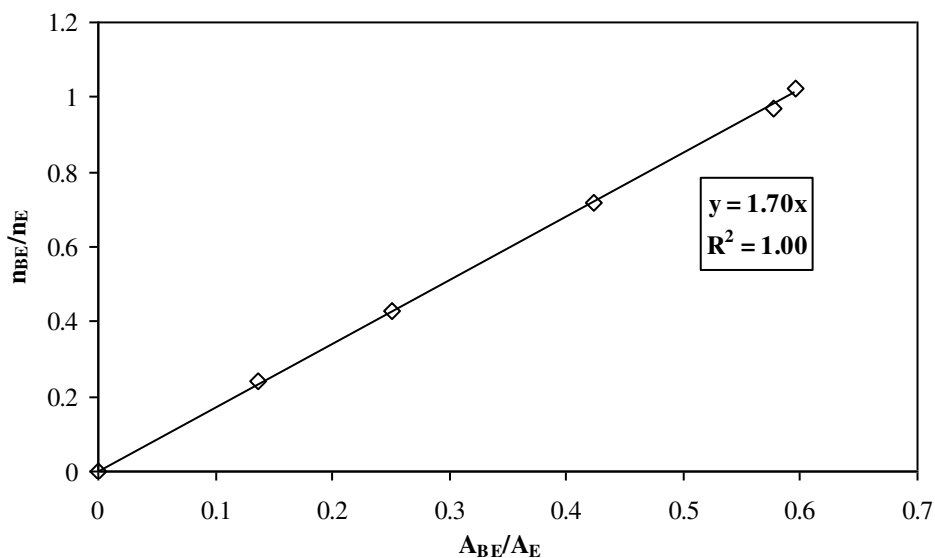
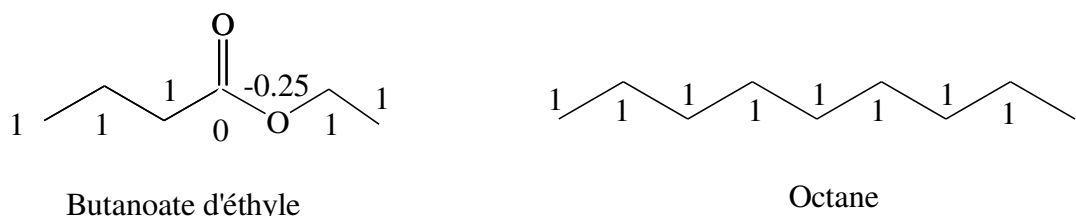


Figure II.14 : Réponse du détecteur FID (PR2100) pour le butanoate d'éthyle.

Le coefficient de réponse du butanoate d'éthyle par rapport à l'étalon interne est la pente de la droite d'étalonnage :

$$K_{i/E}^{n,\text{exp}} = \frac{n_{BE}/n_E}{A_{BE}/A_E} = 1.70 \quad (\text{II.13})$$

Dans notre cas, le composé de référence est l'octane dont le nombre de carbones efficaces $ECN_E=8$. Le calcul du coefficient de réponse théorique pour le butanoate d'éthyle donne :



$$K_{i/E}^{n,\text{théo}} = \frac{ECN_E}{ECN_i} = \frac{8}{5 - 0.25} = 1.68 \quad (\text{II.14})$$

Ce résultat montre que la méthode ECN est tout à fait conforme avec l'étalonnage direct du butanoate d'éthyle. L'annexe (F) illustre les données obtenues avec la méthode ECN et les valeurs expérimentales dans l'évaluation du coefficient de réponse du FID pour les molécules ($K_{i/E}^{\text{exp}}$) qui ont pu être étalonnées directement. Par ailleurs, il présente en détails les conditions d'analyse ainsi que les temps rétention des produits purs passés en CPG sur les colonnes HP-Plot (Q), SGE BP21 et le tamis moléculaire.

Le pilote décrit dans cette partie va permettre de réaliser des réactions d'oxydation. Nos résultats expérimentaux (sans effet catalytique aux parois et réacteur tubulaire avec écoulement proche de l'écoulement piton) seront ensuite comparés à ceux obtenus par la simulation. Le réactif est introduit dans le réacteur avec un débit bien connu. De telles conditions expérimentales n'étaient pas possibles avec le pilote de pyrolyse initial.

Les résultats des expériences d'oxydation du butanoate d'éthyle font l'objet du chapitre III et serviront pour valider ensuite un mécanisme réactionnel détaillé.

II.3 Dispositif expérimental du tube à onde choc

La validation des modèles générés par EXGAS (Warth, 1999) nécessite la comparaison des simulations avec une large gamme de résultats expérimentaux dans des conditions. Disposant d'un tube à onde de choc au laboratoire, nous avons donc décidé de mesurer à l'aide de cet appareillage les délais d'auto-ignition du butanoate d'éthyle, de crotonate d'éthyle, d'acrylate d'éthyle, de crotonate de méthyle et d'acrylate de méthyle à haute température.

II.3.1 Principe du tube à onde de choc

Le tube à choc est un réacteur fermé qui sert en particulier à l'étude de la cinétique des processus chimiques à hautes températures et hautes pressions. Il est le seul dispositif permettant d'étudier les réactions à haute température de manière précise et contrôlée. De plus, il peut être couplé facilement à beaucoup de techniques de détection. Le tube à choc est un tube cylindrique composé de deux parties séparées par une membrane étanche (diaphragme) : une section haute pression et une section basse pression. Dans le compartiment dit « basse pression » se trouve le gaz à étudier (tube de travail) et, dans le compartiment dit « haute pression », un gaz moteur (gaz piston) est introduit. Ce dernier est généralement de l'hélium ou, du moins, un gaz rare.

Après la rupture brutale de la membrane (mécaniquement ou par différence de pression), une onde de choc est produite dans le tube par différence de pression ce qui va permettre une élévation quasi instantanée de la température et de la pression. Cette élévation de la température est trop rapide (de l'ordre de 10^{-10} s) pour que les molécules puissent diffuser vers la paroi froide du tube. On fait donc l'hypothèse d'un écoulement unidirectionnel. En effet le transfert d'énergie aux parois est négligeable durant le temps d'observation qui est de l'ordre de la milliseconde au maximum. Le tube est donc parfaitement adiabatique et les réactions hétérogènes sont négligeables. Notons que cette durée d'observation, à température et pression constantes, dépend de la longueur du tube, des propriétés thermodynamiques des gaz et de la célérité de l'onde de choc.

Afin de simplifier la présentation du tube à onde de choc, introduisons les indices que nous utiliserons par la suite.

Tableau II.6 : Indexation des gaz intervenant dans le tube à onde de choc

Indexation	Type de Gaz
1	Gaz étudié à l'état initial
2	Gaz étudié derrière l'onde de choc incidente
3	Gaz piston entre la surface de contact et le faisceau de détente
4	Gaz piston à l'état initial
5	Gaz étudié derrière l'onde de choc réfléchie

Le gaz piston est introduit à une pression P_4 et une température T_4 et l'échantillon à étudier à une pression P_1 et une température T_1 . Généralement $T_4 = T_1 =$ la température ambiante. Les deux parties séparées par un diaphragme se rompent sous la poussée du gaz piston. Au moment de la rupture du ou des diaphragmes, la différence de pression entre les

deux milieux fait qu'un paquet d'ondes de compression se propage dans l'échantillon alors qu'une onde de détente remonte dans le gaz piston. Comme le montre la figure (II.15), ces ondes de compression ont des vitesses, $C(P)$, de plus en plus élevées lorsque la pression croît (Dayma, 2003).

Ces vitesses, qui correspondent en fait à la célérité locale du son, sont liées à la pression par la relation suivante :

$$C(P) = \sqrt{\left(\frac{\partial P}{\partial \rho}\right)_s} = V \sqrt{-\left(\frac{\partial P}{\partial V}\right)_s} \quad (\text{II.15})$$

Avec : P Pression locale
 ρ Masse volumique
 V Volume massique
 S Entropie

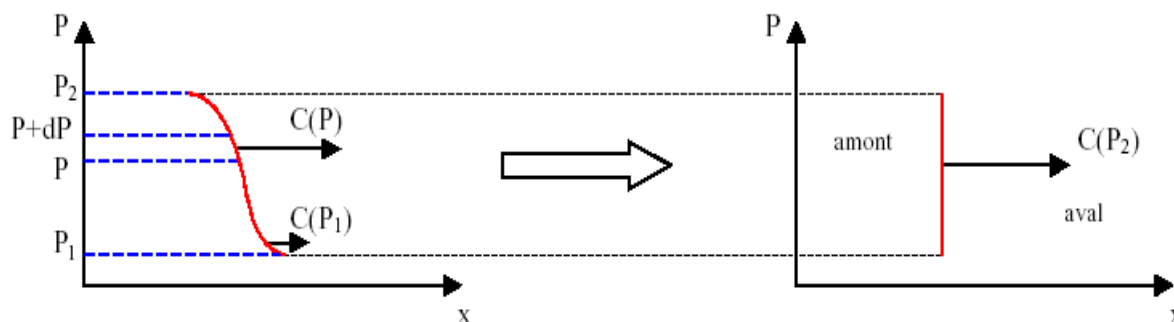


Figure II.15 : Formation de l'onde de choc (Dayma, 2003).

Comme la pression augmente après leurs passages respectifs, ces ondes de compression (figure II.15) se rattrapent les unes les autres jusqu'à s'harmoniser pour former un unique front de choc au bout d'une distance comparable à quelques diamètres de tube. L'échantillon est alors comprimé sous l'effet de cette onde incidente qui se propage à une vitesse supersonique par rapport à l'aval (état 1). De plus, l'onde de choc va plus vite que la surface de séparation entre l'échantillon et le gaz piston. La propagation de cette interface est toutefois suffisamment rapide pour considérer qu'il n'y a pas de diffusion entre les deux gaz. Le gaz moteur (hélium) et le gaz d'étude ne se mélangent pas.

- Le choc incident porte les gaz frais à une pression P_2 et une température T_2 .
- Le gaz piston, initialement à une pression P_4 et une température T_4 , subit diminution isentropique de sa pression et de sa température jusqu'aux valeurs P_3 et T_3 .
- Les ondes de choc et de détente ont également pour effet de mettre le gaz moteur et le gaz d'étude en mouvement. Initialement au repos ($u_1 = u_4 = 0$), la vitesse matérielle de ces gaz devient u_2 pour l'échantillon et u_3 pour le gaz piston. L'équilibre mécanique impose que $P_2 = P_3$ et $u_2 = u_3$.

Lorsque l'onde de choc incidente arrive à l'extrémité du tube, elle est réfléchiée en une nouvelle onde de choc qui comprime et chauffe à nouveau le mélange le portant à une pression P_5 et une température T_5 . Les particules composant le gaz d'étude sont alors stoppées par le passage de cette onde en sens inverse ; $u_5 = 0$. Dans un gaz inerte, les températures et les pressions atteintes derrière l'onde de choc réfléchiée restent relativement constantes tant que cette onde n'a pas rencontré la surface de contact. Dans un milieu réactif, les caractéristiques physiques (température, pression....) sont alors telles que des réactions chimiques se déclenchent au sein du gaz échantillon.

II.3.2 Description du tube à choc du LRGP (ENSIC-Nancy)

Cet appareillage a été antérieurement utilisé lors des travaux d'auto-inflammation de différentes molécules en C_3 , C_4 , C_6 et C_7 (Bauge, 1998; Belmekki, 2001; Da Costa, 2001; Dayma, 2003; Buda, 2006). La figure (II.16), représente un schéma simplifié du montage expérimental utilisé dans cette étude. Ce tube est constitué de deux parties : une partie basse pression d'une longueur de 400.6 cm et d'un diamètre intérieur de 7.8 cm, une partie haute pression d'une longueur de 90 cm et d'un diamètre intérieur de 12.82 cm. Quatre capteurs piézoélectriques de pression affleurent à la paroi intérieure du tube et qui sont espacés de 150 mm. Un dispositif comprenant une fenêtre en quartz transparent aux UV, un monochromateur (Ealing 82415) et un photomultiplicateur (Hamamatsu E717-21) permet de suivre l'émission des radicaux hydroxyles OH^* . Un compartiment intermédiaire (longueur : 5.2 cm; diamètre intérieur: 5.8 cm), placé entre les deux parties précédentes, est délimité par deux membranes de Terphane d'une épaisseur de 75 μm qui résistent à environ 4 bar de pression statique. La mesure du délai d'inflammation s'effectue à 1 mm de l'extrémité du tube grâce à l'enregistrement simultané du passage de l'onde de choc réfléchiée et de l'émission des radicaux OH^* . Cette émission est suivie à une longueur d'onde $\lambda = 306$ nm grâce à un monochromateur couplé à un photomultiplicateur.

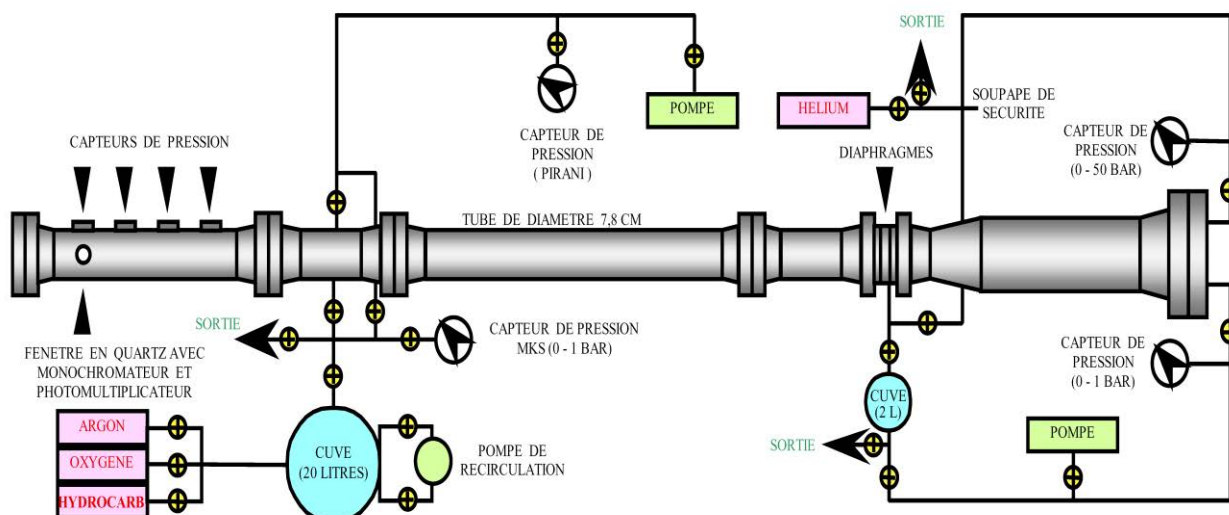


Figure II.16 : Schéma simplifié du tube à onde de choc.

II.3.3 Mise en œuvre du tube à onde de choc

L'ensemble du tube est pompé à l'aide de trois pompes à palettes jusqu'à l'obtention d'un vide de l'ordre de 10^{-2} Torr (1.3 Pa) que l'on vérifie grâce à une jauge de pression de type Pirani (Balzers TPG 251). Avant chaque tir, le tube est purgé deux fois par 1 atm d'argon introduite dans la partie basse pression qui est ensuite évacuée à l'aide des deux pompes. Le mélange gazeux (Carburant, oxygène et argon) est préalablement préparé et stocké dans une cuve de 20 litres à une pression d'environ 800 Torr (soit 105.3 kPa). Ce mélange est préparé par la méthode manométrique des pressions partielles. La précision sur la composition du mélange est de l'ordre d'environ 5%. 100 à 300 Torr (13 à 40 kPa) du mélange gazeux sont introduits dans la partie basse pression du tube. 2.5 bar (250 kPa) d'hélium sont introduits dans le compartiment intermédiaire et 5.3 bar (530 kPa) dans la partie haute pression. Le tir est déclenché par l'ouverture de la vanne permettant l'éclatement des membranes. Une onde de choc incidente est formée et derrière cette onde les gaz sont portés à une température T_2 (500 à 1500 K) et à une pression P_2 (< 5 bar). Cette onde se propage jusqu'à l'extrémité du tube où elle se réfléchit pour porter les gaz à une température T_5 (1000 à 1800 K) et une pression P_5 pouvant atteindre 9 bar. Le tableau (II.7) présente les puretés des gaz utilisés lors des expériences.

Tableau II.7 : Puretés des gaz utilisés en tube à onde de choc.

Nature du gaz (Messer)	Impuretés en ppm (V)
Hélium U	$O_2 < 2$, $C_nH_m < 1.5$, $H_2O < 3$
Argon C	$O_2 < 2$, $C_nH_m < 0.1$, $H_2O < 3$, $N_2 < 5$, $CO + CO_2 < 0.1$
Oxygène C	$H_2O < 5$, $N_2 < 20$, $C_nH_m < 0.5$, $CO + CO_2 < 0.5$

La figure II.17 illustre les élévations de pression enregistrées par les quatre capteurs de pression ainsi que le signal des OH^* fourni par le photomultiplicateur (acquis et lus grâce au logiciel SBENCH5.2).

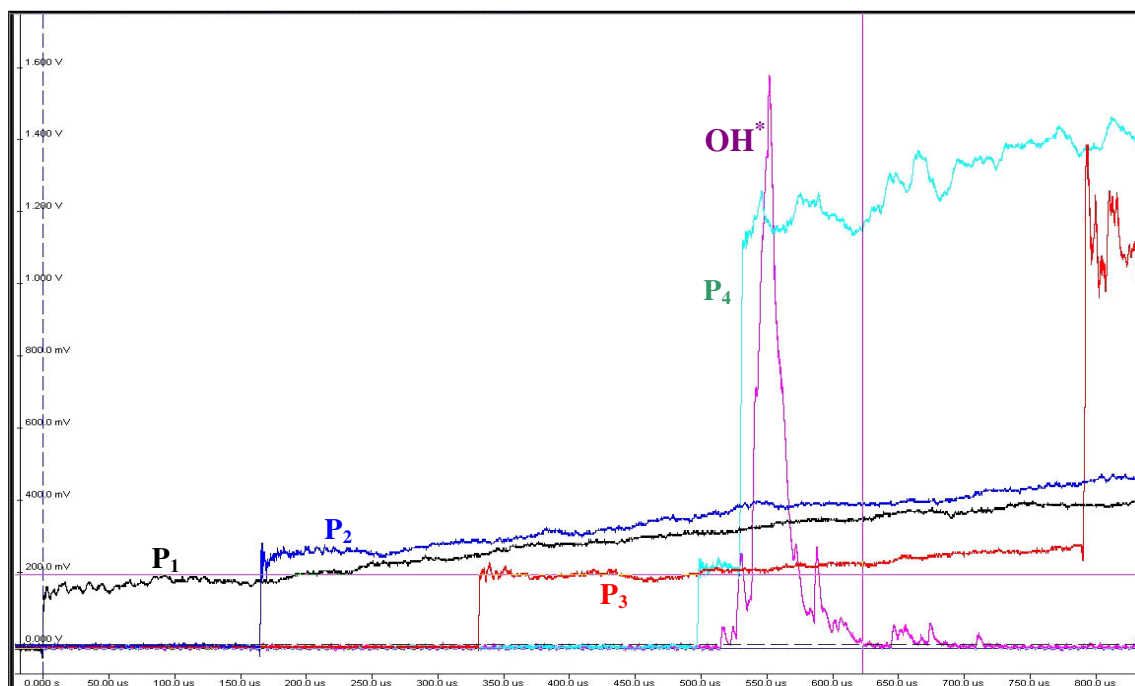


Figure II.17 : Exemple d'enregistrement des 4 signaux de pression et le signal des OH^* .

La célérité de l'onde de choc incidente est déduite à partir des enregistrements des signaux délivrés par des capteurs de pression placés au voisinage de la surface de réflexion de l'onde. En effet, la distance entre les capteurs étant connue avec précision (150 mm), la mesure du temps de passage de l'onde de choc incidente entre deux capteurs donne la vitesse de cette onde. A partir de cette célérité, des conditions initiales du mélange combustible et des propriétés thermodynamiques des gaz (Bradley, 1963), l'état des gaz derrière l'onde de choc réfléchi est calculé à l'aide d'un programme informatique. Par la résolution des équations de Rankine-Hugoniot, les paramètres de choc (pression, température, célérité des ondes incidente et réfléchi, nombre de Mach....) sont calculés par un procédé itératif sur la température (cf. annexe H). Généralement, on considère que l'erreur réalisée sur la détermination de la température T_5 est d'environ 20 K.

Le délai d'auto-inflammation, τ est alors défini comme le temps qui sépare l'arrivée de l'onde de choc réfléchi en face de la fenêtre (deuxième saut du 4^{ème} signal de pression) et l'instant où le signal des radicaux OH excités atteint 50% au maximum du pic comme le montre la figure (II.18). Un autre critère, tout aussi arbitraire est souvent repris dans les publications sur le sujet : à 10 % du signal d'émission total des radicaux hydroxyles.

Néanmoins en se situant à 50% du signal on est sûr d'être en pleine auto-inflammation, alors qu'à 10 % il arrive souvent que l'on ne soit pas sur une montée nette et très franche du signal.

Par ailleurs, on peut remarquer sur le signal fourni par le dernier capteur de pression (4) l'apparition d'une augmentation de la pression lors de l'auto-inflammation. Cette augmentation est due à l'élévation brutale de la pression qui se produit au moment de la libération de chaleur par l'auto-inflammation. Cette augmentation est nettement plus présente quand le mélange est moins dilué. Dans ces conditions, on pourrait envisager de se servir de ce saut pour mesurer le délai d'auto-inflammation (méthode utilisée par Burcat et al., 1985). Cependant ce saut est souvent trop faible et mal défini pour permettre une détermination précise. Les erreurs de mesure du délai d'auto-inflammation liées au dispositif de mesure, sont considérées comme inférieures à 14%. Cette estimation tient compte des temps de réponse des capteurs piézoélectriques, du photomultiplicateur, de la carte d'acquisition, ainsi que des erreurs faites sur la lecture par le manipulateur.

II.3.4 Etudes paramétriques

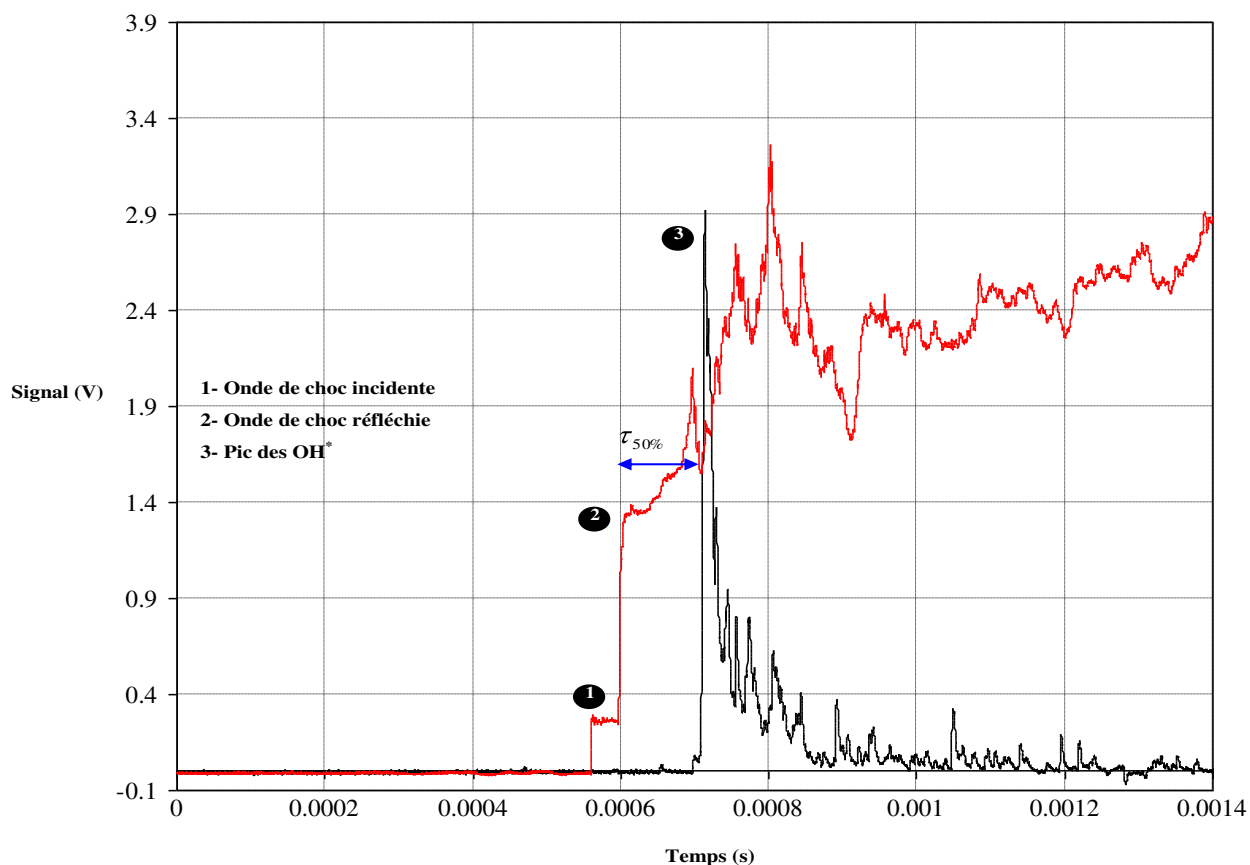
Les délais d'auto-inflammation (τ) de cinq esters: le crotonate de méthyle (CM), l'acrylate de méthyle (ACM) qui représentent des intermédiaires de l'oxydation du butanoate de méthyle (Gail et al., 2007; Hakka et al., 2010) et le butanoate d'éthyle (BE) ainsi que ses intermédiaires: le crotonate d'éthyle (CE) et l'acrylate d'éthyle (ACE) ont été mesurés. La figure II.19 illustre la formule développée de chaque biocarburant étudié.

Les mélanges et les conditions ont été choisis:

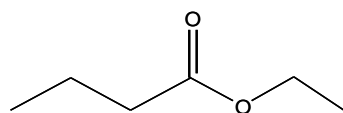
- pour comprendre l'effet de la concentration, de la richesse, ainsi que de l'insaturation sur le délai d'auto-inflammation des carburants étudiés,
- pour comparer les propriétés d'oxydation entre les esters méthyliques et éthyliques.

Les résultats obtenus au cours des expériences font l'objet du chapitre (II) et seront ensuite utilisés pour valider des mécanismes réactionnels détaillés relatif à chaque ester.

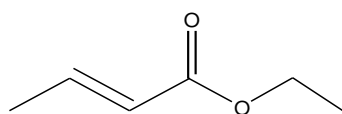
Les conditions opératoires sont regroupées dans le tableau (II.8) ci-après.



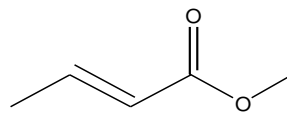
**Figure II.18 : Détermination du délai d'auto-ignition à 50% du pic OH* (Pic à 3 V),
pour : $x_{BE} = 1\%$, $\varphi = 1$, et $P_1 = 200$ torr.**



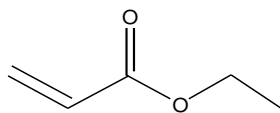
Butanoate d'éthyle (BE)



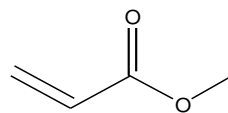
Crotonate d'éthyle (CE)



Crotonate de méthyle (CM)



Acrylate de d'éthyle (ACE)



Acrylate de méthyle (ACM)

Figure II.19 : Structure chimique des esters étudiés en tube à choc.

Tableau II.8 : Composition des mélanges réactionnels, conditions après l'onde de choc réfléchie et délais d'auto-inflammation.

Ester	φ	Composition du mélange réactionnel			P_5 (atm)	T_5 (K)	τ (μ s)
		x_{ester} (%)	x_{O_2} (%)	x_{Ar} (%)			
CM	0.25	0.5	12	87.5	7.2-8.35	1346-1510	7.33-90.8
	1	0.5	3	96.5	7.6-9	1453-1593	18.32-91.12
	1	1	6	93	7.85-8.82	1305-1582	17.34-348
	2	0.5	1.5	98	7.14-8.48	1476-1800	10.96-178.8
ACM	0.25	0.5	9	90.5	7.6-8.74	1388-1521	4.05-46.3
	1	0.5	2.25	97.25	7-8.27	1434-1624	7.14-75.4
	1	1	4.5	94.5	7.26-9.62	1341-1510	10.25-205
	2	0.5	1.125	98.38	7.31-8.58	1485-1765	16.9-95
BE	0.25	0.5	16	83.5	7.75-8.8	1280-1454	4.2-188.6
	1	0.42	3.33	96.25	7.65-9.22	1307-1740	5.5-1485
	1	0.5	4	95.5	7.75-8.5	1385-1635	2.3-112
	1	1	8	91	7.8-9.15	1296-1474	10.95-321.5
	2	0.5	2	97.5	7-8.55	1532-1922	3.5-88.5
CE	0.25	0.5	16	83.5	7.5-8.95	1357-1627	6.4-62.9
	1	0.42	3.13	96.45	6.7-8.6	1411-1817	4.8-176.5
	1	0.5	3.75	95.75	7.5-8.5	1350-1653	22-242
	1	1	7.5	91.5	7.8-9.33	1284-1524	4.7-138
	2	0.5	1.875	97.63	7.24-8.4	1402-1885	12.23-240
ACE	0.25	0.5	12	87.5	7.75-9	1347-1517	4.2-19.6
	1	0.4	2.4	97.2	7.6-8.97	1404-1835	4.37-86.2
	1	0.5	3	96.5	7.74-9.2	1389-1688	7.45-45.84
	1	1	6	93	7.75-9.33	1328-1575	5.22-96.7
	2	0.5	1.5	98	7.42-8.46	1509-1833	4-55.4

Note : P_5 et T_5 sont les pressions et températures derrière l'onde de choc réfléchie, τ est le délai d'auto-inflammation.

III. Description du système EXGAS-ESTERS

III.1 Description générale du système EXGAS-ESTERS

EXGAS-ESTERS permet de générer des mécanismes qui comprennent les réactions associées aux données cinétiques et aux données thermodynamiques. Cette dernière version a été développée à partir de celle d'EXGAS-ALCANES (Biet et al., 2008) en prenant en compte l'effet de la fonction ester. Par la présence de cette fonction, les énergies de certaines liaisons sont différentes de celles des alcanes. Ces énergies ont été fournies à partir des travaux de El-Nahas et al., (2007). Par ailleurs, de nouvelles règles de consommation ont été introduites pour automatiser l'écriture des modèles de combustion des esters. Les mécanismes produits comprennent les réactions et les données cinétiques associées et les données thermodynamiques des espèces. Les mécanismes sont écrits sous un format utilisable par les logiciels de la bibliothèque CHEMKIN II (Kee et al., 1993). Les données thermodynamiques de toutes les espèces sont calculées automatiquement par le logiciel THERGAS (Muller et al., 1995) qui utilise les méthodes d'additivité de groupes (stockées sous forme d'un polynôme de 14 coefficients). Seule l'énergie de dissociation de la liaison C-H de l'atome de carbone au voisinage du groupe carbonyle a été prise égale à $95.6 \text{ kcal.mole}^{-1}$ (Luo, 2003).

Les données cinétiques des réactions d'isomérisations, de combinaisons et de décompositions unimoléculaires sont soit calculées par le logiciel KINGAS (Warth et al., 1998), basé sur les méthodes thermochimiques en utilisant la théorie de l'état de transition ou la théorie des collisions modifiée ; elles peuvent être aussi estimées à partir de corrélations entre structure et réactivité proposées dans la littérature ou déduites de données cinétiques publiées.

Les mécanismes générés avec EXGAS-ESTERS se décomposent en trois parties et gardent la même architecture que celles obtenues avec la version EXGAS-ALCANES :

III.1.1 Base C₀-C₂

Cette base a été construite par Barbé et al. (1995) qui comprend toutes les réactions unimoléculaires et bimoléculaires entre espèces qui contiennent jusqu'à deux atomes de carbone et pour lesquelles les données cinétiques sont disponibles dans la littérature. Les paramètres cinétiques proviennent en grande majorité des bases de données de Tsang et Hampson (1986) et de Baulch et al. (1994), avec des compléments issus de la base développée par le NIST (1993). En effet, pour ces petites espèces, l'écriture des réactions et le calcul des données cinétiques ne répondent pas aux règles appliquées pour les hydrocarbures de taille supérieure. Par ailleurs, l'influence de la pression sur les constantes cinétiques et l'existence de

processus particuliers aux petites espèces sont ainsi pris en compte (Troie, 1974). Cette base est ajoutée à tous les mécanismes générés quelles que soient les conditions de température et de pression étudiées.

III.1.2 Générateur de mécanismes primaires détaillés de consommation des réactifs

Les réactions primaires sont celles qui font uniquement intervenir les réactifs de départ et les radicaux libres qui en sont issus. Les réactifs et radicaux primaires sont soumis aux mêmes règles de génération appliquées à de l'oxydation des alcanes (Buda et al., 2005), et toutes les réactions élémentaires possibles sont écrites systématiquement. Les différents isomères de même formule brute et de même groupement fonctionnel sont globalisés. Le schéma cinétique d'oxydation des esters à une température supérieure à 1000 K inclut uniquement les réactions caractéristiques à haute température :

- Amorçage unimoléculaire par rupture des liaisons C-C et C-O,
- Amorçage bimoléculaire avec l'oxygène conduisant à la formation des radicaux alkyles ou alkenyles ($R\cdot$) et des radicaux hydroperoxy ($HO_2\cdot$),
- Additions des radicaux $\cdot H$ et $\cdot OH$ sur la double liaison (cas des esters insaturés),
- Isomérisations des radicaux alkyles et alkenyles impliquant un état de transition cyclique et un transfert d'un atome d'hydrogène,
- Décompositions des radicaux par β -scission impliquant la rupture des liaisons C-C, C-O, ou C-H,
- Oxydations des radicaux alkyles et alkenyles avec la molécule d'oxygène pour former les alcènes, les diènes et les radicaux hydroperoxy ($HO_2\cdot$),
- Métathèse par l'arrachage d'un atome H du réactif par des petits radicaux ($\cdot O$, $\cdot H$, $\cdot OH$, $HO_2\cdot$ et $\cdot CH_3\dots$), et
- Combinaisons et dismutations des radicaux.

Cependant, dans le cas des températures inférieures à 1000 K, il est nécessaire de tenir compte des réactions à basse température :

- Addition des radicaux alkyles ($R\cdot$) et hydroperoxyalkyle ($\cdot QOOH$) sur une molécule de l'oxygène,
- Isomérisations des radicaux alkylperoxy ($ROO\cdot$) et hydroperoxyalkylperoxy ($\cdot OOQOOH$) impliquant un état de transition cyclique et un transfert d'un atome d'hydrogène,

- Décompositions des radicaux hydroperoxyalkyles ($\dot{\text{QOOH}}$) et dihydroperoxyalkyles $\dot{\text{U}}(\text{OOH})_2$ pour former les éthers cycliques et les radicaux hydroxyle ($\dot{\text{OH}}$), et
- Dismutations des radicaux alkylperoxy ($\text{ROO}\dot{\text{O}}$) avec des radicaux hydroperoxy ($\text{HO}_2\dot{\text{O}}$) pour former des molécules hydroperoxydes (R-O-O-H) et de l'oxygène.

III.1.3 Générateur de mécanismes secondaires de consommation des produits primaires

Le mécanisme secondaire ne concerne plus les réactifs initiaux, mais des produits moléculaires primaires globalisés (Warth et al., 1998). Les réactions mises en jeu regroupent une succession d'étapes élémentaires dégradant les produits primaires sous forme de petites espèces contenues dans la base $\text{C}_0\text{-C}_2$ et sous forme de radicaux qui interviennent dans le mécanisme primaire. La globalisation du mécanisme secondaire permet au modèle de garder des dimensions compatibles avec les temps de calculs de simulation. Les règles utilisées pour l'écriture des réactions des hydroperoxydes, des aldehydes, des cétones et des éthers cycliques sont dérivées à partir de celles des alcanes proposées récemment par Biet et al. (2008).

III.2 Mécanisme d'oxydation de butanoate d'éthyle à haute température

Les mécanismes primaires et secondaires de l'oxydation de butanoate éthylique ont été automatiquement générés à l'aide de la version d'EXGAS-ESTERS en utilisant des règles similaires à celles décrites par Hakka (2010) dans le cas de butanoate de méthyle. Cependant, seules les réactions à haute température ont été considérées dans ce mécanisme. Les énergies d'activation des décompositions par β -scission des radicaux oxygénés sont les mêmes que celles utilisées pour le cas des radicaux oxygénés de l'oxydation du butanoate de méthyle.

Les différences significatives par rapport au mécanisme du butanoate de méthyle sont:

- l'addition de la réaction d'élimination unimoléculaire (cycle centré à six) qui conduit à la formation de l'éthylène et de l'acide butanoïque. La constante de vitesse de cette réaction a été calculée par Kairaitis et Stimson (1968):

$$k = 2.10^{12} \times \text{Exp}\left(-\frac{47300}{RT}\right) \quad (\text{III.1})$$

- les réactions de consommation de l'acide butanoïque, pour lesquels de nouvelles règles de génération ont été considérées (cf. Chapitre III).

III.3 Mécanismes d'oxydation des esters insaturés à haute température

Les mécanismes d'oxydation à haute température des esters méthyliques et éthyliques insaturés : l'acrylate d'éthyle, l'acrylate de méthyle, crotonate d'éthyle et crotonate de méthyle

sont également générés automatiquement en utilisant la nouvelle version d'EXGAS-ESTERS. En effet, ces molécules sont des intermédiaires stables de l'oxydation des butanoates d'éthyle et de méthyle (Gail et al., 2007; Hakka et al., 2010). La génération des mécanismes cinétiques de leur oxydation présente certaines spécificités qui ont nécessité l'addition de nouveaux processus élémentaires au mécanisme initialement généré pour les esters saturés. Ces changements ont été détaillés dans le chapitre (II) du manuscrit et sont donc évoqués très rapidement dans cette partie:

- Réaction de décomposition unimoléculaire des esters éthyliques insaturés qui conduit à la formation de l'éthylène et des acides carboxyliques insaturés.
- Réactions secondaires de consommations de ces acides carboxyliques.
- Amorçage unimoléculaire par rupture des liaisons C-C et C-H impliquant la formation des radicaux stabilisés par résonance (cas des crotonates); où toute forme de mésomères a été prise en compte.
- Les additions des radicaux $\cdot\text{H}$ et $\cdot\text{OH}$ sur la double liaison.
- Décompositions par β -scission des radicaux, où la présence de l'atome de l'oxygène avait un effet significatif sur les énergies d'activation.
- Combinaisons des radicaux stabilisés par résonance avec les petits radicaux.

III.4 Conclusion

Cette partie décrit la nouvelle version d'EXGAS-ESTERS et présente les principales réactions élémentaires introduites dans les mécanismes d'oxydation des esters. Les mécanismes d'oxydation à haute température de l'acrylate d'éthyle, de l'acrylate de méthyle, de crotonate d'éthyle, de crotonate de méthyle et de butanoate d'éthyle ont été générés automatiquement et ont permis de reproduire de façon satisfaisante les délais d'auto-inflammation mesurés en tube à onde de choc.

IV. Etude expérimentale et simulation de l'oxydation des esters méthyliques et éthyliques

Cette partie décrit essentiellement l'étude expérimentale et théorique de l'oxydation des esters éthyliques et méthyliques, principal constituant du biodiesel dans les domaines de basse et de haute température.

Les expériences à haute pression et à haute température ont été réalisées en tube à onde de choc et les expériences à pression atmosphérique et à basse température, dans un réacteur tubulaire à écoulement piston. Cette partie propose aussi les résultats des simulations à haute température, obtenus avec les mécanismes générés automatiquement par la nouvelle version d'EXGAS-ESTERS; nous présentons aussi les analyses de vitesse des voies de consommation et les analyses de sensibilité des réactions.

IV.1 Etude en tube a onde de choc

IV.1.1 Conditions expérimentales

Cinq esters éthyliques et méthyliques (acrylate d'éthyle, acrylate de méthyle, crotonate d'éthyle, crotonate de méthyle et butanoate d'éthyle) ont été étudiés en tube à onde de choc. Des mélanges ester/oxygène/argon ont été préparés aux richesses de 0.25, 1 et 2. La composition des mélanges (en % molaire), la température et la pression derrière l'onde de choc réfléchi sont donnés dans le tableau II.8 dans la partie II.

Les délais d'auto-inflammation de chacun des mélanges d'esters à été mesurés, à des pressions allant de 7 à 9 atm et entre 1200 et 1900 K. On rappelle que P_5 et T_5 sont respectivement la pression et la température derrière l'onde de choc réfléchi et que τ est le délai d'auto-inflammation mesuré à partir de l'enregistrement de l'émission des radicaux hydroxyles (OH^*). Les délais d'auto-inflammation expérimentaux sont alors définis comme le temps s'écoulant entre le passage de l'onde de choc réfléchi et 50 % du pic d'émission des radicaux OH^* .

Les mélanges étudiés sont caractérisés par leur richesse et la concentration initiale de l'ester. Les expressions de la richesse ϕ ou du rapport d'équivalence de chaque ester sont données dans le tableau IV.1 ci-après :

Tableau IV.1 : Les expressions de richesse pour des mélanges ester/oxygène/argon

Ester	Réaction totale	Expression de la richesse φ
Butanoate d'éthyle (BE)	$C_6H_{12}O_2 + 8 O_2 \rightarrow 6 CO_2 + 6 H_2O$	$\varphi = 8 \times \left(\frac{\% BE}{\% O_2} \right)_{\text{expérimental}}$
Crotonate de méthyle (CM)	$C_5H_8O_2 + 6 O_2 \rightarrow 5 CO_2 + 4 H_2O$	$\varphi = 6 \times \left(\frac{\% CM}{\% O_2} \right)_{\text{expérimental}}$
Acrylate de méthyle (AM)	$C_4H_6O_2 + \left(\frac{9}{2} \right) O_2 \rightarrow 4 CO_2 + 3 H_2O$	$\varphi = \left(\frac{9}{2} \right) \times \left(\frac{\% ACM}{\% O_2} \right)_{\text{expérimental}}$
Crotonate d'éthyle (CE)	$C_6H_{10}O_2 + \left(\frac{15}{2} \right) O_2 \rightarrow 6 CO_2 + 5 H_2O$	$\varphi = \left(\frac{15}{2} \right) \times \left(\frac{\% CE}{\% O_2} \right)_{\text{expérimental}}$
Acrylate d'éthyle (AE)	$C_5H_8O_2 + 6 O_2 \rightarrow 5 CO_2 + 4 H_2O$	$\varphi = 6 \times \left(\frac{\% ACE}{\% O_2} \right)_{\text{expérimental}}$

IV.1.2 Etude paramétrique

Les résultats sont représentés sur les figures II.3 à II.7 dans le chapitre (II). Ces figures représentent les délais d'auto-inflammation des esters étudiés en fonction de l'inverse de la température T_5 pour les trois richesses, $\varphi = 0.25$; 1 et 2, et les fractions molaires, allant de 0.4% à 1% en ester. Nous constatons que le délai d'auto-inflammation décroît lorsque T_5 augmente. Ainsi que pour une même température T_5 , le délai d'auto-inflammation le plus court est observé pour le mélange le plus pauvre, c'est-à-dire celui contenant le plus d'oxygène. De plus, on remarque que pour une même température T_5 , plus le mélange est concentré en ester pour une richesse fixe, $\varphi = 1$ et plus le délai d'auto-inflammation est court. En effet, la réactivité du mélange augmente avec la concentration des réactifs: plus le milieu réactionnel est concentré, plus la réaction d'oxydation est accélérée.

Ces résultats nous ont permis à mener une comparaison de réactivité entre les esters étudiés (cf. figure II.8 du chapitre II). Pour avoir une comparaison directe entre les deux types d'esters à une même concentration en atome de carbone, des mélanges stœchiométriques éthyle ester/oxygène/argon à une concentration proche de 0.4 % ester ont été préparés. En effet, la comparaison dans les conditions de cette étude montre qu'il n'y a pas de différence importante entre la réactivité des esters méthyliques et éthyliques insaturés en C_3 et en C_4 . En revanche, la tendance de réactivité diffère pour les esters saturés : le butanoate d'éthyle est plus réactif que butanoate de méthyle en particulier à haute température.

IV.1.3 Approche Statistique

Nous avons également réalisé une approche statistique de nos résultats expérimentaux de manière à pouvoir prévoir tous les délais d'auto-inflammation dans l'intervalle de température et de pression étudié. Une régression multilinéaire est effectuée sur les variables délai d'auto-inflammation, température, concentration en ester, en oxygène et en argon derrière l'onde de choc réfléchie. Ces concentrations sont calculées à partir des concentrations initiales, de la température et de la pression après l'onde de choc réfléchie, en supposant le mélange inerte. Cette approche fait apparaître « l'énergie d'activation apparente » de la réaction globale de combustion de l'ester. Le délai d'auto-inflammation peut alors être décrit par une équation empirique de la forme Arrhénius :

$$\tau = A \exp\left(-\frac{E}{RT}\right) \left[\text{ester} \right]^a \left[\text{O}_2 \right]^b \left[\text{Ar} \right]^c \quad (\text{IV.1})$$

Où τ est le délai d'auto-inflammation mesuré expérimentalement, A : le facteur pré-exponentiel, E : l'énergie d'activation globale ou apparente et a, b et c, les exposants des concentrations des réactifs.

Dans la pratique, le coefficient « c » est pris égal à 0 car la variation de la concentration en argon est si faible dans nos conditions expérimentales que sa valeur est proche de zéro. En supposant que l'énergie d'activation apparente, ou globale, doit être la même pour tous les mélanges si ceux-ci sont soumis aux mêmes processus réactionnels dans l'intervalle de pression et de température considéré, les relations sont regroupées dans le tableau II.1 du chapitre (II).

IV.1.4 Modélisation et simulation des résultats obtenus en tube à choc

IV.1.4.1 Comparaison des simulations et des expériences

Les résultats acquis expérimentalement ont permis aussi de tester la validité des mécanismes cinétiques détaillés d'oxydation dans un domaine de température et de pression élevé des cinq esters étudiés :

- Acrylate d'éthyle avec 111 espèces impliquant 885 réactions,
- Acrylate de méthyle avec 103 espèces impliquant 826 réactions,
- Crotonate d'éthyle avec 128 espèces impliquant 954 réactions,
- Crotonate de méthyle avec 119 espèces impliquant 885 réactions et,
- Butanoate d'éthyle avec 117 espèces impliquant 1035 réactions.

Partie IV Etude expérimentale et simulation de l'oxydation des esters méthyliques et éthyliques

Les modèles cinétiques sont générés automatiquement à l'aide de la nouvelle version d'EXGAS développée pour prendre en compte les produits oxygénés. Les simulations dans le tube à onde de choc ont été réalisées avec le programme SENKIN du logiciel CHEMKIN II (Kee et al., 1993) qui permet de calculer l'évolution de la température, de la pression et des concentrations des espèces chimiques dans un réacteur fermé.

Les figures II.3 à II.7 dans le chapitre (II) illustrent les délais d'auto-inflammation expérimentaux et simulés de l'acrylate d'éthyle, de l'acrylate de méthyle, de crotonate d'éthyle, de crotonate de méthyle et de butanoate d'éthyle respectivement pour différentes conditions de richesse et de concentrations initiales en ester. Là encore les modèles permettent de reproduire de façon satisfaisante les délais mesurés expérimentalement. On peut malgré tout noter que l'écart entre la simulation et l'expérience augmente pour les délais d'auto-inflammation mesurés en mélanges pauvres ($\varphi = 0.25$).

IV.1.4.2 Analyse de flux

L'analyse des flux de consommation des réactifs permet de construire les schémas réactionnels des espèces contenues dans le mécanisme en déterminant leurs voies principales de formation ou de consommation. Les figures II.9 à II.13 (cf. chapitre II) illustrent les principales voies réactionnelles du butanoate d'éthyle, de l'acrylate de méthyle, de l'acrylate d'éthyle, de crotonate de méthyle et de crotonate d'éthyle respectivement, déduites des analyses de vitesse réalisées à une température d'environ 1400 K et à une pression d'environ 8 atm. Les mélanges sont stœchiométriques et la conversion calculée avoisine les 50%. Les voies réactionnelles représentées sur les schémas, bien que non vérifiées expérimentalement par l'analyse des produits, semblent les plus vraisemblables. Comme nous l'avons détaillé dans le chapitre II, la principale voie de consommation du butanoate d'éthyle est la réaction d'élimination unimoléculaire conduisant à la formation de l'éthylène et de l'acide butanoïque; cette voie représente approximativement 75% de la consommation de l'ester. Néanmoins, l'importance de cette voie réactionnelle décroît avec l'augmentation de la température et s'accroît avec l'augmentation de la richesse. Quant à l'acrylate de méthyle, il est essentiellement consommé par la réaction d'addition d'hydrogène sur la double liaison (48%) conduisant à la formation des radicaux: $\cdot\text{CH}_2\text{CH}_2\text{C}(\text{O})\text{OCH}_3$ et $\text{CH}_3\cdot\text{CHC}(\text{O})\text{OCH}_3$. Parmi les voies radicalaires les plus importantes, nous notons les métathèses avec des atomes d'hydrogène et des radicaux hydroxyles conduisant à la formation du radical $\text{CH}_2=\text{CHC}(\text{O})\text{OCH}_2\cdot$ (35% de sa consommation).

Partie IV Etude expérimentale et simulation de l'oxydation des esters méthyliques et éthyliques

L'analyse de vitesse de l'acrylate d'éthyle montre une similarité avec les voies de consommation de l'acrylate de méthyle à l'exception de l'apparition de la voie de formation de l'éthylène et de l'acide acrylique par décomposition unimoléculaire de l'ester (20%).

Par ailleurs, les plus importantes voies de consommation de crotonate de méthyle sont les métathèses avec des atomes d'hydrogène et des radicaux hydroxyles (63%). Elles conduisent principalement à la formation de deux radicaux: $\text{CH}_3\text{CH}=\text{CHC}(\text{O})\text{OCH}_2^\cdot$ et $^\cdot\text{CH}_2\text{CH}=\text{CHC}(\text{O})\text{OCH}_3$ stabilisés par résonance. L'addition d'hydrogène sur la double liaison du crotonate de méthyle constitue une autre voie importante de sa consommation (26%). Cependant, la principale voie de consommation de crotonate d'éthyle est la réaction d'élimination unimoléculaire conduisant à la formation de l'éthylène et de l'acide crotonique (45%). Les réactions de métathèses représentent 37% de la consommation de l'ester. Par contre, les réactions d'addition d'hydrogène sur la double liaison comptent seulement 8% dans le cas de cet ester.

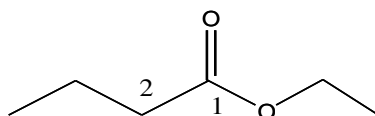
IV.1.4.3 Analyse de sensibilité

Afin de mettre en évidence l'influence des réactions proposées, nous avons effectué une analyse de sensibilité dans les mêmes conditions que celles de l'analyse de vitesse. Cette analyse renseigne sur l'évolution des flux de consommation de l'ester lorsque les constantes de vitesse des principales voies de sa consommation sont multipliées par 10. Un coefficient positif ou négatif est attribué à chaque réaction selon son impact, respectivement sur l'augmentation ou la diminution des délais d'auto-inflammation (cf. Figure II.15 dans le chapitre II).

IV.2 Etude en réacteur tubulaire à écoulement piston

Nous exposerons les résultats expérimentaux de la combustion du butanoate d'éthyle, réalisée dans un réacteur tubulaire à écoulement piston. Ces résultats sont par la suite comparés et confrontés à un modèle cinétique détaillé. La modélisation avec les concentrations des réactifs et des produits issus expérimentalement permet de vérifier les prédictions du modèle. Les manipulations qui ne permettent que la mesure de délais d'auto-inflammation offrent moins de possibilités de validation; seule la réactivité globale du système importe alors, et il est plus difficile d'estimer la validité d'un mécanisme réactionnel détaillé et la pertinence des constantes de vitesses adoptées dans le modèle.

Le but de cette étude est donc d'analyser dans le détail l'oxydation des esters éthyliques en prenant comme molécule modèle le butanoate d'éthyle. La formule développée de cette molécule est illustrée sur la figure (IV.1).



Butanoate d'éthyle

Figure IV.1. Formule développée du butanoate d'éthyle

Les principales propriétés physico-chimiques intervenant dans sa combustion sont récapitulées dans le tableau IV.1 ci-dessous :

Tableau IV.1. Propriétés physico-chimiques du butanoate d'éthyle ($\geq 99.5\%$)
(Fluka/Sigma-Aldrich)

Propriétés	Valeurs
Masse molaire (g.mole ⁻¹)	116.16
Densité (d_4^{15})	0.879
Température d'ébullition	120
Température d'auto-inflammation (°C) à 1 atm	463
Point d'éclair (°C)	26

IV.2.1 Conditions opératoires

Notre étude est réalisée à partir de trois mélanges (butanoates d'éthyle/oxygène/hélium) définis par leur richesse et la dilution des réactifs. Le mélange stœchiométrique a été testé à trois températures différentes et pour des temps de passage allant de 0.65 s à 1.4 s définis dans les conditions normales de pression et de température. Le montage expérimental est à la pression atmosphérique. Les différents mélanges sont fortement dilués (1.3% en ester) dans un gaz inerte, l'hélium, afin de limiter les risques d'auto-inflammation et les variations de température dues à l'exothermicité de la réaction. Le tableau II.2 dans la partie (II) présente les conditions expérimentales imposées pour l'oxydation du butanoate d'éthyle en réacteur piston.

IV.2.2 Identification des produits analysés

L'analyse par chromatographie en phase gazeuse et par analyse Infrarouge non dispersive a montré que les principaux produits identifiés et quantifiés de l'oxydation du butanoate d'éthyle dans nos conditions expérimentales sont :

- Pour les composés condensables : l'acide butanoïque C₃H₇COOH, l'acide acrylique C₂H₃COOH, le propanal C₂H₅CHO, l'acroléine C₂H₃CHO et l'acétaldéhyde CH₃CHO.
- Pour les composés non condensable : le monoxyde de carbone CO, le dioxyde de carbone CO₂, le méthane CH₄, l'acétylène C₂H₂, l'éthylène C₂H₄, l'éthane C₂H₆, le

Partie IV Etude expérimentale et simulation de l'oxydation des esters méthyliques et éthyliques

propène C_3H_6 , l'allène aC_3H_4 , le propyne pC_3H_4 , le buta-1,3-diène $1,3-C_4H_6$, le 1-butène $1C_4H_8$.

- Quelques produits supplémentaires ont pu être identifiés par GC/MS sans être quantifiés. Il s'agit du méthanol CH_3OH , de l'éthanol C_2H_5OH , de l'acide formique $HCOOH$, de l'acide propionique C_2H_5COOH , du 2-butène $2-C_4H_8$, du butanal C_3H_7CHO et de l'oxyde d'éthylène (oxirane) C_2H_4O .

IV.2.3 Bilan de matière

Le bilan de matière en carbone dans le réacteur piston a été traduit par l'égalité qui doit théoriquement exister entre la fraction molaire d'atomes de carbone entrante, $x_{entrée}$ et la fraction molaire d'atomes de carbone sortante, x_{sortie} (cf. annexe A). Généralement, on admet qu'un bilan de carbone boucle correctement lorsque l'écart entre les fractions molaires de carbone à l'entrée et à la sortie n'excède pas 15%. Nous avons pu constater, lors de nos manipulations, que le bilan de carbone varie entre 5% et 10% et évolue en fonction de la conversion.

IV.2.4 Reproductibilité des résultats

Ces expériences se traduisent par les courbes présentées dans le chapitre (III). La plupart des points expérimentaux ont été doublées voire triplées afin d'obtenir des profils cohérents et une estimation expérimentale de la marge d'erreur. Dans l'ensemble, une bonne reproductibilité a été constatée.

IV.2.5 Etude paramétrique

- *L'influence de la température* : sur l'évolution des fractions molaires des réactifs et des produits, les trois autres paramètres étant alors être fixés (richesse, temps de passage et fraction molaire d'entrée en butanoate d'éthyle). Le but est de mettre en évidence l'effet de la température et l'existence éventuelle d'un coefficient négatif de température. Nous avons fait varier la température de consigne du four dans les domaines de basse et haute températures entre 500 et 1200 K. Les figures III.3 à III.5 du chapitre (III) représentent l'évolution des fractions molaires en fonction de la température de consigne du four (pour des richesses $\varphi = 0.5$, $\varphi = 1.1$ et $\varphi = 1.6$). Sur les figures III.3-III.5 (cf. chapitre III), aucun coefficient négatif de température n'apparaît pour le domaine des basses températures.

Partie IV Etude expérimentale et simulation de l'oxydation des esters méthyliques et éthyliques

➤ *Influence de la richesse* : sur l'évolution de la fraction molaire en fonction de la température de consigne, en maintenant constant le temps de passage théorique ($\tau_{TPN} = 930$ ms) et la fraction molaire d'entrée ($x=1.3\%$). Ainsi, les figures III.3, III.4 et III.5 du chapitre (III) montrent l'évolution des fractions moléculaires en fonction de la température pour trois valeurs de richesse ϕ (0.5, 1.1 et 1.6). L'augmentation de la richesse n'a pas d'effet notable sur la réactivité notamment sur la nature des produits analysés.

➤ *Influence du temps de passage* : sur l'évolution des fractions molaires des réactifs et des produits (figures III.7 et III.8 du chapitre (III)) pour les conditions: $\phi = 1$, $x=1.3\%$, $T=700$ K, $T=800$ K et $T=1000$ K,. Nous constatons qu'aux températures de 700 K et 800 K, le butanoate d'éthyle n'est consommé que par décomposition unimoléculaire conduisant à la formation de l'acide butanoïque et de l'éthylène. Cependant, les réactifs sont intégralement consommés à 1000 K. Pour la plupart des produits, la vitesse de consommation devient plus importante pour les temps de passage élevés.

IV.2.6 Modélisation et simulation des résultats obtenus en tube à choc

IV.2.6.1 Comparaison simulation et expérience

Le mécanisme réactionnel de l'oxydation du butanoate d'éthyle à haute température a été généré automatiquement grâce à la nouvelle version d'EXGAS-ESTERS décrite dans la partie (III) précédente. Il contient 117 espèces impliquées dans 1035 réactions. Le mécanisme à basse température n'a pas été développé dans le cadre de ce travail.

La simulation numérique des réacteurs chimiques s'appuie sur l'utilisation de la bibliothèque de programmes CHEMKIN II (Kee et al., 1993). Les modèles implantés sont relatifs à des réacteurs idéaux (parfaitement agités ou à écoulement piston). En conséquence, les dimensions du réacteur tubulaire de l'oxydation permettent un écoulement proche de l'écoulement piston dans les conditions opératoires étudiées. La simulation a été réalisée par le logiciel PSR de CHEMKIN II en modélisant le réacteur piston comme une cascade de 56 réacteurs parfaitement agités (RPA). Les figures III.3-III.5, III.7 et III.8 données dans le dans le chapitre (III) illustrent ces validations. Pour toutes les figures décrites, les symboles représentent les points expérimentaux et les courbes les résultats des simulations. Dans l'ensemble, le modèle reproduit de manière satisfaisante les résultats expérimentaux.

IV.2.6.2 Analyse de flux

Une analyse qualitative des voies réactionnelles est fournie dans le chapitre (III). Cette analyse a été faite à deux températures 800 K et 943 K et pour deux richesses $\varphi = 1.1$ et $\varphi = 1.6$. Les principales réactions de consommation de chaque espèce sont extraites du mécanisme réactionnel. Le schéma de la figure III.10a représentant l'analyse d'un mélange à $\varphi = 1.1$ et $T=943$ K (cf. chapitre III). Celle-ci montre que la principale voie de consommation du carburant est la réaction d'élimination unimoléculaire par passage d'un cycle centré à six menant à la formation de l'éthylène et de l'acide butanoïque (98%). Le reste du carburant subit une métathèse avec les radicaux $\cdot\text{CH}_3$ où l'élimination d'un atome d'hydrogène se fait essentiellement à partir du carbone en position α par rapport au groupe carbonyle. Par ailleurs, l'acide butanoïque est majoritairement décomposé par métathèse avec les radicaux $\cdot\text{H}$, $\cdot\text{OH}$ et $\cdot\text{CH}_3$ conduisant à la formation de quatre radicaux primaires: $\text{CH}_3\text{CH}_2\text{CH}_2\text{OO}\cdot$, $\cdot\text{CH}_2\text{CH}_2\text{CH}_2\text{COOH}$, $\text{CH}_3\text{CH}_2\cdot\text{CHCOOH}$, $\text{CH}_3\cdot\text{CHCH}_2\text{COOH}$. Les mêmes processus de consommations ont été constatés pour l'analyse faite sur le mélange riche $\varphi = 1.6$ à 943 K. De plus, l'analyse de flux réalisée pour une température de 800 K montre aussi que la principale voie de consommation du butanoate d'éthyle est la réaction d'élimination unimoléculaire. Celle-ci contribue à 72% de la consommation du carburant pour $\varphi = 1.1$ et à 77% de sa décomposition pour $\varphi = 1.6$. Les réactions de métathèses avec des petits radicaux ($\cdot\text{OH}$, $\cdot\text{H}$, $\cdot\text{CH}_3$ et $\text{HO}_2\cdot$) représentent les autres voies de consommation du carburant conduisant principalement à la formation d'un radical avec un site actif en position α du groupe carbonyle. Quand à l'acide butanoïque, qui est le produit majoritaire de l'oxydation du butanoate d'éthyle, il réagit principalement par métathèses avec des radicaux $\cdot\text{H}$, $\cdot\text{OH}$ et $\cdot\text{CH}_3$ pour former ses différents radicaux.

IV.2.6.3 Analyse de sensibilité

Une analyse de sensibilité a été réalisée à 943 K et 800 K pour les trois mélanges réactionnels pauvre, stœchiométrique et riche. La figure III.11 du chapitre (III) représente cette analyse pour laquelle les coefficients de sensibilité en concentration du butanoate d'éthyle ont été calculés. Un coefficient positif ou négatif est attribué à chaque réaction selon son impact, respectif sur l'augmentation ou la diminution de la réactivité. Dans ces conditions d'analyse, la concentration en butanoate d'éthyle est essentiellement sensible à la réaction de décomposition unimoléculaire par passage d'un cycle centré à six, où l'augmentation de sa constante de vitesse

fait accroître la consommation du carburant. Par ailleurs, d'autres réactions ont un effet inhibiteur comme celle de la combinaison des radicaux méthyles ($\cdot\text{CH}_3$) pour former l'éthane.

IV.3 Conclusion

Nous avons présenté, dans cette partie, les mesures des délais d'auto-inflammation des esters à courte chaîne carbonée (acrylate d'éthyle, acrylate de méthyle, crotonate d'éthyle crotonate de méthyle et butanoate d'éthyle) dans un tube à onde de choc à haute température et haute pression. L'oxydation des cinq esters étudiés a été modélisée grâce aux mécanismes décrits dans la partie (III). Globalement, les simulations à haute température reproduisent correctement les points expérimentaux. De plus, les analyses de vitesse et de sensibilité ont fourni des indications sur les principales voies de consommation des esters modélisés et sur leurs produits majoritaires de dégradation.

Par ailleurs, nous avons aussi présenté l'étude expérimentale de l'oxydation du butanoate d'éthyle dans un réacteur piston, à pression atmosphérique et dans les domaines de basse et haute température (500 - 1200 K). L'évolution des fractions molaires, mesurées à la sortie du réacteur a été modélisée avec le mécanisme réactionnel utilisé pour le cas du tube à choc. Des voies de consommation du butanoate d'éthyle et de l'acide butanoïque ont pu être écrites, à partir du modèle cinétique et de l'analyse de sensibilité. Ces voies ne représentent pas une liste exhaustive des voies réactionnelles envisageables pour le butanoate d'éthyle mais tentent de reproduire la formation des principaux produits observés expérimentalement. L'écriture des mécanismes incluant les réactions et les espèces caractéristiques présentes à basse température pourrait dans l'avenir compléter cette étude.

Conclusion & perspectives

Cette étude visait à mieux comprendre la chimie de la combustion des composés du biodiesel et a porté sur l'analyse expérimentale et théorique de l'oxydation des esters modèles du biodiesel, en montrant particulièrement l'intérêt d'esters éthyliques d'huiles végétales.

Dans la première partie, une recherche bibliographique a été présentée sur les ressources en matières premières pour la production du biodiesel, sa combustion dans les moteurs et la cinétique l'oxydation des esters alkyliques d'huiles végétales.

La deuxième partie a décrit les deux techniques expérimentales utilisées pour étudier la cinétique d'oxydation de cinq molécules modèles de biodiesel: le butanoate d'éthyle, le crotonate d'éthyle, l'acrylate d'éthyle, le crotonate de méthyle et l'acrylate de méthyle. L'auto-inflammation de ces cinq composés oxygénés a été étudiée dans un tube à onde de choc à haute température et à haute pression. Seule l'oxydation à pression atmosphérique et dans les domaines à basse et à haute température du butanoate d'éthyle a été réalisée dans un réacteur tubulaire à écoulement piston. Le Montage expérimental a été développé et amélioré pendant le temps de cette thèse, les nouvelles techniques d'analyse et de mises en œuvre expérimentales.

La troisième partie a résumé le descriptif de la dernière version d'EXGAS-ESTERS développée à partir de celle d'EXGAS-ALCANES (Biet et al., 2008) en prenant en compte l'effet de la fonction ester. Les mécanismes d'oxydation à haute température des esters étudiés ont été générés automatiquement; ces modèles comptent:

- 111 espèces impliquant 885 réactions pour l'acrylate d'éthyle,
- 103 espèces impliquant 826 réactions pour l'acrylate de méthyle,
- 128 espèces impliquant 954 réactions pour le crotonate d'éthyle,
- 119 espèces impliquant 885 réactions pour le crotonate de méthyle et,
- 117 espèces impliquant 1035 réactions pour le butanoate d'éthyle.

La validation de ces modèles cinétiques générés a consisté à reproduire à l'aide des simulations numériques les résultats expérimentaux obtenus dans des conditions opératoires variées.

La quatrième partie a regroupé les résultats expérimentaux et de simulation de l'oxydation du butanoate d'éthyle, de crotonate d'éthyle, d'acrylate d'éthyle, de crotonate de méthyle et d'acrylate de méthyle. *Les délais d'auto-inflammation* de mélanges ester/oxygène/argon ont été mesurés pour des richesses $\varphi = 0.25, 1$ et 2 , des fractions molaires de 0.4% , 0.5% et 1% en ester, des températures allant de 1200 à 1900 K et des pressions comprises entre 7 et 9 bars. Les simulations à haute température reproduisent correctement les points expérimentaux. De

plus, les analyses de vitesse et de sensibilité ont fourni des indications sur les principales voies de consommation des esters et sur leurs produits majoritaires de dégradation.

L'oxydation du butanoate d'éthyle dans les domaines de basse et de haute température a été réalisée dans un *réacteur piston à pression atmosphérique*. L'évolution des fractions molaires des réactifs (butanoate d'éthyle, O₂) ainsi que des produits majoritaires et minoritaires [CO, CO₂, acides saturés et insaturés, les hydrocarbures (C₁-C₄), des composés oxygénés (aldéhydes, alcools] ont été obtenus par chromatographiques en phase gazeuse (détection par FID et TCD et par analyse Infra-Rouge. Le modèle cinétique a permis de simuler avec un accord satisfaisant les fractions molaires de nombreux produits mesurés dans nos conditions expérimentales. Les voies de consommation du butanoate d'éthyle et de l'acide butanoïque ont pu être explicitées, à partir du modèle cinétique et de l'analyse de sensibilité. Ces voies ne représentent pas une liste exhaustive des voies réactionnelles envisageables pour le butanoate d'éthyle. L'écriture des mécanismes incluant les réactions et les espèces caractéristiques présentes à basse température permettrait d'améliorer encore ce mécanisme.

Les perspectives de ce travail de thèse pourraient être d'améliorer la mesure des profils de température au cours de la réaction d'oxydation tout en s'assurant que la présence du thermocouple n'a pas d'effets catalytiques. Les mesures de l'hydrogène, du formaldéhyde et de l'eau peuvent être aussi améliorées.

Il serait en outre intéressant d'étendre cette étude à l'oxydation de l'oléate d'éthyle (ester majoritaire du biodiesel issu de l'huile de colza) et des acides carboxyliques, des produits majoritaires issus de la combustion des esters éthyliques.

De point de vue théorique, il serait utile d'élargir les modèles d'oxydation des esters étudiés aux domaines de basse température en ajoutant les processus spécifiques à basse température et de valider ensuite ces modèles cinétiques en comparant les résultats simulés et expérimentaux obtenus en (réacteur parfaitement agité, en machine à compression rapide,...)

Publications et communications issues de ce travail de thèse

Les résultats présentés dans ce mémoire ont fait l'objet de publications dans des revues à comité de lecture et de communications à des colloques internationaux. La liste en est donnée ci-après.

Publications

H.BENNADJI, P.A. GLAUDE, L. CONIGLIO, F. BILLAUD

Plug flow reactor and kinetic experimental investigation of ethyl butanoate combustion

Préparé pour soumission dans le journal Green Chemistry

H. BENNADJI, L.CONIGLIO, F. BILLAUD, R. BOUNACEUR, V. WARTH, P.A. GLAUDE., F. BATTIN-LECLERC

Oxidation of small unsaturated methyl and ethyl esters

International Journal of Chemical Kinetics, (soumis en cours de correction).

M.H. HAKKA, H. BENNADJI, J.BIET, M. YAHYAOU, B. SIRJEAN, V. WARTH, L. CONIGLIO-JAUBERT, O. HARBINET, P.A. GLAUDE, F. BILLAUD, F. BATTIN-LECLERC

Oxidation of Methyl and Ethyl Butanoates

International Journal of Chemical Kinetics 42 (2010) 226-252.

Proceedings

H. BENNADJI, J.BIET, L. CONIGLIO-JAUBERT, F. BILLAUD, P.A. GLAUDE, F. BATTIN-LECLERC

Experimental autoignition of C₄-C₆ saturated and unsaturated methyl and ethyl esters

Proceedings of the 4th European Combustion Meeting 2009, Vienne (Autriche).

Conférences sans actes

H.BENNADJI, L. CONIGLIO, P.A. GLAUDE, F. BILLAUD

Kinetic oxidation of ethyl butanoate as surrogate of biodiesel

Communication orale, 1st European Energy Conference 2010, Barcelone (Espagne).

H.BENNADJI, L. CONIGLIO-JAUBERT, F. BILLAUD

Étude expérimentale et modélisation de l'oxydation des esters en tube à onde de choc

Communication orale, Réunion annuelle du Groupe de Cinétique et Photochimie en Phase Gazeuse 2009, Créteil (France).

H. BENNADJI, L. CONIGLIO-JAUBERT, F. BILLAUD

Experimental and kinetic modeling study of ethyl butanoate combustion

Communication par affiche, 2nd International Congress on Green Process Engineering 2009, Venice (Italie).

H. BENNADJI, L. CONIGLIO-JAUBERT, F. BILLAUD

L'étude de l'oxydation du butanoate d'éthyle dans un réacteur tubulaire à écoulement piston

Communication par affiche, Doctoriales de Lorraine 2009, Saint-Dié des Vosges (France).

H. BENNADJI, J.BIET, L. CONIGLIO-JAUBERT, F. BILLAUD, P.A. GLAUDE, F. BATTIN-LECLERC

Experimental autoignition of C₄-C₆ saturated and unsaturated methyl and ethyl esters

Communication par affiche, 4th European Combustion Meeting 2009, Vienne (Autriche).

H. BENNADJI, H. HAKKA, L. CONIGLIO-JAUBERT, F. BILLAUD, J.BIET, P.A. GLAUDE, F. BATTIN-LECLERC

Experimental and kinetic modeling study of the oxidation of saturated and unsaturated ethyl and methyl esters in a shock-tube

Communication par affiche, au séminaire de l'école doctorale RP2E 2009, Nancy (France).

H. BENNADJI, H. HAKKA, L. CONIGLIO-JAUBERT, F. BILLAUD, J.BIET, P.A. GLAUDE, F. BATTIN-LECLERC

Experimental study of the oxidation of saturated and unsaturated ethyl and methyl esters in a shock-tube

Communication par affiche, 32nd International Symposium on Combustion 2008, Montréal (Canada).

Références bibliographiques

AGARWAL A.K. (2007)

Biofuels (alcohols and biodiesel) applications as fuels for internal combustion engines
Progress in Energy and Combustion Science, vol 33, pp 233-271

AMOROSO A., BEINE H.J., SPARAPANI R., NARDINO M., ALLEGRINI I. (2006)

Observation of coinciding arctic boundary layer ozone depletion and snow surface emissions of nitrous acid
Atmospheric Environment, vol 40, pp 1949-1956

BALLERINI D. (2006)

Les Biocarburants - Etats des lieux, perspectives et enjeux du développement
IFP Publications, Editions Technip, Paris, ISBN: 978-2-7108-0869-5

BALLERINI D. (2007)

Le plein de biocarburants? Enjeux et réalités
Editions Technip, Paris, ISBN: 978-2-7108-0882-4 (Institut français du pétrole)

BARBE P., BATTIN-LECLERC F., CÔME G.M. (1995)

Experimental and modelling study of methane and ethane oxidation between 773 and 1573 K
Journal de Chimie Physique, vol 92, pp 1666-1692

BATTIN-LECLERC F. (2008)

Detailed chemical kinetic models for the low-temperature combustion of hydrocarbons with application to gasoline and diesel fuel surrogates
Progress in Energy and Combustion Science, vol 34, pp 440-498

BAUGE J.C. (1998)

Etude de l'oxydation de composés insaturés en réacteur parfaitement agité en tube à onde de choc
Thèse, Institut National Polytechnique de Lorraine, Nancy

BAULCH D.L., COBOS C.J., COX R.A., FRANK P., HAYMAN G.D., JUST T., KERR J.A., MURRELLS T.P., PILLING M.J., TROE J., WALKER R.W., WARNATZ J. (1994)

Summary table of evaluated kinetic data for combustion modelling: supplement 1
Combustion and Flame, vol 98, pp 59-79

BELMEKKI N. (2001)

Etude de l'oxydation de composés insaturés en tube à onde de choc
Thèse, Institut National Polytechnique de Lorraine, Nancy

BELMEKKI N., GLAUDE P.A., DA COSTA I., FOURNET R., BATTIN-LECLERC F. (2002)

Experimental and modeling study of the oxidation of 1-butyne and 2-butyne
International Journal of Chemical Kinetics, vol 34, pp 172-183

BERTRAND T., BARBUSSE S., GAGNEPAIN L. (2008)

Les moteurs thermiques
Prédit 3, ADEME, Carrefour final

BIET J., HAKKA M.H., WARTH V., GLAUDE P.A., BATTIN-LECLERC F. (2008)
Experimental and modeling study of the low-temperature oxidation of large alkanes
Energy and Fuels, vol 22, pp 2258-2269

BRADLEY J.N. (1963)
Chemical applications of the shock tube
Meldola Medal Lecture (Royal Institute of Chemistry)

BUDA F., BOUNACEUR R., WARTH V., GLAUDE P.A., FOURNET R., BATTIN-LECLERC F. (2005)
Progress towards a unified detailed kinetic model for the autoignition of alkanes from C₄ to C₁₀ between 600 and 1200 K
Combustion and Flame, vol 142, pp 170-186

BUDA F. (2006)
Mécanismes cinétiques pour l'amélioration de la sécurité des procédés d'oxydation des hydrocarbures
Thèse, Institut National Polytechnique de Lorraine, Nancy

BURCAT A., SNYDER C., BRABBS T. (1985)
Ignition delay times of cyclopentene oxygen argon mixtures
In Shock Waves and Shock Tubes; Proceedings of the 15th International Symposium Stanford University Press, pp 335-341

Da COSTA I. (2001)
Etude de l'oxydation de composés aromatiques en réacteur parfaitement agité et en tube à onde de choc
Thèse, Institut National Polytechnique de Lorraine, Nancy

DAGAUT P., GAÏL S., SAHASRABUDHE M. (2007)
Rapeseed oil methyl ester oxidation over extended ranges of pressure, temperature, and equivalence ratio: Experimental and modeling kinetic study
Proceedings of the Combustion Institute, vol 31, pp 2955-2961

DAYMA G., GLAUDE P.A., FOURNET R., BATTIN-LECLERC F. (2003)
Experimental and modeling study of the oxidation of cyclohexene
International Journal of Chemical Kinetics, vol 35, pp 273-285

DAYMA. G. (2003)
Etude cinétique de l'oxydation et de la combustion de précurseurs de suies
Thèse, Institut National Polytechnique de Lorraine, Nancy

DEGOBERT P. (1995)
Automobiles and pollution
Editions Technip, Paris, ISBN: 2-7108-0676-2 (ifp)

DOOLEY S., CURRAN H.J., SIMMIE J.M. (2008)
Autoignition measurements and a validated kinetic model for the biodiesel surrogate, methyl butanoate
Combustion and Flame, vol 153, pp 2-32

- EL-NAHAS A.M., NAVARRO M.V., SIMMIE J.M., BOZZELLI J.W., CURRAN H.J., DOOLEY S., METCALFE W. (2007)
Enthalpies of formation, bond dissociation energies and reaction paths for the decomposition of model biofuels: ethyl propanoate and methyl butanoate
Journal of Physical Chemistry A, vol 111, pp 3727-3739
- FISHER E.M., PITZ W.J., CURRAN H.J., WESTBROOK C.K. (2000)
Detailed chemical kinetic mechanisms for combustion of oxygenated fuels
Proceedings of the Combustion Institute, vol 28, pp 1579-1586
- FOURNET R., BAUGE J.C, BATTIN-LECLERC F. (1999)
Experimental and modeling of oxidation of acetylene, propyne, allene and 1,3-butadiene
International Journal of Chemical Kinetics, vol 31, pp 361-379
- GAÏL S., THOMSON M., SARATHY S.M., SYED S.A., DAGAUT P., DIEVART P., MARCHESE A.J., DRYER F.L. (2007)
A wide-ranging kinetic modeling study of methyl butanoate combustion
Proceedings of the Combustion Institute, vol 31, pp 305-311
- GORNAY J. (2006)
Transformation par voie thermique de triglycérides et d'acides gras. Application à la valorisation chimique des déchets lipidiques
Thèse, Institut National Polytechnique de Lorraine, Nancy
- GORNAY J., CONIGLIO L., BILLAUD F., WILD G. (2009)
Steam cracking and steam reforming of waste cooking oil in a tubular stainless steel reactor with wall effects
Energy & Fuels, vol 23, pp 5663-5676
- GORNAY J., CONIGLIO L., BILLAUD F., WILD G. (2010)
Octanoic acid pyrolysis in a stainless-steel tube: What is the role of the coke formed on the wall?
Journal of Analytical and Applied Pyrolysis, vol 87, pp 78-84
- GRABOSKI M.S., Mc CORMICK R.L. (1998)
Combustion of fat and vegetable oil derived fuels in Diesel engines
Progress in Energy and Combustion Science, vol 24, pp 125-164
- GRIFFITHS J.F. (1995)
Reduced kinetic models and their application to practical combustion systems
Progress in Energy and Combustion Science, vol 21, pp. 25-107
- GUO H., WANG T., BLAKE D.R., SIMPSON I.J., KWOK Y.H., LI Y.S. (2006)
Regional and local contributions to ambient non-methane volatile organic compounds at a polluted rural/coastal site in Pearl River Delta, China
Atmospheric Environment, vol 40, pp 2345-2359
- HADJALI K., CROCHET M., VANHOVE G., RIBAUOUR M., MINETTI R. (2009)
A study of the low temperatures autoignition of methyl esters
Proceedings of the Combustion Institute, vol 32, pp 239-246

HAKKA M.H. (2010)

Etude de l'oxydation en phase gazeuse de composants des gazoles et des biocarburants Diesel
Thèse, Institut National Polytechnique de Lorraine, Nancy

HAKKA M.H., BENNADJI H., BIET J., YAHYAOUI M., SIRJEAN B., WARTH V.,
CONIGLIO L., HERBINET O., GLAUDE P.A., BILLAUD F., BATTIN-LECLERC F. (2010)
Oxidation of Methyl and Ethyl Butanoates

International Journal of Chemical Kinetics, vol 42, pp 226-252

HENNICO A., CHODORGE J.A., FORESTIÈRE A. (1995)

Esterfip, a transestérification process to produce bio-diesel from renewable energy sources
pp 763-767.

HERBINET O., PITZ W.J., WESTBROOK C.K. (2008)

Detailed chemical kinetic oxidation mechanism for biodiesel surrogate
Combustion and Flame, vol 154, pp 507-528

KAIRAITIS D.A., STIMSON V.R., (1968)

The thermal decompositions of ethyl trans-crotonate and ethyl n-butyrate
Australian Journal of Chemistry, vol 21, pp 1349-1354

KEE R. J., RUPLEY F.M., MILLER J.A. (1993)

CHEMKIN II: A FORTRAN chemical kinetics package for the analysis of gas-phase chemical kinetics

Sandia Laboratories Report, SAND 89-8009B

LAPUERTA M., HERREROS J.M., LYONS L.L., GARÍA-CONTRERAS R., BRICEÑO Y.
(2008)

Effect of the alcohol type used in the production of waste cooking oil biodiesel on diesel performance and emissions
Fuel, vol 87, pp 3161-3169

LOTERO E., LIU Y., LOPEZ D.E., SUWANNAKARN K., BRUCE D.A., GOODWIN J.G.,
JR (2005)

Synthesis of Biodiesel via Acid Catalysis,
Industrial and Engineering Chemistry Research, vol 44, pp 5353-5363

LUO Y.R. (2003)

Handbook of Bond Dissociation Energies in Organic Compounds
CRC Press LLC: Boca Raton, FL, p 380

MAKAREVICIENE V., JANULIS P. (2003)

Utilization of ethyl ester of waste vegetable oils as fuel in diesel engines
Renewable Energy, vol 28, pp 2395-2403

METCALFE W.K., DOOLEY S., CURRAN H.J., SIMMIE J.M., EL-NAHAS A.M.,
NAVARRO M.V. (2007)

Experimental and modeling study of C₅H₁₀O₂ ethyl and methyl esters
Journal of Physical Chemistry A, vol 111, pp 4001-4014

- METCALFE W.K., TOGBÉ C., DAGAUT P., CURRAN H.J., SIMMIE J.M. (2009)
A jet-stirred reactor and kinetic modeling study of ethyl propanoate oxidation
Combustion and Flame, vol 156, pp 250-260
- MULLER C., MICHEL V., SCACCHI G., COME G.M. (1995)
THERGAS: a computer program for the evaluation of thermochemical data of molecules and free radicals in the gas phase
Journal de Chimie Physique, vol 92, pp 1154-1178
- PLASARI E. (2009)
Génie de la réaction chimique : Conception, dimensionnement et mise en œuvre des réacteurs chimiques
Cours de l'Ecole Nationale Supérieure des Industries Chimiques-INPL de Nancy
- POLING B.E., PRAUSNITZ J.M., O'CONNELL J.P. (2001)
The properties of gases and liquids
Edition McGraw-Hill, 5th Edition ISBN10: 0-07-118971-8
- RAKOPOULOS C.D., ANTONOPOULOS K.A., RAKOPOULOS D.C., HOUNTALAS D.T., GIAKOUMIS E.G. (2006)
Comparative performance and emissions study of a direct injection Diesel engine using blends of Diesel fuel with vegetable oils or bio-diesels of various origins
Energy Conversion and Management, vol 47, pp 3272-3287
- RANZI E., FARAVELLI T., GAFFURI P., SOGARO A. (1995)
Low-temperature combustion: automatic generation of primary oxidation reactions and lumping procedures
Combustion and Flame, vol 102, pp 179-192
- RISTORI A., DAGAUT P., CATHONNET M. (2001)
The oxidation of n-hexadecane: experimental and detailed kinetic modelling
Combustion and Flame, vol 125, pp 1128-37
- SARATHY S.M., GAÏL S., SYED S.A., THOMSON M.J., DAGAUT P. (2007)
A comparison of saturated and unsaturated C₄ fatty acid methyl esters in an opposed flow diffusion flame and jet stirred reactor
Proceedings of the Combustion Institute, vol 31, pp 1015-1022
- SCHÖNBORN A., LADOMMATOS N., WILLIAMS J., ALLAN R., ROGERSON J. (2009)
The influence of molecular structure of fatty acid monoalkyl esters on diesel combustion
Combustion and Flame, vol 156, pp 1396-1412
- SESHADRI K., LU T., HERBINET O., HUMER S., NIEMANN U., PITZ W., SEISER R., LAW C.K. (2009)
Experimental and kinetic modeling study of extinction and ignition of methyl decanoate in laminar non-premixed flows
Proceedings of the Combustion Institute, vol 32, pp 1067-1074

SOVANNA P., SARIN C., SOPHEAK R. (2005)

Moteurs thermiques

Institut de technologie du Cambodge, Département de Génie industriel et mécanique, Agence universitaire de la Francophonie (AUF), pp 1-6

SZYBIST J.P., SONG J., ALAM M., BOEHMAN A.L. (2007)

Biodiesel combustion, emissions and emission control

Fuel Processing Technology, vol 88 (7), pp 679-691

TRANCHANT J., GARDAIS J.F., GORIN P., SERPINET J., UNTZ G. (1982)

Manuel pratique de chromatographie en phase gazeuse

Editions Masson, Paris, France.

TROE J. (1974)

Fall-of curves of unimolecular reactions

Berichte der Bunsengesellschaft Physical Chemistry, vol 78, p 478-485

TSANG W., HAMPSON R.F. (1986)

Chemical kinetic data base for combustion chemistry. Part 1: methane and related compounds

Journal of Physical Chemistry Reference Data, vol 15, pp 1087-1279

UBRICH E., JEULAND N. (2008)

Panorama 2008-ifp : Perspectives des évolutions réglementaires au-delà d'Euro 4 pour les véhicules légers et utilitaires légers (Euro 5, Euro 5+, Euro 6)

<http://www.ifp.fr/information-publications/notes-de-synthese-panorama/panorama-2008>

VILLERMAUX J. (1993)

Génie de la réaction chimique conception et fonctionnement des réacteurs

Edition Tec&Doc, 2^{ème} Edition, ISBN: 2-85206-759-5

WALTON S.M., WOOLDRIDGE M.S., WESTBROOK C.K. (2009)

An experimental investigation of structural effects on the autoignition properties of two C₅ esters

Proceeding of the Combustion Institute, vol 32, pp 255-262

WARTH V., STEF N., GLAUDE P.A., BATTIN-LECLERC F., SCACCHI G., COME G.M. (1998)

Computer-aided derivation of gas-phase oxidation mechanisms: Application to the modeling of the oxidation of n-butane

Combustion and Flame, vol 114, pp 81-102

WARTH V. (1999)

Conception et développement d'un logiciel de génération de mécanismes réactionnels d'oxydation et de combustion de substances organiques

Thèse, Institut National Polytechnique de Lorraine, Nancy

WARTH V., BATTIN-LECLERC F., FOURNET R., GLAUDE P.A., CÔME G.M., SCACCHI G. (2000)

Computer based generation of reactions mechanisms for gas-phase oxidation

Computers and Chemistry, vol 24, pp 541-560

Annexes

- A. Bilan de matière élémentaire et global
- B. Calcul du réacteur piston (Plug flow reactor)
- C. Mesure des profils de température
- D. Courbes d'étalonnage des RDM
- E. Description de la méthode d'étalon interne
- F. Conditions d'analyse des chromatographes et temps de rétention des produits
- G. Calcul du temps de passage
- H. Calcul de l'état des gaz après l'onde de choc

A. Bilans de matière élémentaire et global

Dans cette annexe, nous présentons les équations permettant de calculer les bilans de matière, à partir des grandeurs mesurées sur le pilote. Un schéma simplifié du pilote montrant les courants d'entrée et de sortie est présenté sur la figure (A.1). Les grandeurs mesurables y ont été également spécifiées. Les sources d'erreurs possibles conduisant à des incertitudes sur le bilan de matière global et sur l'élément de carbone sont estimées à $\pm 10\%$.

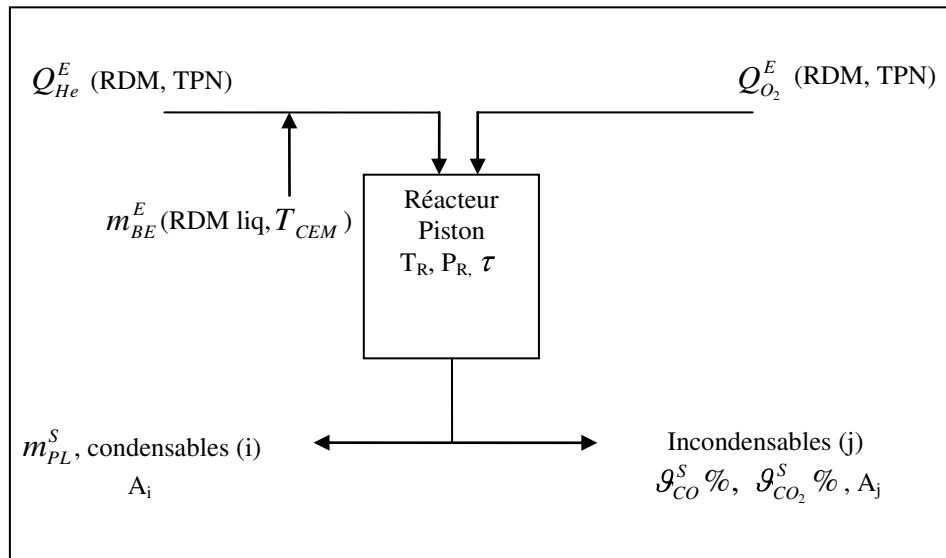


Figure A.1 : Schéma simplifié du réacteur

A.1 Analyse des produits condensables et incondensables

A.1.1 Condensables

Pour établir le bilan de matière global, la quantité d'eau formée durant l'oxydation de butanoate d'éthyle a été déduite par une différence entre la masse totale de la phase liquide (PL) et celle des condensables organiques quantifiés par une analyse CPG.

L'analyse par CPG (PR2100) donne l'aire correspond aux pics des condensables (A_i).

A.1.2 Incondensables

- les pourcentages volumiques en CO et en CO₂ ($g_{CO}^S \%$, $g_{CO_2}^S \%$) sont mesurés par l'analyseur Infra-Rouge (IR)
- l'aire correspond au pic de O₂ résiduel (A_{O_2}) est mesurée par chromatographe en phase gazeuse (CPG-PR1250) muni d'un détecteur catharomètre TCD,
- l'aire correspond aux pics des incondensables (A_j) est mesurée par chromatographe en phase gazeuse (CPG-Agilent 6850) muni d'un détecteur FID.

A.2 Inventaire des grandeurs mesurées et des constantes

$Q_{He,TPN}^E$	débit volumique d'He à l'entrée du réacteur donné dans les conditions TPN, L.min ⁻¹
$Q_{O_2,TPN}^E$	débit volumique d'O ₂ à l'entrée du réacteur donné dans les conditions TPN, L.min ⁻¹
m_{BE}^E	masse d'entrée de butanoate d'éthyle (BE) piégée pendant $\Delta t_{blanc}=10$ min
T_{four}	température de consigne du four, °C
T_i	température du réacteur en différents points, °C
T_a	température ambiante, °C
T_{CEM}	température de la chambre d'évaporation et de mélange du RDM liquide
P_a	pression ambiante, torr
P_R	pression mesurée à l'entrée du réacteur, torr
P_{CPG}	pression mesurée en amont des boucles d'échantillonnage des CPG
ρ_{BE}	masse volumique du réactif, 0.879 g.cm ⁻³
n_C	nombre d'atomes de carbone dans la substance
n_H	nombre d'atomes d'hydrogène dans la substance
n_O	nombre d'atomes d'oxygène dans la substance
Δt_{blanc}	durée de l'expérience réalisée à blanc pour quantifier masse d'ester délivrée par le RDM liquide
Δt_{exp}	durée de l'expérience pour chaque mesure de la masse des produits condensables
$g_{CO}^S \%$	fraction volumique en CO mesuré par IR à T_a, P_a
$g_{CO_2}^S \%$	fraction volumique en CO ₂ mesuré par IR à T_a, P_a
A_j	aire du pic mesurée par analyse CPG du composé incondensable j
A_i	aire du pic mesurée par analyse CPG du composé condensable i
A_E	aire du pic mesurée par analyse CPG de l'étalon interne E
K_E	coefficient de réponse de l'étalon interne (octane), $K_E=1$
$K_{i/E}^{m,exp}$	coefficient de réponse des produits condensables par rapport à l'étalon interne (octane)
K_i^{exp}	coefficient de réponse des produits incondensables (HC) obtenus par un étalonnage externe
m_E	masse d'étalon interne, 0.7 g
(*) m_{PL}^S	masse totale de la phase liquide (PL) obtenue par double pesée
M_{BE}	masse molaire du butanoate d'éthyle, 116.16 g.mol ⁻¹

M_{O_2}	masse molaire d'oxygène, 32 g.mol ⁻¹
M_{He}	masse molaire de l'hélium, 4 g.mol ⁻¹
M_i	masse molaire du produit condensable, g.mol ⁻¹
M_j	masse molaire du produit incondensable, g.mol ⁻¹
V_m	volume molaire d'un gaz parfait dans les conditions TPN, 22.4 L.mol ⁻¹
T_N	température normale, 273.15 K
P_N	pression normale, 760 torr
V_R	volume du réacteur, 27.65 cm ³
R	constante des gaz parfaits, 8.314411 Pa.m ³ .mol ⁻¹ .k ⁻¹
ν_{BE}	coefficient stœchiométrique de butanoate d'éthyle
ν_{O_2}	coefficient stœchiométrique de l'oxygène

(*) Phase liquide (PL) contient l'eau et les produits organiques condensables (i).

A.3 Equations conduisant à la résolution des bilans de matière

A.3.1 Variables spécifiques des courants d'entrée du pilote

Débit massique partiel du butanoate d'éthyle (BE)

$$\bar{F}_{BE}^E = \frac{m_{BE}^E}{\Delta t_{blanc}} \quad (A.1)$$

Débit molaire partiel du BE

$$F_{BE}^E = \frac{m}{\Delta t_{blanc} M_{EB}} \quad (A.2)$$

Débit volumique partiel du BE à l'entrée du réacteur calculé dans les conditions TPN

$$Q_{BE,TPN}^E = \frac{F_{BE}^E \cdot R \cdot T_N}{P_N} \quad (A.3)$$

Débit molaire partiel d'He

$$F_{He}^E = \frac{Q_{He,TPN}^E \times P_N}{R \cdot T_N} \quad (A.4)$$

Débit massique partiel d'He (*)

$$\bar{F}_{He}^E = F_{He}^E \cdot M_{He} \quad (A.5)$$

Masse d'He (*)

$$m_{He}^E = \bar{F}_{He}^E \cdot \Delta t_{exp} \quad (A.6)$$

Débit molaire partiel d'O₂

$$F_{O_2}^E = \frac{Q_{O_2,TPN}^E \times P_N}{R \cdot T_N} \quad (A.7)$$

Débit massique partiel d'O₂

$$\overline{F}_{O_2}^E = F_{O_2}^E \cdot M_{O_2} \quad (\text{A.8})$$

Masse d'O₂

$$m_{O_2}^E = \overline{F}_{O_2}^E \cdot \Delta t_{\text{exp}}$$

Débit molaire total

$$F_T^E = F_{BE}^E + F_{He}^E + F_{O_2}^E \quad (\text{A.9})$$

Masse totale

$$m_T^E = m_{BE}^E + m_{O_2}^E + m_{He}^E = \overline{F}_T^E \cdot \Delta t_{\text{exp}} \quad (\text{A.10})$$

Débit volumique total d'alimentation du réacteur calculé dans les conditions TPN

$$Q_{T,TPN}^S = Q_{He,TPN}^E + Q_{O_2,TPN}^E + Q_{BE,TPN}^E = \frac{F_T^E \cdot R \cdot T_N}{P_N} \quad (\text{A.11})$$

Débit massique total

$$\overline{F}_T = \overline{F}_{BE}^E + \overline{F}_{O_2}^E + \overline{F}_{He}^E \quad (\text{A.12})$$

Fraction molaire du BE

$$x_{BE}^E = \frac{F_{BE}^E}{F_T^E} \quad (\text{A.13})$$

Fraction molaire d'He

$$x_{He}^E = \frac{F_{He}^E}{F_T^E} \quad (\text{A.14})$$

Fraction molaire d'O₂

$$x_{O_2}^E = \frac{F_{O_2}^E}{F_T^E} \quad (\text{A.15})$$

Taux de dilution

$$Di = \frac{x_{He}^E}{x_{He}^E + x_{O_2}^E} \quad (\text{A.16})$$

Temps de passage

$$\tau = \frac{V_R}{Q_{T,T_{\text{four}}},P_R^E} \quad (\text{A.17})$$

Richesse

$$\varphi = \frac{x_{BE} \cdot V_{O_2}}{x_{O_2} \cdot V_{BE}} \quad (\text{A.18})$$

Fraction molaire en carbone

$$x_C^E = 6 \cdot x_{BE}^E \quad (\text{A.19})$$

Fraction molaire en oxygène

$$x_O^E = 2 \cdot x_{BE}^E + 2 \cdot x_{O_2}^E \quad (\text{A.20})$$

Fraction molaire en hydrogène

$$x_H^E = 12 \cdot x_{BE}^E \quad (\text{A.21})$$

(*) Le débit massique de l'hélium ainsi que sa masse ne changent pas entre l'entrée et la sortie du réacteur

A.3.2 Variables spécifiques des courants de sortie du pilote

A.3.2.1 Produits incondensables j (CO, CO₂, O₂, HC)

Pression partielle (O₂, HC)

$$P_j^S = \frac{A_j}{K_j^{\text{exp}}} \quad (\text{A.22})$$

Fraction molaire (O₂, HC)

$$x_j^S = \frac{P_j^S}{P_{CPG}} = \frac{F_j^S}{F_T^S} \quad (\text{A.23})$$

Débit molaire partiel

$$F_j^S = x_j^S \cdot F_T^S \quad (\text{A.24})$$

Débit massique partiel

$$\bar{F}_j^S = F_j^S \cdot M_j \quad (\text{A.25})$$

Masse du produit incondensable

$$m_j^S = \bar{F}_j^S \cdot \Delta t_{\text{exp}} \quad (\text{A.26})$$

Fractions molaire du CO et du CO₂ (considérés comme gaz parfait)

$$g_{CO}^S = x_{CO}^S = \frac{F_{CO}^S}{F_T^S} \quad (\text{A.27})$$

$$g_{CO_2}^S = x_{CO_2}^S = \frac{F_{CO_2}^S}{F_T^S} \quad (\text{A.28})$$

Débits massiques partiels du CO et du CO₂

$$\bar{F}_{CO}^S = g_{CO}^S \cdot F_T^S \cdot M_{CO} \quad (\text{A.29})$$

$$\bar{F}_{CO_2}^S = g_{CO_2}^S \cdot F_T^S \cdot M_{CO_2} \quad (\text{A.30})$$

Masses du CO et du CO₂

$$m_{CO}^S = \bar{F}_{CO}^S \cdot \Delta t_{\text{exp}} \quad (\text{A.31})$$

$$m_{CO_2}^S = \bar{F}_{CO_2}^S \cdot \Delta t_{\text{exp}} \quad (\text{A.32})$$

A.3.2.2 Produits condensables organiques i

Masse du produit i

$$m_i^S = \frac{m_E}{K_{i/E}^{\text{exp}}} \cdot \frac{A_i}{A_E} \quad (\text{A.33})$$

Débit massique partiel du produit i

$$\bar{F}_i^S = \frac{m_i^S}{\Delta t_{\text{exp}}} \quad (\text{A.34})$$

Débit molaire partiel du produit i

$$F_i^S = \frac{\bar{F}_i^S}{M_i} \quad (\text{A.35})$$

Fraction molaire du produit i

$$x_i^S = \frac{F_i^S}{F_T^S} \quad (\text{A.36})$$

A.3.2.3 Quantification de l'eauMasse de H₂O

$$m_{H_2O}^S = m_{PL}^S - \sum_i m_i^S \quad (\text{A.37})$$

Débit massique partiel de H₂O

$$\bar{F}_{H_2O}^S = \frac{m_{H_2O}^S}{\Delta t_{\text{exp}}} \quad (\text{A.38})$$

Débit molaire partiel de H₂O

$$F_{H_2O}^S = \frac{\bar{F}_{H_2O}^S}{M_{H_2O}} \quad (\text{A.39})$$

Fraction molaire de H₂O

$$x_{H_2O}^S = \frac{F_{H_2O}^S}{F_T^S} \quad (\text{A.40})$$

Débit molaire total

$$F_T^S = \sum_j F_j^S + \sum_i F_i^S + F_{He}^S = F_T^E \quad (\text{A.41})$$

$$\text{Et } F_{He}^S = F_{He}^E \quad (\text{A.42})$$

Débit massique total

$$\bar{F}_T^S = \bar{F}_{CO}^S + \bar{F}_{CO_2}^S + \bar{F}_{H_2O}^S + \sum_j \bar{F}_j^S + \sum_i \bar{F}_i^S \quad (\text{A.43})$$

Masse totale

$$m_T^S = m_{CO}^S + m_{CO_2}^S + m_{H_2O}^S + \sum_i m_i^S + \sum_j m_j^S = m_{CO}^S + m_{CO_2}^S + m_{PL}^S + \sum_j m_j^S \quad (\text{A.44})$$

Fraction molaire en carbone du produit condensable i

$$x_{C,i}^S = n_C \cdot x_i^S \quad (\text{A.45})$$

Fraction molaire en carbone du produit incondensable j

$$x_{C,j}^S = n_C \cdot x_j^S \quad (\text{A.46})$$

Fraction molaire totale en carbone

$$x_{C,T}^S = \sum_i x_{C,i}^S + \sum_j x_{C,j}^S \quad (\text{A.47})$$

Fraction molaire totale en hydrogène

$$x_{H,T}^S = 2 \cdot x_{H_2}^S + 2 \cdot x_{H_2O}^S + \sum_i n_H \cdot x_i^S + \sum_j n_H \cdot x_j^S \quad (\text{A.48})$$

Fraction molaire totale en oxygène

$$x_{O,T}^S = 2 \cdot x_{O_2}^S + x_{CO}^S + 2 \cdot x_{CO_2}^S + \sum_i n_O \cdot x_i^S + \sum_j n_O \cdot x_j^S \quad (\text{A.49})$$

A.3.3 Vérifications des bilans

A.3.3.1 Bilans globaux

$$\diamond \text{ Erreur relative au débit massique (\%)} = \frac{\overline{F}_T^E - \overline{F}_T^S}{\overline{F}_T^E} \cdot 100 \quad (\text{A.50})$$

$$\diamond \text{ Erreur relative à la masse (\%)} = \frac{m_T^E - m_T^S}{m_T^E} \cdot 100 \quad (\text{A.51})$$

A.3.3.2. Bilans élémentaires

$$\diamond \text{ Erreur relative au carbone (\%)} = \frac{x_C^E - x_C^S}{x_C^E} \cdot 100 \quad (\text{A.52})$$

$$\diamond \text{ Erreur relative à l'oxygène (\%)} = \frac{x_O^E - x_O^S}{x_O^E} \cdot 100 \quad (\text{A.53})$$

$$\diamond \text{ Erreur relative à l'hydrogène (\%)} = \frac{x_H^E - x_H^S}{x_H^E} \cdot 100 \quad (\text{A.54})$$

Etant donné, qu'on ne pouvait pas quantifier le dihydrogène et l'eau durant les expériences, le bilan élémentaire a été uniquement vérifié pour l'atome de carbone.

B. Calcul du réacteur piston (Plug flow reactor)

B.1 Critères de réalisation d'un réacteur piston

Le mélange réactionnel est en écoulement piston lorsqu'il progresse dans le réacteur par tranches parallèles et indépendantes n'échangeant pas de matière (diffusion axiale négligeable). En pratique, l'hypothèse de l'écoulement piston s'applique souvent à des réacteurs tubulaires où l'écoulement est très turbulent, ou à des réacteurs contenant un garnissage qui rend les profils de vitesse et de température sensiblement plats, tout au moins lorsque la réaction n'est pas très exothermique (Villiermaux, 1993). En effet, le réacteur tubulaire est pratiquement équivalent au réacteur piston s'il satisfait les deux conditions suivantes:

$$\text{Re} = \frac{ud\rho}{\mu} \geq 10^4 \quad (\text{B.1}) \quad \text{et} \quad \frac{L}{d} \geq 10^2 \quad (\text{B.2})$$

Où Re : nombre de Reynolds.

u : vitesse du mélange gazeux dans le réacteur tubulaire, m.s^{-1} .

d : diamètre du tube, m.

L : longueur du réacteur, m.

ρ : masse volumique du mélange gazeux, g.cm^{-3} .

μ : viscosité dynamique du mélange gazeux, Pa.s.

Soit F_i le débit molaire partiel (mol.s^{-1}) du constituant i de masse molaire M_i , g.mol^{-1} . Son débit massique $\bar{F}_i = F_i \times M_i$, g.s^{-1} . (B.3)

Donc le débit massique total d'un mélange gazeux :

$$\bar{F} = \sum \bar{F}_i = \sum F_i \times M_i = Q \times \rho, \text{ Kg.s}^{-1} \quad (\text{B.4})$$

Q : débit volumique total à la température et la pression du mélange gazeux, $\text{m}^3.\text{s}^{-1}$.

On considère que le gaz est parfait en régime continu, d'où le débit molaire F_i est calculé par la

$$\text{relation : } F_i = \frac{PQ_i}{RT}, \text{ mol.s}^{-1} \quad (\text{B.5})$$

Q_i : débit volumique partiel du constituant i , $\text{m}^3.\text{s}^{-1}$.

$$\text{La vitesse d'écoulement : } u = \frac{Q}{S} = \frac{4 \times Q}{\pi d^2} \quad (\text{B.6})$$

S : section droite d'un tube, m^2 .

A partir des relations (A.1), (A.3), (A.4) et (A.5), nous pouvons calculer le nombre de

$$\text{Reynolds par l'égalité : } \text{Re} = \frac{4 \times \bar{F}}{\pi d \mu} \quad (\text{B.7})$$

Le temps de passage τ (s) est défini à partir du débit volumique total d'entrée Q_E , dans les conditions de température et de pression d'entrée (T_E, P_E).

$$\tau = \frac{V}{Q_E} \quad (\text{B.8})$$

V : volume du réacteur tubulaire, m^3 .

Q_E : débit volumique du fluide à la température et la pression d'entrée du réacteur, $\text{m}^3 \cdot \text{s}^{-1}$.

En divisant les deux inégalités (B.1 et B.2), on obtient l'expression: $\tau = \frac{L}{u} \leq 10^{-2} \frac{\rho d^2}{\mu}$ (B.9)

En mettant dans la formule (B.9) les valeurs les plus désavantageuses rencontrées dans la pratique de ρ , d et μ , on vérifie qu'un réacteur piston ne dépasse pas pour les gaz $\tau \leq 100$ s, tandis que pour les liquides $\tau \leq 1$ h (Plasari, 2009).

* Détermination du diamètre et de la longueur des tubes

De l'expression $\text{Re} = \frac{ud\rho}{\mu} = \frac{4Q}{\pi d^2} \times \frac{d\rho}{\mu} = \frac{4Q\rho}{\pi d\mu} \geq 10^4$ on trouve $d \leq \frac{410^{-4}}{\pi} \times \frac{Q\rho}{\mu}$ (B.10)

De plus il faut satisfaire l'inégalité (A.2) $\frac{L}{d} \geq 10^2$ où L est calculé à partir du volume du

réacteur : $L = \frac{4V}{\pi d^2 n}$ (B.11)

Ces relations permettent à calculer d et L .

B.2 Modélisation des écoulements réels

Dans la plupart des cas, l'écoulement des fluides ne satisfait pas la définition des écoulements idéaux: piston ou parfaitement mélangé. L'écoulement réel est situé entre ces deux écoulements idéaux qui représentent les deux cas extrêmes opposés. Généralement, l'écoulement des fluides dans les réacteurs tubulaires est modélisé à l'aide de deux types de modèles: Modèle des réacteurs parfaitement agités en série caractérisé par le nombre équivalent (N) et modèle à dispersion axiale caractérisé par son paramètre de base, le critère de

Péclet calculé par la relation suivante : $Pe = \frac{uL}{D_{ax}}$ (B.12)

Où D_{ax} : coefficient de dispersion axiale, $\text{m}^2 \cdot \text{s}^{-1}$.

La pratique a montré que le modèle à dispersion axiale marche bien pour de faibles écarts par rapport à l'écoulement piston, tandis que le modèle des mélangeurs parfaits en cascade peut caractériser un écoulement réel dans tout son intervalle, du réacteur parfaitement agité ($Pe=0$, $N=1$) au réacteur piston ($Pe \rightarrow \infty$, $N \rightarrow \infty$).

L'équivalence entre les deux modèles est donnée par l'expression:

$$\frac{2}{Pe} - \frac{2}{Pe^2} \times \left(1 - \exp(-pe) \right) \approx \frac{1}{N} \quad (\text{Villiermaux, 1993}) \quad (\text{B.13})$$

Cette équation peut se traduire par la relation : $N = 0.5 \times Pe + 0.65$

$$\text{Où } Pe = 2 \times \left(N - 0.65 \right) \quad (\text{Plasari, 2009}) \quad (\text{B.14})$$

B.2.1 Méthodes d'estimation de D_{ax} dans le cas du tube vide

* En régime laminaire ($Re < 2300$), Taylor et Aris (Villiermaux, 1993) ont trouvé la formule:

$$\frac{D_{ax}}{D} = 1 + \frac{1}{192} \left(Re \cdot Sc \right) = 1 + \frac{1}{192} \left(\frac{ud}{D} \right)^2 \quad (\text{B.15})$$

$$\text{Avec : } Sc = \frac{\mu}{\rho D} \quad (\text{B.16})$$

Où D : coefficient de diffusion moléculaire, $m^2 \cdot s^{-1}$.

Sc : nombre de Schmidt.

* En régime intermédiaire et turbulent ($Re > 3000$), une formule semi-empirique caractérise d'une manière satisfaisante les résultats expérimentaux (Plasari, 2009):

$$\frac{D_{ax}}{ud} = 0.2 \exp \frac{10^4}{Re} \quad (\text{B.17})$$

B.2.2 Calcul du coefficient de diffusion moléculaire

Différentes corrélations empiriques ont été proposées dans la littérature pour estimer le coefficient de diffusion des mélanges gazeux à basse pression. Une corrélation empirique a été proposée par Fuller et al. (1969) (Poling et al., 2001) et qui est en accord avec l'expérience à 4% près dont l'exposant de température (1.75) correspond au cas d'un gaz parfaits.

* Le coefficient de diffusion moléculaire du binaire gazeux est donné par l'expression :

$$\triangleright D_{AB} = 1.4310^{-3} \times \frac{T^{1.75}}{P \times M_{AB}^{1/2} \times \left(\sum \nu_A^{1/3} + \sum \nu_B^{1/3} \right)^2} \quad (\text{B.18})$$

$$M_{AB} = 2 \times \left[\left(\frac{1}{M_A} \right) + \left(\frac{1}{M_B} \right) \right]^{-1} \quad (\text{B.19})$$

$\sum \nu$ est calculé pour chaque composé en faisant la somme des volumes de diffusion atomique (ν) donnés dans le tableau (B.1) suivant (Poling et al., 2001) :

Tableau B.1 : Volume de diffusion atomique

Volume de diffusion atomique ν	
C	15.9
H	2.31
O	6.11
Volume de diffusion des molécules simples	
He	2.67
O ₂	16.3

Une autre expression empirique proposée par Plasari (2005) est obtenue en modifiant la méthode de Wilke et Lee (1955) (Poling et al., 2001). Cette corrélation est généralement adoptée au gaz réel pour des températures élevées et représente un accord de l'ordre de 8% avec l'expérience.

$$\triangleright D_{AB} = 7.2810^{-8} \times \frac{m \times (4.34 - m) \times T^{1.5}}{P \times \left(V_{MA}^{1/3} + V_{MB}^{1/3} \right)^2 \times F(z)} \quad (\text{B.20})$$

Avec D_{AB} : Coefficient de diffusion moléculaire d'un binaire gazeux, $\text{m}^2 \cdot \text{s}^{-1}$.

T : température, K.

P : pression, bar.

M_A et M_B : masses molaires de A et de B, $\text{g} \cdot \text{mol}^{-1}$.

$$m = \left(\frac{1}{M_A} + \frac{1}{M_B} \right)^{1/2} \quad (\text{B.21})$$

$$F(Z) = \left(\frac{0.072}{Z^{4.12}} + \frac{0.0062}{Z^{1.25}} \right)^{0.125} \quad (\text{B.22})$$

$$Z = \frac{T}{0.77 \times \left(T_{CA} \times T_{CB} \right)^{1/2}} \quad (\text{B.23})$$

Le paramètre $F(Z)$ est déterminé expérimentalement et prend en compte les interactions entre les molécules.

T_{CA} et T_{CB} : températures critiques des composés purs A et B, K.

V_{MA} et V_{MB} : volumes molaires des constituants purs A et B, $\text{cm}^3 \cdot \text{mol}^{-1}$.

V_{MA} et V_{MB} sont calculés pour chaque composé en faisant la somme des volumes molaires (v) donnés dans le tableau (B.2) (Poling et al., 2001) :

Tableau B.2 : Volume molaire

Volume molaire v (cm ³ .mol ⁻¹)	
C	7
H	7
O	7
Volume molaires des molécules simples (cm ³ .mol ⁻¹)	
He	32.07
O ₂	25.6

* Calcul du coefficient de diffusion des mélanges gazeux

Dans les mélanges gazeux à plusieurs constituants, le coefficient de diffusion d'une espèce i est calculé par la relation (Poling et al., 2001) :

$$\triangleright D_{im} = \frac{1-x_i}{\sum_{j=1}^n \frac{x_j}{D_{ij}}} \quad i \neq j \quad (\text{B.24})$$

D_{im} : coefficient de diffusion de l'espèce i dans le mélange gazeux, m².s⁻¹.

D_{ij} : coefficient de diffusion de l'espèce i dans le constituant j, m².s⁻¹.

x_i : fraction molaire du constituant i.

x_j : fraction molaire du constituant j.

* Calcul de la viscosité d'un mélange gazeux

L'expression de calcul de la viscosité d'un mélange est donnée par la formule empirique (Poling et al., 2001) :

$$\mu_m = \frac{\sum \left(x_i \times \mu_i \times M_i^{1/2} \right)}{\sum \left(x_i \times M_i^{1/2} \right)} \quad (\text{B.25})$$

μ_i : viscosité dynamique du constituant i, Pas.s.

μ_m : viscosité dynamique du mélange gazeux, Pas.s.

* Calcul de la masse volumique d'un mélange gazeux

L'expression de calcul de la masse volumique d'un mélange gazeux est donnée par la formule empirique (Poling et al., 2001) :

$$\rho_m = \frac{PM_m}{RT}, \text{ kg.m}^{-3}. \quad (\text{B.26})$$

Avec : $M_m = \sum (M_i \times x_i)$: masse molaire moyenne du mélange gazeux, g.mol⁻¹.

B.3 Application numérique

L'application numérique des expressions données est décrite ci-dessous :

Le réacteur tubulaire a un diamètre interne de 8 mm et une longueur de 55 cm

Les données de calcul sont regroupées dans le tableau (B.3) ci-dessous :

Tableau B.3 : caractéristiques du mélange gazeux étudié

Constituant	M_i (g.mol ⁻¹)	V_{Mi} (cm ³ .mol ⁻¹)	* T_{Ci} (K)	Q_i (TPN) (m ³ .s ⁻¹)	F_i (mol.s ⁻¹)	\bar{F}_i (g.s ⁻¹)	x_i
C ₆ H ₁₂ O ₂ (EB)	116	135.34	571.00	3.85E-07	1.72E-05	2.00E-03	0.013
O ₂	32	16.30	154.58	3.00E-06	1.34E-04	4.29E-03	0.103
He	4	2.67	5.20	2.63E-05	1.18E-03	4.72E-03	0.884

* La température critique de chaque constituant a été estimée en utilisant *PRO/II Version 8.1*.

Calcul de la viscosité du mélange gazeux pour une température de 1250 K (cas le plus défavorable) en connaissant la composition du mélange et la viscosité de chaque constituant :

$$\mu_{O_2} = 546E-07 \text{ Pa.s et } \mu_{He} = 519.56E-07 \text{ Pa.s}$$

Compte tenu de la faible teneur en ester (1.3%), on peut négliger sa viscosité dans le calcul de la viscosité du mélange gazeux.

$$(B.25) \Rightarrow \mu_m = \frac{(0.103 \times 546E-07 \times 32^{1/2}) + (0.884 \times 519.56E-07 \times 4^{1/2})}{(0.103 \times 32^{1/2}) + (0.884 \times 4^{1/2})} = 5.26E-05 \text{ Pa.s}$$

D'où

$$(B.7) \Rightarrow Re = \frac{4 \times \sum \bar{F}_i}{\pi d \mu} = \frac{4 \times 1.10E-05}{3.14 \times 8E-03 \times 5.26E-05} \approx 34 \Rightarrow \text{régime laminaire (Re} < 2300),$$

donc on applique la formule de Taylor et Aris (Villermaux, 1993) pour calculer le coefficient

$$\text{de diffusion axiale, } D_{ax} \text{ (B.15) : } D_{ax} = D_m \times \left(1 + \frac{1}{192} \left(\frac{ud}{D_m} \right)^2 \right).$$

Les résultats des calculs sont regroupés dans les tableaux (B.4) et (B.5). Les résultats du tableau (B.4) ont été obtenus en calculant les coefficients de diffusion moléculaire par la formule de Fuller et al. (1969) à différentes températures appliquées durant les expériences menées dans le réacteur tubulaire. Pour les résultats du tableau (B.5), le calcul des coefficients de diffusion moléculaire a été fait en prenant l'expression proposée par Plasari (2005). Les deux expressions donnent des valeurs presque similaires. Ainsi pour les deux types de calcul, le nombre équivalent de réacteur parfaitement agité $N \approx 40$ est le même ce qui démontre que l'écoulement dans le réacteur tubulaire est bien piston.

Tableau B.4 : Résultats obtenus pour D calculé par la formule de Fuller et al. (1969)

T (K)	u (m.s ⁻¹)	D _{EBO2} (m ² .s ⁻¹)	D _{EBHe} (m ² .s ⁻¹)	D _{EBm} (m ² .s ⁻¹)	Pe	N
250	0.51	5.06E-06	1.78E-05	1.41E-05	45.12	24
300	0.62	6.96E-06	2.45E-05	1.94E-05	51.69	27
350	0.72	9.11E-06	3.21E-05	2.54E-05	57.98	30
400	0.82	1.15E-05	4.05E-05	3.21E-05	64.04	33
450	0.93	1.41E-05	4.98E-05	3.94E-05	69.89	34
500	1.03	1.70E-05	6.00E-05	4.74E-05	75.57	39
550	1.13	2.01E-05	7.08E-05	5.60E-05	81.09	41
600	1.24	2.34E-05	8.24E-05	6.52E-05	86.47	44
650	1.34	2.69E-05	9.48E-05	7.50E-05	91.72	47
700	1.44	3.06E-05	1.08E-04	8.54E-05	96.86	49
750	1.54	3.45E-05	1.21E-04	9.64E-05	101.89	52
800	1.65	3.87E-05	1.36E-04	1.08E-04	106.81	54
850	1.75	4.30E-05	1.51E-04	1.20E-04	111.65	57
900	1.85	4.75E-05	1.67E-04	1.32E-04	116.39	59
950	1.96	5.23E-05	1.84E-04	1.45E-04	121.05	61
1000	2.06	5.72E-05	2.01E-04	1.59E-04	125.64	64
1050	2.16	6.23E-05	2.19E-04	1.73E-04	130.14	66
1100	2.26	6.76E-05	2.38E-04	1.88E-04	134.58	68
1150	2.37	7.30E-05	2.57E-04	2.03E-04	138.95	70
1200	2.47	7.87E-05	2.77E-04	2.19E-04	143.25	72
1250	2.57	8.45E-05	2.98E-04	2.36E-04	147.49	74

Tableau B.5 : Résultats obtenus pour D calculé par l'expression de Plasari (2005)

T (K)	u (m.s ⁻¹)	Z _{EBO2}	Z _{EBHe}	F(Z _{EBO2})	F(Z _{EBHe})	D _{EBO2} (m ² .s ⁻¹)	D _{EBHe} (m ² .s ⁻¹)	D _{EBm} (m ² .s ⁻¹)	Pe	N
250	0.51	1.09	5.96	0.70	0.40	4.83E-06	1.86E-05	1.43E-05	45.82	24
300	0.62	1.31	7.15	0.64	0.39	6.92E-06	2.52E-05	1.98E-05	52.63	27
350	0.72	1.53	8.34	0.60	0.38	9.34E-06	3.26E-05	2.59E-05	59.03	30
400	0.82	1.75	9.53	0.56	0.37	1.21E-05	4.07E-05	3.26E-05	65.08	33
450	0.93	1.97	10.73	0.54	0.37	1.51E-05	4.95E-05	4.00E-05	70.83	36
500	1.03	2.19	11.92	0.52	0.36	1.84E-05	5.90E-05	4.80E-05	76.32	39
550	1.13	2.40	13.11	0.50	0.35	2.19E-05	6.91E-05	5.64E-05	81.58	41
600	1.24	2.62	14.30	0.49	0.35	2.57E-05	7.98E-05	6.54E-05	86.63	44
650	1.34	2.84	15.49	0.48	0.35	2.96E-05	9.11E-05	7.50E-05	91.49	46
700	1.44	3.06	16.68	0.47	0.34	3.38E-05	1.03E-04	8.49E-05	96.19	49
750	1.54	3.28	17.88	0.46	0.34	3.82E-05	1.16E-04	9.54E-05	100.75	51
800	1.65	3.50	19.07	0.45	0.33	4.27E-05	1.29E-04	1.06E-04	105.17	53
850	1.75	3.72	20.26	0.44	0.33	4.75E-05	1.42E-04	1.18E-04	109.46	55
900	1.85	3.93	21.45	0.44	0.33	5.24E-05	1.56E-04	1.30E-04	113.65	57
950	1.96	4.15	22.64	0.43	0.33	5.75E-05	1.71E-04	1.42E-04	117.73	60
1000	2.06	4.37	23.83	0.43	0.32	6.28E-05	1.86E-04	1.55E-04	121.72	62
1050	2.16	4.59	25.03	0.42	0.32	6.82E-05	2.02E-04	1.68E-04	125.61	63
1100	2.26	4.81	26.22	0.42	0.32	7.39E-05	2.18E-04	1.81E-04	129.43	65
1150	2.37	5.03	27.41	0.42	0.32	7.96E-05	2.35E-04	1.95E-04	133.17	67
1200	2.47	5.25	28.60	0.41	0.31	8.56E-05	2.52E-04	2.09E-04	136.83	69
1250	2.57	5.46	29.79	0.41	0.31	9.17E-05	2.70E-04	2.24E-04	140.43	71

C. Mesure des profils de température

La figure C.1 ci-dessous regroupe les mesures du profil de température pour les différentes consignes du four sous un milieu inerte (hélium) et sans réactions d'oxydation.

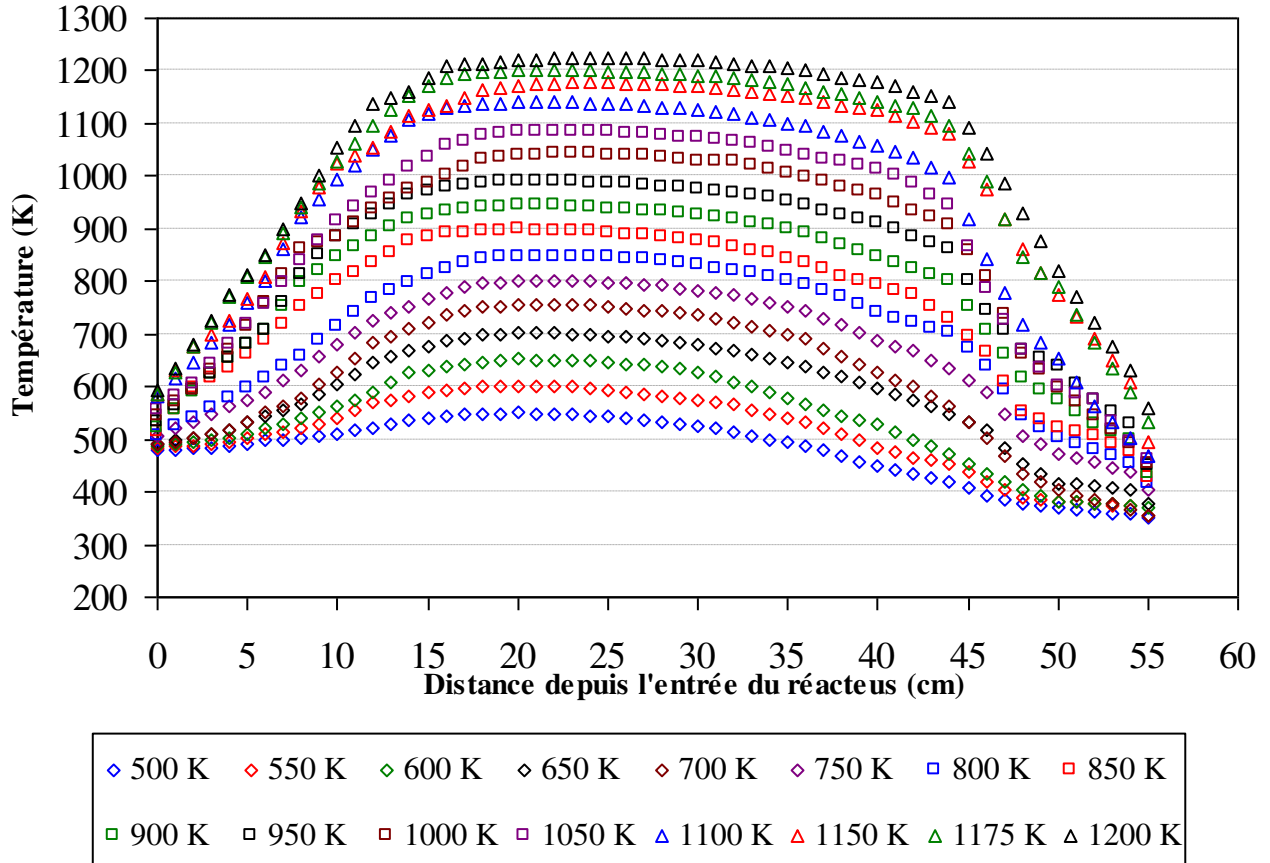


Figure C.1 : Mesure de température du réacteur pour différentes consignes du four

Il a été constaté que la présence du thermocouple dans le réacteur durant les réactions d'oxydation entraîne une instabilité dans les concentrations en monoxyde carbone (CO) et en dioxyde de carbone (CO₂).

D. Courbes d'étalonnage des RDM

Dans cette annexe, on représente les courbes d'étalonnage des différents débitmètres massique (RDM) utilisés pendant ma thèse. Pour tous les RDM, les étalonnages ont été effectués dans les conditions normales de pression (1 atm) et de température (273.15 K).

D.1 Etalonnage du RDM 280 Alphagaz pour l'O₂

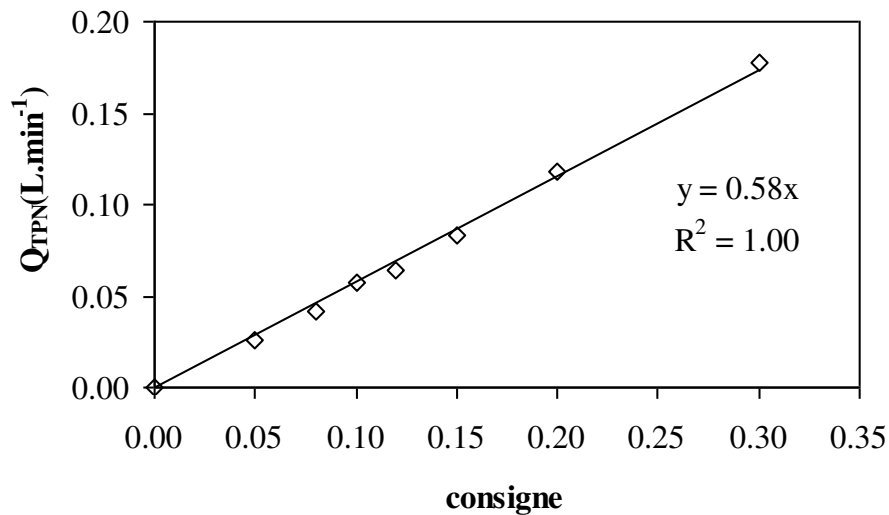


Figure D.1 : Etalonnage du RDM gaz pour l'O₂ (Oxydation)

D.2 Etalonnage du RDM 280 Alphagaz pour l'N₂

Ce RDM a été utilisé pour l'étalonnage zéro de l'analyseur IR COSMA destiné à l'analyse en ligne de monoxyde carbone et de dioxyde de carbone.

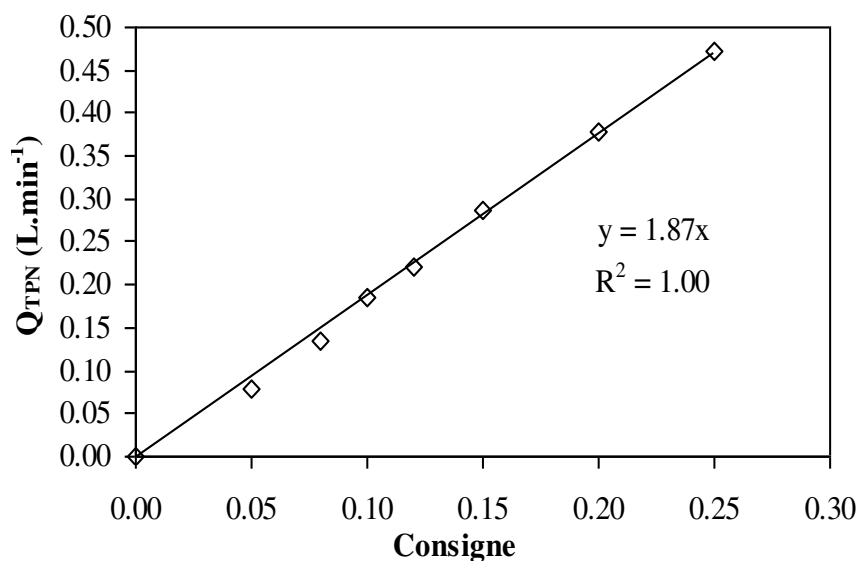


Figure D.2 : Etalonnage du RDM gaz pour N₂ (Etalonnage IR)

D.3 Etalonnage du RDM Bronkhorst (El-Flow)

Ce débitmètre a été utilisé pour régler le débit d'inerte dans la charge d'alimentation du réacteur au cours des réactions d'oxydation. Le RDM El-Flow a été étalonné pour deux gaz inertes l'azote et l'hélium. Les deux courbes d'étalonnage sont représentées sur la figure D.3 suivante.

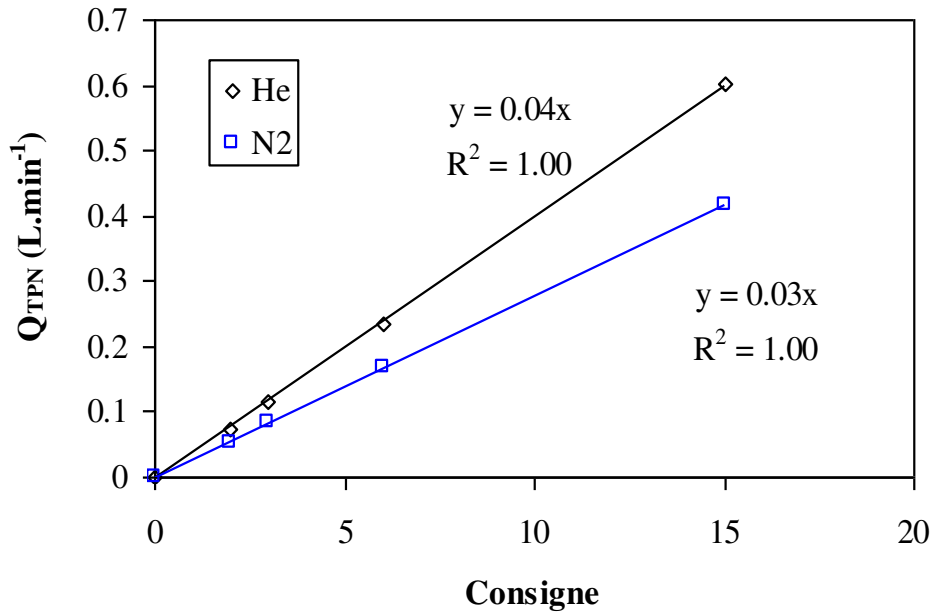


Figure D.3 : Etalonnage du RDM gaz pour He et N₂ (Oxydation)

E. Description de la méthode d'étalon interne

Dans cette annexe est décrite la méthode de l'étalon interne utilisée en chromatographie en phase gazeuse avec un détecteur à ionisation de flamme.

En chromatographie, l'aire d'un pic est en général proportionnelle à la quantité de matière injectée. Pour une injection d'une masse m_i d'un composé quelconque (i), l'aire sous le pic A_i correspondante s'exprime par la relation: $A_i = K_i^m \cdot m_i$ (E.1)

Toutefois, si on injecte un volume v_i de (i), l'aire du pic peut s'exprimer par : $A_i = K_i^v \cdot v_i$ (E.2)

On raisonnera sur m_i ou v_i selon la façon dont ont été préparées les solutions :

* Procédure en titre massique

Soit M_i la masse de (i) dans l'échantillon dont le volume total est V . Si v est le volume injecté : il contient une masse m_i de (i), et on aura :

$$A_i = K_i^m \cdot M_i \cdot \frac{v}{V} \quad (\text{E.3})$$

* Procédure en titre volumique

Soit V_i le volume de (i) dans l'échantillon dont le volume total est V . Si v est le volume injecté : il contient un volume v_i de A , et on aura:

$$A_i = K_i^v \cdot V_i \cdot \frac{v}{V} \quad (\text{E.4})$$

On pourrait donc faire un étalonnage de façon classique, en préparant des solutions de titre massique ou volumique connu et en injectant toujours le même volume v . Or compte tenu de la faible valeur de v , quelques dixièmes de μL , la reproductibilité du volume injecté est insuffisante pour obtenir des résultats précis. La méthode de l'étalon interne rend les résultats indépendants du volume injecté, sous réserve de rester dans le domaine de linéarité de réponse du détecteur (Tranchant et al., 1982).

E.1 Facteur de réponse

On admet avoir pu trouver un produit soluble (E) dans l'échantillon, sortant sous forme de pic isolé, proche du pic analysé et dont on peut introduire une concentration connue dans l'échantillon sans perturber celui-ci. L'injection d'une fraction v de V conduit à :

$$A_i = K_i^m \cdot M_i \cdot \frac{v}{V} \quad (\text{E.3})$$

$$\text{et } A_E = K_E^m \cdot M_E \times \frac{v}{V} \quad (\text{E.5})$$

Où M_i , M_E (ou V_i et V_E), v et V sont connus et A_i ainsi que A_E sont mesurées.

Le rapport des expressions (E.3) et (E.5) donne (E.6) :

$$\frac{A_i}{A_E} = \frac{K_i^m \cdot M_i}{K_E^m \cdot M_E} \quad (\text{E.6})$$

$$\text{Ou } \frac{A_i}{A_E} = \frac{K_i^v \cdot V_i}{K_E^v \cdot V_E} \quad (\text{E.7})$$

Donc le rapport $\frac{A_i}{A_E}$ est indépendant du volume injecté v .

On appelle facteur de réponse la valeur de K_i^m ou de K_i^v rapportée à celle de l'étalon, le facteur de réponse de l'étalon lui-même étant pris égal à 1.

E.2 Etalonnage

On peut faire une courbe d'étalonnage en préparant des solutions connues de (i) et (E),

contenant des rapports: $r_m = \frac{M_i}{M_E}$ (E.8) ou $r_v = \frac{V_i}{V_E}$ (E.9) variables. On obtient alors une droite

$$\text{d'étalonnage en portant } \frac{A_i}{A_E} = f(r), \text{ soit } \frac{A_i}{A_E} = \frac{K_i^m}{K_E^m} \times r_m \quad (\text{E.10})$$

$$\text{Ou } \frac{A_i}{A_E} = \frac{K_i^v}{K_E^v} \times r_v \quad (\text{E.11})$$

E.3 Calcul Direct

Si la courbe d'étalonnage est bien une droite passant par l'origine, on peut faire un calcul direct, après détermination des facteurs de réponse.

Le travail se fait en deux étapes :

1) Solution connue de A et de E pour déterminer $\frac{K_i^m}{K_E^m}$ ou $\frac{K_i^v}{K_E^v}$

2) A un volume connue V_s (ou une masse connue M_s) d'une solution à analyser contenant le composé (i) de volume V_i inconnu (ou de masse M_i inconnue), on ajoute un volume connu V_E (ou une masse connue M_E) de l'étalon.

$$\text{On obtient : } V_i = \frac{A_i}{A_E} \cdot \frac{K_E^v}{K_i^v} \cdot V_E \quad (\text{E.12}) \quad \text{ou} \quad M_i = \frac{A_i}{A_E} \cdot \frac{K_E^m}{K_i^m} \cdot M_E \quad (\text{E.13})$$

La teneur en (i) de l'échantillon peut être calculée soit en :

$$\text{- Teneur volumique} = \frac{V_i}{V_s} \cdot 100, (\%) \quad (\text{E.14})$$

$$\text{- Teneur massique} = \frac{M_i}{M_s} \cdot 100, (\%) \quad (\text{E.15})$$

$$\text{- Concentration massique} = \frac{M_i}{V_s}, (\text{g.L}^{-1}) \quad (\text{E.16})$$

$$\text{- Concentration molaire} \frac{M_i}{\text{Masse molaire de } (i) \times V_s}, (\text{mol.L}^{-1}). \quad (\text{E.17})$$

** Remarques*

a) L'étalon peut être utilisé pour doser simultanément plusieurs espèces, à la condition que la séparation soit satisfaisante.

b) La concentration de l'étalon doit être du même ordre de grandeur que celle de l'espèce à doser.



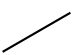
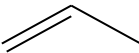
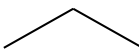
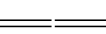
F. Conditions d'analyse des chromatographes et temps de rétention des produits

F.1 Description du chromatographe Agilent 6850 : Analyse et temps de rétention avec la colonne capillaire HP-PLOT Q

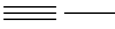
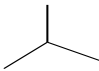
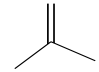
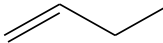
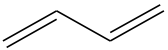
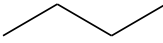
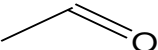
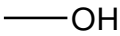
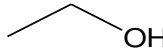
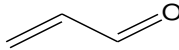
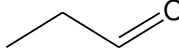
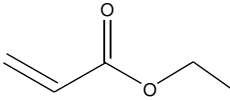
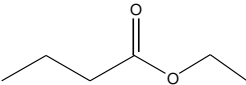
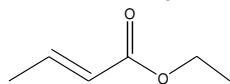
Tableau F.1 : Conditions d'analyse en chromatographie en phase gazeuse

Chromatographe	Agilent 6850 à détecteur FID (analyse en ligne)
Boucle	V=250 μ L T _{boucle} =180°C
Injecteur	T _{inject} =250°C Split=1/100 (Débit total arrivant dans l'injecteur=205 mL.min ⁻¹)
Colonne	HP-Plot Q (colonne capillaire : 30 m x 0.32 mm x 20 μ m) Gaz vecteur : He (P _{entrée colonne} =0.684 bar) Rampe de température : 60°C ->10 min, 5°C/min ->250°C, 250°C ->15 min Q _{He, colonne} =2 mL.min ⁻¹ (débit constant)
Détecteur	T _{détecteur} =300°C Q (H ₂)=30 mL.min ⁻¹ Q (Air)=400 mL.min ⁻¹ Q (He)=25 mL.min ⁻¹ (=débit colonne+makeup)

Tableau F.2 : Liste des molécules identifiées avec la colonne capillaire HP-PLOT Q

Nom de la molécule	Formule brute	Formule développée	Temps de rétention (min)	$A_j = K_j^{\text{exp}} \times P_j$
Méthane	CH ₄	-	2.02	25.95
Ethylène	C ₂ H ₄		3.05	50.05
Acétylène	C ₂ H ₂		3.20	58.05
Ethane	C ₂ H ₆		3.62	47.80
Propène	C ₃ H ₆		11.36	67.05
Propane	C ₃ H ₈		12.54	70.80
1,2- propadiène (allène)	A C ₃ H ₄		12.9	68.85

Annexe F Conditions d'analyse des chromatographes et temps de rétention des produits

Propyne	C_3H_4		13.65	66.75
Isobutane	C_4H_{10}		21.30	75.97
IsoButène	C_4H_8		21.95	83.96
1-Butène	C_4H_8		22.09	87.47
1,3-Butadiène	C_4H_6		22.41	98.17
N-Butane	C_4H_{10}		22.96	85.15
Acétaldéhyde	C_2H_4O		18.30	-
Méthanol	CH_4O		18.57	-
Ethanol	C_2H_6O		25.20	-
2-propenal (acroléine)	C_3H_4O		26.30	-
Propanal	C_3H_6O		26.95	-
Acrylate d'éthyle	$C_5H_8O_2$		38.6	-
Butanoate d'éthyle	$C_6H_{12}O_2$		43.85	-
Crotonate d'éthyle	$C_6H_{10}O_2$		44.70	-

F.2 Description du chromatographe PERICHROM (PR1250) : Analyse et temps de rétention avec la colonne de tamis moléculaire

Tableau F.3 : Conditions d'analyse en chromatographie en phase gazeuse

Chromatographe	PR1250 à détecteur TCD (analyse en ligne)
Boucle	V=3 mL T _{boucle} =Température ambiante (~25°C)
Colonne	Tamis moléculaire (5A°, 2.5m) N ₂ et He sont les gaz vecteurs, P _{entrée colonne} ~190 kPa Programme de température : 40°C =>10 min
Détecteur TCD	Intensité de courant : 80mA Makeup: 10 kPa T _{détecteur} = Température ambiante (~25°C) Polarité négative lorsque l'hélium est utilisé comme gaz vecteur

Tableau F.4 : Liste des molécules identifiées avec la colonne de tamis moléculaire

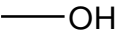
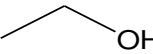
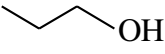
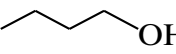
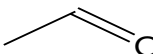
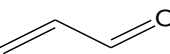
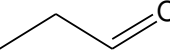
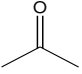



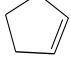
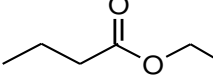
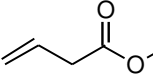
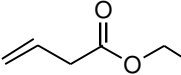
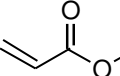
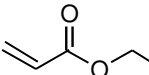
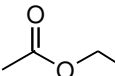
Nom de la molécule	Formule brute	Formule développée	Temps de rétention (min)	$A_j = K_j^{exp} \times P_j$
Dihydrogène	H ₂	H-H	1.15	~ 1.62
Dioxygène	O ₂	O=O	2.55	~ 14.59

F.3 Description du chromatographe PERICHROM (PR2100) : Analyse et temps de rétention avec la colonne capillaire type SGE BP 21

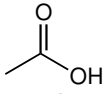
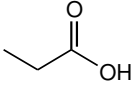
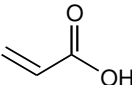
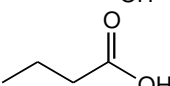
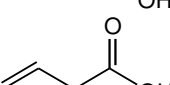
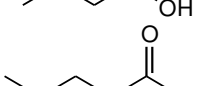
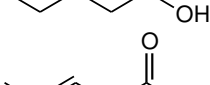
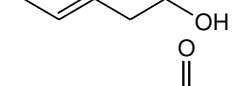
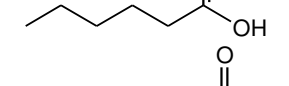
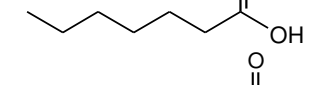
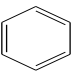
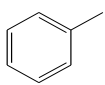
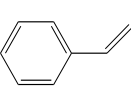
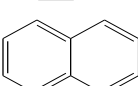
Tableau F.5 : Conditions d'analyse en chromatographie en phase gazeuse

Chromatographe	PR2100 à détecteur FID (analyse en différé)
Passeur automatique ALS 104	V _{injecté} = 0.1 µL Température ambiante (~25°C)
Colonne	SGE BP 21 (colonne capillaire : 30 m x 0.53 mm x 1 µm) N ₂ est le gaz vecteur, P _{entrée colonne} ~0,23 MPa Rampe de température: 40°C ->3 min, 30°C/min ->70°C, 70°C ->1 min, 1°C/min->250°C, 250°C->80 min P (N ₂) : 30 KPa
Détecteur	T _{détecteur} = 260°C P(H ₂)~50 KPa P(Air)~50 KPa

Tableau F.6 : Liste des molécules identifiées avec la colonne capillaire type SGE BP 21

Nom de la molécule	Formule brute	Formule développée	Temps de rétention (min)	$K_{i,E}^{m,exp}$	$K_{i,E}^{n,exp}$	$K_{i,E}^{n,cal}$
Méthanol	CH ₄ O		2.46	0.35	10.04	-
Ethanol	C ₂ H ₆ O		2.85	0.49	5.1	5.7
1- propanol	C ₃ H ₇ OH		5.02	0.63	3.02	3.33
1-Butanol	C ₄ H ₉ OH		9.64	0.63	2.45	2.35
Acétaldéhyde	C ₂ H ₄ O		1.51	0.35	7.41	8
Acroléine	C ₃ H ₄ O		2.1	0.44	4.67	4.21
(*) Propanal	C ₃ H ₆ O		1.9	0.43	4.49	4
Acétone	C ₃ H ₆ O		2	solvant	-	-
N-pentane	C ₅ H ₁₂		1.28	0.96	1.65	1.6
N-hexane	C ₆ H ₁₄		1.35	1	1.33	1.33
N-octane	C ₈ H ₁₈		1.75	1	1	Etalon
Cyclopentène	C ₅ H ₈		1.45	1.02	1.64	1.63
Butanoate d'éthyle	C ₆ H ₁₂ O ₂		4.6	0.58	1.7	1.68
Crotonate de méthyle	C ₅ H ₈ O ₂		7.8	0.52	2.2	2.19
Crotonate d'éthyle	C ₆ H ₁₀ O ₂		9.95	0.56	1.79	1.72
Acrylate de méthyle	C ₄ H ₆ O ₂		3.11	0.46	2.9	3.02
Acrylate d'éthyle	C ₅ H ₈ O ₂		3.7	0.52	2.17	2.19
Acétate d'éthyle	C ₄ H ₈ O ₂		2.34	0.43	3.04	2.91

Annexe F Conditions d'analyse des chromatographes et temps de rétention des produits

Acide acétique	C ₂ H ₄ O ₂		31.32	0,23	8.42	8
Acide propionique	C ₃ H ₆ O ₂		34.12	0.35	4.45	4
Acide Acrylique	C ₃ H ₄ O ₂		37.05	0.25	6.39	4.21
Acide butanoïque	C ₄ H ₈ O ₂		36.7	0.46	2.8	2.67
Acide Butenoïque	C ₄ H ₆ O ₂		39.8	0.39	3.36	2.76
Acide pentanoïque	C ₅ H ₁₀ O ₂		39.5	0.49	2.28	2
Acide 3-pentenoïque	C ₅ H ₈ O ₂		42.97	0.41	2.76	2.05
Acide hexanoïque	C ₆ H ₁₂ O ₂		42.13	0.54	1.84	1.6
Acide heptanoïque	C ₇ H ₁₄ O ₂		45.11	0.53	1.66	1.33
Acide octanoïque	C ₈ H ₁₆ O ₂		2.94	1.09	1.35	1.4
Benzène	C ₆ H ₆		2.94	1.09	1.35	1.4
Toluène	C ₇ H ₈		4.78	1.05	1.18	1.19
Styrène	C ₈ H ₈		19.3	1.04	1.05	1.05
Naphtalène	C ₁₀ H ₈		39.95	0.89	1	0.84

^(*) Pour l'étalonnage du propanal, on a utilisé le N-décane comme solvant.

Le tableau (F.6) montre que la méthode du nombre de carbone effectif (ECN) est tout à fait conforme avec l'étalonnage direct des composés (en particulier pour les hydrocarbures linéaires et aromatiques où un écart moyen de 3.5 % est observé). Un écart important est cependant constaté dans le cas des composés oxygénés. Par ailleurs, certains acides carboxyliques à longue chaîne carbonée et des aromatiques ont été étalonnés dans les perspectives d'étudier un biodiesel réel type ester éthylique d'huile végétale de colza (oléate d'éthyle : C₂₀H₃₈O₂).

G. Calcul du temps de passage

Deux références ont été utilisées pour déterminer le temps de passage dans le réacteur piston. Cette option a été adoptée afin de découpler les deux variables opératoires: température d'expérience et temps de passage, avec l'existence d'un profil de température au sein du réacteur piston.

Pour la comparaison qualitative des expériences menées à différentes conditions opératoires (température, temps de passage, richesse et dilution du mélange réactionnel), les conditions normales de température (273K) et de pression (1atm), invariables d'une expérience à une autre, ont été retenues comme référence.

Pour la comparaison quantitative des expériences avec les simulations, une référence proche des conditions réelles du réacteur a été retenue. Ces conditions correspondent à la pression mesurée durant la détermination expérimentale du profil de température le long du réacteur tubulaire et à la température moyenne correspondant à ce profil. Le temps de passage ainsi défini sera dit «physique», par opposition au temps de passage «théorique» défini dans les conditions normales de température et de pression.

G.1 Programme de calcul de la température moyenne

Le programme de calcul de la température moyenne, établi avec Matlab, est donné ci-dessous:

```

Clear all
clc
%Distance depuis l'entrée du réacteur (cm)
cons=[500 550 600 650 700 750 800 850 900 950 1000 1050 1100 1150 1175 1200];
nc=length(cons);
% Lire les données (les valeurs de température) à partir data.txt
bin=load('data.txt');
dist=bin(:,1);
%boucle sur les consignes. la température est dans bin(:,k+1)
for k=1:nc
Temp=bin(:,k+1);
somme=0;
ST=0; %surface totale
dx=1; % le pas de mesure de la température (cm)
L=55; %longueur du réacteur
for i=2:length(Temp)-1
somme=somme+Temp(i);
end
ST=(dx/2)*(Temp(1)+2*somme+Temp(length(Temp)));
Tmoyen(k)=ST/L;

```

%Affichage de la température moyenne Tmoyen(k)
Tmoyen(k)
End

G.2 Calcul du temps de passage « physique »

En application de la loi des gaz parfaits, l'expression conduisant au temps de passage « physique » est donnée par l'équation (G.1).

$$\tau_{T_{moy}, P_R} = \frac{\tau_{TPN} \cdot T_N \cdot P_R}{T_{moy} \cdot P_N} \quad (G.1)$$

Les résultats de calcul des températures moyennes des profils et des temps de passage correspondants sont regroupés dans les tableaux G.1 et G.2.

Tableau G.1: Calcul du temps de passage à la température moyenne du profil correspondant à chaque consigne du four ($\tau_{TPN} = 0.93 \text{ s}$)

T _{consigne} (K)	T _{moy} (K)	Pression (atm)	τ_{T_{moy}, P_R} (s)
500	481.72	1.05	0.56
550	515.96	1.06	0.52
600	545.89	1.07	0.50
650	594.21	1.08	0.46
700	620.31	1.09	0.45
750	673.59	1.11	0.42
800	713.39	1.13	0.40
850	761.15	1.16	0.39
900	804.35	1.18	0.37
950	846.26	1.19	0.36
1000	877.46	1.21	0.35
1050	906.18	1.23	0.35
1100	958.69	1.26	0.33
1150	1009.97	1.28	0.32
1175	1029.66	1.29	0.32
1200	1057.65	1.29	0.31

Tableau G.2: Calcul du temps de passage à la température moyenne du profil correspondant à trois consignes du four et pour différentes valeurs de τ_{TPN}

τ_{TPN} (s)	T _{moy} (K) / τ_{T_{moy}, P_R} (s) *		
	620.31	713.39	877.46
0.65	0.36	0.31	0.25
0.7	0.39	0.34	0.27
0.8	0.44	0.38	0.31
0.93	0.51	0.45	0.36
1	0.55	0.48	0.39
1.2	0.66	0.57	0.47
1.4	0.77	0.67	0.54

*Une pression moyenne (1.25 atm) a été utilisée pour calculer τ_{T_{moy}, P_R} .

H. Calcul de l'état des gaz après l'onde de choc

H.1 Détermination des paramètres de choc

Pour déterminer les paramètres de choc, on suppose que les gaz sont parfaits, non visqueux, non thermiquement conducteurs et on néglige les effets de paroi. Considérons le passage du gaz à travers une unité de surface du front de choc comme immobile : on se place donc dans un référentiel lié au front de choc. Pour un tube de section constante nous pouvons écrire les équations de conservation de la masse (H.1), de la quantité de mouvement (H.2) et de l'énergie (H.3) concernant par exemple l'onde de choc incidente :

$$\rho_1 \cdot u_1 = \rho_0 \cdot u_0 \quad (\text{H.1})$$

$$P_1 + \rho_1 \cdot u_1^2 = P_0 + \rho_0 \cdot u_0^2 \quad (\text{H.2})$$

$$h_1 + \frac{1}{2} \cdot u_1^2 = h_0 + \frac{1}{2} \cdot u_0^2 \quad (\text{H.3})$$

Où ρ , P , h et u représentent respectivement la masse volumique, la pression, l'enthalpie par unité de masse et la vitesse du gaz dans le référentiel lié au front de choc. Les indices 0 et 1 correspondent à l'aval et à l'amont du front de choc. En exprimant u_0^2 et u_1^2 à partir des relations (H.1) et (H.2), on obtient, avec la relation (H.3), l'équation de Hugoniot caractéristique d'une onde de choc :

$$h_1 - h_0 = \frac{1}{2} \cdot (P_1 - P_0) \cdot \left(\frac{1}{\rho_0} + \frac{1}{\rho_1} \right) \quad (\text{H.4})$$

$$\text{Dans le cas d'un gaz parfait } P = \rho \cdot R \cdot T \quad (\text{H.5})$$

On obtient alors :

$$h_1 - h_0 = \frac{R}{2} \cdot (\rho_1 T_1 - \rho_0 T_0) \cdot \left(\frac{1}{\rho_0} + \frac{1}{\rho_1} \right) \quad (\text{H.6})$$

En éliminant u_1 dans les relations (H.1) et (H.2), on détermine u_0 qui représente la vitesse de l'onde de choc dans un référentiel fixe dans le cas où la vitesse matérielle du gaz en aval serait nulle, ce qui est le cas dans notre tube à onde de choc.

$$u_0 = \sqrt{\frac{R \cdot (\rho_{10} T_1 - T_0)}{1 - \frac{1}{\rho_{10}}}} \quad (\text{H.7})$$

Où ρ_{10} , calculé en résolvant l'équation (H.10) donnée ultérieurement.

Il convient alors d'introduire le concept de nombre de Mach (M) en relation avec l'écoulement du gaz. C'est le rapport de la vitesse du gaz sur la célérité du son, a , dans ce même

$$\text{gaz : } M_0 = \frac{u_0}{a_0} \quad (\text{H.8})$$

$$\text{Avec } a = \sqrt{\gamma \cdot R \cdot T} \quad (\text{H.9}) \text{ et } \gamma = \frac{C_p}{C_v} \quad (\text{H.10})$$

On obtient alors les paramètres de l'onde incidente :

$$\rho_{10} = \frac{\rho_1}{\rho_0} = \frac{(\kappa + 1) M_0^2}{(\kappa - 1) M_0^2 + 2} \quad (\text{H.11})$$

$$\frac{P_1}{P_0} = \frac{2 \cdot \gamma \cdot M_0^2 - (\kappa - 1)}{(\kappa + 1)} \quad (\text{H.12})$$

H.2 Programme de calcul

Le calcul des paramètres après les ondes de choc incidentes et réfléchies est effectué à l'aide du programme « CHOC » (Belmekki, 2001).

H.2.1 Calcul des paramètres du choc incident

On rappelle que dans notre étude, quatre capteurs de pression permettent de suivre le passage de l'onde incidente et permettent d'obtenir la vitesse moyenne de cette onde (V_{inc}). Un premier calcul aux conditions initiales permet d'estimer le nombre de Mach de l'onde incidente (M_{inc}) et la température du mélange derrière l'onde incidente (T_{inc}) :

$$M_{inc} = \frac{V_{inc}}{\sqrt{\frac{1000 \cdot \gamma \cdot R \cdot T_{inc}}{M_{moy}}}} \quad (\text{H.13})$$

Avec : $R=8,314 \text{ J.K}^{-1} \cdot \text{mol}^{-1}$,

M_{moy} , la masse molaire moyenne du mélange étudié,

T_{init} , la température du mélange gazeux à l'état initial (298 K).

$$T_{inc} = \frac{T_{init} \left[\gamma \cdot M_{inc}^2 - (\kappa - 1) \right] \left[(\kappa - 1) M_{inc}^2 + 2 \right]}{M_{inc}^2 \cdot (\kappa + 1)} \quad (\text{H.14})$$

Une boucle sur T_{inc} permet ensuite d'obtenir une valeur calculée de la vitesse de l'onde de choc incidente; à partir de cette température sont successivement calculés h_1 et h_2 (enthalpies du mélange initial et du mélange choqué), ρ_{10} (rapport des densités des mélanges choqué et

initial) et enfin $V_{inc,calc}$ (vitesse calculée de l'onde incidente). La condition d'itération repose sur la comparaison entre V_{inc} (connue expérimentalement) et $V_{inc,calc}$. On obtient alors une nouvelle valeur de T_{init} . Le nombre de Mach calculé ($M_{inc,calc}$) permet, quant à lui, de connaître la pression derrière l'onde de choc incidente ($P_{inc,calc}$) :

$$M_{inc,calc} = \frac{V_{inc,calc}}{\sqrt{\frac{1000 \cdot \gamma \cdot R \cdot T_{init}}{M_{moy}}}} \quad (\text{H.15})$$

$$P_{inc,calc} = \frac{P_{init} \left[\gamma \cdot M_{inc}^2 - (\gamma - 1) \right]}{\gamma + 1} \quad (\text{H.16})$$

H.2.2 Calcul des paramètres du choc réfléchi

La température derrière l'onde de choc réfléchi ($T_{réfl}$) est estimée à partir de l'hypothèse suivante : $T_{réfl} = 2 \cdot T_{inc}$. Comme précédemment, une boucle sur $T_{réfl}$ permet de calculer successivement ρ_{41} (rapport des densités du mélange choqué derrière les ondes réfléchi et incidente) et $V_{réfl}$ (vitesse de l'onde réfléchi). La condition d'itération repose sur une majoration de l'estimation de l'erreur commise sur la vitesse de l'onde réfléchi ($V_{réfl,err}$) :

$$|V_{réfl,err}| = \sqrt{R \cdot \left(\frac{1000}{M_{moy}} \right) \cdot \left[\rho_{41} T_{réfl} - T_{inc} \left(\frac{\rho_{41} - 1}{\rho_{41}} \right) - \frac{V_{inc,calc} \left[\rho_{10} - 1 \right]}{\rho_{10}} \right]} < 0.001 \quad (\text{H.17})$$

La température $T_{réfl}$ obtenue permet de calculer la pression derrière l'onde de choc réfléchi ($P_{réfl,calc}$) :

$$P_{réfl,calc} = \frac{P_{init} \cdot \rho_{10} \cdot \rho_{41} \cdot T_{réfl}}{T_{init}} \quad (\text{H.18})$$

PhD Dissertation

**BIODIESEL: COMBUSTION OF FATTY ACID
ETHYL ESTERS AS ADDITIVES TO
PETRODIESEL**

TABLE OF CONTENTS

Table of contents

Introduction	1
I. Combustion kinetics of biodiesel (methyl and ethyl esters) – A review	4
Abstract	4
Nomenclature	5
I.1 Introduction	7
I.2 Biodiesel production from triglycerides via transesterification	8
I.2.1 Transesterification reaction	9
I.2.2 Industrial transesterification process	10
I.3 Biodiesel properties	12
I.4 Biodiesel as fuel in diesel engine	14
I.4.1 Combustion process in diesel engine	14
I.4.2 Macroscopic key features of fuel combustion	15
I.4.2.1 Heat Release Rate	15
I.4.2.2 Cetane number and ignition delay: relationship, molecular structure, and emissions	17
I.4.2.3 Engine emissions and performance of biodiesel	18
I.5 Biodiesel combustion kinetics	22
I.5.1 Main features of model development and validation	23
I.5.1.1 Detailed chemical kinetic models and their basement	23
I.5.1.2 Model validation: experiments and environment modeling	24
I.5.1.3 Main guidelines of the past research and of the present review	25
I.5.2 General kinetic scheme and classes of elementary reactions in combustion process	26
I.5.3 Negative Temperature Coefficient and related low temperature phenomena	29
I.5.4 Kinetic investigations related to C ₄ -methyl esters	30
I.5.4.1 Oxidation of methyl butanoate as a biodiesel surrogate	30
I.5.4.2 Pyrolysis of methyl butanoate	37
I.5.4.3 Oxidation of methyl crotonate	39
I.5.5 Ethyl ester kinetic investigations: ethyl propanoate versus methyl butanoate	41
I.6 Conclusion	48

I.7 References	50
Appendix AI Oxidation kinetic related to $C_{n(n>4)}$ -methyl and ethyl esters	58
AI.1 Kinetic investigations related to $C_{n(n>4)}$ -methyl esters	58
AI.1.1 Oxidation of model molecules starting to be suitable biodiesel surrogates: methyl hexanoate, methyl decanoate, methyl-5- and methyl-9-decenoate	58
AI.1.2 Oxidation of actual biodiesel molecules: methyl palmitate and methyl oleate	67
AI.1.3 Kinetic oxidation of rapeseed oil methyl ester	71
AI.2 Kinetic investigations related to $C_{n(n>4)}$ ethyl esters: ethyl hexanoate and ethyl nonanoate	73
II. Oxidation of small saturated and unsaturated ethyl and methyl esters under high temperature and moderate pressure	81
Abstract	81
II.1 Introduction	82
II.2 Experimental procedure	84
II.3 Experimental results	85
II.3.1 Auto-ignition times and empirical correlations	85
II.3.2 Comparison between methyl and ethyl esters	93
II.4 Kinetic models	95
II.5 Discussion	97
II.5.1 Computational simulation	97
II.5.2 Reaction flux analysis	98
II.5.3 Sensitivity analysis	106
II.6 Conclusion	107
II.7 References	109
Appendix AII Shock tube measurements	113
III. Experimental and Kinetic Modeling Study of Ethyl butanoate Oxidation in a Tubular Plug Flow Reactor – From Low to High Temperature under Atmospheric Pressure	119
Abstract	119
Nomenclature	120

III.1 Introduction	121
III.2 Experimental setup and materials	124
III.3 Experimental results	127
III.3.1 Theoretical and physical references used for residence time definitions	127
III.3.2 Experimental design features	128
III.3.3 Temperature profiles along the tubular reactor under the investigated conditions	130
III.3.4 Nature of the observed reaction products	131
III.4 Kinetic model	138
III.5 Computational simulation results and discussion	139
III.5.1 Simulation model of the tubular PFR	139
III.5.2 Evaluation of the kinetic model performance	140
III.5.3 Reaction flux analysis	142
III.5.4 Sensitivity analysis	148
III.6 Conclusion	150
III.7 References	152
Appendix AIII Experimental oxidation of ethyl butanoate in a plug flow reactor	156
Conclusions & Prospects	175

INTRODUCTION

Introduction

The present energy scenario has stimulated active research interest in non-petroleum, renewable, and non-polluting fuels. The world reserves of primary energy and raw materials are, obviously, limited. According to an estimate, the reserves will last for 218 years for coal, 41 years for oil, and 63 years for natural gas, under a business-as-usual scenario [1]. The enormous growth of world population, increased technical development, and standard of living in the industrial nations has led to this intricate situation regarding supply and demand of energy. The prices of crude oil keep rising and fluctuating on a daily basis. In such circumstances, the developing and commercializing of fossil fuel alternatives from bio-origin is a real necessity. This may well be the main reason behind the growing awareness and interest for unconventional bio-energy sources and fuels in various developing countries, which are striving hard to offset the oil monopoly.

An increasingly popular biofuel is biodiesel, composed of a mixture of saturated and unsaturated fatty acid methyl or ethyl esters, with a long aliphatic main chain. Transesterification, or alcoholysis, is the reaction of a fat or oil with an alcohol to form biodiesel (esters) and glycerol. The literature clearly shows that transesterification is the best way to use vegetable oil as a fuel in existing diesel engine. Although methanol is the alcohol used in the transesterification process to produce the commercialized biodiesel, ethanol should be preferred because it is derived from agricultural products and is renewable and biologically less objectionable for the environment. In general, the physical and chemical properties, but also the performances of ethyl esters are comparable to those of methyl esters. Methyl and ethyl esters have almost the same heat content. The viscosities of the ethyl esters are slightly higher and the cloud and pour points are slightly lower than those of the methyl esters. Engine tests demonstrated that methyl esters produced slightly higher power and torque than ethyl esters [2]. Some desirable attributes of the ethyl esters over methyl esters are: significantly lower smoke opacity, lower exhaust temperatures, and lower pour point. Nevertheless, the ethyl esters tended to have more injector coking than the methyl esters [3]. Therefore, this investigation is mainly based on the study of fatty acids ethyl esters (FAEE), where the purpose is to make a detailed analysis of the oxidation of this kind of biodiesel. However, direct studies of typical biodiesels are difficult both because laboratory experiments must be carried out on complex and largely nonvolatile mixtures, and also because the modeling and simulation is not sufficiently developed to be able to tackle such large molecules. Furthermore, since biodiesel is mainly composed of fatty acid esters with different degrees of unsaturation, it

is important to understand the impact of the presence of double bonds on the oxidation behavior of fatty acid esters. For this reason, short chain molecules containing the same functional group as real biodiesel are studied to gather insights into the oxidation behavior of the actual fuel.

The **chapter I** of this dissertation provides a *literature review* concerning the origin of biodiesel, its manufacturing process, performance and emissions of diesel engines fueled with biodiesel, and kinetic of oxidation of biodiesel. Efforts were made in this review to highlight the main differences between methyl and ethyl esters while showing the gaps for which the research works still need to be developed or pursued.

Chapter II is devoted to *shock tube oxidation of methyl and ethyl esters containing 3 or 4 carbon atoms with zero or one degree of unsaturation in the aliphatic chain*. Autoignition of five esters were measured behind reflected shock tube: ethyl acrylate, methyl acrylate, ethyl crotonate, methyl crotonate, and ethyl butanoate. Detailed mechanisms for the oxidation of the five studied esters were automatically generated using the version of EXGAS software recently improved to take into account this class of oxygenated reactants. These mechanisms were validated through satisfactory comparison of simulated and experimental results. The main reaction pathways were also derived from flow rate and sensitivity analyses.

Chapter III examines the *experimental and the kinetic modeling combustion of ethyl butanoate as model compounds for Fatty Acid Ethyl Esters (FAEE) in tubular plug flow reactor at atmospheric pressure over wide range of temperature (500-1200 K)*. The results consist of concentration profiles of the reactants, stable intermediates, and final products, identified by Gas Chromatography coupled to Mass Spectrometry (GC/MS), and quantified by off-line and on-line non dispersive infrared ray absorption analyzer, and Gas Chromatography (GC/TCD/FID) analyses. The oxidation of ethyl butanoate under tubular plug flow reactor conditions was simulated using the model previously developed during the shock tube oxidation study of this biodiesel surrogate. The model was again validated satisfactorily by comparison between computed results and the generated experimental data. Sensitivity and flow rate analyses allowed the determination of the main reactional pathways involved in the oxidation of ethyl butanoate.

Finally, on the basis of the objectives and the results obtained, the **conclusions** and **prospects** of this study are expressed at the end of this thesis report.

Literature cited

- [1] A.K. Agarwal, Biofuels (alcohols and biodiesel) applications as fuels for internal combustion engines, *Progress in Energy and Combustion Science* 33 (2007) 233-271.
- [2] J.M. Encinar, J.F. Gonzalez, J.J. Rodriguez, A. Tejedor, Biodiesel fuels from vegetables oils: transesterification of *Cynara cardunculus* L. with ethanol, *Energy and Fuels* 16 (2002) 443 - 450.
- [3] A. Demirbas, Biodiesel production from vegetable oils via catalytic and non-catalytic supercritical methanol transesterification methods, *Progress in Energy and Combustion Science* 31 (2005) 466-487.

CHAPTER I

**COMBUSTION KINETICS OF BIODIESEL
(METHYL AND ETHYL ESTERS) – A REVIEW**

Chapter I

Combustion kinetics of biodiesel (methyl and ethyl esters) – A review

This chapter is planned to be part of a paper entitled "For a sustainable alternative of biodiesel: a review from production to exhaust emissions" and submitted for publication in "Progress in Energy and Combustion Science".

Abstract

Biodiesel is a non petroleum-based fuel consisting of alkyl esters with long aliphatic main chains. Produced by transesterification of bio-lipid raw materials (mainly vegetable oils), biodiesel is intended for use (neat or blended with conventional fuels) in diesel engines. Many studies report tests conducted by using different classes of esters and their blends with petrodiesel. This chapter presents research works from the literature relating to biodiesel, starting from the production by transesterification, for ending by the engine performance and emissions, and going through the kinetic aspects of biodiesel combustion.

Keywords: Biodiesel; Surrogates; Transesterification; Combustion; Diesel engine; Performance and emissions; Chemical kinetics of oxidation.

Nomenclature

ASTM: American Society of Testing and Materials	HCCI: homogeneous-charge compression-ignition
BDC: bottom-dead-center	HMN: 2,2,4,4,6,8,8- heptamethylnonane
BSFC: brake specific fuel consumption	HRR: Heat Release Rate
BTE: brake thermal efficiency	HTHR: high-temperature-heat-release
BXX: Biodiesel blend, where XX indicate the amount of biodiesel on volume basis	ICE: internal combustion engine
CAD: crank angle degree	ID: ignition delay
CFNPF: coflowing laminar non-premixed flame	iPrAc: isopropyl acetate
CFR: cooperative fuel research engine used for testing, research, and instruction in the performance of fuels and lubricants for the internal combustion engines	IQT: ignition quality tester
CN: cetane number	JSR: jet-stirred reactor
CR: compression ratio	k: rate constant expressed by the modified Arrhenius equation as $k(T)=AT^n \exp(-E_a/RT)$, where units are mole, cm, sec, cal, and K.
CSTR: continuous stirred-tank reactor	K_c : equilibrium constant on concentration basis
E_a : Activation energy (cal)	KOEE: Karanja oil ethyl esters
EB: ethyl butanoate	KOME: Karanja oil methyl esters
EGR: exhaust gas recirculation	$K_{reverse(forward)}$: rate constant for the reverse (forward) reaction
EHX: ethyl hexanoate	LTHR: low-temperature-heat-release
EN: ethyl nonane	MB: methyl butanoate
EP: ethyl propanoate	MC: methyl crotonate
FAEE: fatty acid ethyl esters	MD: methyl decanoate
FAME: fatty acid methyl esters	MD5EN: methyl-5 decenoate
FFA: free fatty acids	MH: methyl heptanoate
FID: flame ionization detector	MHX: methyl hexanoate
FR: flow reactor	MiBu: methylisobutyrate
FTIR: Fourier transformed infrared	MN: methyl nonane
GC-DET: gas chromatography coupled with DET as detector with DET=MS, FID, or TCD.	MN2EN: methyl-2 nonenoate
	MN3EN: methyl-3 nonenoate
	MO: methyl oleate
	MOEE: Mahua oil ethyl esters

Nomenclature (continued)

MP: methyl palmitate	ST: shock tube
MS: mass spectroscopy	T: temperature (K)
NO _x : nitrogen oxides	TCD: thermal conductivity detector
NTC: negative temperature coefficient	THC: total hydrocarbons
nC7: n-heptane	UHC: unburned hydrocarbons
nC10: n-decane	V: volume of the reactor
nC16: n-hexadecane	VOC: volatile organic compounds
OFDF: opposed flow diffusion flame	VPFR: variable pressure flow reactor
P: pressure (atm)	WCOEE: waste cooking oil ethyl esters
PM: particulate matter	WCOME: waste cooking oil methyl esters
PME: phenyl methyl ether	x _{fuel} : fuel molar fraction
PrAc: propyl acetate	x _{O₂} : oxygen molar fraction
Q: volumetric flow rate	v _{fuel} : stoichiometric coefficient of the fuel
R: ideal gas constant	v _{O₂} : stoichiometric coefficient of the oxygen
RCM: rapid compression machine	φ: equivalence ratios defined, as example for
REE: rapeseed oil ethyl esters	reaction C _n H _m + (n + m/4) O ₂ → n CO ₂ + m/2 H ₂ O, as
RME: rapeseed oil methyl esters	φ = (x _{fuel} /x _{O₂})/(v _{fuel} /v _{O₂}) with, here v _{fuel} = 1 and v _{O₂}
RRKM: Rice-Ramsperger-Kassel-Marcus	= (n + m/4) ^a
SP: species profile	τ: residence time τ=V/Q
SO _x : sulfur oxides	

^a This definition corresponds to the traditional equivalence ratio considering that oxygen atoms contained in a fuel molecule is still part of the fuel, which actually function as oxidizers during the oxidation process. Therefore, was introduced in the literature (Zhang et al., 2009 [101]) the concept of oxygen equivalence ratio considered to be a more appropriate representation of the mixture stoichiometry for oxygenated fuels than the traditional equivalence ratio. Indeed, the oxygen equivalence ratio was defined as the oxygen content available in the reactant mixture divided by the amount of oxygen required for stoichiometric combustion.

I.1 Introduction

Energy demand around the world is continuously increasing, specifically the demand for petroleum-based energy. Petroleum is the largest single source of energy which has been consumed by the world's population, exceeding the other energy resources such as natural gas, coal, nuclear and renewable materials. According to the International Energy Outlook 2007 published by the Energy Information Administration [1], the world consumption for petroleum and other liquid fuel will grow from 83 million barrels/day in 2004 to 97 million barrels/day in 2015 and just over 118 million barrels/day in 2025. Under these growth assumptions, approximately half of the world's total resources would be exhausted by 2025. Also, many studies estimated that the world oil production would peak sometime between 2007 and 2025 [1]. Therefore, with this depletion of oil resources as well as the negative environmental impact associated with the use of fossil fuels, there is a renewed interest in alternate energy sources. As world reserves of fossil fuels and raw materials are limited, active research in nonpetroleum, renewable, and nonpolluting fuels was stimulated. Biofuels are the only viable source of energy for the foreseeable future and can still form the base for sustainable development in terms of socioeconomic and environmental concerns. Indeed, biofuels come from agricultural products such as sugarcane, oleaginous plants, forest biomass, or other sources of organic matter. Also, biofuels can be used either neat or added to conventional fossil fuels in blends. As typical examples, it is possible to mention biodiesel blended with petroleum diesel (petrodiesel) for use as fuel in compression-ignition engines and bioethanol blended with gasoline for use as fuel in spark-ignition engines. Therefore, biodiesel and bioethanol appear to be promising future energy sources. Biodiesel (i.e. *bio* from life in Greek and *diesel* from Rudolf Diesel) is defined as the monoalkyl esters of long-chain fatty acids derived from renewable biolipids. Biodiesel is typically produced through the reaction (transesterification) of vegetable oils or animal fats with methanol or ethanol in the presence of a catalyst to yield methyl or ethyl esters (biodiesel) and glycerol (by-product). Generally, methanol is preferred for transesterification because it is less expensive than ethanol (Graboski and McCormick, 1998) [2]. However, biodiesel is 100% renewable only when the alcohol used in the transesterification process is also renewable, but this proportion is reduced to around 90% (if the balance is made in mass) when fossil alcohol (methanol) is used (Lapuerta et al., 2008) [3]. Furthermore, biodiesel is an oxygenated fuel containing from 10% to 15% oxygen by weight and also a sulfur-free fuel. These facts lead biodiesel to more complete combustion and less exhaust emissions from diesel engine. Nevertheless, comparing the fuel properties of biodiesel

and petrodiesel, biodiesel has higher viscosity, density, pour point, flash point and cetane number than petrodiesel (Myo, 2008) [4]. By the way, it should be mentioned the poor engine performance and emission characteristics of vegetable oils as fuel, even when blended with petrodiesel. Indeed, engine failures were observed when fuelled with blends of vegetable oil and petrodiesel and these failures were attributed to the high viscosity of vegetable oils leading to injector coking and contamination of the lubricating oil (Basha et al., 2009) [5]. Also, Krahl et al. (2009) [6] highlighted that strong mutagenicity of extracts and condensates from combustion of rapeseed vegetable oil was denoted.

The subject of this study is to present research works from the literature relating to biodiesel, starting from the production by transesterification, for ending by the engine performance and emissions, and going through the kinetic aspects of biodiesel combustion that makes up the core of this study. In addition, the characteristics of methyl biodiesel (commercial biodiesel) are compared, when this has been possible, to those of ethyl biodiesel. As there will be illustrated, this study has been motivated by the highly controversial arguments about the engine performance and emission characteristics (nature and proportions) when the engine is fuelled with methyl or ethyl esters as biodiesel (neat or blended). Also, an additional argument is the necessity of a comprehensive knowledge of the kinetic aspects related to biodiesel combustion in order to predict the important characteristics of exhaust emissions for a class of fuel, and longer terms, to formulate a biodiesel blend which would lead to harmless and cleaner emissions. In such circumstances, it seemed urgent to draw a state-of-the-art in order to highlight the main residual difficulties and the progress to make. Thus, this work is complementary to the review published very recently by Kohse-Höinghaus et al. (2010) [7] which was focused on biofuels combustion chemistry from ethanol to biodiesel, with particular attention to the analysis of the species composition of laminar premixed flames by molecular-beam mass spectrometry and appropriate combustion models.

I.2 Biodiesel production from triglycerides via transesterification

Biodiesel is currently defined by two technical regulations: either the EN 14214 inside the European Union or the ASTM D6751 inside the USA. Governmental regulations define biodiesel as Fatty Acid Methyl Esters (FAME), as these are the alkyl esters commonly produced industrially from lipid raw materials (vegetable oils) and methanol (as alcohol). However, FAME are only 90% renewable due to methanol that is chemically produced from synthesis gas. Therefore, discussions are underway to change the definition of biodiesel and include other products, such as Fatty Acid Ethyl Esters (FAEE). In the FAEE process

production, methanol is replaced by bioethanol, giving a product that is fully biological (100% renewable) and would further contribute to reduce life-cycle greenhouse emissions from vehicles. Moreover, researchers devise new methods and technologies to produce second or third generation biodiesel (Lois, 2007) [8].

Neat biodiesel, i.e. with a composition equal to 100% in biodiesel, is referred to B100, and is called “neat” fuel. Thus, neat biodiesel blended with petrodiesel are referred to BXX, where XX indicates the volume percent of neat biodiesel blended with petrodiesel. As example, B20 designates a biodiesel blend containing 20% volume by neat biodiesel and 80% volume by petrodiesel.

I.2.1 Transesterification reaction

Historically, transesterification of triglycerides in oils is not a new process. Duffy and Patrick had conducted transesterification as early as 1853. Use of the diesel engine began in 1893, when the famous German inventor Dr. Rudolph Diesel published a paper entitled "The theory and construction of a rational heat engine". Diesel designed the original diesel engine to run on vegetable oil. He also believed that engines running on plant oils had potential and that these oils could one day be as important as petroleum-based fuels. Since the 1980, biodiesel plants have opened in many European countries, and some cities have run buses on biodiesel, or blends of petrodiesel and biodiesel. More recently, Renault and Peugeot have approved the use of biodiesel in some of their truck engines (Demirbas, 2008) [9].

Transesterification is the reaction of vegetable oil or animal fat with methanol or ethanol in the presence of a catalyst to yield methyl or ethyl esters (biodiesel) and glycerol (by-product). Various types of catalyst can be used: alkali catalyst (Zhang et al., 2003) [10], acid catalyst (Furuta et al., 2004) [11], or enzymes (Noureddini et al., 2005) [12]. Various studies have been carried out using different lipid sources as raw materials (virgin vegetable oils, non-edible oils, animal fats, waste cooking oils, ...), different alcohols (methanol, ethanol, butanol), as well as different catalysts including homogeneous ones such as sodium or potassium hydroxide, sodium methoxide, and sulfuric acid (Demirbas, 2003 [13]; Rathore et al., 2007 [14]) and heterogeneous ones such as lipases (Marchetti et al., 2007) [15] or mixture of zinc and aluminum oxides (Bournay et al., 2005) [16]. Transesterification process is conducted to reduce together viscosity, specific gravity (relative density) and flash point of the lipid source used as feedstock. Figure I.1 depicts the transesterification reaction.

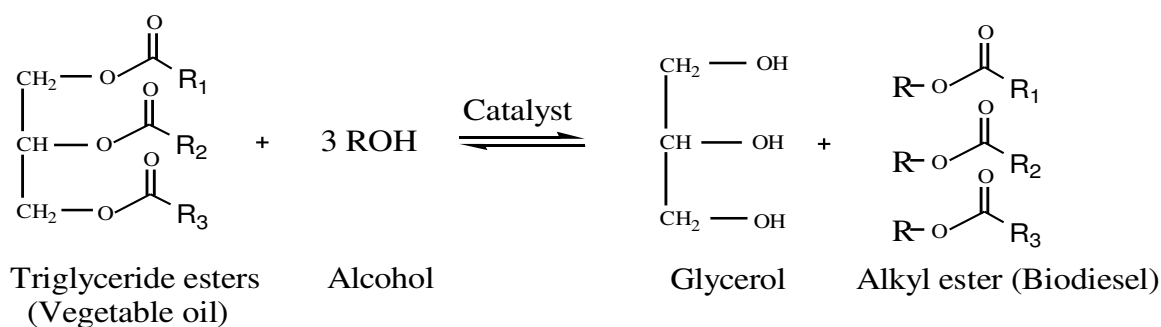


Figure I.1: Chemical equation of transesterification reaction

(R = alkyl group; R₁, R₂, R₃: identical or different alkyl chains with one to three unsaturated bond(s) –CH=CH–)

As mentioned previously, a large variety of biolipids can be used to produce biodiesel. These are (a) virgin vegetable oils among which rapeseed and soybean oils are the most commonly used, though other crops such as mustard, palm oil, sunflower, hemp, cottonseed oil, safflower, coconut and even algae show promise potentialities; (b) waste cooking oils (frying oils); (c) animal fats including tallow, lard, and yellow grease; and (d) non-edible oils such as jatropha oil, neem oil, mahua oil, castor oil, or tall oil. The choice of the feedstock depends largely on its geographical availability. Depending on the origin and quality of the feedstock, changes to the production process may be necessary. As can be seen in table I.1, palmitic (C16:0) and stearic (C18:0) acids are the two most common saturated fatty acids whereas oleic (C18:1) and linoleic (C18:2) acids are the most common unsaturated fatty acids, occurring in every vegetable oil with at least small amounts of each one (Demirbas, 2008) [9].

Table I.1: Fatty acid compositions of some vegetable oils and fats^a (Demirbas, 2008) [9]

Vegetable oil	C16:0	C16:1	C18:0	C18:1	C18:2	C18:3	Others
Cottonseed	28.7	0	0.9	13.0	57.4	0	0
Rapeseed	3.8	0	2.0	62.2	22.0	9.0	0
Safflowerseed	7.3	0	1.9	13.6	77.2	0	0
Sunflowerseed	6.4	0.1	2.9	17.7	72.9	0	0
Linseed	5.1	0.3	2.5	18.9	18.1	55.1	0
Palm	42.6	0.3	4.4	40.5	10.1	0.2	1.1
Soybean	11.9	0.3	4.1	23.2	54.2	6.3	0
Tallow	23.3	0.1	19.3	42.4	2.9	0.9	2.9

^a Cxx:y: xx number of carbon atoms; y: number of double bonds.

I.2.2 Industrial transesterification process

Regarding fatty acid methyl ester (FAME) production, Figure I.2 shows a schematic diagram of typical processes involved in biodiesel production from feedstocks containing low levels of free fatty acids (FAA). These include soybean oil, rapeseed oil, and the higher grades of waste cooking oils (Knothe et al., 2005) [17]. For methylic biodiesel, alcohol (methanol), catalyst, and oil are introduced in a reactor and agitated for ~1 h at 60°C. Smaller plants often

use batch reactors but larger plants (>4 million L/yr) use continuous flow processes involving continuous stirred-tank reactors (CSTR) or plug flow reactors. The reaction is sometimes done in two steps in which ~80% of the alcohol and catalyst is added to the oil in a first-stage CSTR. Then, the product stream from this reactor goes through a glycerol removal step before entering a second CSTR. The remaining 20% of the alcohol and catalyst is added in this second reactor. This system provides a very complete reaction with the potential of using less alcohol than single-step systems. At the end of the reaction, glycerol is removed from the methyl esters. Due to the low solubility of glycerol in the esters, this separation generally occurs quickly and can be accomplished with either a settling tank or a centrifuge. The excess methanol tends to act as a solubilizer and can slow the separation. However, this excess methanol is usually not removed from the reaction stream until after the glycerol and methyl esters are separated due to concern about the reversing of the transesterification reaction. Additional glycerol may be added to the reaction mixture after the transesterification is complete to improve the separation of glycerol. After separation from the glycerol, the methyl esters enter a neutralization step and then pass through a methanol stripper, usually a vacuum flash process or a falling film evaporator, before water washing. Acid is added to the biodiesel product in order to neutralize any residual catalyst and to split any soap that may have formed during the reaction. The glycerol refining process takes the purity up to 99.5-99.7% using vacuum distillation or ion exchange processes. Methanol that is removed from the methyl ester and glycerol streams will tend to collect any water that may have entered the process (for example during neutralization). This water should be removed in a distillation column before methanol is returned to the process. This step of rectification is more difficult if an alcohol forming an azeotrope with water, such as ethanol or isopropanol, is used. In such circumstances, separation by molecular sieve or by membrane pervaporation is preferred in that case to remove water (Knothe et al., 2005) [17]. Other technical difficulties may be encountered when using ethanol instead of methanol as alcohol for transesterification (Baiju et al., 2009) [18]. First, tests showed that the reaction proceeds slower if ethanol is used, most probably because of its inferior reactivity. Secondly, whereas solubility of oils in methanol is low, inducing limitation by mass transfer during transesterification, ethanol possesses instead a higher solubility and reduces the effect of the mass transfer limitation. Nevertheless, this higher solubility may lead to a more difficult separation of the glycerol-rich phase from the ethyl ester-rich phase. This phenomenon could, however, be improved by addition of supplementary glycerol during the settling stage, as mentioned previously regarding FAME production. All these technical drawbacks that are not well defined or controlled, together with the low cost of

methanol compared to ethanol, may explain why fatty acid ethyl ester (FAEE) production facilities are still very scarce and pilot scale.

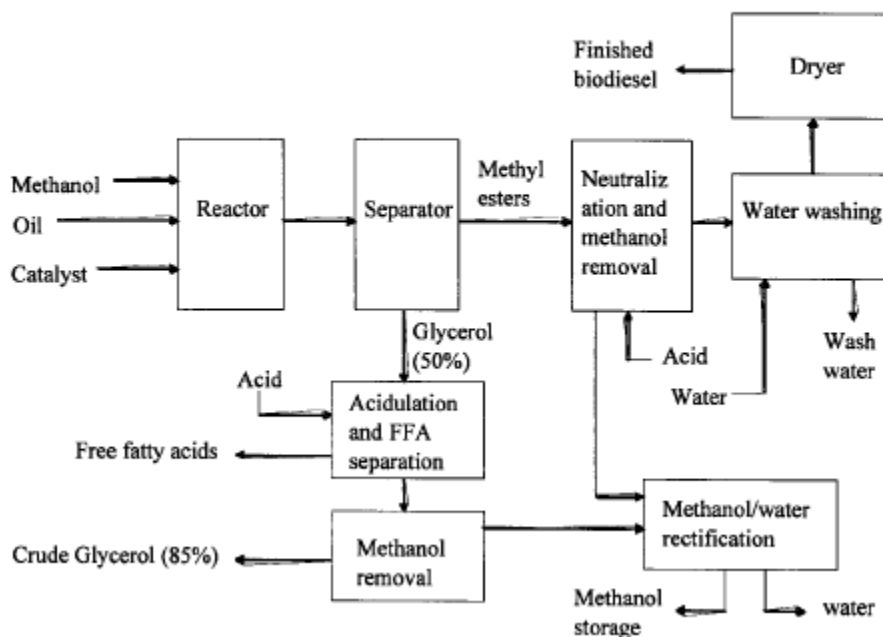


Figure I.2: Process flow scheme for fatty acid methyl ester production

(Knothe et al., 2005) [17].

I.3 Biodiesel properties

As expected, biodiesel fuel properties are strongly influenced by the nature and structure of its components (mainly the fatty acid alkyl esters). Therefore, quality specifications or requirements for biodiesel as fuel were established according to ASTM D6751 and EN 14214 standards (Knothe et al., 2005 [17]; Monteiro et al., 2008 [19]; Ramos et al., 2009 [20]). As illustrated in Table I.2 giving ranges of some quality specifications related to biodiesel and petrodiesel (Van Gerpen et al., 2004 [21]; Lapuerta et al., 2008 [3]), both of the fuels are very similar for some properties and quite different for others, highlighting their advantages and disadvantages. The most evident ones are shortly mentioned below (Murugesan et al., 2009) [22] whereas others will be discussed further in the following section related to engine emission and performance characteristics.

Among *advantages of biodiesel compared to petrodiesel*, it may be mentioned:

- Derivation from a renewable resource.
- Biodegradability (Biodiesel degrades 4 times faster than petrodiesel and degrades 85-88% in water.)
- No production of greenhouse effects due to equal balance between the amount of CO₂ emissions and the amount of CO₂ absorbed by the plants producing vegetable oil used as raw materials.

- Excellent lubricity.
- Essentially free from sulfur and aromatics, leading to 90% reduction in cancer risks.
- Oxygenated fuel, which is expected to improve combustion in engine and exhaust emissions by “cleaner” burning.
- Can be used directly in compression ignition engines with no substantial modifications of the engine.
- Higher flash point, leading to safer handling and storage.

Regarding the *disadvantages associated with biodiesel*, it should be mentioned its inherent higher price of production, which is mainly due to the cost of the raw materials used (up to now, mainly virgin vegetable oils). This drawback can however be partially offset by the use of less expensive feedstocks, such as waste cooking oils (Ramos et al., 2009) [20]. Also, compared to typical petrodiesel, biodiesel has significantly higher density and viscosity in cold weather, poorer low temperature properties, and is inherently less stable to air and high temperature exposures (due to unsaturation present in biodiesel components).

Table I.2: Ranges of some quality specifications related to biodiesel and petrodiesel

(Van Gerpen et al., 2004 [21]; Lapuerta et al., 2008 [3]).

Specifications ^a	Biodiesel	Petrodiesel
Density (15°C) (kg/m ³)	870 – 895	810 – 860
Kinematic viscosity (40°C) (cSt)	3.5 – 5.5	2 – 3.5
Flash point (°C)	130 minimum	38 – 55
Cetane number	45 – 65	40 – 50
Cloud point (°C)	-5 to 10	-20 to 0
Pour point (°C)	-15 to 10	-35 to 0
Lower heating value (MJ/kg)	36.5 – 38	42.5 – 44
Water content (mg/kg)	0 – 500	
Acid number (mg KOH/g)	0 – 0.60	
Ester content (% w/w)	> 96	
Total glycerin content (% w/w)	0 – 0.25	
Sulfur content (% w/w)		15 – 500

^a Definition of most specific properties are given here, with the exception of *cetane number* and *lower heating value* which will be explained in section related to engine emissions and performance characteristics. *Flash point* (lowest temperature corrected to a pressure of 101.3 kPa at which application of an ignition source causes the vapors of a specimen to ignite under the specified conditions of test, i.e. measure of residual alcohol in the B100). *Cloud point* (temperature at which a cloud of wax crystals first appears in a liquid when it is cooled down under conditions prescribed by the specific test method). *Pour point* (lowest temperature at which a liquid will pour or flow under conditions prescribed by the specific test method). *Lower heating value* (enthalpy of combustion by considering that water is in the vapor state in the exhaust product). *Acid number* (quantity of base, expressed as milligrams of potassium hydroxide per gram of sample, required to titrate a sample to a specified end point). *Total glycerin content* (sum of the free glycerin and bonded glycerin as glycerides).

I.4 Biodiesel as fuel in diesel engine

Understanding the basis concept of combustion process in diesel engine, together with the macroscopic key features of fuel combustion, is necessary for converging to the requirement of a good knowledge of the governing microscopic phenomena, i.e. biodiesel combustion kinetics.

I.4.1 Combustion process in diesel engine

The *diesel engine* or *compression ignition engine* is commonly a four-stroke cycle engine. During the first stroke (intake), air is drawn into the cylinder engine and then, compressed to a high pressure and temperature during the second stroke (compression). Next, the fuel is injected into the turbulent compressed air and, after a certain time period, spontaneously ignites during the third stroke (power). Afterward, the products of combustion are exhausted during the fourth stroke (exhaust). The diesel engine relies on high compression ratio (typically from 15 to 22) to occur combustion. Indeed, this is necessary to bring the air temperature to a level where autoignition is promoted when the fuel is injected into the cylinder at the end of the compression stroke (Myo, 2008) [4]. Thus, it appears clearly that a principal requirement of a fuel for diesel engine is that must be auto ignited easily.

Furthermore, it is worth mentioning that two classes of diesel engine exist depending on the fuel injection mode used; these are direct and indirect injection engines. *Direct injection* means the fuel is directly injected into the combustion chamber under high pressure through a nozzle fitted with one or more tiny holes to reach atomization of the fuel in a spray of very fine droplets making easier fuel evaporation. On the other hand, in the *indirect injection* engines, fuel is injected first into a pre-chamber that is adjacent and connected to the main combustion chamber. Combustion begins in the pre-chamber from which burning gases leave with high velocities creating turbulence and greater ability for mixing fuel and air (Myo, 2008) [4]. Nevertheless, modern diesel engines commonly make use of direct injection method.

Further downstream technical considerations previously mentioned, *combustion process* in diesel engine generally comprises *four stages* (Van Gerpen et al., 2004) [21]. The *first stage* is “*ignition delay*” during which the fuel fine droplets heat up, vaporize, mix with air and undergo chemical precombustion reactions that produce the radical species necessary for spontaneous ignition or autoignition. Hence, this period combines both physical and chemical phenomena occurring simultaneously, with vaporization and mixing processes called the “*physical delay*” and the precombustion reaction process named the “*chemical delay*”. Thus, it is clear that ignition delay time depends on size of injected fuel droplets, air temperature,

extent of fuel-air mixing, and fuel oxidation stability. The *second stage* is “ignition” that occurs spontaneously and independently at multiple locations of the combustion chamber in regions of fuel-air mixture that have fuel-air ratios close to the chemically correct ratio, namely the stoichiometric ratio (except for Homogenous Charge Compression Ignition – HCCI – engine operating at lean-fuel mixtures). The *third stage* called “*premixed combustion*” corresponds to initial combustion that proceeds and propagates very rapidly in the combustion chamber due to the backlog of prepared fuel-air mixtures formed during the ignition delay period. The rapidly rising in temperature and pressure in the combustion chamber accelerates the combustion in an uncontrolled manner until the backlog is depleted. This portion of the combustion process consumes about 5 to 10% of the injected fuel. The *fourth stage* is called “*mixing controlled*” or “*diffusion controlled*” burning, during which the remainder of the fuel in the spray core is too rich (in fuel) to burn, and then, leads to slowing down of combustion which is thus controlled by the rate at which the air is entrained and a combustible mixture is formed. This portion of the combustion process consumes all the remainder fuel. Thus, while chemical kinetics dominates the ignition delay, the high temperatures and pressures of the post-ignition gases promote very fast reaction rates that make fuel-air mixing the rate determining process (Van Gerpen et al., 2004) [21].

I.4.2 Macroscopic key features of fuel combustion

Some macroscopic key features basically used for discussing global fuel behavior during combustion are shortly described here. These are heat release rate, cetane number and ignition delay and finally engine emissions and performance of biodiesel during combustion.

I.4.2.1 Heat Release Rate

The heat release rate (HRR) or combustion rate is the rate of heat emitted rapidly just after ignition. Although determined indirectly during combustion in diesel engine, HRR can provide meaningful information related to the combustion process as shown in Figure I.3 (Dubreuil et al., 2007) [23].

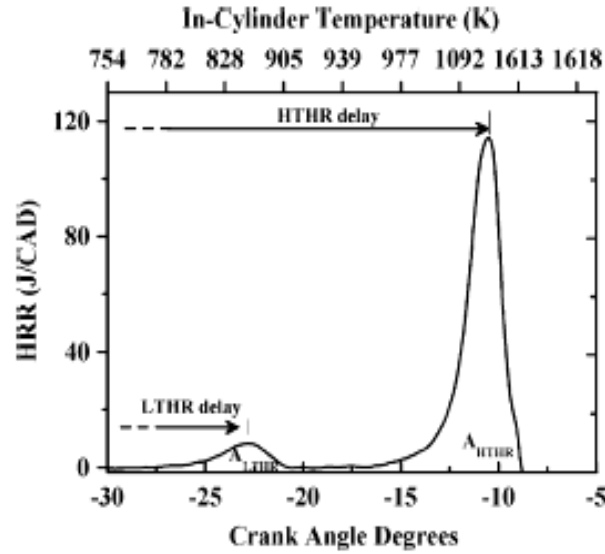


Figure I.3: Definition of combustion parameters determined from heat release rate data

(Dubreuil et al., 2007) [23]

From the pressure history in the combustion chamber of the test engine recorded in function of the crank angle, the HRR can be determined by the following equation:

$$\frac{dQ}{d\alpha} = \frac{\gamma}{\gamma-1} \cdot P \cdot \frac{dV}{d\alpha} + \frac{1}{\gamma-1} \cdot V \cdot \frac{dP}{d\alpha}, \quad (\text{eq. I.1})$$

where γ is the air-fuel mixture adiabatic constant, P and V are the instantaneous cylinder pressure and volume, α is the crank angle, and Q the net heat release. This expression, deriving from the first law of thermodynamics applied to the combustion chamber as system, is based on three assumptions: the first is that the air-fuel mixture inside the combustion chamber behaves as an ideal gas; the second is that the mixture in the cylinder is a uniform single zone of constant composition; the third is that the energy released is due to fuel combustion.

The cylinder volume per crank angle $dV/d\alpha$ can be derived from the following equation including geometrical engine data (Myo, 2008) [4]:

$$\frac{dV}{d\alpha} = \frac{\pi A_S}{180} \cdot r_C \cdot \left\{ \sin\left(\frac{\pi\alpha}{180}\right) + \left[\lambda \sin^2\left(\frac{\pi\alpha}{180}\right) / \left(2\sqrt{1-\lambda^2 \sin^2\left(\frac{\pi\alpha}{180}\right)} \right) \right] \right\} \quad (\text{eq. I.2})$$

where A_S is the cross-section area of the piston, r_C the crank radius, and λ the connecting rod length. As illustrated by Figure I.3, HRR history in function of crank angle degrees (CAD) may show one or two peaks, depending on the fuel nature and combustion conditions. In case of two peak occurrences, the first designated by Low-Temperature-Heat-Release (LTHR) delay corresponds to the ignition delay of the first-stage combustion representative of the low temperature oxidation, namely cool flames. The second designated by High-Temperature-Heat-Release (HTHR) delay corresponds to the second-stage ignition delay, representative of the

main part of the combustion. In case of one peak occurrence, this one may correspond to LTHR or HTHR phenomena. Parameters LTHR and HTHR correspond to the CAD after Bottom-Dead-Center (BDC) when each heat release maximum is reached. A_{LTHR} is defined as the area of the first-stage of combustion, in other words, as the net energy (in J) which is released during this phase and A_{HTHR} is defined as the net energy (in J) released during the second-stage of combustion (Dubreuil et al., 2007) [23].

I.4.2.2 Cetane number and ignition delay: relationship, molecular structure, and emissions

As mentioned previously (section I.4.1), one of the most important properties required to a diesel fuel is ignition delay (i.e. the period between the start of injection and the start of combustion) showing its readiness to auto ignite at the temperatures and pressures present in the engine cylinder when the fuel is injected. The laboratory test used to measure this tendency is the Cetane Number (CN) test, giving a dimensionless descriptor of the autoignition quality of the considered diesel fuel. Fuels with a high CN will have short ignition delays (IDs) and a small amount of premixed combustion since little time is available to prepare the fuel for combustion.

The CN of a diesel fuel is directly influenced by the molecular structure of its components. Regarding hydrocarbons, saturated and unbranched molecules with long aliphatic chains are known to have suitable CN, and thus good ignition ability as diesel fuel, against unsaturated or branched molecules (Freedman et al., 1990) [24]. Besides, the two primary reference fuels used for CN measurements are both alkanes with 16 carbon atoms; however, the high cetane standard (n-hexadecane, trivial name cetane, with an assigned CN=100) has a linear skeleton, whereas the low cetane standard (2,2,4,4,6,8,8-heptamethylnonane, HMN, with an assigned CN=15) has a branched skeleton. Hence, regarding biodiesel components, two structural effects may influence the fuel CN: first, the skeleton of the aliphatic main chain (chain length and number of double bonds) and secondly, the nature of the alcohol moiety (methyl, ethyl, propyl, butyl,...). Knothe et al. (2003) [25] determined the CNs of 29 mono-alkyl esters of fatty acids by using an Ignition Quality Tester (IQT). Globally, the authors found the same tendency as the one commonly experienced by hydrocarbons: CNs increased with chain length (in other words, the more sequential methylene CH_2 groups in the fatty compound, the higher the CN) whereas increasing the number of double bonds or branching in the aliphatic main chain caused lower CNs (with subsequent longer ID times and poorer combustion performance). Hence, among the investigated fatty esters, the lower CN was

observed for the esters of linolenic acid and the higher CN for the esters of stearic acid, with CN increasing in the order linolenic < linoleic < oleic < palmitic < stearic acid (see Table I.1 for molecular structure description). The effect of the alcohol moiety on the CNs was, however, less well-defined, according to Knothe et al. (2003) [25]. Nevertheless, all ethyl esters experienced clearly higher CNs (i.e. lower IDs) than the corresponding methyl esters; additionally, the esters of 2-ethylhexanol, the most CH₂-rich alcohol used in the work, prominently displayed the highest CNs of all tested esters. On the basis of their CN measurements conducted in the IQT, Knothe et al. (2003) [25] provided the following relationship between ID and CN:

$$\text{CN} = 83.99 \cdot (\text{ID} - 1.512)^{-0.658} + 3.547, \quad (\text{eq. I.3})$$

showing that small changes at shorter ID times result in greater changes in CN than at longer ID times.

Although CN (and consequently molecular structure of fuel components) was observed to be closely linked to engine emissions, the relationship between CN and engine emissions is complicated by many factors including the type of engine technology and engine operating conditions (Lee et al., 1998) [26]. Particularly, it was observed that exhaust emissions of nitrogen oxides (NO_x) and unburnt hydrocarbons (UHC) decreased with increasing CN, due to the reduction in ID times and amount of premixed fuel burnt, resulting lower average combustion temperatures and advanced combustion (Ladommatos et al., 1996) [27].

I.4.2.3 Engine emissions and performance of biodiesel

- *FAME-biodiesel versus petrodiesel.* There have been many investigations relating combustion performance and emission characteristics of common biodiesel (i.e. fatty acid methyl esters, FAME) in diesel engines. Recently, Basha et al. (2009) [5] published a literature review gathering the scientific works on biodiesel that appeared between 1980 and 2008. Earlier, Lapuerta et al. (2008) [3] focused their review on the effect of biodiesel fuels on diesel engine performance and emissions compared to conventional diesel fuels (also named fossil diesel or petrodiesel fuel), by analyzing exhaustively the problem and by listing explanations and eventual measures proposed in the literature.

Typically, researchers are all agreed to report that combustion of biodiesel (irrespective to the feedstock) in diesel engines results in a decrease in the emissions of particulate matter (PM), unburned hydrocarbons (UHC), sulfur oxides (SO_x), volatile organic compounds (VOCs), and carbon monoxide (CO) with respect to petrodiesel fuel. Biodiesel is also said to be carbon neutral as it contributes no net CO₂ to the atmosphere (the balance between the

amount of CO₂ emissions and the amount of CO₂ absorbed by the plants producing vegetable oil is equal; Lapuerta et al., 2008 [3]; Basha et al., 2009 [5]).

Nevertheless, a slight increase in nitrogen oxides (NO_x) emissions was commonly observed in the research literature, although no unanimity has been found; indeed, some works found NO_x increases only in certain engine operating conditions, some others did not find differences between petrodiesel and biodiesel fuels, and others still found decreases in NO_x emissions when using biodiesel. One reason for this disagreement is the large number of different engine technologies tested, the varying operating conditions, the different biodiesel fuels used, and the various measurement techniques and procedures applied (Lapuerta et al., 2008 [3]). Anyway, some measures to compensate the effect of biodiesel on NO_x emissions have been proposed in the literature, such as delaying injection (which is slightly advanced with biodiesel due to its physical properties, i.e. viscosity, density, compressibility, and sound velocity) in combination with increasing exhaust gas recirculation (EGR) and this without involving any penalty of PM reductions favored by advanced injection/combustion (Lapuerta et al., 2008 [3]). Other examples of proposed measures are the use of advanced injection strategies with low-temperature combustion modes (Fang and Lee, 2009) [28], or even the modification of the fuels to be used (Lapuerta et al., 2008 [3]). Indeed, it is generally admitted that formation of NO_x during combustion is mainly controlled by the ignition delay of the fuel, and thus by the relative amounts of heat released during the premixed combustion phase and the diffusion controlled combustion phase. A lower degree of ignition delay was observed to strongly increase NO_x formation (Schönborn et al., 2009) [29]. According to the relationship shown in the previous section between ignition delay (ID) and cetane number (CN), and their evolution relating the molecular structural features of the fuel components, it is expected that increasing fatty acid chain length, increasing saturation, and increasing the chain length of the alcohol moiety should decrease the ID, and thus should decrease NO_x formation (Knothe et al., 2003 [25]; McCormick et al., 2001 [30]).

Moreover, the emissions of aromatic and polyaromatic compounds, as well as their toxic and mutagenic effect, have been generally observed to be reduced with biodiesel (contrary to neat vegetable oil used as fuel, Krahl et al., 2009 [6]). However, no conclusive trend has been found regarding the decrease in the mean diameter of the particle size distributions obtained when biodiesel fuel is used (mainly caused by a sharp decrease in the number of large particles, but also a certain increase in the number of the smallest ones) or the emissions of oxygenated compounds such as aldehydes and ketones (Lapuerta et al., 2008) [3].

Regarding engine performance, conventional internal combustion engines can be operated with biodiesel without major modification. In comparison to petrodiesel, the higher CN of biodiesel (resulting in shorter ID, longer combustion duration, and lower particulate emissions) yields hence minimum carbon deposits on injector nozzles (Murugesan et al., 2009) [22]. Additionally, biodiesel does not cause any loss of power output unless the maximum power is demanded. A surplus in fuel consumption (involving an increase in the brake specific fuel consumption, BSCF, defined as the fuel consumption rate divided by the power produced) that was reported by a majority of authors would, in any case, compensate the lower heating value of biodiesel as compared with petrodiesel fuel (Table I.2, Lapuerta et al., 2008 [3]).

Among the various blends of biodiesel with petrodiesel tried, B20 (a blend of 20% by volume FAME-biodiesel with 80% by volume petrodiesel) giving the maximum improvement in terms of diesel engine emissions and performance was recommended as optimum blend for long-term engine operation (Murugesan et al., 2009) [22].

- *FAEE-biodiesel and analysis in terms of various bio-lipid raw materials.* The number of studies about the effect of ethanol-derived biodiesel (i.e. fatty acid ethyl esters, FAEE) on diesel engine performance and emissions is, however, still much lower than that of methanol-derived one (FAME).

Peterson et al. (1996) [31] tested exhaust emissions from a 1994 Dodge pickup with a direct injected, turbocharged and intercooled, 5.9 Liter Cummins diesel engine fuelled with 100% rapeseed oil ethyl esters (REE). The authors reported that, compared to petrodiesel fuel, emissions of UHC, CO and NO_x decreased by 55.6%, 50.6%, and 11.8% respectively. An increase in CO₂ (1.1%) and PM (10.3%) was however observed. Nevertheless, a blend of 20% REE and 80% petrodiesel led to a decrease in PM emission of 5.7% compared to neat petrodiesel fuel. The authors also indicated that the dynamometer test at 2500 rpm showed 1.8% less power, 8.9% less fuel consumption, and 31.8% less opacity when operated on neat REE in comparison to petrodiesel neat fuel.

Al-Widyan et al. (2002) [32] studied the use of different blends of waste vegetable oil ethyl esters (WOEE) with petrodiesel as fuel in a single-cylinder, direct injection diesel engine. The tests showed that the blends produced less CO and UHC emissions than neat petrodiesel fuel. Additionally, with the exception of 100% WOEE, CO₂ concentration decreased with engine speed. The authors also indicated that the blends burned more efficiently with less fuel consumption and higher power output. Overall, the best engine performance were obtained for

100% WOEE and 75:25 WOEE/petrodiesel blend while the 50:50 blend consistently gave the lowest amounts of emissions.

Puhana et al. (2005) [33] carried out the performance and emission engine of non-edible Mahua oil ethyl esters (MOEE) in a 4-stroke direct injection natural aspirated diesel engine. The authors reported that the brake specific fuel consumption (BSFC) for MOEE was higher than for petrodiesel fuel, explaining this result by the combined effect of low heating value and high density of MOEE. Nevertheless, equivalent thermal efficiency was observed for both MOEE and petrodiesel fuels. Moreover, a much higher exhaust gas temperature was observed for MOEE compared to petrodiesel (439°C and 249°C, respectively) due to a better combustion of MOEE. Concerning emissions of CO, UHC, and NO_x, these were reduced around 58, 63, and 12% respectively, in case of MOEE compared to petrodiesel fuel. However, the CO₂ emission was greater from MOEE, indicating that the ester fuel burned more efficiently than the petrodiesel one.

• *FAME versus FAEE as biodiesel and analysis in terms of various bio-lipid raw materials.* Makarevicienne et al. (2003) [34] compared the environmental effect of rapeseed oil methyl and ethyl esters (RME and REE, respectively) as biodiesel fuel. Exhaust emission tests were conducted by using a direct injection 4 cylinders diesel Audi 80 engine, fuelled with petrodiesel, blends of biodiesel/petrodiesel (25%, 50%, and 75% by volume esters), or neat biodiesel. Globally, their investigations showed that REE has less negative environmental effect than RME. Emissions of CO, UHC and smoke density decreased by 7.2%, 53%, and 72.6% respectively when substituting petrodiesel by neat REE. Even CO₂ emissions decreased by 782.87 g/kWh when neat REE was used against 782.26 g/kWh with neat RME. Concerning NO_x emissions, comparison of petrodiesel fuel with neat REE confirmed however that the latter leads to slight increase (around 8.3%). Nevertheless, petrodiesel blends with 25 - 50% by volume REE experienced slightly decrease in NO_x emissions. Finally, REE is more easily biodegradable in an aqua environment than RME.

Lapuerta et al. (2008) [28] studied the diesel performance and engine emissions of waste cooking oil methyl and ethyl esters (WCOM and WCOE, respectively). These biodiesels were tested neat and blended at 30% and 70% (volume basis) with a low sulphur petrodiesel fuel, which was evaluated too. All experiments were conducted in a 4 cylinder, 4-stroke, turbocharged, direct injection, 2.2 L Nissan diesel engine. Exhaust analysis showed a certain reduction of NO_x emissions from WCOE compared to those from WCOM. The authors explained this trend by a slight increasing in CN with the number of carbon atoms of the alcohol used, leading to lower premixed combustion. Moreover, the authors reported that the

type of alcohol used in the biodiesel production process had a significant effect on the total hydrocarbon (THC) emissions and on the PM composition. As the alcohol used was more volatile, both the THC emissions and volatile organic fraction of the PM were observed to increase (meaning that WCOM were again less favorable than WCOE). Nevertheless, slightly higher reduction in opacity was observed in the case of WCOM, consistently with its higher oxygen content.

Baiju et al. (2009) [18] carried out a comparative evaluation of compression ignition characteristics using methyl and ethyl esters of Karanja oil (KOME and KOEE respectively), a non-edible oil which can be extensively grown in the waste lands of India. KOME and KOEE samples were prepared by atmospheric homogeneous alkali catalysis with potassium hydroxide as catalyst. Compared to KOME, KOEE showed slightly higher viscosity, but better cold flow properties and a higher flash point. These observations helped to conclude that KOEE make the storage and transport safer than KOME. Performance and exhaust emission characteristics of the engine fuelled with blends of biodiesel and petrodiesel, or neat biodiesel, or also neat petrodiesel were conducted on a single cylinder four-stroke, compression ignition engine. Regarding blends and neat fuels, results obtained are in a agreement with those found in the open literature. Regarding specifically the behavior of KOME- or KOEE-biodiesels as fuel, the authors observed that KOME blends showed better performance and emission characteristics.

I.5 Biodiesel combustion kinetics

Oxidation kinetics of hydrocarbons has been the subject of numerous investigations, as presented in recent literature reviews related to this subject (Simmie et al., 2003 [36]; Battin-Leclerc, 2008 [37]). On the other hand, very few kinetic studies related to the oxidation of biodiesel have been carried out, at both experimental and modeling levels. The main reason of this lack of information is the molecular structure of actual biodiesel components (i.e. saturated and unsaturated fatty acid methyl or ethyl esters) involving large aliphatic main chains of 14 to 20 carbon atoms with allyl and ester groups (Figure I.1, Table I.1); such a complexity in the molecular structure of reactants poses a real challenge to modeling and also experimental kinetic studies.

Therefore, this part of the review was focused on oxidation modeling by detailed chemical kinetic mechanisms of biodiesel (surrogates and neat fuel) and on the experiments that are a prerequisite for the development and validation of the corresponding models which are built by using theoretical-based approaches accounting thermodynamic and kinetic phenomena.

I.5.1 Main features of model development and validation

I.5.1.1 Detailed chemical kinetic models and their basement

Models based on detailed chemical kinetic mechanisms showed very good performance for the prediction of hydrocarbon reactivity in the presence of oxygen (Simmie et al., 2003 [36]; Battin-Leclerc, 2008 [37]). This success is mainly due to the core methodology they are based on, according to which chemical changes occurring during reactions are described at the molecular level. Nevertheless, this molecular approach has two results. First, most of the proposed mechanisms have been detailed on a systematical way by using similar classes of reactions drawing a commonly admitted general kinetic scheme related to the primary oxidation reactions of the fuel molecule and its derived species (molecular and radical species). The slight differences between the classes of reactions used are described exhaustively in the Battin-Leclerc (2008) [37] literature review. Secondly, fuels comprising a large number of atoms involve mechanisms of large size. Therefore, two types of approach were adopted in the development of mechanisms and derived kinetic models, depending on the use or not of computer. Mechanisms (and derived kinetic models) based on non-computer help generation were generally built iteratively starting with small esters and progressing to larger ones. On the other hand, mechanisms based on computer-aided generation did not need to be developed iteratively, and were usually of smaller size by tailoring the sought mechanisms to the operating conditions of study. Hence, with EXGAS software (Touchard et al., 2005 [38]) which is to our knowledge the only automatic system of gas-phase oxidation mechanisms used for biodiesels and derivatives, only the significant classes of reactions for the temperature range of study may be activated via a menu. Summarily, EXGAS provides reaction mechanisms made of three parts (Battin-Leclerc, 2008) [37]:

- A C₀-C₂ reaction base, including all the reactions involving radicals or molecules containing less than three carbon atoms (periodically updated).
- A comprehensive primary mechanism based exclusively on elementary steps, and involving as molecular reactants only the initial organic compounds (fuel and oxygen).
- A secondary mechanism, containing reactions consuming the molecular products of the primary mechanism which do not react in the reaction base. In order to have a manageable size, the secondary mechanism involves lumped reactants (i.e., the molecules formed in the primary mechanism with the same molecular formula and the same functional groups are lumped into one unique species without distinguishing between the different isomers) and includes global reactions that produce, in the smallest number of steps, C₂₊ molecules or

radicals that can further decompose according to reactions included in the primary mechanism.

For all mechanisms, thermodynamic properties were determined by softwares, i.e. THERM (Ritter and Bozzelli, 1991 [39]) regarding non-computer based mechanisms and THERGAS (Muller et al., 1995 [40]) regarding computer-aided mechanisms. When not available in the literature or stored in the software databank, the thermodynamic properties were automatically computed by using the implemented method, i.e. usually Benson (1976) [41] method with updated group contribution and bond additivity values. Concerning kinetic properties (i.e. rate constants of each reaction) information available in the literature and stored in the software databank was used as first option. When not available, the kinetic properties were usually calculated by thermochemical kinetics or, when this procedure was not possible, were estimated by correlations based on quantitative structure-reactivity relationships or from quantum calculations. More precisely, each elementary reaction of the mechanism was written as reversible reaction and the reverse rate constant was computed from the corresponding the forward rate constant and the appropriate equilibrium constant $K_c = k_{\text{forward}}/k_{\text{reverse}}$ calculated from the appropriate thermochemical data. Concerning EXGAS (computer-based system for automatic generation of detailed kinetic models), KINGAS software (Warth et al., 1998 [42]) was devoted to this task of kinetic property calculation.

I.5.1.2 Model validation: experiments and environment modeling

Regarding oxidation experiments, they were conducted in various physical environments. The equipments used were selected for covering a wide range of reactors with different geometry (shock tube, premixed flames, diffusion flames, continuous jet stirred reactor, plug flow reactor, variable pressure flow reactor, or internal combustion engines) in which experiments could be conducted in large ranges of temperature, pressure, and biodiesel/oxygen equivalence ratios ϕ (i.e. $\phi < 1$ for fuel-lean mixtures and $\phi > 1$ for fuel-rich mixtures, see nomenclature for definition. Most of them (with the exception of shock tube yielding integrated information such as ignition delay) provide species-dependent and time-dependent information that is particularly valuable and relevant for model development and validation. As a result, experimental information generated from this large panel of physical environments warrants a wide-ranging kinetic modeling. However, while kinetic modeling aims to account for chemical phenomena, a suitable and reliable reactor modeling is required in turn to account for the physical environments. All these features need to be gathered to perform successfully reliable predictions of the fuel behavior during ignition, combustion, and

emissions in diesel and homogeneous compression ignition (HCCI) engines. Within this context, CHEMKIN II library software (Kee et al., 1993 [43]) offering the possibility of modeling a wide range of reactors was the most widely used tool among the scientist community relating to kinetics. Standardization of CHEMKIN II input data format for describing reactions, rate parameters, thermodynamic data, and transport properties of species favored this common use by facilitating the exchange of models between scientists (Battin-Leclerc, 2008 [37]).

I.5.1.3 Main guidelines of the past research and of the present review

Globally, if one wants to identify the main guidelines of the past research in the area of biodiesel oxidation for reliable prediction of engine behavior, it should be said that two major paths were followed. The first path is devoted to oxidation experiments and kinetic modeling oriented to small methyl and ethyl esters with 1 to 4 carbon atoms (C_1 - C_4) in their aliphatic main chain. These works allowed focusing attention on the special features of methyl and ethyl ester group reactivity. The second path is devoted to the generation of experimental information by conducting oxidation of actual biodiesel fuel and components followed by the comparison with simulation results obtained from oxidation mechanisms of large n-alkanes. This approach assumes that large n-alkanes and fatty acid methyl or ethyl esters with the same number of carbon atoms in their aliphatic main chain have approximately the same behavior during oxidation.

Nevertheless, authors agreed themselves that all alkyl esters with an aliphatic main chain in C_1 - C_2 were too small molecules to be considered as potential biodiesel surrogates (i. e. methyl and ethyl formate or acetate; Dagaut et al., 1997 [44]; Gasnot et al., 2005 [45]; Osswald et al., 2007 [46]; Westbrook et al., 2009 [47]). The firstly minded acceptable biodiesel surrogate among the small alkyl esters investigated was methyl butanoate with an aliphatic main chain in C_4 and the challenge of the further research work was to extend the kinetic modeling capabilities to alkyl esters with larger aliphatic main chain in order to reproduce reliably the reactivity of actual biodiesel components: early (low temperature) CO_2 production from the ester group and burning similarly to petrodiesel. These features are described in more details in the following sections, once some chemical basements of the combustion process would shortly be given.

Nevertheless, since the subject of the present PhD dissertation concerns short ethyl esters as biodiesel surrogates with the corresponding methyl esters as comparative references, the core of this literature survey has been restricted to this class of compounds, whereas the

oxidation related to longer alkyl (ethyl and methyl) esters was reported to the appendix AI. Hence, this first chapter may be of more reasonable length and focused on the core subject of the PhD work, while providing to the reader the possibility to refer to the appendix AI at his option.

In the following, alkyl (methyl or ethyl) esters with aliphatic main chains comprising n carbon atoms will be designated C_n -alkyl esters; in others words C_n -methyl (ethyl) esters will designate molecules with $n+1$ ($n+2$) carbon atoms. The experimental data generated for the oxidation of alkyl esters selected as biodiesel surrogates were summarized in Table I.9 whereas the main features related to the developed chemical kinetic models were shortly given in Table I.10. Both Tables were located at the end of the section (I.5.4).

I.5.2 General kinetic scheme and classes of elementary reactions in combustion process

The general kinetic scheme and classes of elementary reactions used for the development of the detailed chemical kinetic mechanisms proposed in the open literature for the oxidation of esters with aliphatic main chains in C_n , $n \geq 4$ are similar to those established by Curran et al. (1998) [48], (2002) [49] for the oxidation of *n*-heptane and iso-octane. Extension to alkyl ester molecules was achieved by including the chemistry information specific to the ester moiety. The resulting general kinetic scheme is shown in Figure I.4 (Herbinet et al., 2008 [50]), while the classes of elementary reactions considered for the generation of alkyl ester oxidation mechanisms are listed in Table I.3. Note that the main changes to these elementary reactions compared to the work by Curran et al. (1998) [48], (2002) [49] are firstly the class of reaction 26 which is specific to esters (Metcalf et al., 2007 [51]) and secondly the chemical nature of the species hidden behind the notation R^\bullet , R' , Q , and X . By the way, the naming conventions commonly adopted both in Figure I.4 and Table I.3 are R^\bullet and R' , denote alkyl or alkyl ester radicals or structures while Q and X denoting C_nH_{2n} or $C_nH_{2n}COO$ species and structures.

As shown in Figure I.4, two main reaction pathways, with a three-way branching on one of them, clearly stand out depending on the temperature range. First, the oxidation process of the ester RH is initiated by abstraction of a hydrogen atom (H-abstraction or metathesis) from RH (at both low and high temperature) and by unimolecular decomposition of RH (at high temperature only) leading to the formation of alkyl and alkyl ester radicals R^\bullet (reaction 1, Figure I.4). These radicals may then follow either the *high temperature* or the *low temperature* dominate pathway. At *high temperature* (approximately above 800K), unimolecular decomposition by β -scission is the dominant route yielding olefins or olefinic esters (stable

molecules) plus smaller radical species R^{\bullet} (reaction 2, Figure I.4), with contribution of isomerizations.

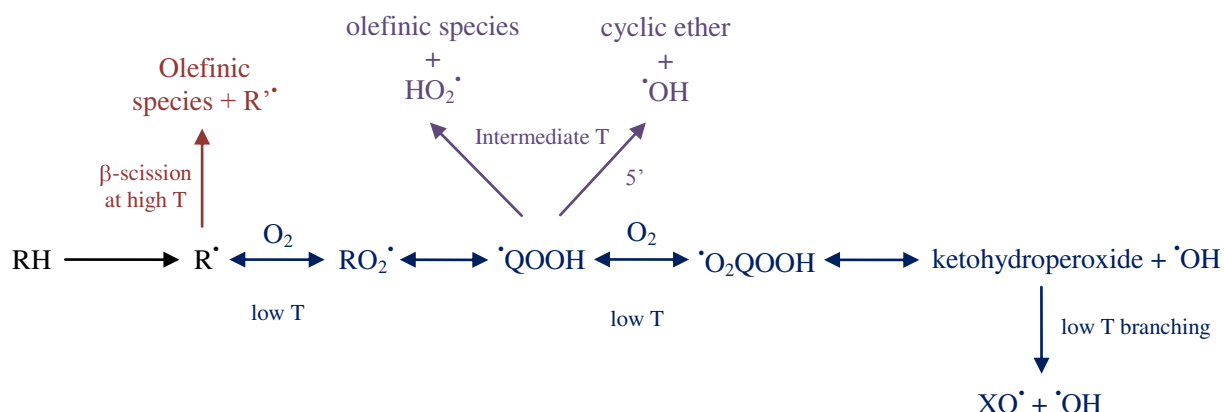


Figure I.4: Primary oxidation reaction pathways common to methyl and ethyl esters (aliphatic main chain $C_n, n \geq 4$) – Adaptation from Curran et al. (1998) [48] work (Herbinet et al., 2008 [50]).

Olefins and olefinic esters formed through these primary routes react in turn through the same types of reactions as the fuel molecule and through other reactions specifically due to the presence of the double bond: additions of radicals to the double bond, decomposition by retro-ene reactions (Herbinet et al., 2008 [50]). On the other hand, at *low temperatures* (approximately around 500-600K), the alkyl and alkyl ester radicals R^{\bullet} mainly undergo addition to O_2 leading to alkyl and alkyl-ester peroxy radicals RO_2^{\bullet} (reaction 3, Figure I.4), which in turn react by isomerizations to hydroperoxy alkyl and hydroperoxy alkyl ester radicals $\bullet QOOH$ (reaction 4, Figure I.4). At this point of the oxidation scheme, a three-way branching allow $\bullet QOOH$ radicals for undergoing three pathways, the first two dominating at intermediate temperatures: (reaction 5, Figure I.4) a C-O β -scission decomposition to olefinic alkyl or alkyl ester stable molecule plus HO_2^{\bullet} ; (reaction 5', Figure I.4) a decomposition to cyclic ether plus $\bullet OH$; (reaction 6, Figure I.4) a second addition to O_2 leading to hydroperoxy peroxy radicals $\bullet O_2QOOH$. The product of this second addition leads to $\bullet OH$ and ketohydroperoxyde species (reaction 7, Figure I.4) which then undergo through low temperature branching reaction with decomposition in two radicals (reaction 8, Figure I.4) (Battin-Leclerc, 2008 [37]; Herbinet et al., 2008 [50]). Thus, it can be seen clearly that at two points of the general oxidation scheme, intermediate radicals (R^{\bullet} formed by reaction 1- Figure I.4, and then, $\bullet QOOH$ formed by reaction 4- Figure I.4) are involved in competitive reaction pathways that are dominant in different temperature range and additionally lead to chain reactions of different modes. Globally, these competitive reaction pathways are of two classes:

(i) unimolecular decomposition by β -scission occurring at high and intermediate temperature and leading to *chain-propagation* reactions that produce one radical flux (reactions 2, 5, or 5' in Figure I.4), and (ii) addition to O_2 occurring at lower temperature and leading to *chain-branching* reactions that produce two radical flux (reactions 3 and 6 leading to reaction 8 in Figure I.4). This competition repeated twice between branching channels and propagation channels may involve global variation in reactivity over some temperature range. Of course, there is a direct relationship between these features of the general kinetic scheme related to the oxidation of alkyl esters and the fuel molecule behavior during actual combustion. This is in fact the subject of the following section.

Table I.3: Major classes of elementary reactions used as basement by oxidation mechanisms proposed in the literature (extension of the work by Curran et al., 1998 [48]; 2002 [49] to methyl and ethyl ester oxidation).

1.	Unimolecular fuel decomposition
2.	H-atom abstraction from the fuel (ester)
3.	Alkyl or alkyl ester radical decomposition
4.	Alkyl or alkyl ester radical + O_2 to produce olefinic molecule + HO_2^\bullet directly
5.	Alkyl or alkyl ester radical isomerization
6.	Abstraction reactions from olefinic molecule by $^\bullet OH$, H^\bullet , O^\bullet , and $^\bullet CH_3$
7.	Addition of radical species to olefinic molecules
8.	Alkenyl radical decomposition
9.	Olefinic molecule decomposition
10.	Addition of alkyl or alkyl ester radicals to O_2
11.	$R^\bullet + R'O_2^\bullet \rightarrow RO^\bullet + R'O^\bullet$
12.	Alkyl peroxy radical isomerization ($RO_2^\bullet = ^\bullet QOOH$)
13.	$RO_2^\bullet + HO_2^\bullet \rightarrow RO_2H + O_2$
14.	$RO_2^\bullet + H_2O_2 \rightarrow RO_2H + HO_2^\bullet$
15.	$RO_2^\bullet + CH_3O_2^\bullet \rightarrow RO^\bullet + CH_3O^\bullet + O_2$
16.	$RO_2^\bullet + R'O_2^\bullet \rightarrow RO^\bullet + R'O^\bullet + O_2$
17.	$RO_2H \rightarrow RO^\bullet + ^\bullet OH$
18.	RO^\bullet decomposition
19.	$^\bullet QOOH \rightarrow QO + ^\bullet OH$ (cyclic ether formation via cyclization of diradical)
20.	$^\bullet QOOH \rightarrow$ olefinic molecule + HO_2^\bullet (radical site β to OOH group)
21.	$^\bullet QOOH \rightarrow$ olefinic molecule + carbonyl + $^\bullet OH$ (radical site γ to OOH group) ^a
22.	Addition of $^\bullet QOOH$ to O_2

Table I.3 (Continued)

-
- | | |
|-----|--|
| 23. | Isomerization of $\cdot\text{O}_2\text{QOOH}$ and formation of ketohydroperoxide and $\cdot\text{OH}$ |
| 24. | Decomposition of ketohydroperoxide to form oxygenated radical species and $\cdot\text{OH}$ |
| 25. | Cyclic ether reactions with $\cdot\text{OH}$ and $\text{HO}_2\cdot$ |
| 26. | Unimolecular elimination involving a six-membered transition state and leading to the formation of ethylene and a carboxylic acid molecule for ethyl esters or ethylene and a shorter ester for methyl esters (Metcalfé et al., 2007 [51]) |
-

^a This class of reaction was most often neglected.

I.5.3 Negative Temperature Coefficient and related low temperature phenomena

The negative temperature coefficient (NTC) region signifies a zone of temperature in which the overall reaction rate decreases with temperature (Figure I.5). Occurring usually around 500 to 800 K, this phenomena is specific to low temperature oxidation process. As mentioned in the previous section, some explanations can be directly deduced from the general oxidation scheme (Figure I.4). At low temperature, *chain-branching* is mainly due to the O_2 addition reaction pathway leading through the ketohydroperoxide species (reaction 7, Figure I.4). As temperature increases, the *chain-propagation* reactions of $\cdot\text{QOOH}$ species (reactions 5 and 5', Figure I.4) increase because the energy barrier to their formation is more easily overcome, leading to the formation of cyclic ether species and olefinic molecules at the expense of the reaction pathways through the ketohydroperoxide species (reaction 8, Figure I.4). The increasing importance of these propagation channels leads to a lower reactivity of the system, which is observed as the NTC region. However, propagation channel related to high temperature β -scissions should also start to contribute partially to these phenomena. In other words, NTC phenomena could be considered as a chemical transient regime allowing going continuously from established chemical low to high temperature regimes. This feature commonly encountered in case of hydrocarbon combustion (Curran et al., 1998 [48]; 2002 [49]) is also observed when operating in engine conditions with esters comprising aliphatic main chains in C_n , $n \geq 5$ (HadjAli et al., 2009 [52]) for which oxidation mechanisms may involve temperature range dependent competition between chain-propagating channels and chain-branching channels.

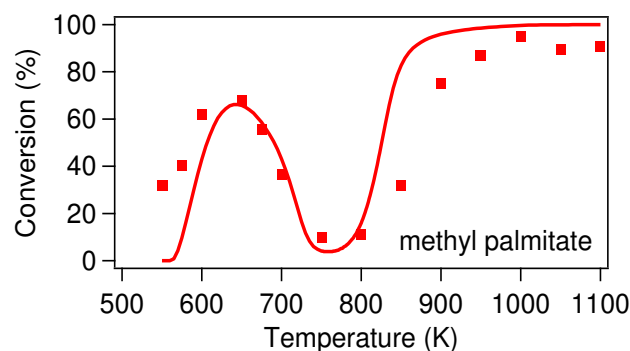


Figure I.5: Illustration of the negative temperature coefficient region

(Herbinet et al., 2010 [53]).

Other intimately related low-temperature phenomena are usually encountered when NTC behaviour is exhibited. These are cool flame phenomena occurring at temperatures several hundred degrees below the minimum autoignition temperature and transition from single-stage low-temperature heat release (LTHR) to two-stage ignition with the increase of engine compression ratio. During a cool flame (or multiple cool flames) the temperature and the pressure increase strongly over limited temperature range (typically up to 500 K), but the reaction stop before combustion is complete due to the decrease in reactivity in the NTC region (Battin-Leclerc, 2008 [37]). Hence, cool flames are actually the first-stage of two-stage ignition and thus lead to the appearance of LTHR. LTHR is initiated by the decomposition of ketohydroperoxides at low-temperature (Figure I.4, reactions 1, 3, 4, 6, 8) while HTHR is induced by the rapid dissociation of H_2O_2 into $\cdot\text{OH}$ radicals (Zhang and Boehman, 2010) [54].

I.5.4 Kinetic investigations related to C_4 -methyl esters

Kinetic investigations related to methyl esters are presented first for methyl butanoate (molecule firstly selected as biodiesel surrogate) and then, for methyl crotonate (methyl (E)-2-butenate), while studies related to methyl hexanoate, methyl decanoate (much closer and closer in size to actual biodiesel components), and finally for a commercial biodiesel (methyl ester rapeseed oil) are given in appendix AI.

I.5.4.1 Oxidation of methyl butanoate as a biodiesel surrogate

Firstly selected as a biodiesel surrogate, methyl butanoate (MB) ($\text{C}_3\text{H}_7(\text{C}=\text{O})\text{OCH}_3$) has been the subject of many published kinetic studies [51, 52, 55-66]. This C_4 -methyl ester was originally chosen as the mimetic model molecule of larger biodiesel components (C_{16} - C_{22} methyl esters, Table I.1) in order to limit the number of possible products formed to a manageable level and to handle a reaction mechanism of manageable size from which it would be possible to focus on the kinetic description of the methyl ester moiety. The main chemical

structure features that are relevant to account for the combustion characteristic of biodiesel *i.e.*, ester moiety and aliphatic main chain of sufficient length, were thought to be saved. Indeed, MB is large enough to allow the fast RO_2^\bullet isomerization reaction (class of reactions 12 in Table I.3; reaction 4 in Figure I.4) that play a key role in the low-temperature chemistry and control fuel autoignition under conditions found in diesel engines.

The first detailed chemical kinetic mechanism for the combustion of MB was developed by Fisher et al. (2000) [55]. This first proposal comprised 264 species and 1219 reactions (Table I.10) and was established by introducing to the existing oxidation mechanism for n-heptane by Curran et al. (1998) [48] (with updated data by Curran et al., 2002 [49]) the submechanism describing the specificity of MB oxidation. Fisher et al. (2000) [55] model was tested against the limited combustion data available at this time in the literature. These were conducted in closed vessels, under low temperature and subatmospheric conditions (Parson and Dandy, 1936 [67]; Parsons and Hinshelwood, 1956 [68]; Parson, 1956 [69]; Hoare et al., 1967 [70]). SENKIN software (Lutz et al., 1988 [71]) was used to perform the chemical kinetic calculations in which thermodynamic properties of the involved species were estimated by Benson (1976) [41] group and bond additivity methods. Some qualitative agreement was obtained; however, calculations consistently indicated higher overall reactivity by a factor of 10-50 compared with experiments. Also, accordingly to the same experimental data, Fisher et al. (2000) [55] model predicts a weak NTC behavior for MB oxidation that the authors explained thanks to their proposed low- and high temperature reaction pathways (Figure I.6). Obviously, part of the general kinetic scheme given in Figure I.4 for alkyl ester oxidation can be seen again when applied to the MB molecule, as this one directly derives from Fisher et al. work which got the original idea. Particularly, it can be seen again at two points of Fisher et al. scheme (Figure I.6), competition between chain-propagation channels (from unimolecular decomposition at high temperature) and chain-branching channels (from O_2 addition at low temperature), which usually involves NTC phenomena.

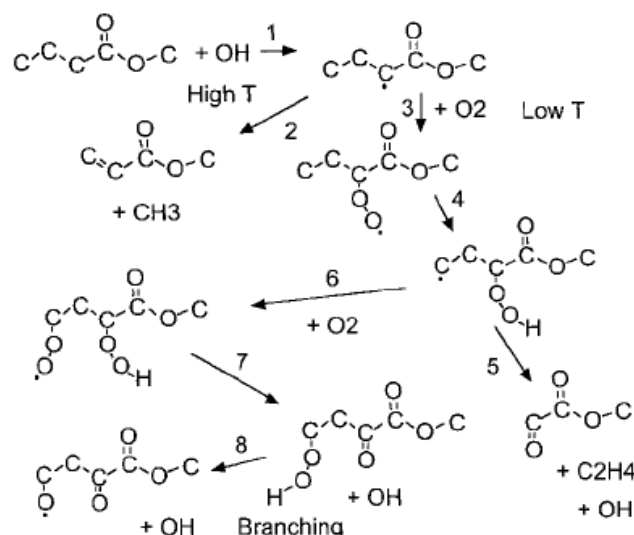


Figure I.6: Key low- and high-temperature reaction pathways of methyl butanoate oxidation for one of the four possible hydrogen abstraction sites (Fisher et al., 2000 [55])^a.

^a The three other possible sites of H-abstraction are on the carbon in α - or β - to the radical site illustrated in the figure and on the methyl group of the ester function.

Later, Marchese et al. (2004) [56] conducted MB oxidation in a flow reactor operating under moderate pressures, over low to medium temperatures, with various equivalence ratios, and a residence time set to a constant value (Table I.9). Profiles of the reactant, intermediate and product species determined during experiments were compared with simulation results obtained from Fisher et al. (2000) [55] mechanism. Good agreement was obtained under stoichiometric conditions, but the model over-predicted the experimentally observed reactivity under fuel rich conditions whilst under-predicting it under fuel-lean conditions.

More recently, Gail et al. (2007) [57] proposed a revised version of Fisher et al. (2000) [55] mechanism, developed and validated on the basis of new experimental results they generated over a wide range of operating conditions by using various equipments: a jet-stirred reactor (JSR), a Princeton variable pressure flow reactor (VPFR), and an opposed flow diffusion flame (OFDF) (Table I.9). Molar fraction profiles for a large number of molecular species were obtained from JSR and VPFR experiments: - MB and O₂ (reactant); - H₂, CO, CO₂, acetylene, methane, ethylene, ethane, propene, propane, formaldehyde, methanol, methyl propenoate, propanal, methyl crotonate (major products); allene, acrolein, acetaldehyde, 1-butene, 1,3-butadiene (minor products); - methyl vinyl ketone (traces). Similar trends were observed for the profiles of the molecular species obtained from OFDF experiments. Gail et al. (2007) [57] new model consists of 295 species and 1498 reactions. Several rate constant parameters of the original mechanism by Fisher et al. (2000) [55] were modified as described

in Table I.4, and a C₄-submechanism taken from the work by Dagaut (2002) [72] was added to simulate the measured 1-butene and 1,3-butadiene profiles. The kinetic modeling is in reasonable agreement with the experimental results. However, under JSR conditions, reactivity of MB was under-predicted by the model at low temperature. Concerning OFDF data, the same model showed, in general, higher reactivity for intermediate species and lower reactivity for MB than observed in experiment. On the other hand, the model reproduced quite well the VPFR data at stoichiometric conditions, and neither the model nor the experiments show evidence of NTC region. It was only for the leanest investigated equivalence ratios that very little NTC behavior could be observed between 600 and 800K.

Table I.4: Reaction rate constants modified by Gail et al. (2007) [57] (bold) in the Fisher et al. (2000) [55] MB mechanism.

Reaction	A	n	E _a
CH ₃ CH ₂ CH ₂ (C=O)OCH ₃ + H [•] = H ₂ + CH ₃ CH ₂ •CH(C=O)OCH ₃	2.52E + 14	0.00	7300
CH₃CH₂CH₂(C=O)OCH₃ + H[•] = H₂ + CH₃CH₂•CH(C=O)OCH₃	1.00E + 14	0.00	7300
CH ₃ O [•] (+M) = CH ₂ O + H [•] (+M)	5.45E + 13	0.00	13500
CH₃O[•] (+M) = CH₂O + H[•] (+M)	1.38E + 21	-6.65	33190
C ₂ H ₃ [•] + O ₂ = CH ₂ O + HCO [•]	1.70E + 29	-5.31	6500
C₂H₃[•] + O₂ = CH₂O + HCO[•]	1.66E + 13	-1.39	1013

The same year, Metcalfe et al. (2007) [51] reported the oxidation of MB in shock tube. Ignition delay times were measured behind reflected shock waves at two low pressures (1 and 4 atm), over the temperature range 1100-1670 K, and for various equivalence ratios (Table I.9). Their experimental results showed that at both pressures, the ignition delay times increased as MB concentration increased. Furthermore, the detailed mechanism proposed by the authors for MB oxidation was derived from the Fisher et al. (2000) [55] model to which some changes were made as mentioned in the following.

- The H₂/O₂ mixture submechanism has been replaced with that published recently by O’Conaire et al. (2004) [73].
- The bond enthalpy of the C-H bond α to the carbonyl group has been reduced to 93.6 kcal·mol⁻¹ from 96.2 kcal·mol⁻¹, due to recent quantum theory-based estimations by El-Nahas et al. (2007) [74]. Note that the value adopted by Metcalfe et al. (2007) [51] corresponds to the group additivity estimates and not to the *ab initio* calculations (94.2 kcal·mol⁻¹) made by El-Nahas et al. (2007) [74].

- The rate constants for MB radical decomposition have been adjusted taking into account alkyl and alkoxy radical decomposition according to the work by Curran (2006) [75].
- The high-pressure limit rate constant expressions for unimolecular ester fuel decomposition reactions have been decreased by 66% (multiplied by 0.33).
- Unimolecular fuel decomposition reactions have been treated using quantum Rice-Ramsperger-Kassel theory to account for pressure falloff (variation of the rate constant as a function of pressure).
- A six-centered unimolecular elimination reaction that yields ethylene and methyl ethanoate (methyl acetate) was added (Figure I.7) with an activation energy of 68 kcal·mol⁻¹ (El-Nahas et al., 2007 [74]).

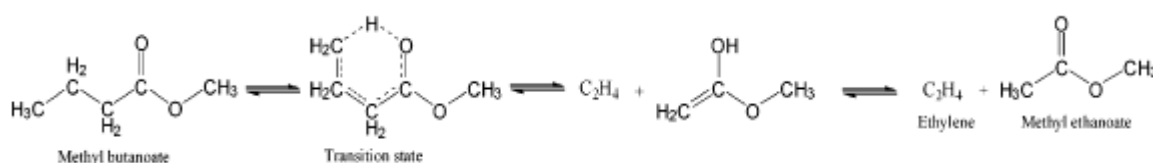


Figure I.7: Six-centered unimolecular elimination for methyl butanoate producing methyl ethanoate and ethylene (Metcalf et al., 2007 [51]).

However, the authors found that this last pathway (Figure I.7) contributes very little (<1%) to the MB decomposition for the conditions investigated during the work.

Following this work, measurements of ignition delay for MB were carried out by Dooley et al. (2008) [58] at low temperatures (640-949 K) in a rapid compression machine (RCM) and at higher temperatures (1250-1760 K) in a shock tube (Table I.9). The auto-ignition of methyl butanoate was observed to follow the Arrhenius law ($\tau = A \cdot \exp(-E/RT)$) over all conditions studied. The authors also proposed a detailed chemical kinetic mechanism which is an extensively modified version of their previous work (Metcalf et al., 2007 [51]). The main changes are shortly listed below (an exhaustive description is given in Dooley et al., 2008 [58] paper):

- Some bond enthalpy values originally given in Fisher et al. (2000) [55] work were reevaluated employing THERM (Ritter and Bozzelli, 1991 [39]) with updated H/C/O and bond dissociation groups (Lay et al., 1995 [76]; Sumathi and Green, 2003 [77]). These values concern the $n\text{C}_3\text{H}_7\text{C}(\text{O})\text{O}-\text{CH}_3$ and $n\text{C}_3\text{H}_7-\text{C}(\text{O})\text{OCH}_3$ bonds reduced to 86.8 and 89.9 kcal·mol⁻¹ from 101.2 and 92.0 kcal·mol⁻¹, respectively. These values are

in substantial agreement with the work by El-Nahas et al. (2007) [74] who proposed from *ab initio* calculations 87.0 and 93.4 kcal·mol⁻¹, respectively.

- Due to the intrinsically hierarchical nature of their detailed chemical kinetic mechanism, the C₃-submechanism (involving species with 3 carbon atoms) to which the MB chemistry was added had been updated according to recent works by Petersen et al. (2007) [75].
- Also, a C₄-submechanism (involving species with 4 carbon atoms) was added based on the work by Curran et al. (1998 [48], 2002 [49]) to account for C₄ species observed in Gaïl et al. (2007) [57] experiments.
- The low-temperature chemistry describing isomerization of alkylperoxyl radicals to hydroperoxyl alkyl radicals (reaction 4, Figure I.4) was not included. This choice was motivated by the experimentally non-observed low temperature reactivity.

The new mechanism consists of 275 species and 1545 reactions and was validated against the data generated by the authors (in RCM and shock tube), but also against the data reported in the literature (in a flow reactor by Marchese et al., 2004 [56], a shock tube by Metcalfe et al., 2007 [51], a JSR and an OFDF by Gaïl et al., 2007 [57]). Simulations were in good agreement with the whole experimental data selected. However, the agreement with the RCM ignition delays was less accurate. In addition, analysis of the kinetic model confirmed that depending on operating conditions of temperature, pressure, and equivalence ratio, different reaction pathways become prominent. In particular, the importance of unimolecular fuel decomposition at high temperatures (reaction 1, Figure I.4), the processes of the HO₂[•] radical at low to intermediate temperatures (steps successive to reaction 5, Figure I.4), and the importance of fuel alkyl radical decomposition (reaction 2, Figure I.4) under fuel-rich conditions were highlighted. Also, from their results in shock tube and RCM, Dooley et al. (2008) [58] concluded that MB did not exhibit NTC behavior.

In order to meet the internal combustion engine conditions, Walton et al. (2009) [59] performed recently experimental ignition of MB by using a RCM over low temperature (935-1117 K) and moderate pressure (4.7 - 19.6 atm) conditions (Table I.9). Rate constants of some MB reactions from Metcalfe et al. (2007) [51] mechanism were slightly modified to improve the agreement between computed and experimental results. These reactions are gathered in Table I.5. Overall, the agreement between the computed and experimental results was excellent for all temperatures. Also, the results obtained by the authors support the assumption that MB consumption would be dominated by relatively slow bimolecular H-atom abstraction reactions.

Table I.5: Reaction rate constants modified by Walton et al. (2009) [59] from Metcalfe et al. (2007) [51] mechanism related to MB oxidation. ^a

Reaction	A	n	E _a
$\text{CH}_3\text{CH}_2\text{CH}_2(\text{C}=\text{O})\text{OCH}_3 + \text{HO}_2^\bullet = \text{H}_2\text{O}_2 + \bullet\text{CH}_2\text{CH}_2\text{CH}_2(\text{C}=\text{O})\text{OCH}_3$	1.90E + 12	0.00	20440
$\text{CH}_3\text{CH}_2\text{CH}_2(\text{C}=\text{O})\text{OCH}_3 + \text{HO}_2^\bullet = \text{H}_2\text{O}_2 + \text{CH}_3\bullet\text{CHCH}_2(\text{C}=\text{O})\text{OCH}_3$	1.30E + 12	0.00	17690
$\text{CH}_3\text{CH}_2\text{CH}_2(\text{C}=\text{O})\text{OCH}_3 + \text{HO}_2^\bullet = \text{H}_2\text{O}_2 + \text{CH}_3\text{CH}_2\bullet\text{CH}(\text{C}=\text{O})\text{OCH}_3$	1.30E + 12	0.00	17690
$\text{CH}_3\text{CH}_2\text{CH}_2(\text{C}=\text{O})\text{OCH}_3 + \text{HO}_2^\bullet = \text{H}_2\text{O}_2 + \text{CH}_3\text{CH}_2\text{CH}_2(\text{C}=\text{O})\text{O}\bullet\text{CH}_2$	1.90E + 12	0.00	20440
$\text{CH}_3\text{CH}_2\text{CH}_2(\text{C}=\text{O})\text{OCH}_3 + \text{H}^\bullet = \text{H}_2 + \bullet\text{CH}_2\text{CH}_2\text{CH}_2(\text{C}=\text{O})\text{OCH}_3$	1.88E + 05	2.75	6280
$\text{CH}_3\text{CH}_2\text{CH}_2(\text{C}=\text{O})\text{OCH}_3 + \text{H}^\bullet = \text{H}_2 + \text{CH}_3\bullet\text{CHCH}_2(\text{C}=\text{O})\text{OCH}_3$	1.30E + 06	2.40	4471
$\text{CH}_3\text{CH}_2\text{CH}_2(\text{C}=\text{O})\text{OCH}_3 + \text{H}^\bullet = \text{H}_2 + \text{CH}_3\text{CH}_2\bullet\text{CH}(\text{C}=\text{O})\text{OCH}_3$	1.30E + 06	2.40	4471
$\text{CH}_3\text{CH}_2\text{CH}_2(\text{C}=\text{O})\text{OCH}_3 + \text{H}^\bullet = \text{H}_2 + \text{CH}_3\text{CH}_2\text{CH}_2(\text{C}=\text{O})\text{O}\bullet\text{CH}_2$	1.88E + 05	2.75	6280

^a The remainder of the mechanism from Metcalfe et al. (2007) [51] was unchanged. The rate coefficients are listed in the generalized Arrhenius form ($k=A\cdot T^n\cdot\exp(-E_a/RT)$) where units are mole, cm, s, cal, and K.

Later on, Hakka et al. (2009) [61] carried out an experimental and modeling study of the oxidation of MB and ethyl butanoate (EB) in shock tube (ST) and jet-stirred reactor (JSR). From JSR experiments (operating conditions: atmospheric pressure, at two moderate temperatures 800 and 850 K, for various residence times, Table I.9), molar fraction profiles vs. residence time could be generated for various molecular species: - MB and O₂ relating the reactants; - CO, CO₂, methane (CH₄), acetylene (C₂H₂), ethylene (C₂H₄), propane (C₂H₆), methyl acrylate (methyl propenoate), and methyl crotonate (methyl (E)2-butenate) relating the intermediates and final products. Concerning the new experimental data generated in shock tube, ignition delay times were performed by recording $\bullet\text{OH}$ emissions behind reflected shock waves for various operating conditions (moderate pressure, over a large range of high temperature (1250-2000 K), and for fuel-rich, stoichiometric and fuel-lean compositions, (Table I.9). A new mechanism for MB was proposed by using a version of EXGAS software (Touchard et al., 2005 [38]) improved for taking into account oxygenated reactants (Hakka et al., 2009 [61]; Biet et al., 2008 [78]). In the case of esters, the bond enthalpy of the C-H bond α to the carbonyl group was taken equal to 95.6 kcal·mol⁻¹ as proposed by Luo (2003 [79]) for ethyl propanoate. The mechanism of MB oxidation could be applied from low to high temperatures and involved 203 species and 1317 reactions (Table I.10). The simulations were performed using SENKIN (for ST related results) and PSR (for JSR related results) modules of

CHEMKIN II software (Kee et al., 1993 [43]). The authors reported that the agreement between experimental and simulated ignition delays of MB was satisfactory. The same trend was observed with the ignition delay times previously measured by Metcalfe et al. (2007) [51] and Walton et al. (2009) [59]. Nevertheless, concerning experimental results obtained in JSR, the kinetic model overpredicted MB consumption and productions in CO and CO₂ but underpredicted ethylene formation. However, consumption of O₂ and formation of CH₄, methyl acrylate, and methyl crotonate were correctly reproduced. Reaction flux analysis performed under ST and JSR conditions (at 1370 and 800 K, respectively and for 50% conversion in MB) showed that MB is mainly consumed by H-abstractions with H[•], [•]OH, and HO₂[•] radicals, the main contributors.

Very recently, to provide complementary data on MB autoignition, Akih-Kumgeh and Bergthorson (2010) [60] measured ignition delay times behind reflected shock waves (by CH emissions) at moderate pressures (1.2–11.4 atm) and high temperatures (1060–1632 K) for various equivalence ratios in oxygen/argon mixtures (Table I.9). Measurements were also carried out for n-heptane as fuel (instead of MB) for comparison. The generated experimental results for MB were compared with simulations obtained by using the modified version of Fisher et al. (2000) [55] model by Dooley et al. (2008) [58], together with Hakka et al. (2009) [61] model. CANTERA software by Goodwin (2003) [80] was used for modeling the shock tube ignition process as a constant volume adiabatic reactor. The authors found that MB and n-heptane had comparable high-temperature ignition delay times under stoichiometric conditions, but differences were observed at other conditions. Also, good agreement was observed between the data generated by the authors and previous published data (Metcalfe et al., 2007 [51]; Hakka et al., 2009 [61]) while some deviations were obtained between the two test models (Dooley et al., 2008 [58]; Hakka et al., 2009 [61]). The authors highlighted that generally the model by Dooley et al. (2008) [58] predicted longer ignition delays than the model by Hakka et al. (2009) [61], with good agreement at low-temperatures and more pronounced deviations at higher temperatures. Additionally, the two test models deviated from experiments under rich-conditions (while good agreement was obtained at stoichiometric conditions).

I.5.4.2 Pyrolysis of methyl butanoate

Oxidation mechanisms at high temperatures include characteristic reactions of pyrolysis as a purely thermal process (for example, fuel-unimolecular decompositions or bimolecular H-abstractions from the fuel). Therefore, it is interesting to quote some works on ester pyrolysis as they can be used as core partial submechanism to study the combustion of ester species.

Farooq et al. (2009) [63] studied the high-temperature thermal decomposition of three methyl esters (methyl acetate, methyl propionate, and MB) in a shock tube, by measuring the CO₂ mole fraction time-histories during pyrolysis. Measurements were conducted at high temperatures (1260-1653 K), with high reactant compositions (favorable for H-abstractions), and under low pressure (Table I.9). It was found that the CO₂ yields during pyrolysis were high and not strongly dependent on the aliphatic main chain length of the methyl ester. The incorporation of the theoretical work by Huynh and Violi (2008) [62] into the Fisher et al. (2000) [55] model allowed Farooq et al. (2009) [63] to account accurately the CO₂ yields experimentally observed, except at the highest temperatures. The theoretical work by Huynh and Violi (2008) [62] consisted in the development of a new computed kinetic sub-model for MB thermal decomposition including both pyrolysis and oxidation processes by using *ab initio* techniques. The rate constants for the unimolecular and bimolecular reactions in the temperature range of 300-2500 K were calculated using Rice-Ramsperger-Kassel-Marcus (RRKM) and transition state theories, respectively. Due to the rather low barrier of the H-abstraction reactions between MB and flame radicals H[•], [•]OH, and CH₃[•], Huynh and Violi (2008) [62] focused their work to this class of reactions. Thirteen pathways (Figure I.8) were identified for MB thermal decomposition initiated by H-abstraction reactions and leading to the formation of small species such as [•]CH₃, [•]C₂H₃, CO, CO₂, and formaldehyde (H₂CO). Kinetic simulation results for a high temperature pyrolysis environment showed that the H[•] + MB reaction was the most important one in the initial stage of MB breakdown. In addition, the [•]C(O)OCH₃ = CO + CH₃O[•] reaction was found to be the main source of CO formation.

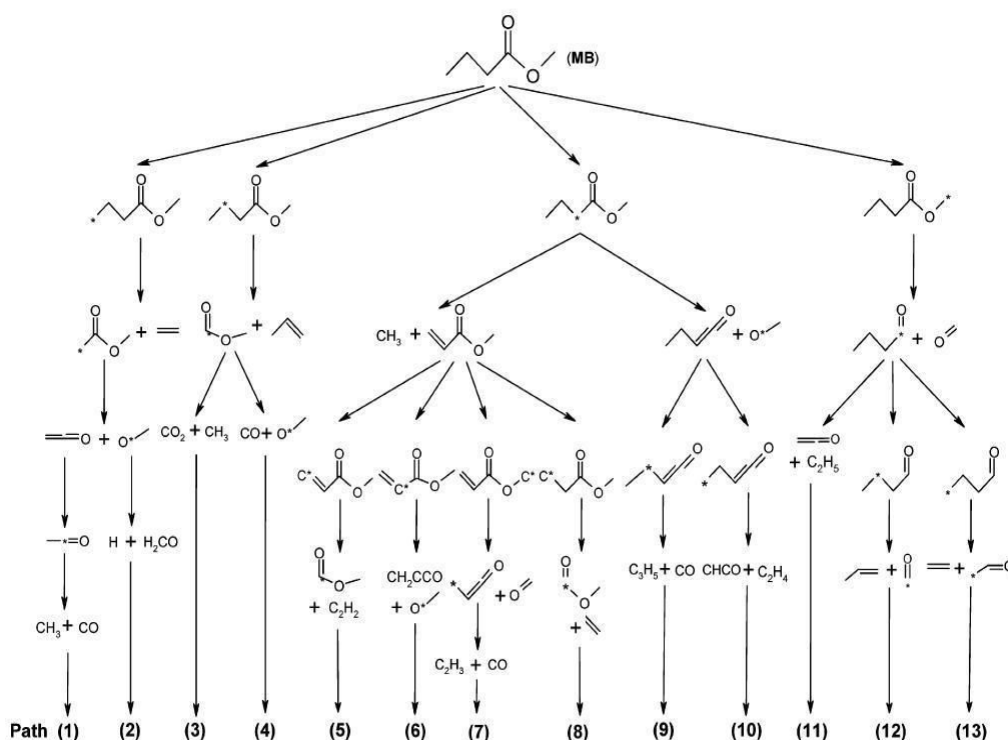


Figure I.8: The thirteen pathways for methyl butanoate thermal decomposition initiated by hydrogen abstraction reactions (Huynh and Violi, 2008 [62]).

I.5.4.3 Oxidation of methyl crotonate

Since biodiesel is mainly composed of fatty acid esters with one or two degrees of unsaturation, it is important to understand the impact of the presence of double bonds on the combustion chemistry. Therefore, various studies were conducted on methyl (E)-2-butenate, i.e. under its trivial name methyl crotonate (MC), that corresponds to one of the unsaturated C₄-methyl ester (CH₃CH=CH(C=O)OCH₃) for which oxidation behavior can be compared with the corresponding saturated C₄-methyl ester, MB (CH₃CH₂CH₂(C=O)OCH₃) firstly selected as biodiesel surrogate. Also, these studies are very helpful for increasing information related to MB oxidation since MC is one of the intermediate products formed during MB combustion (Gaïl et al., 2007 [57]; Hakka et al., 2009 [61]).

In their comparative study of MC and MB oxidation, Sarathy et al. (2007) [64] carried out experiments in an opposed flow diffusion flame (OFDF) and a jet-stirred reactor (JSR). Details related to operating conditions are given in Table I.9. Mole fraction profiles of major intermediates, final products and reactants were measured. The authors observed that both fuel molecules had globally similar reactivity. Nevertheless, the experimental results showed that, compared to MB, MC oxidation produced much higher levels of aldehydes (2-propenal and

acetaldehyde: toxic products) and light unsaturated hydrocarbons (acetylene, propyne, 1-butene, and 1,3-butadiene: soot precursors). On the other hand, the MB combustion had higher levels of ethylene (C₂H₄). Also, in OFDF, MC produced benzene which was not detected for MB oxidation. These results led the authors to conclude that unsaturated esters would have a greater tendency to form soot than saturated esters.

Later, Gail et al. (2008) [65] carried on Sarathy et al. (2007) [64] work by extending the oxidation experiments made in JSR for MC and MB (at atmospheric pressure, over the temperature range 850-1350 K, and under stoichiometric conditions) to fuel-lean mixtures (Table I.9). Additionally, Gail et al. (2008) [65] used these new experimental results joined to those of Sarathy et al. (2007) [64] for validating a new version of the detailed chemical kinetic model they proposed previously for MB oxidation (Gail et al., 2007 [57]) and extended to MC by adding several specific reactions (Table I.6). The rate constants of the new added reactions were derived using analogies with reactions occurring in the already established MB model. The thermochemical properties of the new species were calculated from THERGAS software (Muller et al., 1995 [40]) while the transport quantities were estimated from species of similar size and structure. The new revised mechanism consisted of 1516 reactions involving 301 species (Table I.9). Overall, the new kinetic model reproduced the experimental data fairly well and confirmed the conclusions experimentally observed by Sarathy et al. (2007) [64].

Table I.6: Reactions added to the Gail et al. (2007) [57] model for representing MC oxidation (Gail et al., 2008 [65])^a.

Reaction	A	n	E _a
CH ₃ CH=CH(C=O)O [•] + [•] CH ₃ = CH ₃ CH=CH(C=O)OCH ₃	8.00E + 13	0.00	0
CH ₃ CH=CH [•] C=O + CH ₃ O [•] = CH ₃ CH=CH(C=O)OCH ₃	6.00E + 13	0.00	0
CH ₃ CH=CH [•] + CH ₃ O [•] CO = CH ₃ CH=CH(C=O)OCH ₃	8.00E + 13	0.00	0
[•] CH ₂ CH=CH(C=O)OCH ₃ = CH ₂ =CH- [•] CH(C=O)OCH ₃	4.00E + 12	0.00	60000
CH ₃ CH=CH(C=O)OCH ₃ + [•] CH ₃ = CH ₃ CH=CH(C=O)OCH ₂ [•] + CH ₄	1.00E + 12	0.00	7300
CH ₃ CH=CH(C=O)OCH ₂ [•] + H [•] = CH ₃ CH=CH(C=O)OCH ₃	1.00E + 14	0.00	0
CH ₃ CH=CH(C=O)OCH ₂ [•] = CH ₃ CH=CH [•] C=O + CH ₂ O	5.01E + 12	0.00	19000
CH ₃ CH=CH(C=O)OCH ₂ [•] + [•] OH = CH ₃ CH=CH(C=O)OCH ₃ + [•] O	3.50E + 11	0.00	29900
CH ₃ CH=CH(C=O)OCH ₃ + [•] CH ₃ = [•] CH ₂ CH=CH(C=O)OCH ₃ + CH ₄	1.00E + 12	0.00	7300
CH ₃ CH=CH(C=O)OCH ₃ + H [•] = [•] CH ₂ CH=CH(C=O)OCH ₃ + H ₂	3.70E + 13	0.00	3900
CH ₃ CH=CH(C=O)OCH ₃ + O ₂ = [•] CH ₂ CH=CH(C=O)OCH ₃ + HO ₂ [•]	3.00E + 13	0.00	52800
[•] CH ₂ CH=CH(C=O)OCH ₃ + [•] OH = CH ₃ CH=CH(C=O)OCH ₃ + [•] O	7.00E + 11	0.00	29900

Table I.6 (Continued) ^a

$\text{CH}_3\text{CH}=\text{CH}(\text{C}=\text{O})\text{OCH}_3 + \cdot\text{OH} = \cdot\text{CH}_2\text{CH}=\text{CH}(\text{C}=\text{O})\text{OCH}_3 + \text{H}_2\text{O}$	3.00E + 13	0.00	1230
$\text{CH}_3\text{CH}=\text{CH}(\text{C}=\text{O})\text{OCH}_3 + \text{HO}_2\cdot = \cdot\text{CH}_2\text{CH}=\text{CH}(\text{C}=\text{O})\text{OCH}_3 + \text{H}_2\text{O}_2$	1.50E + 11	0.00	14190
$\cdot\text{CH}_2\text{CH}=\text{CH}(\text{C}=\text{O})\text{OCH}_3 + \text{H}\cdot = \text{CH}_3\text{CH}=\text{CH}(\text{C}=\text{O})\text{OCH}_3$	5.00E + 12	0.00	0
$\cdot\text{CH}_2\text{CH}=\text{CH}(\text{C}=\text{O})\text{OCH}_3 + \cdot\text{O}\cdot = \cdot\text{CH}=\text{CH}(\text{C}=\text{O})\text{OCH}_3 + \text{CH}_2\text{O}$	1.58E + 07	1.80	-1216
$\text{CH}_3\text{CH}=\text{CH}(\text{C}=\text{O})\text{OCH}_3 + \cdot\text{OH} = \text{CH}_3\text{CH}=\text{CH}(\text{C}=\text{O})\text{OCH}_2\cdot + \text{H}_2\text{O}$	3.00E + 13	0.00	1230
$\text{CH}_3\text{CH}=\text{CH}(\text{C}=\text{O})\text{OCH}_3 + \text{H}\cdot = \text{CH}_3\text{CH}=\text{CH}(\text{C}=\text{O})\text{OCH}_2\cdot + \text{H}_2$	3.70E + 13	0.00	3900

^a The rate coefficients are listed in the generalized Arrhenius form ($k = A \cdot T^n \cdot \exp(E_a/RT)$) where units are mole, cm, s, T, and cal.

1.5.5 Ethyl ester kinetic investigations: ethyl propanoate versus methyl butanoate

Researches related to the oxidation of fatty acid ethyl esters (FAEE) are very scarce, likely because commercial biodiesel components are still fatty acid methyl esters (FAME). Consequently, researches are still at the stage of mechanism development for small model molecules that are known not to be good biodiesel surrogates but will give significant information on ethyl ester oxidation behaviour. Additionally, the few published studies give oxidation results for FAEE by comparison with the ones for FAME, highlighting thus advantages and disadvantages of both biodiesel alternatives as fuels. As a result, the same approach will be adopted here for presenting investigations in an effective way. They will be shown in the main text for ethyl propanoate and ethyl butanoate (vs. methyl butanoate), and then for ethyl nonanoate (vs. methyl nonanoate) in the appendix AI.

The original tendency was to compare esters with the same chemical formula (isomers) while varying the length of the alkyl and aliphatic chains in order to investigate the effect of the molecular structure on the oxidation chemistry. Once different mechanisms were elucidated for various alkyl esters, the studies were devoted to compare, for molecules with the same aliphatic main chain length, the oxidation behaviour of the functional groups, methyl ester and ethyl ester as a whole.

Schwartz et al. (2006) [66] studied five different isomer esters with the chemical formula $\text{C}_5\text{H}_{10}\text{O}_2$: methyl butanoate (MB), methyl isobutyrate (MiBu), ethyl propanoate (EP), propyl acetate (PrAc), and isopropyl acetate (iPrAc). Their experiments were performed at atmospheric pressure in methane/air coflowing non-premixed flames doped separately with 5000 ppm of each ester (Table I.9). Such flames are typical of many practical combustors, especially soot-producing systems such as diesel engines and gas turbine, and yet simple enough to permit basic understanding. Major species from within the flame were measured using mass spectrometry. The authors determined that the main decomposition pathway in non-

premixed flames for EP, together for the acetate esters (PrAc and iPrAc), was a unimolecular-six-centered dissociation reaction, leading to a carboxylic acid and a 1-alkene (propanoic acid and ethylene for EtPr, reaction I.1). On the other hand, MB and MiBu, which cannot undergo a unimolecular six-centered dissociation reaction, had decomposition rates that were consistent with a unimolecular C-O fission mechanism, leading to two radicals (reaction I-2 for MB).



The authors also found propene (whose presence correlates to the formation of aromatics and soot) to be a major decomposition product for all esters investigated. Nevertheless, EP and MB produced the lowest concentrations of propene which is in agreement with the suggested primary reaction pathways (reactions I.1 and I.2).

Simultaneously to MB behavior as fuel at high temperature, Metcalfe et al. (2007) [51] also studied, in the same work, the oxidation of EP in shock tube. For EP/O₂/Ar mixtures, ignition delay times were measured behind the reflected-shock waves over the temperature range 1140-1675 K, at two low reflected-shock pressures and various equivalence ratios, including fuel-lean and fuel-rich conditions (Table I.9). The authors reported that as EP concentration was increased (from 1 to 1.5%) with the O₂ concentration constant (at 6.5%), the ignition delay times increased. Reversely, increasing O₂ concentration (from 6.5 to 26.0%), with a constant EP concentration (of 1%), led to a significant reduction in delay times. The authors pointed out that this negative power dependence of O₂ is in accordance with previous work on hydrocarbons (Curran et al., 1998 [48]). Indeed, because the chain-branching mechanism at the high temperatures investigated in their work (1140-1675 K) are due to the H[•] + O₂ = O[•] + [•]OH reaction, fuel-lean mixtures are more reactive in this regime (however, at low temperatures, because chain-branching is dependent on radical species formed directly from the parent fuel, fuel-rich mixtures are oxidized more quickly).

Metcalfe et al. (2007) [51] also observed that EP was consistently faster to ignite than MB, particularly at low temperatures. Theoretical interpretation was given to this behavior based on the detailed chemical kinetic mechanism they developed for the EP combustion. This mechanism contained 139 species and 786 reversible reactions in which the EP submechanism was built by analogy with MB. However, some changes were made as mentioned in the following.

- The six-centered unimolecular elimination reaction producing propanoic acid and ethylene, as evocated previously by Schwartz et al. (2006) [66], has been added and characterized by an activation energy of approximately 50 kcal·mol⁻¹ (Figure I.9).

- The EP mechanism contained also the recently published H₂/O₂ submechanism by O’Conaire et al. (2004) [73].
- Like for MB mechanism, unimolecular decomposition reactions were treated to account for pressure falloff.
- The ethylene submechanism was based on that which had been published previously by Curran et al. (1998) [48].
- The authors developed for the circumstances a propanoic acid submechanism on the basis of the n-heptane and iso-octane kinetic mechanisms published previously by Curran et al. (1998) [48] and (2002) [49].

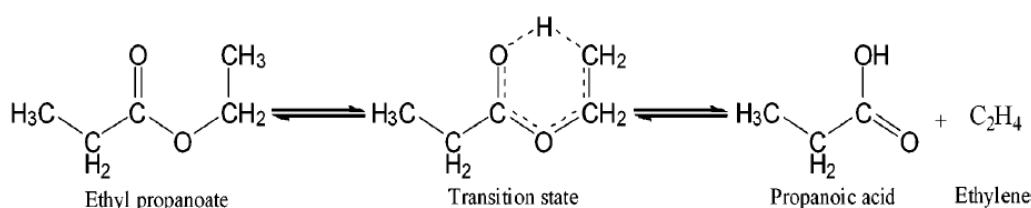


Figure I.9: Six-centered unimolecular elimination for ethyl propanoate producing propanoic acid and ethylene (Metcalfé et al., 2007 [51]).

Metcalfé et al. (2007) [51] pointed out that the simulations were in good agreement with the experimental data. Additionally, rate of production analyses using the proposed detailed mechanisms helped the authors to explain the faster reactivity of EP (compared to that of MB) by the six-centered unimolecular decomposition reaction which has a relatively low activation energy barrier and produces propanoic acid and ethylene. According the authors, it is actually the faster reactivity of these two products that is responsible of EP behavior.

Following this work, Metcalfé et al. (2009) [81] recently carried out experiments in JSR for EP oxidation that they used to further validate their previously proposed kinetic model (Metcalfé et al., 2007 [51]). Measurements were conducted under high pressure (10 atm), for various equivalence ratios, and at temperatures in the range 750-1100 K (Table I.9). Fuel (EP), intermediate and final product species were recorded as a function of temperature. The authors reported that the main intermediate species observed were ethylene, propanoic acid, formaldehyde, and methane among which ethylene and propanoic acid were the most abundant (Figure I.9) while the major products were H₂O, CO₂, and CO.

In order to obtain a better agreement with the JSR species profiles, the authors brought some changes to the original EP oxidation mechanism previously published (Metcalfé et al., 2007 [51]).

- The rate constant for the unimolecular elimination reaction $EP = C_2H_4 + C_2H_5COOH$ was increased by a factor of four from $4.0 \cdot 10^{12} \exp(-50,000/RT)$ to $1.6 \cdot 10^{13} \exp(-50,000/RT) s^{-1}$ (E_a in $cal\ mol^{-1}$).
- The abstraction reactions listed in Table I.7 were decreased by a factor of two.
- An updated C_3 submechanism developed by the authors and collaborators was incorporated.

Table I.7: Abstraction reactions modified by Metcalfe et al. (2009) [81]^a.

Reaction	A	n	E_a
$EP + HO_2^{\cdot} = H_2O_2 + CH_3^{\cdot}CH(C=O)OC_2H_5$	2.16E+12	0.0	14 400
$EP + HO_2^{\cdot} = H_2O_2 + CH_3CH_2(C=O)O^{\cdot}CHCH_3$	3.61E+03	2.5	10 530
$C_2H_5COOH + HO_2^{\cdot} = H_2O_2 + CH_3^{\cdot}CHCOOH$	2.16E+12	0.0	14 400

^a The rate coefficients are listed in the generalized Arrhenius form ($k=A \cdot T^n \cdot \exp(-E_a/RT)$) where units are mole, cm, s, cal, and K.

The revised mechanism was reported to be in very good agreement with experiments (both those carried out in JSR during this last study and in shock tube (ST) during their previous study, Metcalfe et al., 2007 [51]). Nevertheless, the authors observed better performance at stoichiometric and lean conditions than at rich ones. Also, the rate of production analysis led the authors to observe that the elimination reaction played a much smaller role in the decomposition of EP relative to H-abstraction reaction under the JSR conditions compared to the ST ones. Furthermore, the sensitivity analysis highlighted the importance of ethylene chemistry on the overall reactivity of the system.

Walton et al. (2009) [59] also performed in the same work as the one mentioned previously for MB oxidation, low temperature ignition of EP using a RCM (Table I.9). The authors confirmed the observation made by Schwartz et al. (2006) [66] and Metcalfe et al. (2007) [51] according to which, under the investigated conditions, EP ignited more rapidly than MB and gave the same explanation of this reactivity through the faster unimolecular decomposition of EP leading to the formation of ethylene and propanoic acid. Additionally, Walton et al. (2009) [59] proposed a new mechanism for EP oxidation on the basis of Metcalfe et al. (2007) [51] model that they improved to match more closely experiments, particularly at low temperatures. The modified reactions and rate constants are summarized in Table I.8.

Table I.8: Reactions modified by Walton et al. (2009) [59] from the Metcalfe et al. (2007) [51] mechanism for EP oxidation. ^a

$\text{CH}_3\text{CH}_2(\text{C}=\text{O})\text{OC}_2\text{H}_5 + \text{HO}_2^\cdot = \text{H}_2\text{O}_2 + \cdot\text{CH}_2\text{CH}_2(\text{C}=\text{O})\text{OC}_2\text{H}_5$	8.30E + 03	2.55	16490
$\text{CH}_3\text{CH}_2(\text{C}=\text{O})\text{OC}_2\text{H}_5 + \text{HO}_2^\cdot = \text{H}_2\text{O}_2 + \text{CH}_3\cdot\text{CH}(\text{C}=\text{O})\text{OC}_2\text{H}_5$	1.50E + 12	0.00	14400
$\text{CH}_3\text{CH}_2(\text{C}=\text{O})\text{OC}_2\text{H}_5 + \text{HO}_2^\cdot = \text{H}_2\text{O}_2 + \text{CH}_3\text{CH}_2(\text{C}=\text{O})\text{O}\cdot\text{CHCH}_3$	2.50E + 03	2.55	10530
$\text{CH}_3\text{CH}_2(\text{C}=\text{O})\text{OC}_2\text{H}_5 + \text{HO}_2^\cdot = \text{H}_2\text{O}_2 + \text{CH}_3\text{CH}_2(\text{C}=\text{O})\text{OCH}_2\cdot\text{CH}_2$	8.30E + 03	2.55	16490

^a The remainder of the mechanism was unchanged from Metcalfe et al. (2007) [51] mechanism. The rate coefficients are listed in the generalized Arrhenius form ($k=A\cdot T^n\cdot\exp(-E_a/RT)$) where units are mole, cm, s, cal, and K.

Table I.9: Summary of the main experimental data generated for oxidation of C₄-alkyl esters selected as biodiesel surrogates.

Fuel	Equipment (Data type)	Temperatur e /K	Pressure /atm	Equivalence ratio ϕ (Fuel molar fraction %)	Reference
MB	FR (SP)	500 – 900	12.5	0.35 - 1.5 (800 ppm)	Marchese et al. (2004) [56]
	CFNPF (SP)	-	1	- (5000 ppm + CH ₄)	Schwartz et al. (2006) [66]
	JSR (SP)	800 - 1350	1	1.13 (0.075)	Gail et al. (2007) [57]
	OQDF (SP)	-	1	- (4.7)	
	PVPFR (SP)	500 - 900	12.5	0.35 - 1.5 (-)	
	ST (ID)	1100 - 1670	1 - 4	0.25 - 1.5 (-)	Metcalfe et al. (2007) [51]
	JSR (SP)	850 - 1350	1	1.0 (0.075)	Sarathy et al. (2007) [64]
	OQDF (SP)	-	1	- (4.7)	
	JSR (SP)	850 - 1400	1	0.375 and 0.75 (0.075)	Gail et al. (2008) [65]
	RCM (ID)	640 - 949	10 - 40	0.33 - 1.0 (1.59 - 3.13)	Dooley et al. (2008) [58]
	ST (ID)	1250 - 1760	1 - 4	0.25 - 1.5 (1.0 - 1.5)	

Table I.9 (Continued)

	RCM (ID)	935 - 1117	4.7 - 19.6	0.3 - 0.4 (0.95 - 1.27)	Walton et al. (2009) [59]
	RCM (ID)	650 - 850	3.9 - 19.7	1.0 (-)	HadjAli et al. (2009) [52]
	ST (CO ₂ yields)	1260 - 1653	1.4 - 1.7	Pyrolysis study (2 - 3)	Farooq et al. (2009) [63]
	JSR (SP)	800 - 850	1	0.5 - 1.0 (2)	Hakka et al. (2010) [61]
	ST (ID)	1250 - 2000	7.6 - 9.1	0.25 - 2 (0.5 - 1)	
	ST (ID)	1060 - 1632	1.2 - 11.4	0.5 - 2.0 (0.64 - 3.32)	Akih-Kumgeh and Bergthorson (2010) [60]
MC	OFDF (SP)	-	1	- (4.7)	Sarathy et al. (2007) [64]
	JSR (SP)	850 - 1350	1	1 (0.075)	
	JSR (SP)	850 - 1400	1	0.375 and 0.75 (0.075)	Gail et al. (2008) [65]
EP with MiBu, PrAc, and iPrAc for comparison	CFNPF (SP)	-	1	- (5000 ppm + CH ₄)	Schwartz et al. (2006) [66]
EP	CFNPF (SP)	-	1	- (5000 ppm + CH ₄)	Schwartz et al. (2006) [66]
	ST (ID)	1140 - 1675	1 - 4	0.25 – 1.5 -	Metcalfe et al. (2007) [51]
	JSR (SP)	750 - 1100	1	0.3 – 1 (0.1)	Metcalfe et al. (2009) [81]
	RCM (ID)	935 - 1117	4.7 - 19.6	0.3 - 0.4 (0.95 - 1.27)	Walton et al. (2009) [59]

Table I.10: Summary of the main features related to the chemical kinetic models proposed for the oxidation of C₄-alkyl esters selected as biodiesel surrogates

Fuel ^a	Model features		Software features			Model applicability conditions				Ref.	
	Nb. of reactions	Nb. of species	Thermochemical property estimation	Kinetic rate estimation ^b	Mechanism generator ^c	ChemKin module used	Low T (≈ 500 K)	High T (≈ 1300 K)	Low P (≈ 1 atm)		Moderate P (≈ 10 atm)
MB	1219	264	THERM [39]	N.C.H.	None	SENKIN [71]	✓	-	✓	-	Fisher et al. (2000) [55]
	1498	295	THERM [39, 76, 77]	N.C.H.	None	ND ^d	✓	✓	✓	✓	Gaïl et al. (2007) [57]
	N.D. ^e	N.D. ^e	THERM [39, 76, 77]	N.C.H.	None	HCT [103] ^f	-	✓	✓	-	Metcalfé et al. (2007) [51]
	1545	275	THERM [39, 76, 77]	N.C.H.	None	HCT [103] ^f	✓	✓	✓	✓	Dooley et al. (2008) [58]
	Metcalfé et al. (2007) [51]		THERM [39]	N.C.H.	None	HCT [103] ^f	✓			✓ (≈ 20 atm)	Walton et al. (2009) [59]
	1317	203	THERGAS [40]	KINGAS [42]	EXGAS [49]	SENKIN PSR	✓	✓	✓	✓	Hakka et al. (2009) [61]
MC	1516	301	THERGAS [40]	N.C.H.	None	PSR OPPDIFF	✓	✓	✓	-	Gaïl et al. (2008) [65]
EP	786	139	THERM [39]	N.C.H.	None	HCT [103] ^f	-	✓	✓	-	Metcalfé et al. (2007) [51]
	N.D. ^d	N.D. ^d	THERM [39]	N.C.H.	None	HCT [103] ^f	✓	✓	✓	✓	Metcalfé et al. (2007) [51] + Walton et al. (2009) [59]
EB	1101	115	THERGAS [40]	KINGAS [42]	EXGAS [49]	SENKIN	-	-	✓	✓	Hakka et al. (2009) [61]

^a See nomenclature for species names ^b N.C.H.: non-computer-helped method: the rate constants for the reverse reactions k_{reverse} were computed from the forward rate constants k_{forward} and the equilibrium constants K_c calculated using the appropriate thermochemical data according to $K_c = k_{\text{forward}}/k_{\text{reverse}}$. ^c No mechanism generator was used from developing the kinetic models which were instead built hierarchically. ^d N.D.: No details mentioned. ^e Model derived from Fisher et al. (2000) [55] proposal with some changes, but resulting number of reactions and species involved are not mentioned in the manuscript. ^f HCT was used instead of ChemKin. ^g NO formation (GRI-Mech 3.0 mechanism).

I.6 Conclusion

The present literature review has shown that biodiesel can be obtained by transesterification of vegetable oil (neat or used) with alcohol (methanol, ethanol...) in presence of a catalyst (alkali, acid or enzyme). This transformation reaction aims to reduce together viscosity, specific gravity and flash point of the lipid source used as feedstock. It was also inferred that esters (biodiesel) obtained from branched alcohols have lower melting points and could points than those derived from straight-chain alcohols. Disadvantages of using branched or long chain alcohols are their higher cost and the needed changes in the transesterification process.

The different studies reviewed in this work have shown that biodiesel has almost similar combustion characteristics as petrodiesel. It was found that the biodiesel combustion involves a decrease in the emissions of particulate matter (PM), unburned hydrocarbons (UHC), sulfur oxides (SO_x), volatile organic compounds (VOCs), and carbon monoxide (CO) with respect to petrodiesel fuel. On the other hand, the exhaust emissions in nitrogen oxides from the engine were found to be higher. It should be also noted that the decomposition of fatty acid esters leads to the formation of a considerable amount of CO₂ at low temperature regime as reported by Szybist et al. (2007) [83, 85].

Furthermore, experimental oxidation and modeling by detailed chemical kinetic mechanisms of esters, particularly methyl esters as surrogates of the commercial biodiesel, have been the subject of many investigations, as presented in recent literature reviews. However, actual biodiesel components (i.e. saturated and unsaturated fatty acid methyl or ethyl esters) are molecules with long aliphatic main chains of 14 to 20 carbon atoms with allyl and ester functional groups. Such a complexity in the molecular structure poses a real challenge for modeling and also experimental kinetic studies. Therefore, esters molecules with a short aliphatic main chain containing the same functional group as actual biodiesel components were studied to gather insights into the oxidation behavior at low and high temperatures of the practical fuel. Nevertheless, it is regrettable that the number of studies developed for the ethyl esters is much smaller than for methyl esters. Moreover, the nature and relative proportions of engine emissions regarding methyl esters as fuel and even more ethyl esters are still very controversial. Accordingly, there still seems necessary to continue work on the oxidation of ethyl esters, starting with molecules of short aliphatic chains allowing to focus on the combustion chemistry of the ethyl ester chemical function, and for continuing with ethyl esters with at least 10 carbon atoms in the aliphatic main chain in order to study potentially excellent

surrogates for green biodiesel (as the equivalent methyl esters showed themselves to be excellent surrogates for commercial biodiesel). Kinetic models developed on the basis of data generated for this class of molecules will help to better understand the emissions produced by combustion of this class of biodiesel in a diesel engine, or even help in the formulation of a cleaner biofuel.

I.7 References

- [1] International Energy Outlook 2007 by Energy Information Administration, Office of Integrated Analysis and Forecasting, U.S. Department of Energy, Washington, DC 20585 (2007).
- [2] M.S. Graboski, R.L. McCormick, Combustion of fat and vegetable oil derived fuels in Diesel engines, *Progress in Energy and Combustion Science* 24 (1998) 125-164.
- [3] M. Lapuerta, O. Armas, J. Rodriguez-Fernandez, Effect of biodiesel fuels on diesel engine emissions, *Progress in Energy and Combustion Science* 34 (2008) 198-223.
- [4] T. Myo, The effect of fatty acid composition on the combustion characteristics of biodiesel, Graduate School of Science and Engineering, Kagoshima University, Japan (2008).
- [5] S.A. Basha, K.R. Gopal, S. Jebaraj, A review on biodiesel production, combustion, emissions and performance, *Renewable and Sustainable Energy Reviews* 13 (2009) 1628-1634.
- [6] J., Krahl, G. Knothe, A. Munack, Y. Ruschel, O. Schröder, E. Hallier, G. Westphal, J. Bünger, Comparison of exhaust emissions and their mutagenicity from the combustion of biodiesel, vegetable oil, gas-to-liquid and petrodiesel fuels, *Fuel* 88 (2009) 1064-1069.
- [7] K. Kohse-Höinhaus, P. Oßwald, T.A. Cool, T. Kasper, N. Hansen, F. Qi, C.K. Westbrook, P.R. Westmoreland, *Biofuel Combustion Chemistry: From Ethanol to Biodiesel*, *Angewandte Chemie International Edition* 49 (2010) 3572-3597.
- [8] E. Lois, Definition of biodiesel, *Fuel* 86 (2007) 1212-1213.
- [9] A. Demirbas, *Biodiesel: a realistic fuel alternative for diesel engines*, ISBN-13: 9781846289941, Springer (2008).
- [10] Y. Zhang, M.A. Dubé, D.D. McLean, M. Kates, Biodiesel production from waste cooking oil: 1. Process design and technological assessment, *Bioresource Technology* 89 (2003) 1-16.
- [11] S. Furuta, H. Matsuhashi, K. Arata, Biodiesel fuel production with solid superacid catalysis in fixed bed reactor under atmospheric pressure, *Catalysis Communication* 5 (2004) 721-723.
- [12] H.Noureddini, X.Gao, R.S. Philkana, Immobilized *Pseudomonas cepacia* lipase for biodiesel fuel production from soybean oil, *Bioresource Technology* 96 (2005) 769-777.
- [13] A. Demirbas, Biodiesel fuels from vegetable oils via catalytic and non-catalytic supercritical alcohol transesterifications and other methods: a survey, *Energy Conversion and Management* 44 (2003) 2093-2109.

- [14] V. Rathore, G. Madras, Synthesis of biodiesel from edible and non-edible oils in supercritical alcohols and enzymatic synthesis in supercritical carbon dioxide, *Fuel* 86 (2007) 2650-2659.
- [15] J.M. Marchetti, V.U. Miguel, A.F. Errazu, Possible methods for biodiesel production, *Renewable and sustainable energy reviews* 11 (2007) 1300-1311.
- [16] L. Bournay, D. Casanave, B. Delfort, G. Hillion, J.A. Chodorge, New heterogeneous process for biodiesel production: A way to improve the quality and the value of the crude glycerin produced by biodiesel plants, *Catalysis Today* 106 (2005) 190-192.
- [17] G. Knothe, J.V. Gerpen, J. Krahl, *The biodiesel Handbook*, ISBN-13: 9781893997790, AOCS Publishing (2005).
- [18] B. Baiju, M.K. Naik, L.M. Das, A comparative evaluation of compression ignition engine characteristics using methyl and ethyl esters of karanja oil, *Renewable Energy* 34 (2009) 1616-1621.
- [19] M.R. Monteiro, A.R.P. Ambrozin, L.M. Liao, A.G. Ferreira, Critical review on analytical methods for biodiesel characterization, *Talanta* 77 (2008) 593-605.
- [20] M.J. Ramos, C.M. Fernández, A. Casas, L. Rodríguez, Á. Pérez, Influence of fatty acid composition of raw materials on biodiesel properties, *Bioresource Technology* 100 (2009) 261-268.
- [21] J. Van Gerpen, B. Shanks, R. Pruszko, D. Clements, G. Knothe, August 2002-January 2004, National Renewable Energy Laboratory (NREL), Colorado, July 2004 [NREL/SR-510-36240].
- [22] A. Murugesan, C. Umarani, R. Subramanian, N. Neduzchezain, Bio-diesel as an alternative fuel for diesel engines-A review, *Renewable and Sustainable Energy Reviews* 13 (2009) 653-662.
- [23] A. Dubreuil, F. Foucher, C. Mounaïm-Rousselle, G. Dayma, P. Dagaut, HCCI combustion: Effect of NO in EGR, *Proceedings of the Combustion Institute* 31 (2007) 2879-2886.
- [24] B. Freedman, M.O. Bagby, T.J. Callahan, T.W. Ryan III, Cetane Numbers of Fatty Esters, Fatty Alcohols, and Triglycerides Determined in a Constant Volume Combustion Bomb, SAE Paper no. 900343 (1990).
- [25] G. Knothe, A.C. Matheus, T.W. Ryan III, Cetane numbers of branched and straight-chain fatty esters determined in an ignition quality tester, *Fuel* 82 (2003) 971-975.
- [26] R. Lee, C.H. Hobbs, J.F. Pedley, A Fuel quality impact on heavy duty diesel emissions: a literature review. SAE paper no. 982649 (1998).

- [27] N. Ladommatos, M. Parsi, A. Knowles, The effect of fuel cetane improve on diesel pollutant emissions, *Fuel* 75 (1996) 8-14.
- [28] T. Fang, C.F. Lee, Biodiesel effects on combustion processes in an HSDI diesel engine using advanced injection strategies, *Proceedings of the Combustion Institute* 32 (2009) 2785-2792.
- [29] A. Schönborn, N. Ladommatos, J. Williams, R. Allan, J. Rogerson, The influence of molecular structure of fatty acid monoalkyl esters on diesel combustion, *Combustion and Flame* 156 (2009) 1396–1412.
- [30] R.L. McCormick, M.S. Graboski, T.L. Alleman, A.M. Herring, Impact of biodiesel source material and chemical structure on emissions of criteria pollutants from a heavy-duty engine, *Environmental Science & Technology* 35 (2001) 1742-1747.
- [31] C.L. Peterson, D. L. Reece, J.C. Thompson, S.M. Beck, C. Chases, Ethyl ester of rapeseed used as a biodiesel fuel-A case study, *Biomass Bioenergy* 10 (1996) 331-336.
- [32] M. Al-Widyan, G. Tashtoush, M. Abu-Qudais, Utilisation of ethyl ester of waste vegetable oils as fuel in diesel engines, *Fuel Processing Technology* 76 (2002) 91-103.
- [33] S. Puhana, N. Vedaramana, G. Sankaranarayanan, B.V. Bharat Rama, Performance and emission study of Mahua oil (*madhuca indica* oil) ethyl ester in a 4-stroke natural aspirated direct injection diesel engine, *Renewable Energy* 30 (2005) 1269-1278.
- [34] V. Makareviciene, P. Janulis, Utilization of ethyl ester of waste vegetable oils as fuel in diesel engines, *Renewable Energy* 28 (2003) 2395-2403.
- [35] M. Lapuerta, J.M. Herreros, L.L. Lyons, R. Garía-Contreras, Y. Briceño, Effect of the alcohol type used in the production of waste cooking oil biodiesel on diesel performance and emissions, *Fuel* 87 (2008) 3161-3169.
- [36] J.M. Simmie, Detailed chemical kinetic models for the combustion of hydrocarbons fuel, *Progress in Energy and Combustion Science* 29 (2003) 599-634.
- [37] F. Battin-Leclerc, Detailed chemical kinetic models for the low-temperature combustion of hydrocarbons with application to gasoline and diesel fuel surrogates, *Progress in Energy and Combustion Science* 34 (2008) 440-498.
- [38] S. Touchard, R. Fournet, P.A. Glaude, V. Warth, F. Battin-Leclerc, G. Vanhove, M. Ribaucour, R. Minetti, Modeling of the oxidation of large alkenes at low temperature, *Proceedings of the Combustion Institute* 30 (2005) 1073-1081.
- [39] E.R. Ritter, J.W. Bozzelli, THERM: Thermodynamic property estimation for gas phase radicals and molecules, *International journal of chemicals kinetics* 23 (1991) 767-778.

- [40] C. Muller, V. Michel, G. Scacchi, G.M. Côme, A computer program for the evaluation of thermochemical data of molecules and free radicals in the gas phase, *Journal of Chemical Physics* 92 (1995) 1154-1177.
- [41] S. W. Benson, *Thermochemical Kinetics*, Edition John Wiley, 2nd edition (1976), New York.
- [42] V. Warth, N. Stef, P.A. Glaude, F. Battin-Leclerc, G. Scacchi, G.M. Côme, Computer-Aided Derivation of Gas-Phase Oxidation Mechanisms: Application to the Modeling of the Oxidation of n-Butane, *Combustion and Flame* 114 (1998) 81-102.
- [43] R.J. Kee, F.M. Rupley, J.A. Miller, CHEMKIN II: A fortran chemical kinetics package for the analysis of gas phase chemical kinetics, Sandia Laboratories Report, SAND 89-8009B, (1993).
- [44] P. Dagaut, N. Smoucovit, M. Cathonnet, Methyl acetate oxidation in a JSR: Experimental and detailed kinetic modeling study, *Combustion science and technology* 127 (1997) 275-291.
- [45] L. Gasnot, V. Decottignies, J.F. Pauwels, Kinetics modeling of ethyl acetate oxidation in flame conditions, *Fuel* 84 (2005) 505-518.
- [46] P. Osswald, U. Struckmeier, T. Kasper, K. Kohse-Höinghaus, J. Wang, T. A. Cool, N. Hansen, P. R. Westmoreland, Isomer-specific fuel destruction pathways in rich flames of methyl acetate and ethyl formate and consequences for the combustion chemistry of esters, *Journal of Physical Chemistry A* 111 (2007) 4093-4101.
- [47] C.K. Westbrook, W.J. Pitz, P.R. Westmoreland, F.L. Dryer, M. Chaos, P. Osswald, K. Kohse-Hoinghaus, T.A. Cool, J. Wang, B. Yang, N. Hansen, T. Kasper, A detailed chemical kinetic reaction mechanism for oxidation of four small alkyl esters in laminar premixed flames, *Proceedings of the Combustion Institute* 32 (2009) 221-228.
- [48] H.J. Curran, P. Gaffuri, W.J. Pitz, C.K. Westbrook, A comprehensive modeling study of n-heptane oxidation, *Combustion and Flame* 114 (1998) 149-177.
- [49] H.J. Curran, P. Gaffuri, W.J. Pitz, C.K. Westbrook, A comprehensive modeling study of iso-octane oxidation, *Combustion and Flame* 129 (2002) 253-280.
- [50] O. Herbinet, W.J. Pitz, C.K. Westbrook, Detailed chemical kinetic oxidation mechanism for a biodiesel surrogate, *Combustion and Flame* 154 (2008) 507-528.
- [51] W.K. Metcalfe, S. Dooley, H. J. Curran, J. M. Simmie, A. M. El-Nahas, M. V. Navarro, Experimental and modeling study of C₅H₁₀O₂ ethyl and methyl esters, *Journal of Physical Chemistry A* 111 (2007) 4001-4014.

- [52] K. HadjAli, M. Crochet, G. Vanhove, M. Ribaucour, R. Minetti, A study of the low temperatures autoignition of methyl esters, *Proceedings of the Combustion Institute* 32 (2009) 239-246.
- [53] O. Herbinet, W.J. Pitz, C.K. Westbrook, Detailed chemical kinetic mechanism for the oxidation of biodiesel fuels blend surrogate, *Combustion and Flame* 157 (2010) 893-908.
- [54] Y.Zhang, A.L. Boehman, Experimental study of the autoignition of C₈H₁₆O₂ ethyl and methyl esters in a motored engine, *Combustion and Flame* 157 (2010) 546-555.
- [55] E.M. Fisher, W.J. Pitz, H.J. Curran, C.K. Westbrook, Detailed chemical kinetic mechanisms for combustion of oxygenated fuels, *Proceedings of the Combustion Institute* 28 (2000) 1579-1586.
- [56] A.J. Marchese, M. Angioletti, F.L. Dryer, Flow reactor studies of surrogate biodiesel fuels, *International Symposium on Combustion* (2004), Work-in progress poster 1F1-03.
- [57] S. Gail, M. Thomson, S.M. Sarathy, S.A. Syed, P. Dagaut, P. Diévert, A.J. Marchese, F.L.Dryer, A wide-ranging kinetic modeling study of methyl butanoate combustion, *Proceedings of the Combustion Institute* 31 (2007) 305-311.
- [58] S. Dooley, H.J. Curran, J.M. Simmie, Autoignition measurements and a validated kinetic model for the biodiesel surrogate, methyl butanoate, *Combustion and Flame* 153 (2008) 2-32.
- [59] S.M. Walton, M.S. Wooldridge, C.K. Westbrook, An experimental investigation of structural effects on the autoignition properties of two C₅ esters, *Proceeding of the Combustion Institute* 32 (2009) 255-262.
- [60] B. Akih-Kumgeh, J.M. Bergthorson, Comparative Study of Methyl Butanoate and n-Heptane High Temperature Autoignition, *Energy & Fuels*, 24 (2010) 2439-2448.
- [61] M.H. Hakka, H. Bennadji, J. Biet, M. Yahyaoui, B. Sirjean, V. Warth, L. Coniglio, O. Herbinet, P.A. Glaude, F. Billaud, F. Battin-Leclerc, Oxidation of methyl and ethyl butanoates, *International journal of chemicals kinetics* 42 (2010) 226-252.
- [62] L.K. Huynh, A. Violi, Thermal decomposition of methyl butanoate: Ab initio study of a biodiesel fuel surrogate, *Journal of Organic Chemistry* 73 (2008) 94-101.
- [63] A. Farooq, D.F. Davidson, R.K. Hanson, L.K. Huynh, A. Violi, An experimental and computational study of methyl ester decomposition pathways using shock tube, *Proceedings of the Combustion Institute* 32 (2009) 247-253.
- [64] S.M. Sarathy, S. Gail, S.A. Syed, M.J. Thomson, P. Dagaut, A comparison of saturated and unsaturated C₄ fatty acid methyl esters in an opposed flow diffusion flame and jet stirred reactor, *Proceedings of the Combustion Institute* 31 (2007) 1015-1022.

- [65] S. Gail, S.M. Sarathy, M.J. Thomson, P. Diévar, P. Dagaut, Experimental and chemical kinetic modeling study of small methyl esters oxidation: Methyl (E)-2-butenate and methyl butanoate, *Combustion and Flame* 155 (2008) 635-650.
- [66] W.R. Schwartz, C.S. McEnally, L.D. Pfeifferle, Decomposition and hydrocarbon growth process for esters in non-premixed flames, *Journal of Physical Chemistry A* 110 (2006) 6643-6648.
- [67] B.I. Parsons, C.J. Dandy, The oxidation of hydrocarbons and their derivatives. Part I. The observation of the progress of the reaction by pressure change and by analysis, *Journal of the Chemical Society* (1956) 1795-1798.
- [68] B.I. Parson, C. Hinshelwood, The oxidation of hydrocarbons and their derivatives. Part II. Structural effects in the ester series, *Journal of the Chemical Society* (1956) 1799-1803.
- [69] B.I. Parson, The oxidation of hydrocarbons and their derivatives. Part III. The role of intermediates, *Journal of the Chemical Society* (1956) 1804-1809.
- [70] D.E. Hoare, T.M. Li, A.D. Walsh, Cool flames and molecular structure, *Proceedings of the Combustion Institute* 11 (1967) 879-887.
- [71] A.E. Lutz, R.J. Kee, J.A. Miller, SENKIN: A Fortran Program for Predicting Homogeneous Gas Phase Chemical Kinetics with Sensitivity Analysis, Report No (1988), SAND87-8248, Sandia National Laboratories.
- [72] P. Dagaut, G. Pengloan, A. Ristori, Oxidation, ignition and combustion of toluene: Experimental and detailed chemical kinetic modeling, *Physical Chemistry Chemical Physics* 4 (2002) 1846-1854.
- [73] M. O’Conaire, H.J. Curran, J. M. Simmie, W.J. Pitz, C.K. Westbrook, A comprehensive modeling study of hydrogen oxidation, *International Journal of Chemical Kinetics* 36 (2004) 603-622.
- [74] A.M. El-Nahas, M.V. Navarro, J.M. Simmie, J.W. Bozzelli, H.J. Curran, S. Dooley, W. Metcalfe, Enthalpies of Formation, Bond Dissociation Energies and Reaction Paths for the decomposition of Model Biofuels: Ethyl Propanoate and Methyl Butanoate, *Journal of Physical Chemistry A* 111 (2007) 3727-3739.
- [75] H.J. Curran, Rate constant estimation for C₁ to C₄ alkyl and alkoxy radical decomposition, *International journal of chemicals kinetics* 38 (2006) 250-275.
- [76] T. Lay, J.W. Bozzelli, A.M. Dean, E.R. Ritter, Hydrogen Atom Bond Increments for Calculation of Thermodynamic Properties of Hydrocarbon Radical Species, *Journal of Physical Chemistry B* 99 (1995) 14514-14527.

- [77] R. Sumathi, W.H. Green Jr., Oxygenate, oxyalkyl, and alkoxy carbonyl thermochemistry and rates for hydrogen abstraction from oxygenates, *Physical Chemistry Chemical Physics* 5 (2003) 3402-3417.
- [78] J. Biet, M.H. Hakka, V. Warth, P.A. Glaude, F. Battin-Leclerc, Experimental and Modeling Study of the Low-Temperature Oxidation of Large Alkanes, *Energy and Fuel* 22 (2008) 2258-2269.
- [79] Y.R. Luo, *Handbook of Bond Dissociation Energies in Organic Compounds*, CRC Press: Boca Raton (2003), FL.
- [80] D.G. Goodwin, An open-source extensible software suite for CVD process simulation, *Proceedings of CVD XVI and EuroCVD Fourteen*, *Electrochemical Society* 14 (2003) 155-162.
- [81] W.K. Metcalfe, C. Togbé, P. Dagaut, H.J. Curran, J.M. Simmie, A jet-stirred reactor and kinetic modeling study of ethyl propanoate oxidation, *Combustion and Flame* 156 (2009) 250-260.
- [82] G. Dayma, S. Gail, P. Dagaut, Experimental and kinetic modeling study of the oxidation of methyl hexanoate, *Energy and Fuel* 22 (2008) 1469-1479.
- [83] J.P. Szybist, J. Song, M. Alam, A.L. Boehman, Biodiesel combustion, emissions and emission control, *Fuel Processing Technology* 88 (2007) 679-691.
- [84] R.A. Yetter, F.L. Dryer, Inhibition of moist carbon monoxide oxidation by trace amounts of hydrocarbons, *Proceedings of the Combustion Institute* 24 (1992) 757-767.
- [85] J.P. Szybist, A. Boehman, D.C. Haworth, H. Koga, Premixed ignition behavior of alternative diesel fuel-relevant compounds in a motored engine experiment, *Combustion and Flame* 149 (2007) 112-128.
- [86] P. Dagaut, S. Gaïl, M. Sahasrabudhe, Rapeseed oil methyl ester oxidation over extended ranges of pressure, temperature, and equivalence ratio: Experimental and modeling kinetic study, *Proceedings of the Combustion Institute* 31 (2007) 2955-2961.
- [87] D.F. Davidson, J.T. Herbon, D.C. Horning DC, R.K. Hanson, OH concentration time histories in *n*-alkane oxidation, *International Journal of Chemical Kinetics* 33 (2001) 775-783.
- [88] P.A. Glaude, W.J. Pitz, M.J. Thomson, Chemical kinetic modeling of dimethyl carbonate in an opposed-flow diffusion flame, *Proceedings of the Combustion Institute* 30 (2005) 1111-1118.
- [89] K. Seshadri, T. Lu, O. Herbinet, S. Humer, U. Niemann, W. Pitz, R. Seiser, C.K. Law, Experimental and kinetic modeling study of extinction and ignition of methyl decanoate in laminar non-premixed flows, *Proceedings of the Combustion Institute* 32 (2009) 1067-1074.

- [90] S.R. Hoffmann, J. Abraham, A comparative study of n-heptane, methyl decanoate, and dimethyl ether combustion characteristics under homogeneous-charge compression-ignition engine conditions, *Fuel* 88 (2009) 1099-1108.
- [91] R.J. Kee, F.M. Rupley, J.A. Miller, M.E. Coltrin, J.F. Gear, E. Meeks, Theory Manual CHEMKIN Release 4.0.1 Reaction Design, Inc., 2004.
- [92] G.P. Smith, D.M. Golden, M. Frenklach, N.W. Moriarty, B. Eiteneer, M. Goldenberg, GRI-Mech version 3.0, 1999.
- [93] M.H. Hakka, P.A. Glaude, O. Herbinet, F. Battin-Leclerc, Experimental study of the oxidation of large surrogates for diesel and biodiesel fuels, *Combustion and Flame* 156 (2009) 2129-2144.
- [94] S. Bax, M.H. Hakka, P.A. Glaude, O. Herbinet, F. Battin-Leclerc, Experimental study of the oxidation of methyl oleate in a jet-stirred reactor, *Combustion and Flame* 157 (2010) 1220-1229.
- [95] J.R. Pedersen, A. Ingemarsson, J.O. Olsson, Oxidation of Rapeseed Oil, Rapeseed Methyl Ester (RME) and Diesel Fuel Studied with GC/MS, *Chemosphere* 38 (1999) 2467-2474.
- [96] A. Ristori, P. Dagaut, M. Cathonet, The oxidation of n-hexadecane: Experimental and detailed kinetic modeling, *Combustion and Flame* 125 (2001) 1128-1137.
- [97] P. Dagaut, S. Gail, Chemical kinetic study of the effect of a biofuel additive on jet-A1 combustion, *Journal of Physical Chemistry A* 111 (2007) 3992-4000.
- [98] V.I. Golovitchev, J. Yang, Construction of combustion models for rapeseed methyl ester bio-diesel fuel for internal combustion engine applications, *Biotechnology Advances* 27 (2009) 641-655.
- [99] V.I. Golovitchev. <http://www.tfd.chalmers.se/~valeri/MECH.html>, accessed (2003).
- [100] A.A. Amsden, KIVA-3V, a block-structured KIVA program for engines with vertical or canted valves. Report LA-13313-MS, UC-1412, Los Alamos, New Mexico 87545 (1997).
- [101] Y. Zhang, Y. Yang, A.L. Boehman, Premixed ignition behavior of C₉ fatty acid esters: A motored engine study, *Combustion and Flame* 156 (2009) 1202-1213.
- [102] C.K. Westbrook, Chemical Kinetics of Hydrocarbon Ignition in Practical Combustion Systems, *Proceedings of the Combustion Institute*. 28 (2000) 1563-1577.
- [103] C.M. Lund, L. Chase, HCT-A general computer program for calculating time dependent phenomena involving one-dimensional hydrodynamics, transport, and detailed chemical kinetics, Lawrence Livermore National Laboratory report UCRL-52504, revised (1995).

Appendix AI Oxidation kinetic related to $C_{n(n>4)}$ -methyl and ethyl esters

This part gives a summary of the main oxidation kinetic studies conducted for methyl and ethyl esters with an aliphatic main chain comprising more than four carbon atoms ($C_{n(n>4)}$ -methyl or ethyl esters). Experimental data generated for this class of biodiesel surrogates are listed in Table AI.4 whereas the main features relating the modeling are shown in Table AI.5. Both Tables were located at the end of this section.

AI.1 Kinetic investigations related to $C_{n(n>4)}$ -methyl esters

AI.1.1 Oxidation of model molecules starting to be suitable biodiesel surrogates: methyl hexanoate, methyl decanoate, methyl-5- and methyl-9-decenoate

Although investigations related to C_4 -methyl esters helped to improve knowledge related the impact of the methyl ester group on the combustion chemistry, these molecules firstly selected as biodiesel surrogates revealed to be not suitable. Particularly, no evidence of cool flame or NTC region (excepting few sources like Fisher et al., 2000 [55] or Sarathy et al., 2007 [64] claiming weak NTC behaviour) was experimentally observed or predicted by modelling. Nevertheless, actual biodiesel components, like long chain alkanes, should show these two kinds of phenomena (indicating competition between temperature dependent oxidation channels, Figure I.4). It is now admitted that this deficiency encountered with C_4 -methyl esters is actually due to their too short aliphatic main chains that avoid easy internal H-atom transfer onto the peroxy radicals RO_2^\bullet (reaction 3, Figure I.4) via formation of low strain cyclic intermediate to yield hydroperoxy radicals $^\bullet QOOH$ (reaction 4, Figure I.4). Methyl hexanoate and, a fortiori methyl decanoate, methyl-5- and methyl-9-decenoate revealed to be more suitable biodiesel surrogates.

- *Oxidation of methyl hexanoate.* Dayma et al. (2008) [82] were the first to carry out methyl hexanoate (MHX) oxidation in a jet-stirred reactor (JSR) at high pressure (10 atm) and in a range from low to high temperatures (500-1000 K), with additionally various equivalence ratios and a constant residence time (Table AI.4). Concentration (mole fraction) profiles of 23 species were measured (O_2 , H_2 , CO, CO_2 , formaldehyde, methane, acetaldehyde, ethane, ethene, acetylene, propene, propanal, propenal, 1-butene, 1-pentene, and unsaturated methyl esters from C_4 to C_7). Under the investigated operating conditions, the authors reported that MHX showed three main reaction regimes similarly to large hydrocarbons:
 - A cool flame zone (560-660 K) characterized by fuel consumption at low temperature and the production of small aldehydes and methyl hexenoates,

- A NTC zone (660-760 K) where the total reactivity decreases with increasing of temperature,
- A high temperature zone (>760 K), with the total consumption of the fuel.

This new set of experimental data was used by the authors to develop and validate a detailed chemical kinetic model for MHX oxidation, consisting of 435 species and 1875 reactions (Table AI.5). The mechanism was built in a hierarchical and systematic way. The first edifice was based on the comprehensive MB oxidation mechanism developed by Fisher et al. (2000) [55] to which was added a 1-butene submechanism validated under various experimental conditions (Dagaut, 2002 [72]) and including 1,3-butadiene, butyl and butenyl radicals. Nevertheless, four reactions from the Fisher et al. (2000) [55] model were modified to get better predictions, particularly for ethylene (C₂H₄) and methyl 2-propenoate (CH₂=CHC(=O)OCH₃) profiles (Table AI.1). Additionally, a submechanism of 551 reactions was implemented to model the oxidation of MHX and related compounds from low to high temperatures. For similar reactions, the rate constants were those proposed by Fisher et al. (2000) [55] for MB. Nevertheless, due to the larger length of the aliphatic main chain for MHX, some rate constants had to be taken from the literature using structure-reactivity relationships (with computation of the reverse rate constants from the corresponding forward rate constants and the appropriate equilibrium constants $K_c = k_{\text{forward}}/k_{\text{reverse}}$ calculated from thermochemistry). Thermochemical data were taken from Fisher et al. (2000) [55] model while they were estimated from THERGAS software (Muller et al., 1995 [40]) for species belonging to MHX submechanism. The kinetic modeling was performed using the PSR code of CHEMKIN II (Kee et al., 1993 [43]). The proposed kinetic model yielded overall good agreement with experimental results. Thanks to reaction path analysis (Figures AI.1, AI.2), the authors highlighted that, over the investigated temperature and pressure ranges, the oxidation behavior of MHX was mainly controlled by the weakness of the C-H bond on the carbon adjacent to the methyl ester group.

Table AI.1 Reactions and rate constants modified by Dayma et al. (2008) [82] (bold) in MB Fisher et al. (2000) [55] model^a.

$C_2H_4 + \cdot C(=O)OCH_3 = \cdot CH_2CH_2(C=O)OCH_3$	2.11E + 11	0.00	3350
$\cdot CH_2CH_2C(=O)OCH_3 = C_2H_4 + \cdot C(=O)OCH_3$	2.00E + 13	0.00	30500
$CH_2=CHC(=O)OCH_3 + H\cdot = \cdot CH_2CH_2C(=O)OCH_3$	1.00E + 13	0.00	2900
$\cdot CH_2CH_2C(=O)OCH_3 = H\cdot + CH_2=CHC(=O)OCH_3$	3.00E + 13	0.00	37500
$CH_2=CHC(=O)OCH_3 + \cdot OH \rightarrow CH_2O + C_2H_3CO + H_2O$	5.25E + 09	0.97	1590

Table AI.1 (Continued)^a.

$\text{CH}_2=\text{CHC}(=\text{O})\text{OCH}_3 + \cdot\text{OH} \rightarrow \cdot\text{CH}_2\text{C}(=\text{O})\text{OCH}_3 + \text{CH}_2\text{O}$	4.00E + 12	0.00	-928
$\text{CH}_2=\text{CHC}(=\text{O})\text{OCH}_3 + \cdot\text{OH} \rightarrow \cdot\text{O}=\text{CHC}(=\text{O})\text{OCH}_3 + \cdot\text{CH}_3$	6.90E + 11	0.00	-928
$\text{C}_2\text{H}_4\text{OH} = \text{C}_2\text{H}_4 + \cdot\text{OH}$	1.293E + 12	-0.37	26850
$\text{C}_2\text{H}_4 + \cdot\text{OH} = \text{CH}_2\text{O} + \cdot\text{CH}_3$	1.40E + 12	0.00	3250

^a The rate constants were expressed using the modified Arrhenius equation $k = A \cdot T^n \cdot \exp(E_a/RT)$ with units cm, mole, s, T, and cal.

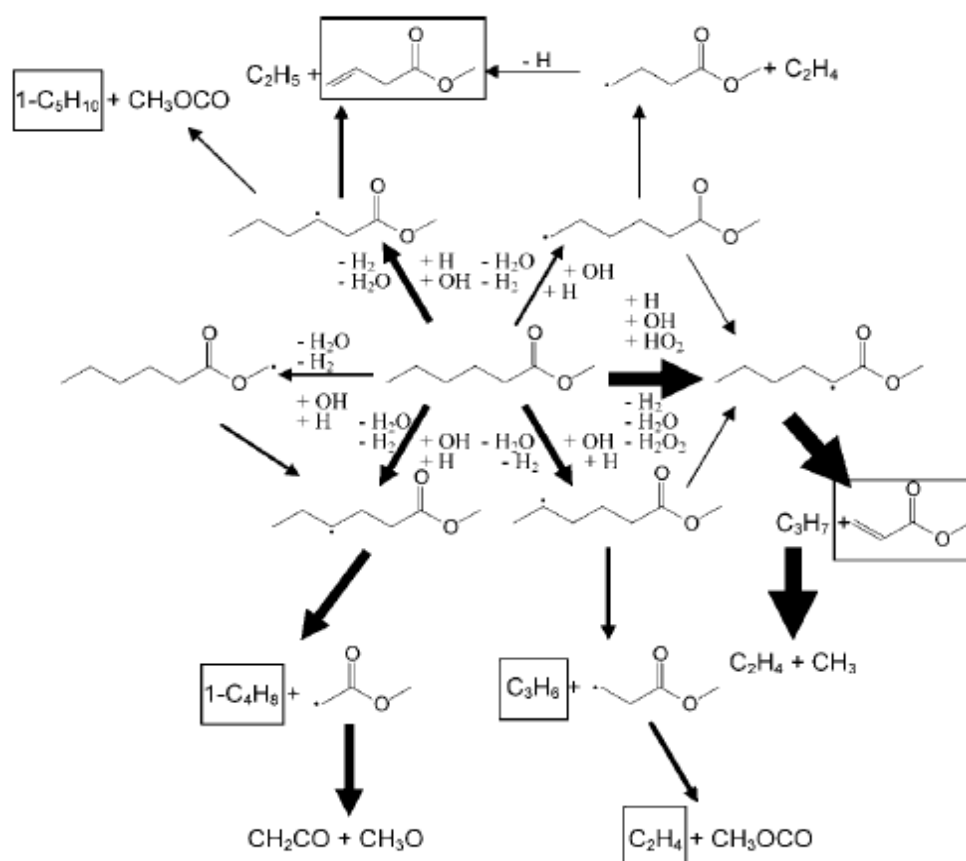


Figure AI.1 Reaction path analysis for the oxidation of methyl hexanoate at $T=950\text{ K}$, $\phi=1$, $\tau=1\text{ s}$, and $P=10\text{ atm}$ (Dayma et al., 2008 [82])^a.

^a The thickness of the arrows is proportional to the importance of the reaction path. The framed products were quantified.

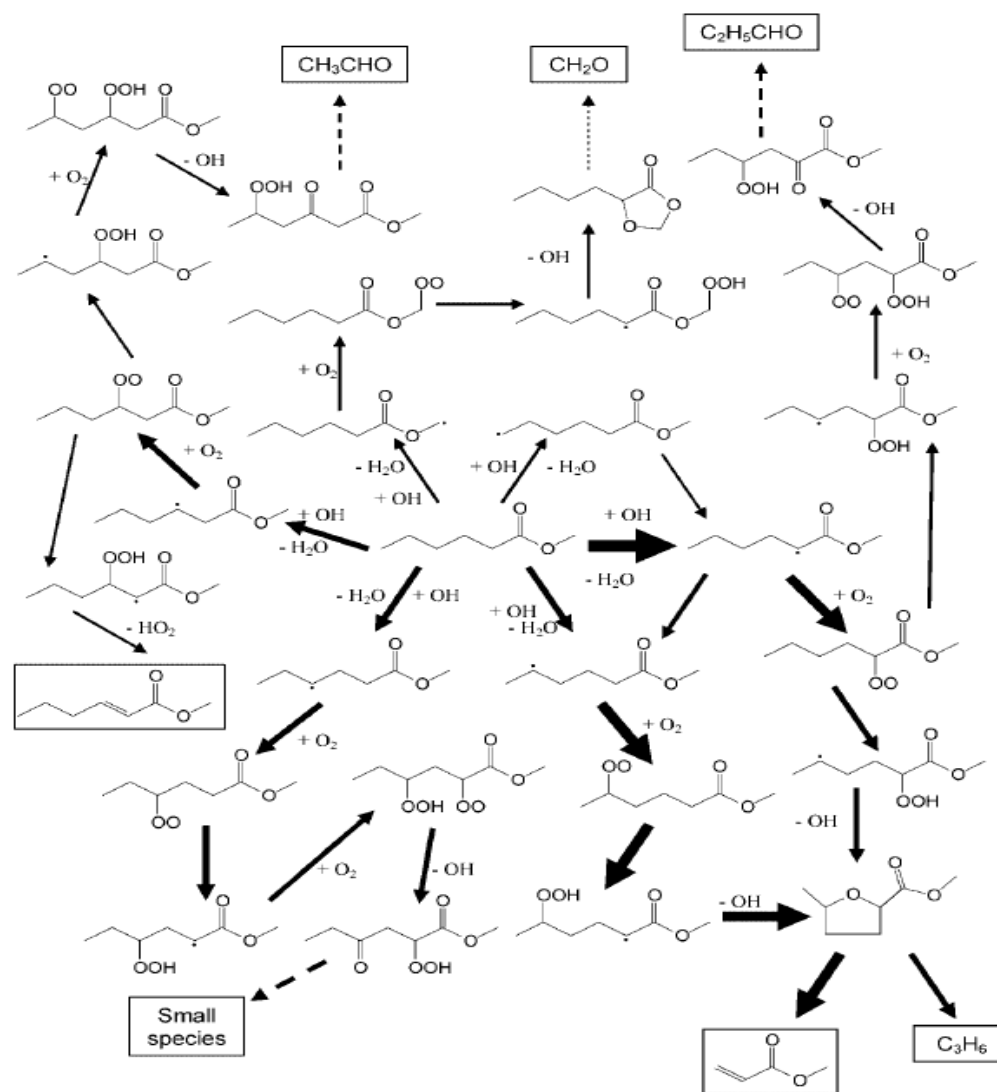


Figure AI.2 Reaction path analysis for the oxidation of methyl hexanoate at $T=650$ K, $\phi=1$, $\tau=1s$, and $P=10$ atm (Dayma et al., 2008 [82])^a.

^a The thickness of the arrows is proportional to the importance of the reaction path. The framed products were quantified (dashed arrows mean a several step production).

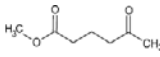
HadjAli et al. (2009) [52] examined the autoignition of five linear methyl esters of butanoic to octanoic acids in a rapid compression machine (RCM), at operating conditions useful for compression ignition engine model validation (over low and intermediate temperature range: 650-850K, under medium to high pressures: 4-20 bar, with stoichiometric mixtures, and the same dilution of oxygen as in air; (Table AI.4). Nevertheless, under the conditions investigated, the vapor pressures of methyl heptanoate and octanoate were too low to permit valid autoignition experiments. Therefore, the authors selected MHX for a full investigation of its autoignition phenomenology, including the identification and quantification of the intermediate products of low temperature oxidation. The oxidation scheme and overall

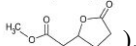
reactivity of MHX were examined and compared to the reactivity of C₄ to C₇ n-alkanes, in the same experimental conditions, to evaluate the impact of the methyl ester function on the reactivity of the n-alkyl chain. The low temperature reactivity of MHX leading to the first stage of autoignition (cool flame event) is similar to that of n-heptane. However, the NTC region is located at lower temperature than in the case of n-pentane and n-butane. The authors also gave the main reaction pathways leading to the detected products (for the lighter species: acetic acid, propenal, 1-pentene, propanal, methyl acetate, butanone, and butanal; for the C₄-C₇ species: unsaturated methyl esters, methyl epoxy esters with 3-5 atom rings, and 5-butyl-1,3-dioxolane-4-one).

- *Oxidation of methyl decanoate.* Szybist et al. (2007) [83] reported the autoignition behavior of methyl decanoate (MD) in a variable compression ratio (CR) octane rating engine charged with premixed MD and air. The spark plug was disabled for this study so that combustion is initiated kinetically and ignition occurs simultaneously at multiple points throughout the cylinder as with HCCI combustion. The engine CR was adjusted over a range of 4.0 to 13.75, at multiple equivalence ratios (Table AI.4). During each CR sweep, exhaust composition in CO, CO₂, formaldehyde, and acetaldehyde was monitored via FTIR (Fourier transformed infrared) spectrometry and condensable exhaust gas was collected for subsequent GC-MS (gas chromatography/mass spectrometry) analysis. The authors observed that, for sufficiently high compression ratios (CR ≈ 9.1), MD exhibited two-stage ignition with low-temperature heat release (LTHR) followed by the main combustion event or high-temperature heat release (HTHR). For lower compression ratios (CR ≈ 5.6), MD underwent only LTHR. GC-MS speciation of the LTHR exhaust condensate revealed formation of various classes of species, a selection of which are listed in Table AI.2. In addition to a number of saturated and unsaturated methyl esters with shorter aliphatic main chains than MD, a number of saturated oxo-methyl esters with additional carbonyl group on the aliphatic main chain were also identified. This result revealed that the long aliphatic main chain acts similarly to n-paraffins during LTHR, while the ester group remains intact. On the other hand, FTIR analysis revealed significant amounts of CO₂ produced during LTHR. On the basis of results commonly established according to which oxidation of CO to CO₂ does not occur at low-temperature conditions when hydrocarbon chains are present in the medium (Yetter and Dryer, 1992 [84]), the authors concluded that the CO₂ produced by MD during LTHR was due to decarboxylation of the ester group. Thus, by collecting both FTIR and GC-MS data, the decarboxylation of MD should not occur until the aliphatic main chain has been largely consumed by LTHR reactions, incorporating the contribution of oxygen in the molecule. The authors thus highlighted that due

to this lost of CO₂ directly from decomposition of the parent molecule (and not by oxidation), the oxygen present in the fuel is used less effectively to remove carbon from the pool of soot precursors, revealing that esters should reduce particulate matter emissions less efficiently than ethers.

Table AI.2 Selected identified species from the low-temperature heat release exhaust condensate of methyl decanoate oxidation (Szybist et al., 2007 [83],[85])^a.

Methyl esters	Oxo-methyl esters
2-methyl butanoic acid methyl ester	4-oxopentanoic acid methyl ester
Methyl hexanoate	
Methyl heptanoate	5-oxopentanoic acid methyl ester
Methyl octanoate	5-oxohexanoic acid methyl ester
Methyl octanoate	6-oxoheptanoic acid methyl ester
Methyl nonenoate (isomers)	4-oxooctanoic acid methyl ester
Methyl nonanoate	2-oxodecanoic acid methyl ester
Methyl decenoate (isomers)	9-oxodecanoic acid methyl ester
Methyl decanoate	

^a Additional detected species: organic acids (from butanoic to decanoic acid), 2-nonanone, heptanal, nonanal, 5-methylcarbonylpentan-4-olide (result of a cyclic ester being formed at the aliphatic chain with the methyl ester group remaining intact ).

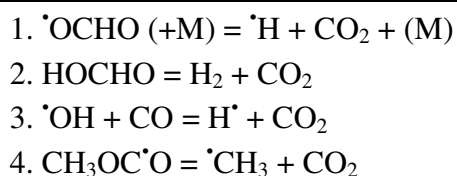
In a complementary approach to the experimental work by Szybist et al. (2007) [83], [85], Herbinet et al. (2008) [50] developed a detailed kinetic model for MD oxidation by combining the mechanisms previously proposed for n-heptane, iso-octane (Curran et al., 1998 [48], 2002 [49]), and MB (Fisher et al., 2000 [55]) with the low- and high-temperature chemistry specific to MD. Kinetic parameters and thermochemical properties were updated according to recent literature information, including quantum theory based estimations. Particularly, the C-H bond dissociation energy (bond enthalpy) of the carbon atom adjacent to the carbonyl group has been updated according to El-Nahas et al. (2007) [74] work as was done previously by Metcalfe et al. (2007) [51] and Dooley et al. (2008) [58] (value adopted by Herbinet et al., 2008 [50] and obtained by El-Nahas et al., 2007 [74] from *ab initio* estimations: 94.1 kcal·mol⁻¹). Based on the overall primary oxidation reaction pathways and reaction classes, deriving from the work by Curran et al. and extended to methyl- and ethyl esters (Figure I.4 and Table I.3, respectively), the resulting mechanism proposed by Herbinet et al. includes 8820 reactions involving 3012 species (Table AI.5). The large numbers of reactions and species are mainly caused by the fact that MD is not a symmetric molecule (unlike an n-alkane) and also by the numerous types of reactions that were taken into account. Particularly, isomerizations of RO₂[•] to [•]QOOH radicals in the low-temperature regime (reaction 4 in Figure

I.4) were considered of going through 5-, 6-, 7-, and 8-member cyclic transition states yielding numerous permitted H-shifts. Model validation was conducted by comparing computed results with various classes of experimental information ranging from low to high temperature regions: the only available experimental data for MD obtained in a motored engine (Szybist et al., 2007 [83], [85]), together with rapeseed methyl ester oxidation results in a JSR (Dagaut et al., 2007 [86]) and n-decane ignition in shock tube (Davidson et al., 2001 [87]). The first two classes of experimental information yielding species profiles helped to highlight the ability of the model to reproduce the chemistry of most products formed, particularly the early production of CO₂ that is specific to biodiesel and due to the presence of the ester group into the reactant. This important feature of the mechanism was obtained thanks to the insertion of low-temperature reactions leading to the formation of CO₂. The main of these reactions are listed in Table AI.3. Reactions 1 and 4 derive uniquely from the methyl ester group in MD and would not occur in hydrocarbon oxidation. Also, the authors pointed out that concerning reaction 4 of Table AI.3, the kinetic parameters were updated according to the recent work by Glaude et al. (2005) [88] relative to dimethyl carbonate. Successive reactions from an alkyl-ester radical to the formation of CO₂ via the [•]OCHO radical are reported in Figure AI.3 as illustrated by the authors. As the later pointed out, one oxygen atom in CO₂ comes from the non-carbonyl part of the ester group and the other oxygen atom from the oxygen molecule involved in the reaction of addition.

Additionally, Herbinet et al. (2008) [50] also obtained very good agreement with n-decane experiments in shock tube (ignition delay times and OH profiles), with a NTC region occurring around 780-920 K at 12 atm. This result shows that the reactivity of large methyl esters is very similar to the reactivity of n-alkanes of similar size. Nevertheless, fine kinetic details like early CO₂ production occurring at low-temperature during biodiesel combustion can only be predicted by considering actual methyl ester fuels.

Table AI.3 The main reactions leading to the formation of CO₂ at low temperature

(Herbinet et al., 2008 [50])



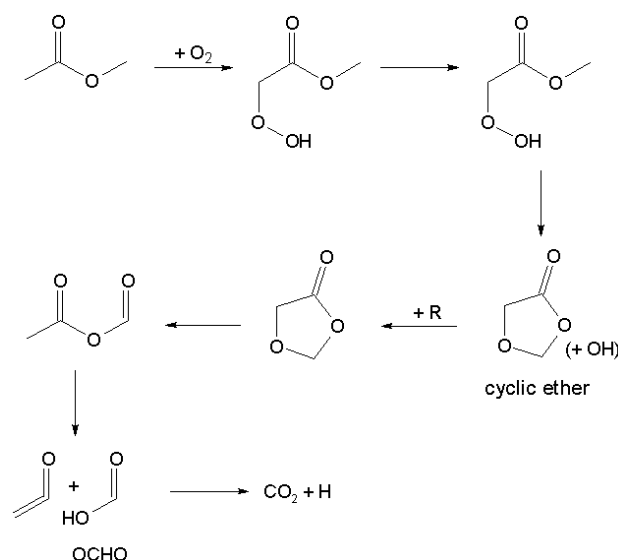


Figure AI.3 Successive reactions from an alkyl-ester radical to the formation of CO_2 via the radical $\cdot OCHO$ (Herbinet et al., 2008 [50]).

Following this work, an experimental and kinetic modeling study of extinction and ignition of MD in non-premixed, aerodynamically strained flows, was investigated by Seshadri et al. (2009) [89]. These characteristics were investigated under such conditions because flame extinction in high strained flows is an important problem in gas turbine engines and because fuel/air mixtures must be ignited in flows in internal combustion engines. Critical conditions of counter flow extinction and ignition were measured with a fuel stream made up of vaporized MD in nitrogen, and an oxidizer stream of air (Table AI.4). The detailed chemical kinetic model for MD by Herbinet et al. (2008) [50] includes unfortunately too large numbers of reactions and species for being directly used in current flame codes. Therefore, a skeletal mechanism was deduced from this detailed mechanism using the directed relation graph method. The derived skeletal mechanism involves only 713 elementary reactions and 125 species. Predictions of extinction and ignition of MD in non-premixed counter flows were found to agree well with the experimental data. Also, the authors pointed out that the derived skeletal mechanism showed minor importance of the low temperature chemistry under the considered counter flow conditions. The reaction chemistry of most importance was found to be the high-temperature reactions of fuel decomposition, radical abstraction, isomerization, and radical decomposition. Formation and consumption of olefin intermediates with ester moieties were also found to be significant.

The same year, Hoffman and Abraham (2009) [90] investigated ignition delay and NO formation rates for MD and n-heptane (mineral diesel surrogate) under conditions of varying O_2 concentration by employing the CHEMKIN homogeneous constant-pressure reactor model

and the homogeneous-charge compression-ignition engine model (Lee et al., 2004 [91]). Ignition delay time was defined in this study as the time for the gas mixture to reach a temperature of 1500 K in the homogeneous reactor. Calculations were performed in a wide temperature range (700-1350 K), at two pressures (12.5 and 40 atm), and for stoichiometric mixtures of fuel and air (21% in O₂). Reduced O₂ molar concentrations (18%, 15%, and 12%) were obtained by replacing a portion of the initial oxidizer O₂ by N₂. This procedure was adopted to simulate the dilution effect of exhaust-gas-recirculation (ERG). The MD detailed chemical kinetic model proposed by Herbinet et al. (2008) [50] was used without any modification. Nevertheless, the GRI-Mech 3.0 mechanism (Smith et al. 1999 [92]), involving 105 reactions and 20 species, was added to predict NO formation (Table AI.5). Computed results led the authors to observe that reducing O₂ concentration increased ignition delay for all fuels. As previously observed by Herbinet et al. (2008) [50] for MD and n-decane, MD and n-heptane showed qualitatively similar autoignition characteristics, with NTC region occurring in different temperature ranges (for MD in the range 750–900 K at 12.5 atm and 820-950 K at 40 atm, while for n-heptane at 50 K higher). Ignition delay was roughly the same for n-heptane and MD in the NTC region; however, outside the NTC region, the delay for MD was 30-60% shorter. The authors also highlighted the effect of pressure onto NTC region. They observed that at higher pressures, NTC region shifted towards higher temperatures and became less pronounced (due to H₂O₂ dissociation in 2 HO· at relatively lower temperatures when pressure increases). Furthermore, addition of NO to simulate exhaust-gas-recirculation (EGR) reduced the ignition delay time. However, in practical applications, the increase in ignition delay due to lower O₂ concentrations dominates over any decrease due to NO.

- *Oxidation of methyl-5- and methyl-9-decenoate.* Although Herbinet et al. (2008) [50] model revealed to be a very powerful tool for predicting biodiesel combustion, methyl decanoate (MD) on which was based the model has no double bond, unlike most of actual biodiesel components. Therefore, in order to capture the impact of this chemical specificity on biodiesel reactivity and further refine kinetic modeling, the same authors (Herbinet et al., 2010 [53]) investigated the oxidation of two C₁₀-methyl esters with a double bond located at different position on the aliphatic main chain: methyl-5-decenoate (MD5EN) and methyl-9-decenoate (MD9EN). Due to the similar molecular structures of the selected biodiesel surrogates, the two detailed chemical kinetic sub-mechanisms for the oxidation of MD5EN and MD9EN were built from the previous MD oxidation model by adding the low- and high-temperature chemistry specific to the unsaturated species (presence of double bonds, vinylic and allylic H-atoms). Both models for MD5EN and MD9EN oxidations were compared

with rapeseed oil methyl esters experiments in JSR (Dagaut et al., 2007 [86]). It could be observed that MD9EN performed better than MD5EN in reproducing the reactivity and the mole fraction profiles of major species. Computed ignition delay times for MD5EN and MD9EN were also compared, showing that MD9EN was more reactive than MD5EN, particularly in the NTC region, leading to the conclusion that MD9EN would be a better biodiesel surrogate than MD5EN. The authors attributed the lower reactivity of MD5EN to more difficult isomerizations over the double bond because of its location in the middle of the aliphatic main chain. Thus, the authors (Herbinet et al., 2010 [53]) highlighted that it is actually the length of the continuously-saturated carbon chain in the reactant that determines its reactivity because this chain sets the range of possible RO_2^{\bullet} isomerizations.

In order to obtain a detailed chemical kinetic mechanism more representative of biodiesel/petrodiesel blends, the authors (Herbinet et al., 2010 [53]) combined the three models of oxidation related to MD, MD9EN, and n-heptane (petrodiesel surrogate) oxidation; The resulting “blend surrogate models” was used to simulate the previously mentioned rapeseed oil methyl ester experiments conducted in JSR by Dagaut et al., (2007) [86]. The “blend surrogate models” performed slightly better than the model for MD9EN, by reproducing the experimental mole fraction profiles of most species with good agreement. These results led the authors to recommend this “blend surrogate models” for simulating combustion of biodiesel fuels whatever their origins, just by adjusting the mole fractions of the three components in the surrogate blend.

AI.1.2 Oxidation of actual biodiesel molecules: methyl palmitate and methyl oleate

As mentioned previously (Table I.1), methyl palmitate (MP) and methyl oleate (MO) are two components of methyl biodiesels derived from vegetable oils. The first MP is a saturated C_{16} -methyl ester, mainly encountered in palm oil, while the second MO is a monounsaturated C_{18} -methyl ester, mainly encountered in rapeseed oil. In the following two mentioned studies conducted by Hakka et al. (2009) [93] and Bax et al. (2010) [94], MP and MO were experimentally investigated in mixture with n-decane in order to simulate biodiesel fuel oxidation behaviour when blended with petrodiesel. Comparisons were also conducted with n-decane/n-hexadecane as blend surrogate for petrodiesel fuels (indeed, n-hexadecane is a reference molecule for the calculation of the cetane number which is assigned to 100 and has also 16 carbon atoms like the MP aliphatic main chain). For all surrogate blends, experiments were performed in a JSR over a wide range of temperature covering both low and high-temperatures (550-1100 K), at quasi atmospheric pressure and stoichiometric conditions (Table AI.4). Numerous reaction products were identified and quantified. Comparisons of

observed results highlighted the similarities and differences in the oxidation of large n-alkanes, monounsaturated and saturated methyl esters of similar size.

• *Methyl palmitate versus n-hexadecane* by Hakka et al. (2009) [93]. MP and n-hexadecane (nC16) showed very similar reactivities and the same NTC behaviour over the temperature range of study, confirming results previously observed by Herbinet et al. (2008) [50] for MD and n-decane. Furthermore, most of the observed species were formed with the two surrogate blends, n-decane/MP and n-decane/nC16. These common products are small oxygenated species (carbon oxides, methanol, acetaldehyde), small hydrocarbons (methane, acetylene, ethylene, ethane), and 1-olefins. The products specifically observed depend on the temperature of oxidation. At high temperature, these were monounsaturated esters with the double bond at the extremity of the aliphatic main chain (molecule of type A, Figure AI.4) for MP but 1-olefins for nC16. At low temperature, these specific products were methyl esters with a cyclic ether group located onto the aliphatic main chain and a 5-membered ring cyclic ether including the ester group branched to a long aliphatic main chain for MD (molecules of type B and C respectively, Figure AI.4) but 5-membered ring cyclic ethers and ketones branched onto aliphatic chain with 16 carbon atoms for nC16. The first class of compounds occurring at high temperature was also observed by Szybist et al. (2007) [83], [85] for MD, whereas for the second class of compounds occurring at low temperatures, the same authors rather observed oxo-alkanoic acid methyl esters and cyclic esters, probably because of the shorter aliphatic main chain of the ester MD (Table AI.2).

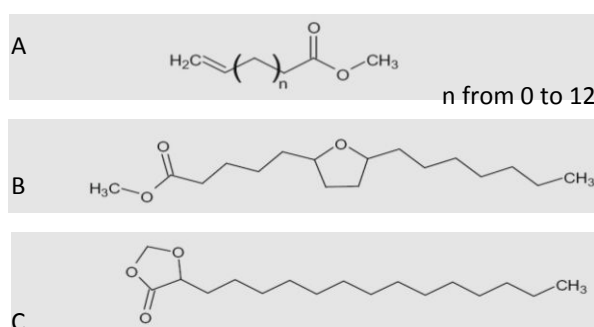


Figure AI.4 Samples of molecules observed by Hakka et al. (2009) [93] during methyl decanoate oxidation.

• *Methyl oleate versus methyl palmitate by Bax et al. (2010) [94].* The authors reported that both molecules (i.e. MO and MP) exhibited similar reactivity with a NTC zone occurring around 650-750 K. Nevertheless, due to the presence of the double bond in the middle of the aliphatic main chain for MO, specific reactivity features and reaction products were denoted by the authors. First, MO seemed to be slightly less reactive than MP in the low temperature range (below 750 K), despite its two additional carbon atoms relative to MP, whereas the opposite trend was observed beyond the NTC region. The authors attributed this behaviour to the presence of the double bond which disfavoured low-temperature chain-branching reactions, mainly isomerizations of peroxy radicals into hydroperoxy radicals (reaction 4, Figure I.4). Concerning the reaction products specific to MP oxidation, dienes and esters with two double bonds (resulting from decomposition of the two allylic radicals from H-abstraction of MO, Figure AI.5) were observed at high temperatures (around 800 K). On the other hand, at low and intermediate temperatures (around 550-650 K), oxygen containing compounds were observed, namely aldehydes conjugated with one double bond (Figure AI.6a) and C₁₈-methyl esters with either one 3-member ring cyclic ether functional group (oxirane esters, Figure AI.6b) or one ketone functional group (oxo esters, Figures AI.6c) branched onto the aliphatic main chain. These species were supposed by the authors to come likely from combination of HO₂[•] radicals with the resonance stabilized radicals from MO (conjugated aldehydes) or from addition of HO₂[•] or HO[•] to the double bond in MO (leading respectively to oxirane or oxo esters). The authors concluded their work by highlighting that, based on recent investigations related to large methyl esters modelling (Herbinet et al., 2008 [50], 2010 [53]), a detailed chemical kinetic model for methyl oleate generated by EXGAS software (Biet et al., 2008 [78]; Hakka et al., 2009 [61]) would contain more than 50,000 reactions and 6000 species, making its applicability very difficult.

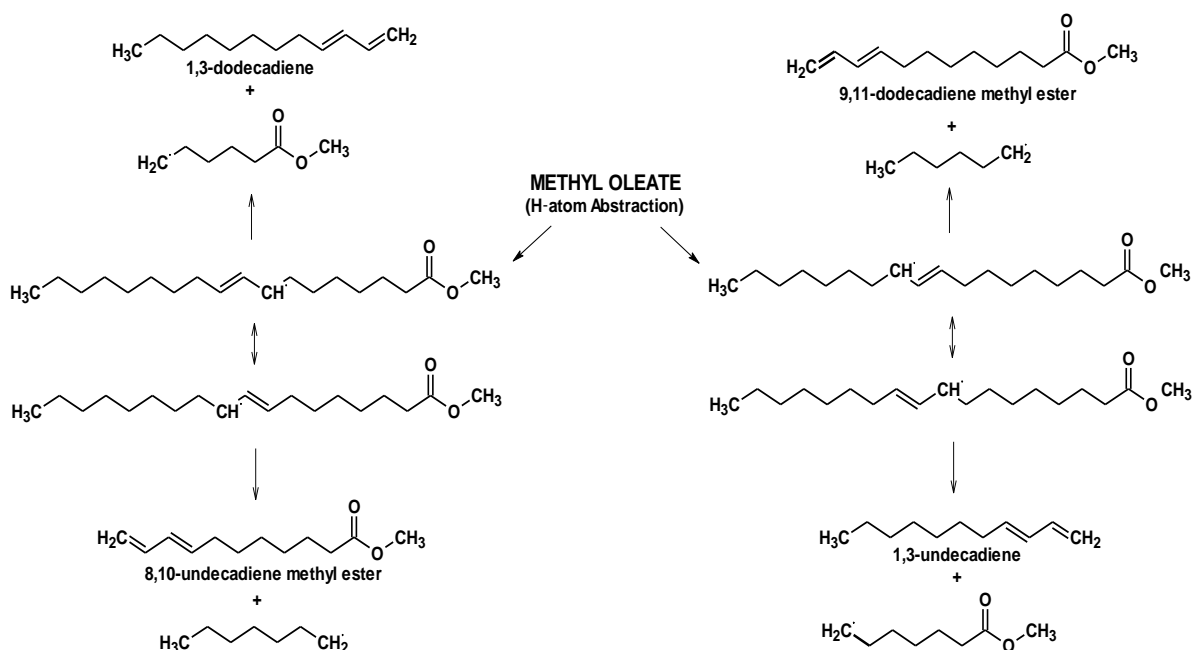


Figure AI.5 Illustration of dienes and esters with two double bonds formed during n-decane/methyl oleate oxidation (decomposition by β -scission of the two allylic radicals resulting from H-abstraction of methyl oleate and stabilized by resonance) (Bax et al., 2010 [94]).

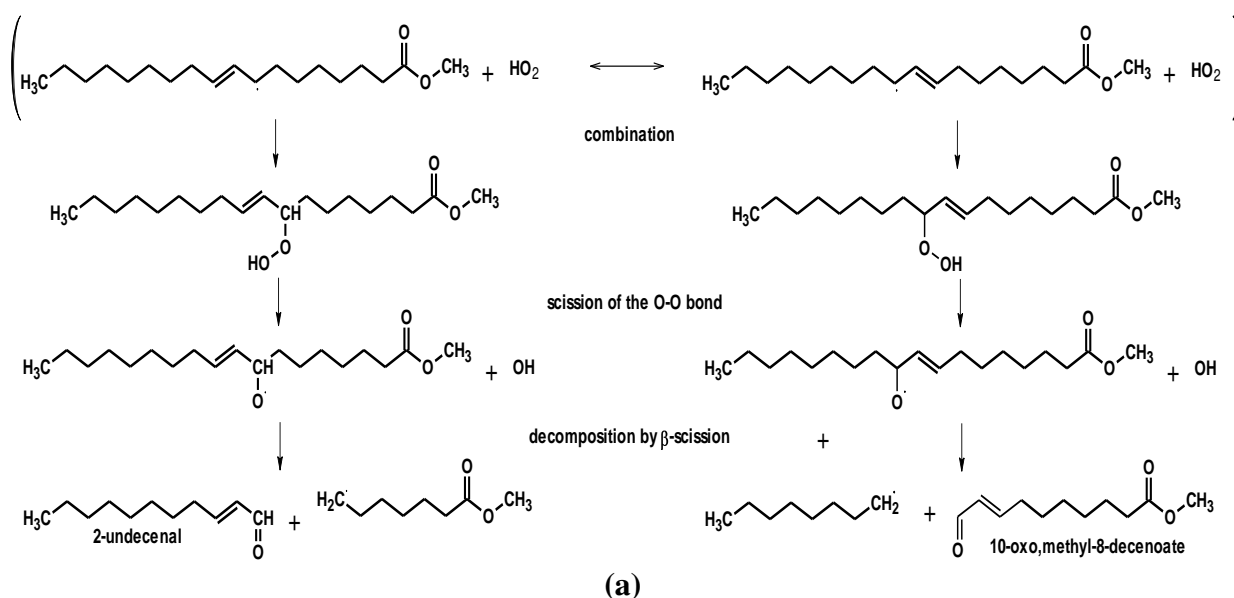
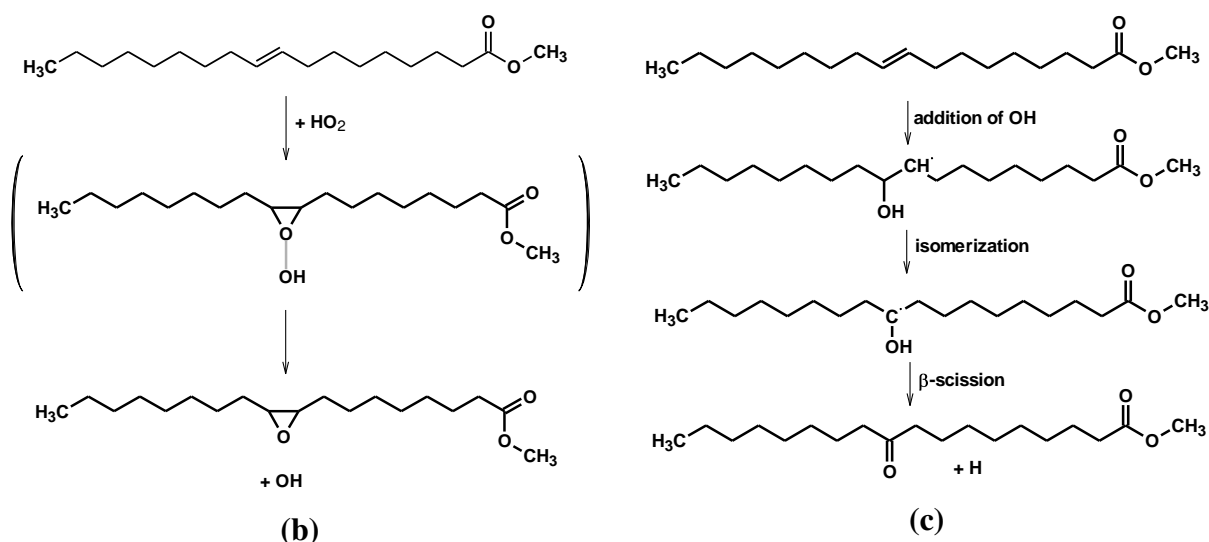


Figure AI.6 Illustration of oxygen containing compounds formed during n-decane/methyl oleate oxidation and their possible channels of formation. (a) Aldehydes conjugated with one double bond; (b) C_{18} -methyl esters with one 3-member ring cyclic ether functional group (oxirane esters illustrated here by 2-octyl, 3-(methyl octanoate)-oxirane); (c) C_{18} -methyl esters with one ketone functional group (oxo esters illustrated here by 10-oxo, methyl octadecanoate).

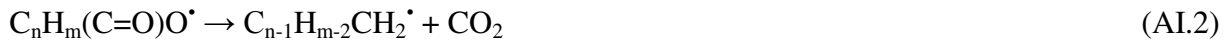


AI.1.3 Kinetic oxidation of rapeseed oil methyl ester

Pedersen et al. (1999) [95] performed a qualitative study of the species formed during oxidation of rapeseed oil and rapeseed oil methyl esters (RME) in a stainless steel tubular reactor at 823 K. GC-MS analysis of the two fuel gaseous emissions led the authors to conclude that rapeseed oil and RME react in a similar way during oxidation regarding formation of hydrocarbon products (1-alkenes, dienes, and benzene). Nevertheless, the authors observed that rapeseed oil oxidation produced high amounts of acrolein and other aldehydes, whereas RME oxidation produced significant amounts of methyl acrylate (methyl-2-propenoate) and other unsaturated esters like methyl-3-butenate, methyl-5-hexenoate, and methyl-6-heptenoate. The formation of methyl-4-pentenoate was not observed.

Quantitative investigation of RME oxidation was conducted for the first time in a JSR by Dagaut et al. (2007) [86]. Thus, as mentioned previously in sections related to biodiesel surrogate oxidation, the work developed by these authors was extensively used by researchers performing kinetic modeling investigations in order to validate their detailed chemical kinetic model on actual biodiesel oxidation experiments (Herbinet et al., 2008 [50]; 2010 [53]). Details related to this significant experimental work are given in this paragraph at last. Experiments by Dagaut et al. were conducted in dilute conditions over a wide range of temperature (800 to 1400 K), under low to moderate pressures (1-10 atm), and for various equivalence ratios and residence times (Table AI.4). Analysis of mole fractions for measured species led the authors to observe a strong similarity between oxidation of RME and oxidation of large n-alkanes. Then, experimental species profiles were compared with computed mole fractions from a mechanism previously developed for the oxidation of n-hexadecane (nC16), consisting of 225

species and 1841 reversible reactions (Ristori et al., 2001 [96]). The agreement was shown to be satisfactory and n-hexadecane appeared to be a good surrogate for RME under the investigated conditions. However, as it can be expected at this stage of the review, the nC16 mechanism was unable to predict the early production of CO₂ that was observed in the experiments. According to assumptions reported by Szybist et al., (2007) [83], [85], Dagaut et al. suggested reactions responsible for this phenomenon but without giving further mechanistic considerations:



More recently, Dagaut and Gaïl (2007) [97] investigated the oxidation of a blend of RME and kerosene Jet-A1 (20/80, mol/mol) in a JSR. As far as this review is concerned with biodiesel fuels, only results related to RME oxidation will be reported. Experiments that were performed over a wide temperature range (740-1200 K) and at 10 atm, for various equivalence ratios and a constant residence time (Table AI.4) revealed the formation of monounsaturated methyl esters with a double bond at the extremity of the aliphatic main chain (methyl-2-propenoate, methyl-3-butenate, methyl-4-pentenoate, and methyl-5-hexenoate).

More recently, Golovitchev and Yang (2009) [98] developed a RME combustion model for internal combustion engine applications. Assigning RME to the chemical formula C₁₉H₃₄O₂ (methyl linoleate) the authors based their RME combustion mechanism on the global decomposition reaction:



leading to products for which detailed oxidation sub-mechanisms were available in the literature. C₅H₁₀O₂ species designated methyl butanoate (MB) for which Fisher et al. (2000) [55] mechanism was used, whereas C₇H₁₆ and C₇H₈O species designated respectively n-heptane and phenyl methyl ether for which mechanisms by Golovitchev (2003) [99] were selected. The resulting biodiesel surrogate blend model produced a detailed RME combustion mechanism consisting of 309 species and 1472 reactions, including soot and NO_x formation processes, and was validated successfully using shock-tube ignition-delay data related to RME surrogate components (MB, n-heptane, and phenyl methyl ether). Nevertheless, for modeling and simulation of diesel engine (Volvo D12C) combustion (via the KIVA-3V code; Amsden, 1997 [100]), the authors had to reduce the detailed mechanism to 88 species participating in 363 reactions. The simulation results showed that RME combustion could be achieved with

low soot and NO concentrations, if moderate exhaust gas recirculation (EGR) loads, inducing a reduction in the combustion temperature, were used.

AI.2 Kinetic investigations related to $C_{n(n>4)}$ ethyl esters: ethyl hexanoate and ethyl nonanoate

Given the way investigations were conducted for methyl esters, researchers have realized that although the work developed for the short esters has greatly helped the understanding of the chemistry of oxidation of the alkyl esters, only esters with a long aliphatic main chain may exhibit the cool flame behavior characteristic of biodiesel. Hence, investigations were forwarded directly from ethyl propanoate to long-aliphatic main chain ethyl esters.

Quite obviously, these investigations were not directed to the development of detailed chemical kinetic mechanisms for oxidation of long-aliphatic main chain ethyl ester but rather to the generation of experimental information focused on application related to modern engine designs and from which it was possible to propose major reaction pathways. This is the subject of the following sub-sections illustrated for ethyl hexanoate and ethyl nonanoate.

- *Ethyl hexanoate versus methyl heptanoate.* In order to examine the applicability of two $C_8H_{16}O_2$ ethyl and methyl esters as biodiesel surrogates for application in modern engine designs employing low temperature combustion strategies, Zhang and Boehman (2010) [54] performed an experimental study of the autoignition of ethyl hexanoate (EHX) and methyl heptanoate (MH) in a motored CFR (Cooperative Fuel Research) engine. For each test fuel, while operating under fuel-lean condition (equivalence ratio of 0.25) and at 600 rpm, the engine compression ratio (CR) was gradually increased from the lowest point (4.43) to the point where significant high temperature heat release (HTHR) occurred. Also, to draw major low temperature oxidation pathways of the two esters, the engine exhaust was sampled and analyzed through GC-MS and GC-FID/TCD at various CRs for which only low temperature heat release (LTHR) occurred (Table AI.4).

From the performed heat release analyses, the authors observed that both EHX and MH exhibited evident cool flame and experienced a transition from single-stage LTHR to two-stage ignition with the increase of engine CR, which led to the conclusion that these two esters are likely suitable biodiesel surrogates in terms of low temperature oxidation characteristics. Furthermore, at a given CR, EHX revealed to have both a later onset and a lower magnitude of LTHR than MH, indicating that EHX is less reactive in the low temperature region than MH (Figure AI.7). The authors attributed this feature to the different aliphatic main chain length between the two esters.

Based on the literature mentioned above, this result seems to be in contradiction with the experimental or simulated observations done in previous works by other researchers on the oxidation of EP and MB, both at high and low temperatures (Schwartz et al., 2006 [66]; Metcalfe et al., 2007 [51]; 2009 [81]; Walton et al., 2009 [59]). Yet, EP also differs from MB like EHX does from MH in one CH_2 group on the aliphatic main chain, additionally to the nature of the ester functional group, e. g. ethyl or methyl ester group. The main difference between on one hand EP and MB and on the other hand EHX and MH is that the first class of esters account for short esters whereas the second class account for long esters; however, no evident relation between this structure-based feature and reactivity with a critical length of the aliphatic main chain has been highlighted yet. Moreover, differences between the chemistry of oxidation low- and high-temperature should also be taken into account in this evaluation. As a result, it might seem that the reactivity order between ethyl- and methyl esters against temperature still requires more investigations to get a better understanding.

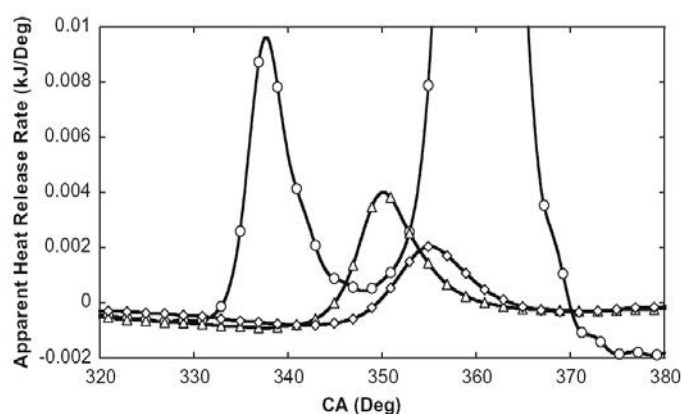


Figure AI.7. Comparison in heat release profiles between methyl heptanoate (triangle) and ethyl hexanoate (rhombus) at CR = 7.05 (Zhang and Boehman, 2010 [54]).

^a n-Heptane (round) was also introduced by the authors for illustrating that the presence of ester moiety inhibits low-temperature reactivity. Indeed, n-heptane and methyl heptanoate have the same carbon chain length and yet n-heptane experiences two-stage ignition while both esters only exhibit single-stage at the operating CR.

Concerning results obtained by Zhang and Boehman (2010) [54] relating the exhaust species produced under engine conditions where only LTHR occurred, GC analyses showed that the aliphatic main chain of the two esters, EHX and MH, experienced the typical paraffin-like low temperature oxidation sequence, with formation of unsaturated esters, epoxy esters, oxo-esters, aldehydes, and carboxylic acids. Similarly to Dayma et al. (2008) [82], the authors also observed that the abstraction of H-atoms on the α -carbon of the ester carbonyl group, further involving the cleavage of the C-C bond γ to the ester carbonyl group to form alkyl

(ethyl or methyl) propenoate, played an important role in the oxidation of long aliphatic main chain esters. Moreover, in the case of EHX oxidation, higher concentration of ethylene was observed compared to MH, with additionally formation of hexanoic acid, all confirming the existence of the six-centered unimolecular elimination reaction during low temperature oxidation of ethyl esters, as previously reported by Schwartz et al. (2006) [66], Metcalfe et al. (2007) [51], (2009) [81], and Walton et al. (2009) [59]. On the basis of these observations, the authors proposed major low temperature oxidation pathways of EHX (Figure AI.8). As expected, this scheme is very similar to the one adapted from Curran et al. (1998) [48] work by Herbinet et al. (2008) [50] for both high and low temperature oxidation of methyl esters (Figure I.4). The only difference is the insertion in the low temperature channels of the unimolecular decomposition of the ester RH into a carboxylic acid and ethylene, together with two additional decomposition paths of the hydroperoxy alkyl ester radicals ($\dot{Q}OOH$), prominent at intermediate temperatures, to form either unsaturated esters with a terminal double-bond, aldehydes and hydroxyl radicals, or oxo-esters and hydroxyl radicals. These two last reaction paths were also proposed with slight differences by Bax et al. (2010) [94] for MO oxidation.

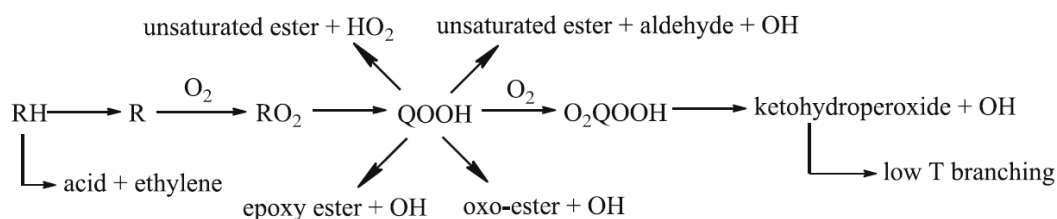


Figure AI.8 Major low temperature oxidation pathways of ethyl hexanoate (Zhang and Boehman, 2010 [54]).

- *Ethyl nonanoate versus methyl nonanoate.* With the aim of gaining insight into the low temperature oxidation of fatty acid esters produced from different alcohols and with unsaturation site located at different positions in the aliphatic main chain, Zhang et al. (2009) [101] investigated experimentally with the same engine environment as the one used previously by Zhang and Boehman (2010) [54] the premixed ignition behavior of four C₉ fatty acid esters, accounting methyl- and ethyl nonanoate (MN and EN respectively) together with two monounsaturated methyl esters, i.e. methyl 2- and methyl 3- nonenoate (MN2EN and MN3EN respectively) (Figure AI.9). Attention was also focused on the further understanding of the primary reaction paths responsible for the early CO₂ production during low temperature

oxidation of fatty acid esters, since this process is directly linked to the reduction of soot formation.

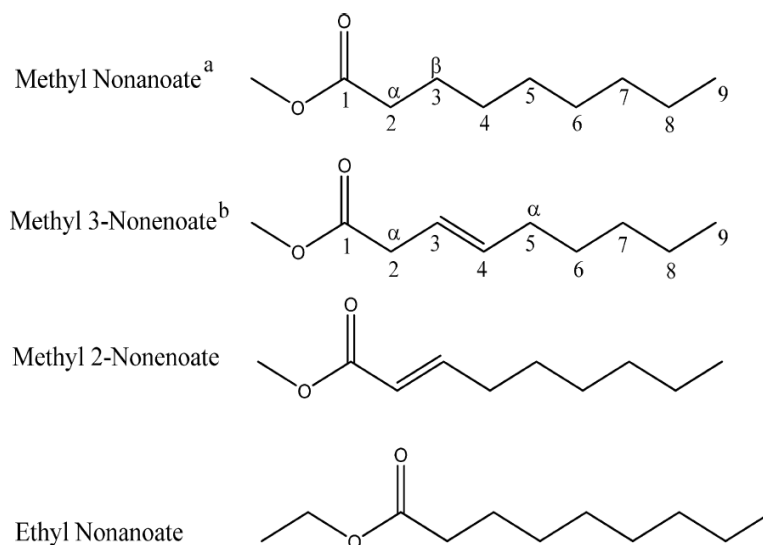


Figure AI.9 Molecular structures of the four C₉ esters investigated by Zhang et al. (2009) [101].^{a, b}

^a The carbon atom of the carbonyl group is carbon no. 1. Carbon no. 2 corresponds to the α -carbon of the carbonyl group. ^b The α -carbons of the ethylenic bond correspond to the carbon no. 2 and carbon no. 5 for methyl 3-nonenoate.

By following the same experimental operating conditions and procedure as those adopted by Zhang and Boehman (2010) [54], Zhang et al. (2009) [101] reported that, from exhaust species analyses, the four tested C₉ fatty acid esters showed different ignition behavior; MN and EN exhibited evident cool flame behavior and experienced two-stage ignition, whereas MN2EN and MN3EN experienced only single-stage ignition. The magnitude of low temperature heat release (LTHR) was observed to follow the order: EN > MN >> MN2EN > MN3EN. Furthermore, the comparison in percent of LTHR (defined as $[\text{LTHR}/(\text{LTHR} + \text{HTHR})] \times 100\%$) revealed that EN has the highest fraction of LTHR, indicating that EN has the highest low temperature oxidation reactivity among the test fuels. As discussed in the previous sub-section, the higher low temperature reactivity of the ethyl ester compared to that of the methyl ester was already reported by various authors (Schwartz et al., 2006 [66]; Metcalfe et al., 2007 [51]; 2009 [81]; Walton et al., 2009 [59]) who also explained this feature by the occurrence of the six-centered unimolecular elimination reaction of fatty acid ethyl esters likely facilitating ignition because of a relatively low activation energy. Further to this structure-reactivity relationship that they confirmed, Zhang et al. (2009) [101] gave a second structure-based argument relative to the presence of additional secondary C-H bonds in the

ethyl ester group enhancing the internal H-atom shift and then forming more seven-membered transition state rings with rapid reaction rate (analogously to six-membered transition state rings, Westbrook, 2000 [102]), which might then contribute to a higher oxidation rate of the ethyl esters at low temperature. Nevertheless, it is worth to notice that a reverse trend for the low temperature oxidation reactivity was concluded for ethyl hexanoate (EHX) and methyl heptanoate (MH) by Zhang and Boehman (2010) [54], likely due to the difference in length of the aliphatic main chain of the two esters. As a result, further investigations relating this subject seem to be still necessary in order to draw clearer conclusions, and to determine whether a critical length of aliphatic main chain actually exists from which ethyl esters start being more or less reactive than methyl esters depending of the low or high temperature regime. Concerning the lower oxidation reactivity of the unsaturated fatty acid esters in the low temperature regime, the authors attributed this feature to the reduction of the possible number of six- or seven-membered transition state rings that could be formed during the oxidation due to the presence of a double bond in the aliphatic main chain. Also, it was deduced from the observed products that the inhibition effect of the double bond on the low temperature oxidation reactivity of fatty acid esters became more pronounced as the double bond moved toward the central position of the aliphatic main chain. These trends were also observed by Herbinet et al. (2010) [53] for methyl-5- and methyl-9-decenoate.

Moreover, similarly to the work done by Zhang and Boehman (2010) [54] for EHX and MH oxidation, GC analysis of exhaust condensates collected under the engine conditions where only LTHR occurred also showed that the aliphatic main chain of the saturated fatty acid esters participated in typical paraffin-like low temperature oxidation sequences, with formation of the same classes of products as those observed for EHX and MH. In contrast, the unsaturated fatty acid methyl esters (MH2EN and MH3EN) were observed to exhibit olefin-like autoignition behavior (with the double bond in the aliphatic main chain being attacked by either hydroxyl or hydroperoxy radicals, eventually leading to the formation of either methyl esters with a terminal double bond and aldehydes or cyclic ethers, methyl esters, and hydroxyl radicals. For all test compounds, the ester functional group remained largely intact during the early stage of oxidation.

Also, the authors concluded from observed products for MN2EN and MN3EN oxidation that the presence and the position of the double bond in the aliphatic main chain of the fatty acid esters could affect the primary route for early CO₂ production. Indeed, for MN3EN it was suggested that early CO₂ production might mainly come from the direct decomposition of the methoxy carbonyl radical (CH₃OC[•]O) according to reaction pathway no. 4 in Table AI.3

(Herbinet et al., 2008 [50]). On the other hand, it was proposed that MN2EN might experience the production of the radical $\cdot\text{CH}_2(\text{CO})\text{OCH}_3$ which could then follow the reaction pathway illustrated by Figure AI.3 (Herbinet et al., 2008 [50]) to form CO_2 at low temperature. Finally, the authors observed that the extent of CO_2 production in the low temperature regime followed the order: $\text{EN} \approx \text{MN} > \text{MN2EN} > \text{MN3EN}$.

Table AI.4 Summary of the main experimental data generated for oxidation of $\text{C}_{n(n>4)}$ -alkyl esters selected as biodiesel surrogates.

Fuel	Equipment (Data type)	Temperature /K	Pressure /atm	Equivalence ratio ϕ (Fuel molar fraction %)	Reference
MHX	JSR (SP)	500 - 1100	10	0.5, 1, 1.5 (0.1)	Dayma et al. (2008) [82]
	RCM (ID)	650 - 850	3.9 - 19.7	1.0 (-)	HadjAli et al. (2009) [52]
MD	Variable CR octane rating (HRR vs. CAD and exhaust SP)	400 - 2000	CR range 4.0 - 13.75	0.25 - 2	Szybist et al. (2007) [83] [85]
	Flame (Counter flow extinction and ignition critical conditions)	900 - 1600	1	0.5 - 1.5 (-)	Seshadri et al. (2009) [89]
MP (nC10/MP)	JSR (SP)	500 - 1000	1	1 (0.002)	Hakka et al. (2009) [93]
MO (nC10/MO)	JSR (SP)	550 - 1100	1	1 (0.002)	Bax et al. (2010) [94]
RME	JSR (SP)	800 - 1400	1 - 10	0.25, 0.5, 1, 1.5 (0.05)	Dagaut et al. (2007) [86]
RME/kerosene (20/80 mol./mol.)	JSR (SP)	740 - 1200	1	0.5 - 1.5 (-)	Dagaut and Gail (2007) [97]
EN with: MN, MN2EN, and MN3EN for comparison	CFR motored engine (exhaust SP)	650 – 1850 (bulk cylinder gas temperature)	CR range 4.43 - 15	0.25 (-)	Zhang et al. (2009) [101]
EHX with MH for comparison	CFR motored engine (exhaust SP)	600 – 1650 (bulk cylinder gas temperature)	CR range 4.43 – 10.5	0.25 (-)	Zhang and Boehman (2010) [54]

Table AI.5 Summary of the main features related to the chemical kinetic models proposed for the oxidation of long alkyl esters selected as biodiesel surrogates

Fuel ^a	Model features		Software features			Model applicability conditions				Ref.	
	Nb. of reactions	Nb. of species	Thermochemical property estimation	Kinetic rate estimation ^b	Mechanism generator ^c	ChemKin module used	Low T (≈ 500 K)	High T (≈ 1300 K)	Low P (≈ 1 atm)		Moderate P (≈ 10 atm)
MHX	1875	435	Fisher et al. [55] + THERGAS [40]	N.C.H.	None	PSR	✓	✓	✓	✓	Dayma et al. (2008) [82]
MD	8820	3012	THERM [39]	N.C.H.	None	ICE [60] PSR AURORA	✓	✓	✓	✓	Herbinet et al. (2008) [50]
	713	125	Skeletal mechanism derived from Herbinet et al. (2008) [50] model			Flame Master	✓	✓	✓	-	Seshadri et al. (2009) [89]
	8820 + 105	3012 + 20	Herbinet et al. (2008) [50] + Smith et al. (1999) [92]			H CPR ^h HCCI ^h	✓	✓	-	✓	Hoffman and Abraham (2009) [90]
MD5EN	N.D. ^d	N.D. ^d	THERM [39] ^j	N.C.H.	None	PSR SENKIN	✓	✓	✓	✓	Herbinet et al. (2010) [53]
MD9EN	N.D. ^d	N.D. ^d	THERM [39] ^j	N.C.H.	None	PSR SENKIN	✓	✓	✓	✓	Herbinet et al. (2010) [53]
nC16 (RME)	1841	225	THERGAS [40]	N.C.H.	None	PSR	✓	✓	✓	✓	Ristori et al. (2001) [96] + Dagaut et al. (2007) [86]
MB+nC7+PME (RME)	1472	309	THERM [39]	N.C.H.	None	SENKIN	-	✓	-	✓	Golovitchev and Yang (2009) [98]
EB	1101	115	THERGAS [40]	KINGAS [42]	EXGAS [49]	SENKIN	-	-	✓	✓	Hakka et al. (2009) [61]

Chapter I Combustion kinetics of biodiesel (methyl and ethyl esters) – A review

^a See nomenclature for species names ^b N.C.H.: non-computer-helped method: the rate constants for the reverse reactions k_{reverse} were computed from the forward rate constants k_{forward} and the equilibrium constants K_c calculated using the appropriate thermochemical data according to $K_c = k_{\text{forward}}/k_{\text{reverse}}$. ^c No mechanism generator was used from developing the kinetic models which were instead built hierarchically. ^d N.D.: No details mentioned. ^e Model derived from Fisher et al. (2000) [55] proposal with some changes, but resulting number of reactions and species involved are not mentioned in the manuscript. ^f HCT was used instead of ChemKin. ^g NO formation (GRI-Mech 3.0 mechanism). ^h Homogeneous constant-pressure reactor model. ⁱ Homogeneous charge compression-ignition. ^j Herbinet et al. (2010) [53] also took the opportunity to mention openly that the activation energy for abstraction of secondary H-atoms by HO^{*} radicals needed to be corrected from $-3500 \text{ cal}\cdot\text{mol}^{-1}$ (as used in the initial version of MD oxidation model) to $-35 \text{ cal}\cdot\text{mol}^{-1}$.

CHAPTER II

**OXIDATION OF SMALL SATURATED AND
UNSATURATED ETHYL AND METHYL
ESTERS UNDER HIGH TEMPERATURE AND
MODERATE PRESSURE**

Chapter II

Oxidation of small saturated and unsaturated ethyl and methyl esters under high temperature and moderate pressure

This chapter has been the subject of two papers: (i) M. H. Hakka, H. Bennadji, J. Biet, M. Yahyaoui, B. Sirjean, V. Warth, L. Coniglio, O. Herbinet, P. A. Glaude, F. Billaud, F. Battin-Leclerc, « Oxidation of Methyl and Ethyl Butanoates », International Journal of Chemical Kinetics 2010, 42(4), 226-252; (ii) H. Bennadji, L. Coniglio, F. Billaud, R. Bounaceur, V. Warth, P. A. Glaude, F. Battin-Leclerc, « Oxidation of small unsaturated methyl and ethyl esters », submitted for publication in International Journal of Chemical kinetics. The work related to the experimental part of this study, together with part of the discussion of the models performance via reaction flux and sensitivity analyses have been carried out by the author, H. Bennadji of the PhD dissertation , whereas the model developments were achieved by J. Biet, R. Bounaceur, V. Warth, P. A. Glaude, and F. Battin-Leclerc.

Abstract

The ignition delay times were measured behind reflected shock waves for temperatures from 1280 to 1930 K, pressures from of 7 to 9.65 atm, fuel concentrations of 0.4, 0.5, and 1%, and equivalence ratios equal to 0.25, 1.0, and 2.0 in the cases of five esters: ethyl acrylate, methyl acrylate, ethyl crotonate, methyl crotonate, and ethyl butanoate. Ignition delay times were measured using chemiluminescence emission from OH^* at 306 nm and piezoelectric pressure measurements made at the shock tube sidewall. No important difference of reactivity was observed between methyl and ethyl unsaturated esters, methyl and ethyl crotonate having the same reactivity as methyl butanoate. The reactivity of acrylates is more important than that of crotonates especially at the lowest investigated temperatures. Detailed mechanisms for the combustion of the five studied esters have been automatically generated using the version of EXGAS software recently improved to take into account this class of oxygenated reactants. These mechanisms have been validated through satisfactory comparison of simulated and experimental results. The main reaction pathways have been derived from flow rate and sensitivity analyses.

Keywords: combustion, chemicals kinetics, biodiesel, ethyl esters, methyl esters, shock tube.

II.1 Introduction

Because of the reduced amount of petroleum components and its rising price, alternative fuels are intensively investigated for the full or partial replacement of the diesel fuel. Biodiesel is an alternative fuel made from renewable sources which can be used directly in a diesel engine without noticeably modifying the engine system or the fuel distribution infrastructure. Biodiesel can be produced from various feedstocks (vegetable oil, animal fat or waste cooking oil) using a chemical process called transesterification [1, 2, 3, 4]. Biodiesel has been the focus of a considerable amount of recent research because it is a renewable source of energy. The most important difference in composition between petro-diesel fuel and biodiesel is the oxygen content. Biodiesel contains 10 - 12 wt% oxygen, which lowers energy density and affects the fuel mutagenicity [5], as well as the formation of pollutants. The use of biodiesel in conventional diesel engines results in substantial reduction in unburned hydrocarbons, carbon monoxide, particulate matter emissions [6, 7] and smoke in exhaust gases, but also in an increase of NO_x formation [4, 5].

Biodiesel is composed of saturated and unsaturated methyl or ethyl esters containing carbon chains of twelve or more atoms in length [8, 9]. Because of this chemical structure, both the experimental and theoretical investigations of their oxidation are difficult. A first step before developing detailed kinetic models for the oxidation of real components of biodiesel requires to get a better understanding of the reactivity of the oxygenated part of these molecules by studying small chain methyl/ethyl esters. Small saturated esters, especially methyl butanoate have then been the subject of many experimental and theoretical studies [10-20]. While the major components of biodiesel are mono or multi-unsaturated esters (e.g. about 95 wt% in biodiesel deriving from rapeseed oil and about 85 wt% in that produced from soybean oil [9]), there are only very few kinetic studies concerning these molecules, which are also important products of the oxidation of saturated esters [12, 20]. The presence of unsaturations in esters has been shown to greatly influence ignition properties and to lower cetane number (e.g. cetane numbers are 101 for methyl stearate, deriving from octadecanoic acid, 59.3 for methyl oleate, the ester of similar structure but with one unsaturation, and 38.2 for methyl linoleate, which includes again the same number of atoms of carbon, but with two unsaturations [21]).

Chapter II Oxidation of small saturated and unsaturated ethyl and methyl esters at high temperature and moderate pressure

Very few studies have been performed on the oxidation of unsaturated esters. Sarathy et al. [22] performed a comparative experimental study of the oxidation of methyl crotonate (methyl butenoate) and of methyl butanoate. The experiments were carried out at atmospheric pressure in an opposed flow diffusion flame, with the fuel stream containing 4.7% fuel diluted in N₂ and the oxidizer stream including 42% O₂ and 58% N₂, and in a jet stirred reactor, at a residence time of 70 ms, over the temperature range 850-1350 K for a mixture of 0.075% fuel under stoichiometric conditions. Mole fraction profiles of major intermediates, final products and reactants were measured by gas chromatography. Sarathy et al. [22] concluded that both fuels have a similar reactivity, but that unsaturated esters would have a greater tendency to form soot than saturated esters. Recently, Gail et al. [23] completed the jet-stirred reactor measurements by studying mixtures with equivalence ratios of 0.375 and 0.75 under the same conditions. In addition, based on their mechanism for methyl butanoate [12], Gail et al. [23] have developed a detailed kinetic model for the oxidation of methyl crotonate. This model, which involves 301 species and 1516 reactions, reproduces well the experimental data obtained in a jet-stirred reactor. Concerning larger unsaturated methyl esters, a recent experimental study of the oxidation of a blend containing n-decane and methyl oleate has been studied in a jet stirred reactor over a range of temperature from 550 to 1100 K [24].

Since no study about the ignition of small unsaturated esters is available, the purpose of this chapter is to present experimental data about the ignition behind reflected shock wave of four small unsaturated esters: ethyl acrylate (C₅H₈O₂, M = 100 g/mol), methyl acrylate (C₄H₆O₂, M = 86 g/mol), ethyl crotonate (C₆H₁₀O₂, M = 114 g/mol), and methyl crotonate (C₅H₈O₂, M = 100 g/mol). In all these species, the double C=C bond is conjugated with the carbonyl group. Combined with results previously obtained on the ignition of ethyl and methyl butanoates under similar conditions [20], trends about the influence of the structure of the ester on its ignition properties have been derived. Note that the four unsaturated esters studied here are primary products of the oxidation of ethyl or methyl butanoate [20]. The chemical structures of the esters studied under shock tube conditions are presented in Figure II.1.

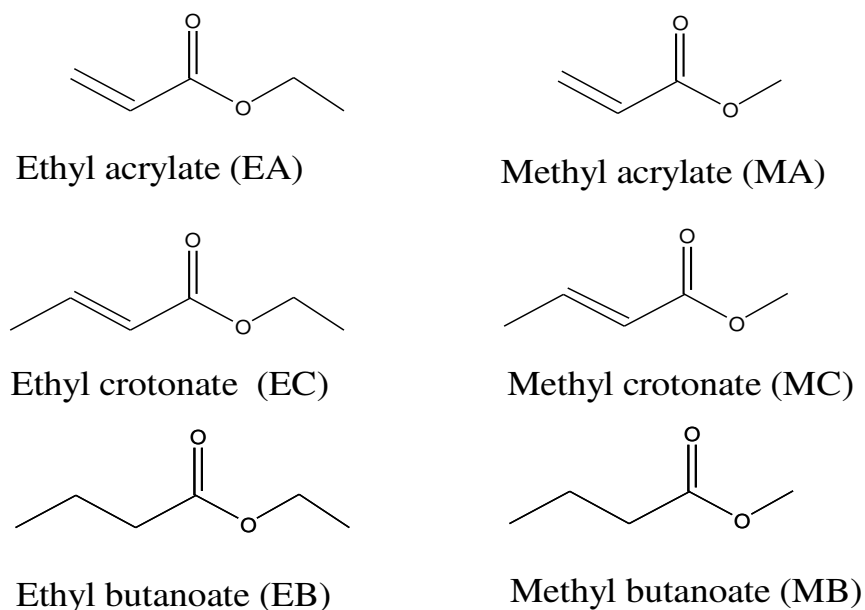


Figure II.1: Developed structure of ethyl and methyl esters included in this study.

II.2 Experimental procedure

As the method of measurement of ignition delay times in the used shock tube has been described in several papers [20, 25-27], the main features of this experimental device will just be recalled here. Autoignition delay times have been measured in a stainless steel shock tube made of two sections. The length of the high-pressure section is 90 cm with an internal diameter of 12.82 cm, and that of the low-pressure section is 400.6 cm with an internal diameter of 7.8 cm. The high and low-pressure sections are separated by an auxiliary chamber equipped with two terphane diaphragms (thickness of 7.5 μm) intended for bursting by decreasing the pressure of this chamber. The driver gas was helium. Incident and reflected shock velocities were calculated based on the measurements of four piezoelectric pressure transducers equally spaced (15 cm between each of them) and linearly spread over the last 50 cm of the reaction section. The pressure P_5 and temperature T_5 of the test gas behind the reflected shock wave were derived from the values of the initial pressure (P_1) in the low pressure section and of the incident shock velocity (V) by using ideal one-dimensional shock equations and thermodynamic parameters calculated using THERGAS software [28] which is based on Benson's group additivity method [29]. The error on the temperature was about 20 K.

The onset of ignition was detected by following hydroxyl radical emission at 306 nm. It is worth noting that the experimental OH^* emission at 306 nm is related to electronically excited OH^* concentration and is not directly proportional to OH radical concentration. Nevertheless,

Chapter II Oxidation of small saturated and unsaturated ethyl and methyl esters at high temperature and moderate pressure

previous work [25] has shown a correct agreement between the shapes of the profiles of experimental emission and calculated OH^* concentration during the rise of the signal, which is the part of the curve needed for determining autoignition delay times. Light emission from OH^* chemiluminescence was collected through a quartz window, located at the same place as the last pressure transducer, i.e. at 2 mm from the sidewall. The time resolution of the emission measurements is better than 2 μs . Both pressure and emission signals were transferred and registered by a digital card which consists of twelve acquisition ways mounted on computer. Research grade argon, helium, and oxygen specified to be 99.995% pure, were supplied by Messer and were used without further purification. Methyl and ethyl esters (>99% pure) were supplied by Sigma-Aldrich and were frozen and degassed a number of times before the mixtures were prepared. Fresh reaction mixtures were prepared every day using the method of partial pressures. Before each introduction of the reaction mixture, the reaction section was flushed with pure argon and evacuated, to ensure the residual gas to be mainly argon.

II.3 Experimental results

II.3.1 Auto-ignition times and empirical correlations

This study was performed under the following experimental conditions after the reflected shock wave allowing delay times from 5 up to 250 μs to be obtained:

- Temperature range from 1280 to 1930 K,
- Pressure ranging from 7.0 to 9.6 atm,
- Argon / ester / oxygen mixtures corresponding to three different equivalence ratios ($\varphi = 0.25, 1$ and 2) and to two different concentrations of esters (0.5 and 1%). For each ethyl ester, a supplementary concentration has been studied to allow the comparison with its counterpart methyl ester for the same mole fraction of carbon atoms under stoichiometric conditions.

Figure II.2 presents the record of the signal of the last pressure transducer and of the excited OH^* emission for a typical experiment in the case of methyl crotonate. The pressure profile displayed three rises, which were due to the incident shock wave, pointed as 1, the reflected shock wave pointed as 2, and ignition. This last pressure rise is too weak to be used for determining the delay time, while the rise of OH^* emission, pointed as 3, is much steeper and allows the delay time to be known with a precision better than 10 %. The ignition delay time (τ) is given by the time interval between the pressure rise measured by the last pressure

Chapter II Oxidation of small saturated and unsaturated ethyl and methyl esters at high temperature and moderate pressure

transducer due to the arrival of the reflected shock wave and the rise of the optical signal by the photomultiplier up to 50% of its maximum value as shown in Figure II.2.

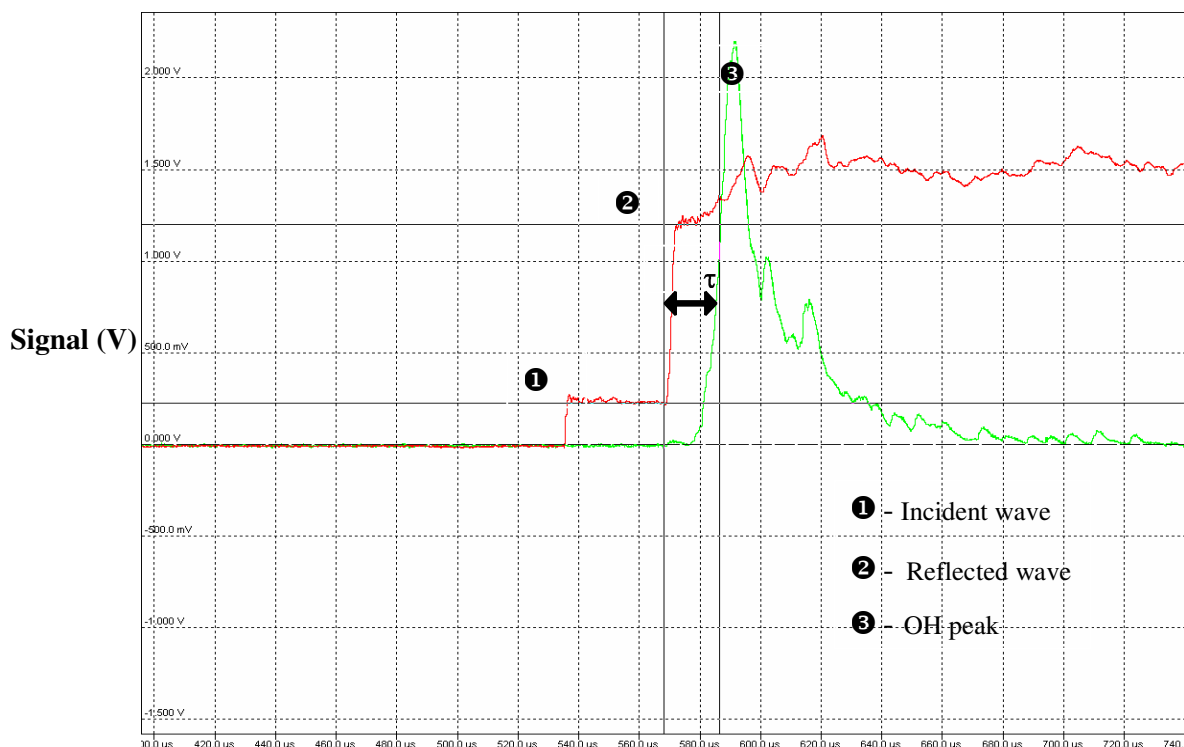


Figure II.2: Typical experimental profiles of pressure and OH* emission obtained from an experiment at $\phi = 1$ and mixture of 0.5% methyl crotonate, 3% O₂ and 96.5% Ar.

The tables AII.1 to AII.5 in appendix AII present the complete set of experimental conditions and measurements performed in this study for ethyl acrylate, methyl acrylate, ethyl crotonate, methyl crotonate, and ethyl butanoate respectively. We consider that the range of ignition delay times that can be measured in this shock tube while maintaining ideal conditions (adiabatic for long ignition delay times and reasonable uncertainties for short ignition delay times) is between 10 and 1500 μs . Beside, we present here a few points with ignition delay times shorter than 10 μs and then with a larger uncertainty.

Figures II.3 to II.7 present the experimental results obtained for the ignition of ethyl acrylate, methyl acrylate, ethyl crotonate, methyl crotonate, and ethyl butanoate respectively. Figures II.3a-II.7a correspond to mixtures containing 0.5 % of ester, for three equivalent ratios. Figures II.3b-II.7b display the experimental results obtained for different ester concentrations with a constant equivalence ratio of 1. On the whole, the results show that in each case, ignition delay times increase when equivalence ratio increases (by decreasing O₂ concentration

Chapter II Oxidation of small saturated and unsaturated ethyl and methyl esters at high temperature and moderate pressure

at constant ester content) and decrease when dilution decreases (by decreasing Ar concentration at constant ratio of percent content in fuel and O₂).

For organic compound / oxygen / argon mixtures, the determination of power dependences is often proposed from the overall statistical correlation between τ and the gas concentrations:

$$\tau = A \times \exp(E/RT) \times [OC]^a \times [O_2]^b \times [Ar]^c \quad (\text{eq.II.1})$$

where A is the pre-exponential factor, E the apparent “activation energy”, R the gas constant and OC designates the organic compound [30]. For a restricted range of pressure and temperature, a, b and c are usually constant. Such a statistical correlation has been derived from the present experiments, but since the mole fraction of argon had limited variations under the different initial conditions (from 84.5 to 98.375%) and seems not to affect the delay times, it was chosen to keep $c = 0$.

A multi-linear regression gave the parameters summarized in Table II.1. All these statistical correlations show a strong negative O₂ power dependence, while the fuel power dependence is small.

Table II.1: Summary of the parameters used in the correlations found under the form:

$$\tau = A \times \exp(E/RT) [ester]^a \times [O_2]^b$$

Ester	Parameters			
	A	E	a	b
Ethyl acrylate	2.26×10^{-15}	35.0	0.219	-1.120
Methyl acrylate	3.85×10^{-25}	69.0	-0.337	-1.326
Ethyl crotonate	2.64×10^{-22}	47.4	-0.550	-1.122
Methyl crotonate	7.09×10^{-19}	46.2	-0.034	-1.220
Ethyl butanoate*	1.88×10^{-20}	57.5	0.250	-1.520
Methyl butanoate*	2.54×10^{-20}	55.6	0.140	-1.450

Notes: Concentrations are in mol/cm³, τ in s, T in K, the activation energy (E) in kcal/mol, and R is the universal gas constant in kcal/mol/K. * the parameters are taken from reference [20].

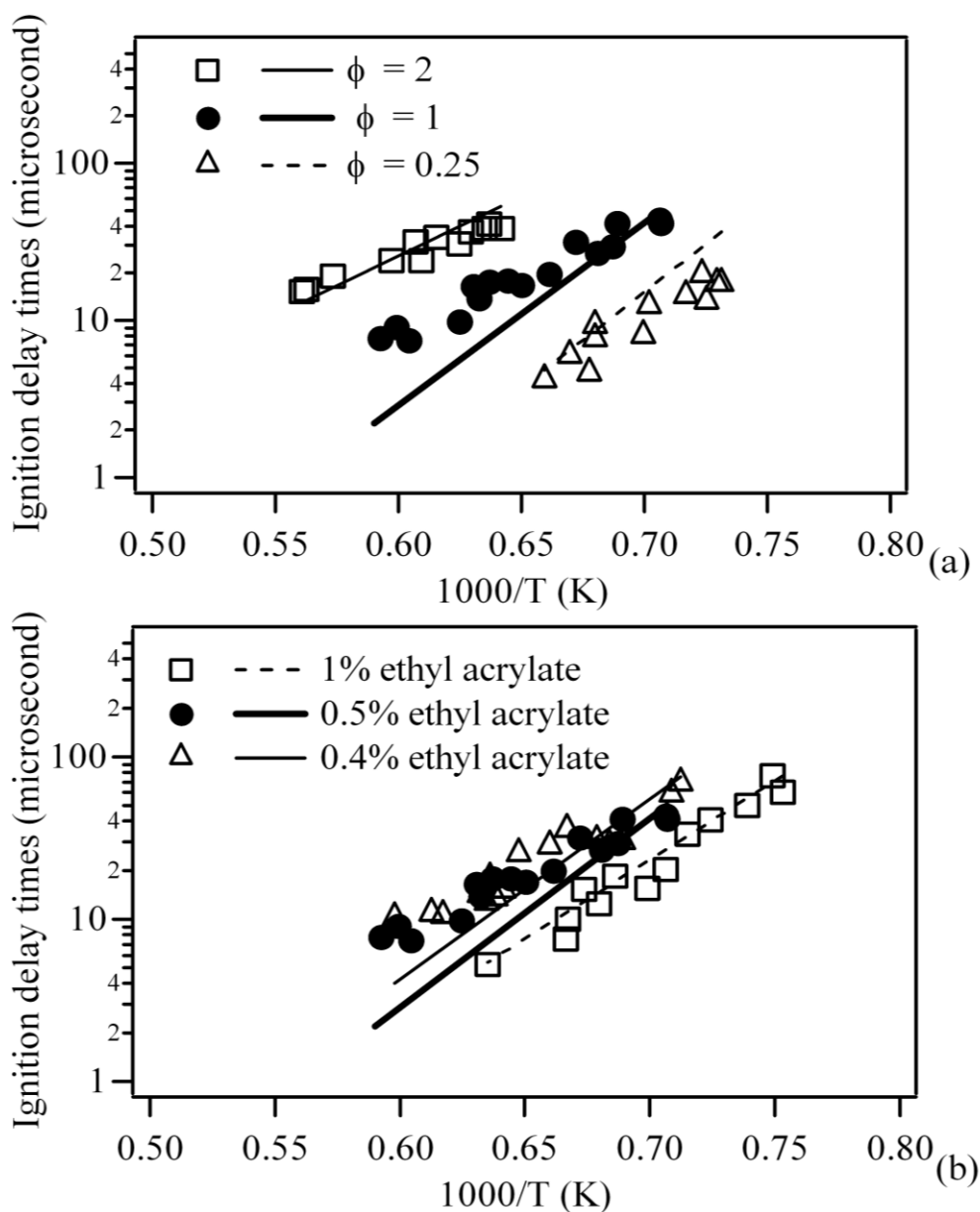


Figure II.3: Ignition delay times of ethyl acrylate in a shock tube for (a) equivalence ratios of 0.25, 1 and 2 and a concentration of ester of 0.5 % and (b) an equivalence ratio of 1 and concentrations of ester of 0.4, 0.5 and 1%. Points correspond to experimental results and lines to simulations.

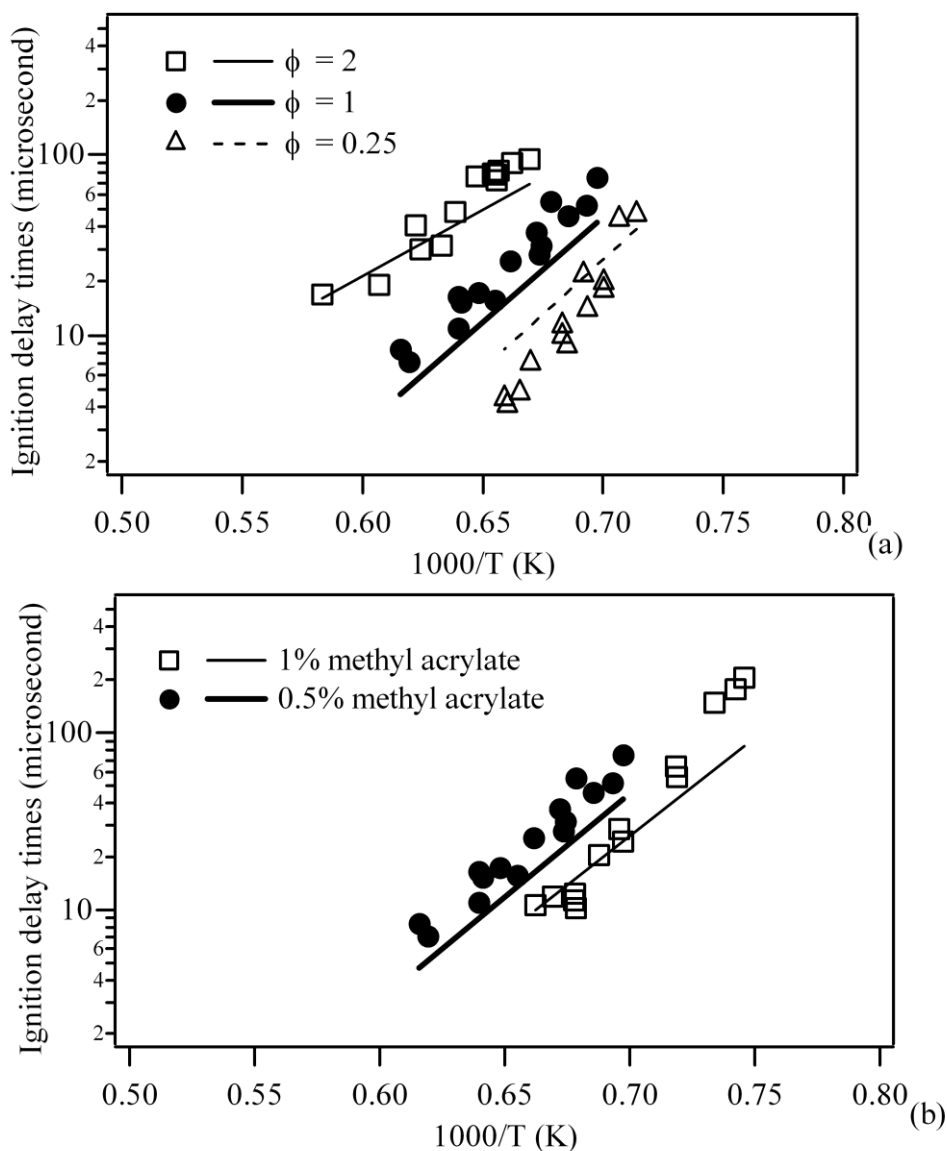


Figure II.4: Ignition delay times of methyl acrylate in a shock tube for (a) equivalence ratios of 0.25, 1 and 2 and a concentration of ester of 0.5 % and (b) an equivalence ratio of 1 and concentrations of ester of 0.5 and 1%. Points correspond to experimental results and lines to simulations.

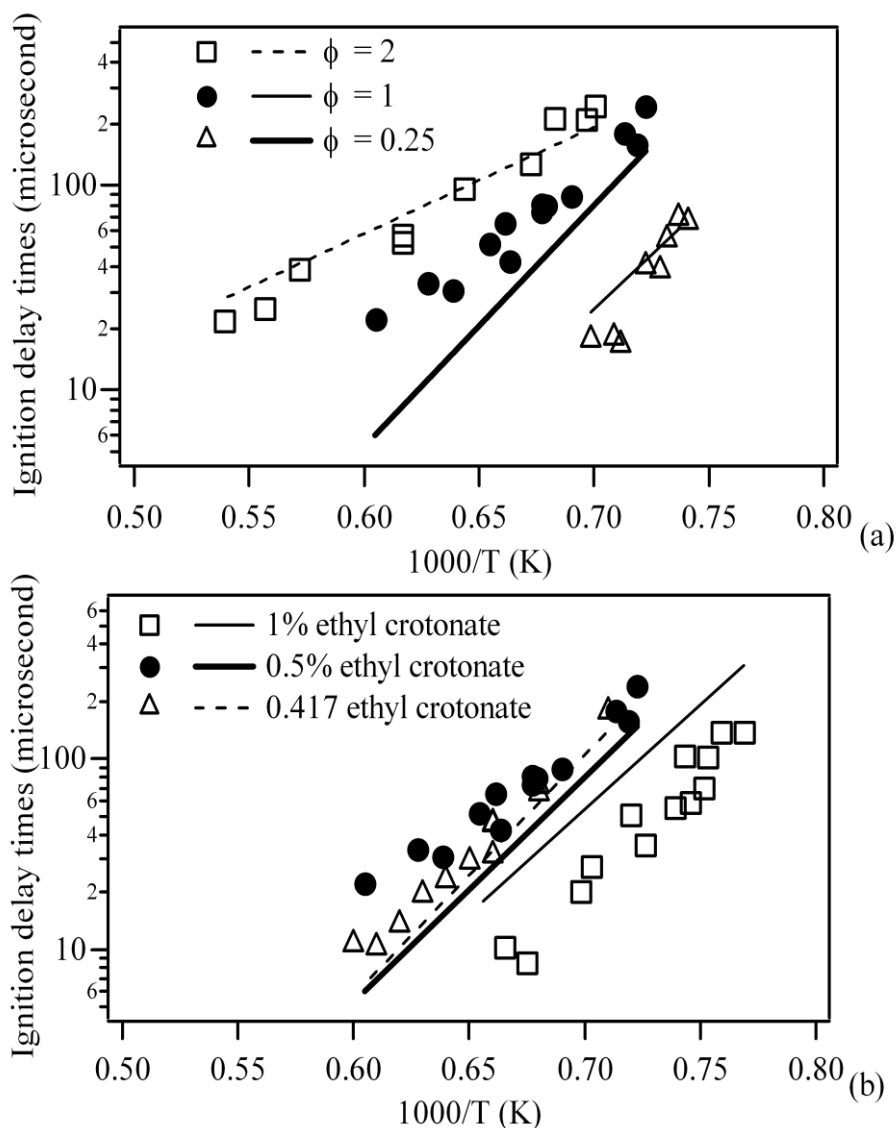


Figure II.5: Ignition delay times of ethyl crotonate in a shock tube for (a) equivalence ratios of 0.25, 1 and 2 and a concentration of ester of 0.5 % and (b) an equivalence ratio of 1 and concentrations of ester of 0.417, 0.5 and 1%. Points correspond to experimental results and lines to simulations.

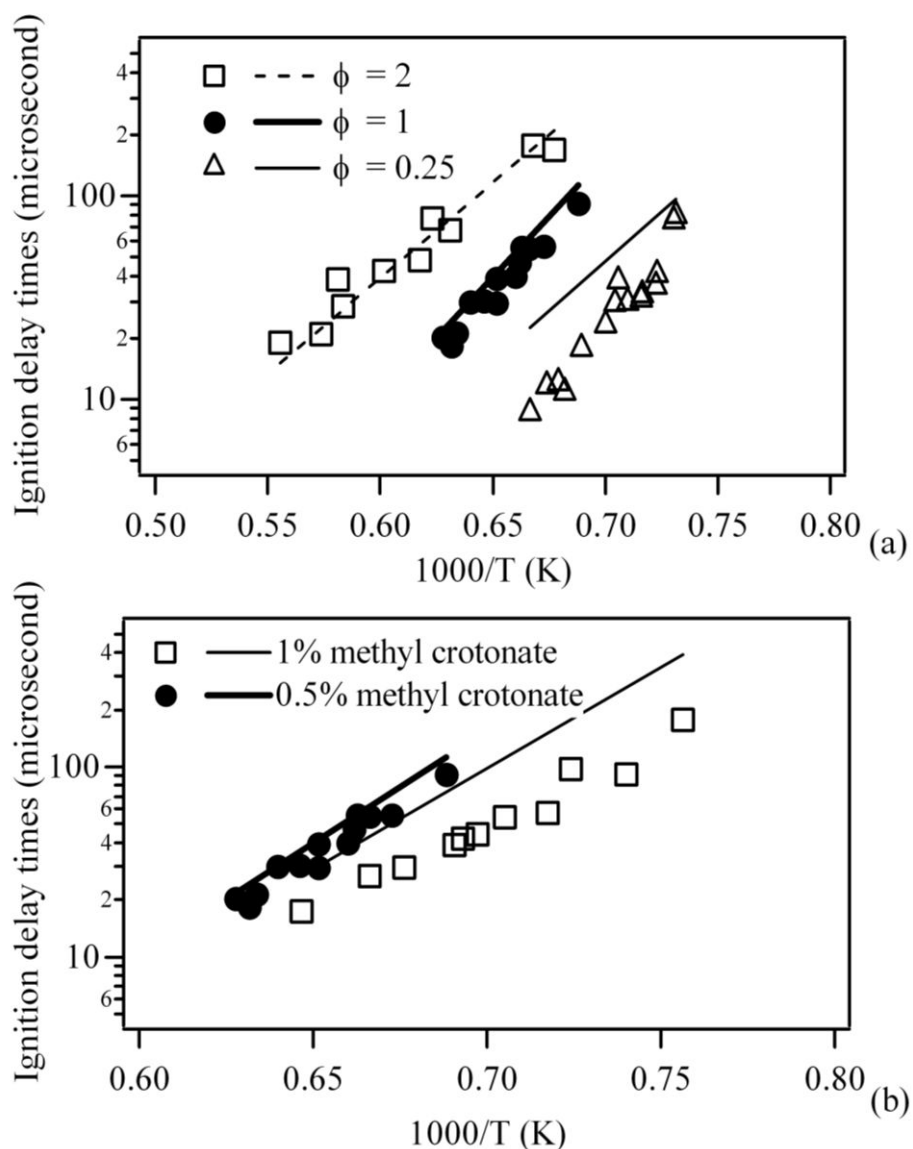


Figure II.6: ignition delay times of methyl crotonate in a shock tube for (a) equivalence ratios of 0.25, 1 and 2 and a concentration of ester of 0.5 % and (b) an equivalence ratio of 1 and concentrations of ester of 0.5 and 1%. Points correspond to experimental results and lines to simulations.

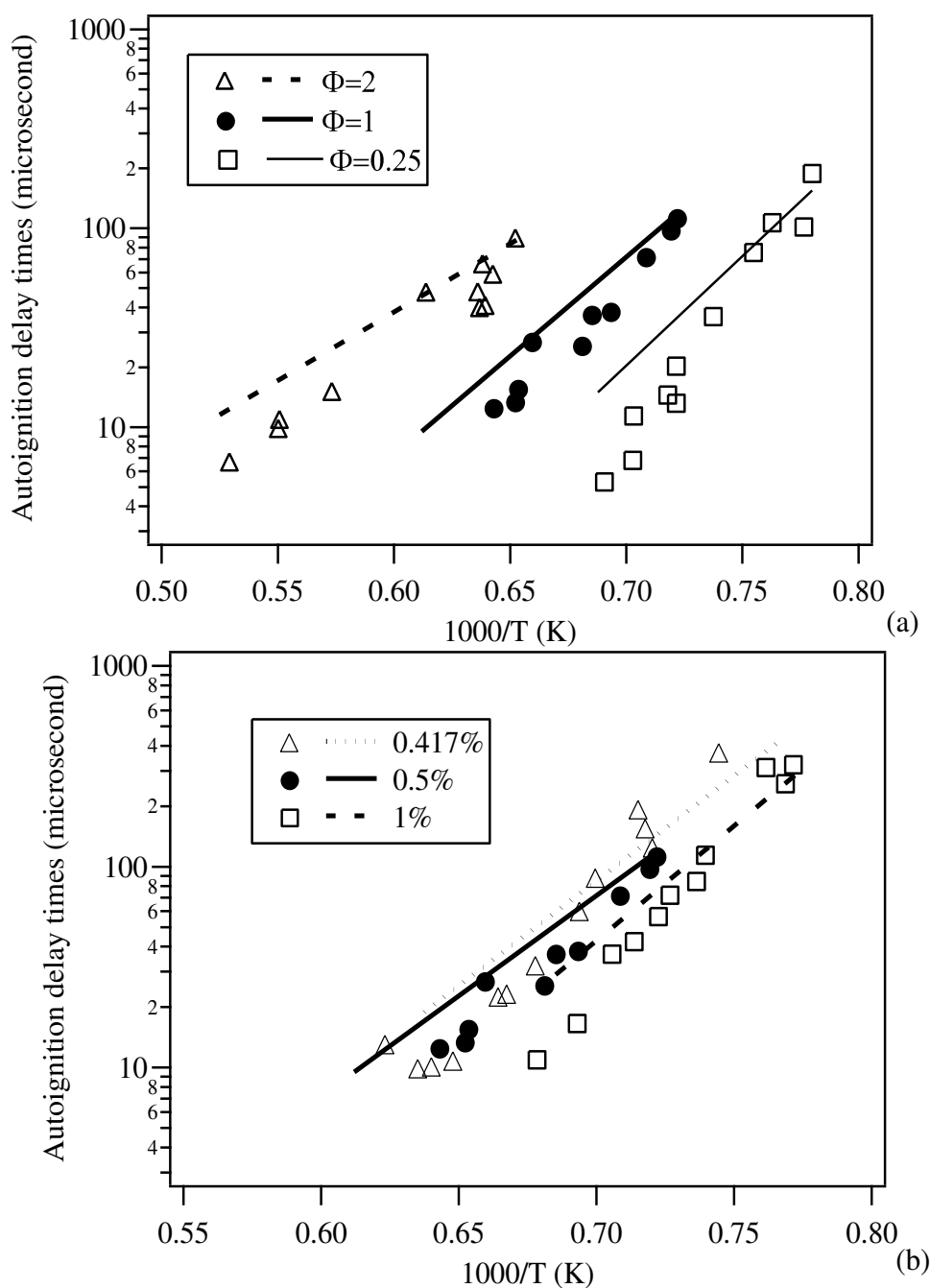


Figure II.7: Ignition delay times of ethyl butanoate in a shock tube for (a) equivalence ratios of 0.25, 1 and 2 and a concentration of ester of 0.5 % and (b) an equivalence ratio of 1 and concentrations of ester of 0.417%, 0.5%, and 1%. Points correspond to experimental results and lines to simulations.

II.3.2 Comparison between methyl and ethyl esters

Based on the previous results obtained under similar conditions for ethyl and methyl saturated C₄ esters [20], Figure II.8 presents a series of comparison of the reactivity of ethyl and methyl acrylates, butanoates and crotonates for an equivalence ratio of 1 and a concentration of ester equal to 0.5% for methyl ester. However, in order to obtain a direct comparison between similar compounds with the same concentration of carbon atoms and the same C/O ratio, a concentration 0.4% has been shown for ethyl acrylate and of 0.417 for ethyl crotonate and butanoate. Figures II.8a and II.8b indicate that, under the conditions of this study, in the case of unsaturated C₃ and C₄ esters, there is no important difference of reactivity between ethyl and methyl compounds. That differs to what is obtained for C₄ saturated esters, for which ethyl butanoate is more reactive than methyl butanoate, especially at high temperature (see Figure II.8b). Note, however, the difference of slope obtained for ethyl and methyl acrylates, for which the apparent “activation energies” given in Table II.1 differ noticeably. In addition, Figure II.8b shows that ethyl and methyl crotonates have the same reactivity as methyl butanoate. That is in agreement with the results obtained by Sarathy et al. [22] in a jet-stirred reactor, since these authors observed the same reactivity for methyl butanoate and methyl crotonate. As shown in Figure II.8b, ethyl butanoate is the only one, amongst methyl and ethyl C₄ esters, which has a different reactivity since it leads to lower ignition delay times at the highest temperatures. Figure II.8c shows that ethyl acrylate is more reactive than methyl crotonate, and consequently than methyl butanoate, i.e. below 1500 K the ignition delay times of ethyl acrylate are shorter by more than a factor 2 compared to those of methyl crotonate. That is in agreement with the large difference of apparent “activation energy” between these two compounds displayed in Table II.1. The results obtained by Metcalfe et al. [13] concerning the ignition of methyl butanoate and ethyl propanoate also show the ethyl ester to be considerably more reactive at low temperature. These authors explain this difference of reactivity by the fact that the formation of ethylene and propanoic acid through the molecular reaction of ethyl ester increases the reactivity.

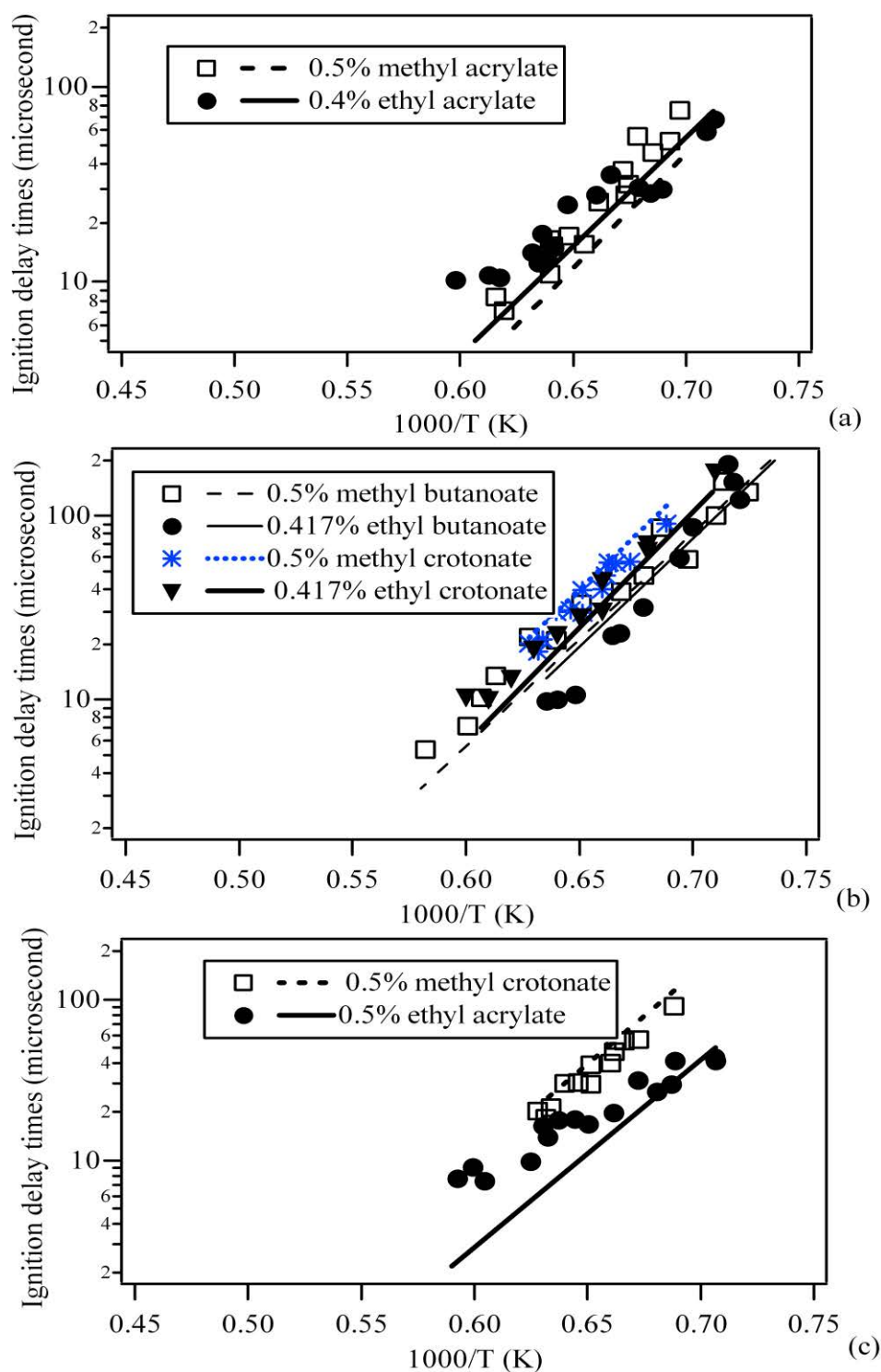


Figure II.8: Comparison between experimental autoignition delay times obtained for an equivalence ratio of 1 with (a) methyl and ethyl acrylates (0.5 % of methyl ester, 0.4% of ethyl esters), (b) with methyl and ethyl butanoates and methyl and ethyl crotonates (0.5 % of methyl ester, 0.417% of ethyl esters) and (c) with methyl crotonate and ethyl acrylate (0.5% of both esters).

II.4 Kinetic models

The detailed chemical kinetic reaction mechanisms presented here have been developed using the version of EXGAS software recently improved to take into account methyl and ethyl esters [20]. As the use of EXGAS to model the oxidation of alkanes [31-33] and alkenes [34, 35], as well as saturated esters [20] has already been extensively described, we will recall here only its main features. However the reactions and rate constants specific to the unsaturated esters studied here are more detailed. Concerning ethyl butanoate, its detailed mechanism of oxidation will be described exhaustively further in chapter III.

The EXGAS system provides reaction mechanisms made of three parts which are used together:

➤ **A comprehensive primary mechanism**, in which the only molecular reactants considered are the initial organic compounds and oxygen. For modeling results obtained above 1000 K, the mechanism can only include high temperature reactions, which are in the case of unsaturated esters:

- Molecular reactions

As shown in the case of ethyl butanoate [20], the main specificity of ethyl esters compared to methyl ones is the inclusion of the molecular elimination leading to the formation of ethylene and carboxylic acids and of the secondary reactions of these oxygenated species, for which new rules of generation have to be considered.

- Unimolecular initiations

The reactions involving the breaking of a C-C bond have been considered, as well as those involving the breaking of a C-H bond and leading to the formation of resonance stabilized radicals, e.g. in the case of crotonates. In further reactions of resonance stabilized radicals, both mesomer forms have been taken into account.

- Bimolecular initiations with oxygen to produce alkenyl and HO₂ radicals.
- Additions of H-atoms and OH radicals to the double bond.

Reactions are possible on both side of the double bond. The additions of H-atoms lead to alkyl radicals. In the case of the additions OH radicals, the formation of a stabilized adduct is not considered, but the formation of decomposition products is written. Kinetic data are those used by Touchard et al. [34] for 1-pentene.

- Isomerizations of alkyl and alkenyl radicals involving a cyclic transition state and the transfer of an H-atom.

Chapter II Oxidation of small saturated and unsaturated ethyl and methyl esters at high temperature and moderate pressure

According to the work of Bounaceur et al. [35], the isomerizations of alkenyl radicals involving a transition state including a double bond in the cycle were not considered.

- Decompositions of radicals by β -scission involving the breaking of C-C, C-O or C-H bonds for all types of radicals.

In agreement with recent values of the literature for the decomposition of alkyl radicals [36], the value of the activation energy for a C-H scission of alkylic radicals in the primary mechanism has been reduced by 2 kcal/mol compared to the values given by EXGAS [32]. The presence of oxygen atoms in the involved radicals can have a significant impact on the values of the activation energies of the decomposition by β -scission. We have then used here the value calculated for saturated esters using quantum calculations as given in below Table II.2 [20].

Table II.2: activation energies used for the decompositions by β -scission of oxygenated radicals involved in the oxidation of methyl and ethyl esters [20]

Types of reaction	E_a (Kcal/mol)
$R/C(//O)/O^\bullet \rightarrow R^\bullet + CO_2^a$	5.1
$R/C(//O)/O/CH_2^\bullet \rightarrow R/C^\bullet/O + CH_2//O^a$	31.9
$R/CH^\bullet/C(//O)/O/CH_3 \rightarrow R/CH//C/O + CH_3O^{\bullet b, c}$	49.0
$R/CH^\bullet/CH_2/C(//O)/O/CH_3 \rightarrow R/CH//CH_2 + CH_3O/C^\bullet/O^{\bullet b, c}$	30.7
$R/CH_2/C^\bullet/O \rightarrow R^\bullet + CH_2//C/O^d$	39.9
$R/CH^\bullet/CH_2/C(//O)/O/CH_3 \rightarrow H^\bullet + R/CH//CH/C(//O)/O/CH_3^{\bullet b, c}$	34.9
$R/C(//O)/O/CH_2/CH_2^\bullet \rightarrow R/C//O/O^\bullet + C_2H_4^a$	25.1

Notes: ^a the calculation has been performed for $R^\bullet = CH_3^\bullet$, ^b for $R^\bullet = H^\bullet$, ^c the same value is used in the case of ethyl esters, and ^d the calculation has been performed for $R^\bullet = C_2H_5^\bullet$.

- Oxidations of alkyl and alkenyl radicals with O_2 .

These reactions lead to the formation of hydroperoxy radicals and, alkenes and dienes, respectively.

- Metatheses between radicals and the initial reactants (H-abstractions).

For all the reaction involving the abstractions of an H-atom (bimolecular initiations, isomerizations and metatheses), those involving an H-atom bound to an atom of carbon included in a double bond have not been written.

Chapter II Oxidation of small saturated and unsaturated ethyl and methyl esters at high temperature and moderate pressure

- Combinations of resonance stabilized radicals with small radicals.
- **A lumped secondary mechanism**, containing reactions consuming the molecular products of the primary mechanism which do not react in the reaction bases. In order to have a manageable size, the lumped secondary mechanisms [31] involved lumped reactants: the molecules formed in the primary mechanism, with the same molecular formula and the same functional groups, are lumped into one unique species without distinction between the different isomers. To avoid a too important formation of allyl radicals with a strong inhibiting behavior, the values of the rate constants of the metatheses on unsaturated carboxylic acids have been divided by a factor of 10, compared to what was used for saturated acid [20].
- **A C₀-C₂ reaction base**, including all the reactions involving radicals or molecules containing less than three carbon atoms. As this part of the mechanism concerns small species, pressure-dependent rate constants follow the formalism proposed by Troe [37] and efficiency coefficients have been included, which is not the case in the primary and secondary mechanisms.

Thermochemical data for molecules or radicals are automatically computed using software THERGAS [28] based on group additivity [29], and stored as 14 polynomial coefficients, according to the CHEMKIN II formalism [380].

The kinetic data of isomerizations, recombinations and the unimolecular decompositions are calculated using software KINGAS [31], based on the thermochemical kinetic methods [29] using the transition state theory or the modified collision theory. The kinetic data, for which the calculation is not possible by KINGAS, are estimated from correlations, which are based on quantitative structure-reactivity relationships and obtained from a literature review [20, 32 and 34].

II.5 Discussion

II.5.1 Computational simulation

Simulations were performed with SENKIN software of CHEMKIN II [38] by using the mechanisms previously described. The mechanism for the oxidation of ethyl acrylate (C₅H₈O₂) involves 111 species and globally contains 885 reactions, the mechanism for the oxidation of methyl acrylate (C₄H₆O₂) involves 103 species and globally contains 826 reactions, the mechanism for the oxidation of ethyl crotonate (C₆H₁₀O₂) involves 128 species and globally contains 954 reactions, the mechanism for the oxidation of methyl crotonate (C₅H₈O₂) involves

Chapter II Oxidation of small saturated and unsaturated ethyl and methyl esters at high temperature and moderate pressure

119 species and globally contains 885 reactions, and the mechanism for the oxidation of ethyl butanoate ($C_6H_{12}O_2$) involves 117 species and globally includes 1035 reactions. The conditions behind the reflected shock waves have been assumed to be those in a homogeneous adiabatic reactor at constant volume. Simulated ignition delay times have been defined as the time at 10 % of the maximum concentration of excited OH^* radicals using the mechanism for excited species developed by Hall et al. [39].

Figures II.3 to II.7 show the agreement between experimental and simulated ignition delay times for the four unsaturated esters and ethyl butanoate. This agreement is fairly good, with differences between prediction and experiment of at most a factor of three, but for many of the conditions the simulations fall within the $\pm 20\%$ uncertainty in measurements. Particularly important deviations are encountered for stoichiometric mixtures containing 1% methyl or ethyl crotonate.

Figure II.8 shows that these mechanisms are able to reproduce the similarities and differences in reactivity experimentally observed between the studied compounds. Simulations show well the higher reactivity of ethyl acrylate compared to methyl crotonate.

II.5.2 Reaction flux analysis

Figures II.9 to II.13 display a flow rate analysis performed for the four unsaturated esters and ethyl butanoate for 50% of fuel conversion at a temperature around 1400 K (1370 K for ethyl butanoate and 1440 K for the four other compounds) at pressure around 8 bar, for an equivalence ratio of 1 and a 0.5% initial ester concentration.

- Under the conditions of Figure II.9 ($T=1370$ K, $\phi=1$), *the main consumption pathway of ethyl butanoate* is the molecular reaction to give ethylene and butanoic acid, which is the major C_{2+} oxygenated product obtained. Due to the low activation energy barrier of 47.29 kcal/mol, this elimination reaction accounts for approximately 75% of the fuel consumption. However, the importance of this channel decreases when temperature increases, e.g., it accounts for only 40% of the ester consumption $T = 1635$ K still at $\phi = 1$ and at 50% ester conversion. Nevertheless, it slightly increases when equivalence ratio increases, as it represents 78% of the ester consumption at $\phi = 2$ and $T = 1370$ K at 50% ester conversion. It can be seen clearly in Figure (II.10a) that all of the fuel has disappeared ($\approx 60 \mu s$) long before the ignition event takes place ($160 \mu s$), with ethylene and butanoic acid effectively behaving as the fuel.

Chapter II Oxidation of small saturated and unsaturated ethyl and methyl esters at high temperature and moderate pressure

In addition, minor channels involve H-abstractions (22% of the ester consumption) by H-atoms and hydroxyl radicals to give mainly R_{EB-1} radicals and unimolecular decomposition (3% of the ester consumption). R_{EB-1} radicals mainly isomerise to produce radicals that decompose to ethylene and radicals that in turn decompose to carbon dioxide and propyl radicals. These last radicals yield ethylene and methyl radicals. A small part of R_{EB-1} radicals directly decomposes to give methyl radicals and *ethyl acrylate*, the second main C_{2+} -oxygenated product obtained from ethyl butanoate.

Butanoic acid is mainly consumed by H-abstractions (56% of its consumption) and yields mainly R_{EB-2} radicals and to a lower extent R_{EB-3} , R_{EB-4} , and R_{EB-5} radicals. R_{EB-2} radicals are decomposed to give methyl radicals and *acrylic acid*, another very minor C_{2+} -oxygenated product obtained from ethyl butanoate. R_{EB-3} radicals decompose to produce carbon dioxide and propyl radicals, a source of ethylene and methyl radicals. The decomposition of R_{EB-4} radicals leads to propene and radicals, the decomposition of which gives carbon monoxide and hydroxyl radicals, $\cdot OH$. Finally, the breaking of a C-C bond in R_{EB-5} radicals produces ethylene and radicals, the decomposition of which yields carbon dioxide and methyl radicals.

Unimolecular initiations, which lead to ethyl radicals, a source of H-atoms, and radicals the decomposition of which produces methyl radical and carbon dioxide, are responsible for 32% of the consumption of butanoic acid. The unimolecular initiation yielding ethyl radicals is made easier in the acid due to lower activation energy, 78.9 kcal/mol, compared to those for the ethyl ester, 81.2 kcal/mol, and also to a larger A-factor in the case of the acid.

The fact that about 24% ($75\% \times 32\%$) of the consumption of ethyl butanoate leads to unimolecular initiations involving the production of branching agents, H-atoms, (while it is only the case for 15% from methyl butanoate in identical conditions [20]) might explain the higher reactivity observed for the ethyl butanoate (Figure II.8b).

- Under the conditions of Figure II.10, *methyl acrylate* reacts mainly by addition of H-atoms (48% of the ester consumption) which produces R_{MA-1} and R_{MA-2} radicals. R_{MA-1} radicals are a source of ethylene and of radicals the decomposition of which yields carbon dioxide and methyl radicals. As R_{MA-2} radicals cannot easily decompose (the breaking of a C-H bond has an activation energy of 39 kcal/mol and that of a C-C bond leading to CH_3O radicals has an activation energy of 49 kcal/mol), its main reaction is by isomerization with an activation energy of 17.8 kcal/mol. The decomposition of the obtained radicals yields

Chapter II Oxidation of small saturated and unsaturated ethyl and methyl esters at high temperature and moderate pressure

formaldehyde and radicals which can easily break down to give carbon monoxide and ethyl radicals, a source of ethylene and H-atoms. The addition of OH radicals (10% of the ester consumption) produces formaldehyde and radicals, which can decompose to give again formaldehyde and CH₃CO radicals or a C₂ methyl ester with an aldehyde function and methyl radicals. The second important channel consuming methyl acrylate is the H-abstractions by hydrogen atoms and hydroxyl radicals to give R_{MA-4} radicals (35% of the ester consumption). The decomposition of R_{MA-4} radicals yields formaldehyde and radicals which can easily break down to give carbon monoxide and vinyl radicals, a source of acetylene and H-atoms. Unimolecular initiations are the least important channel (7% of the ester consumption) and produce methyl radicals and radicals, which can decompose to give carbon dioxide and vinyl radicals.

- Figure II.11 shows that the reaction pathways are very similar for ethyl acrylate. Note however that 20% of this ethyl ester is consumed to give ethylene and acrylic acid and that the importance of metatheses is larger due to more H-atoms available. In this case, initiation reactions are also a source of H-atoms.

- The relative importance of the ways of consumption differs more in the case of methyl crotonate. Under the conditions of figure II.12, *methyl crotonate* is mainly consumed by H-abstractions by hydrogen atoms and hydroxyl radicals, which accounts for globally 63% of the ester consumption. Two types of radicals can be thus produced, R_{MC-1} radicals, which are resonance stabilized and then the most abundantly formed and R_{MC-2} radicals. A mesomer form of R_{MC-1} radicals can isomerize to produce radicals which can easily decompose to produce formaldehyde and radicals, the decomposition of which leads to carbon monoxide and allyl radicals (C₃H₅). The combination of allyl radicals with HO₂ radicals yields acrolein, OH radicals and H-atoms. The decomposition of R_{MC-2} radicals leads to formaldehyde and radicals which can easily break down to give carbon monoxide, acetylene, and methyl radicals.

Another important channel consuming methyl crotonate is the addition of H-atoms (26% of the ester consumption) which produces R_{MC-3} and R_{MC-4} radicals. The decomposition of R_{MC-3} radicals leads to *methyl acrylate* and methyl radicals, that of R_{MC-4} radicals is a source of propene and of radicals which can easily break down to give carbon dioxide and methyl radicals. Another type of addition is also noticeable, the addition of OH radicals (8% of the ester consumption) which produces acetaldehyde and radicals, which can decompose to give formaldehyde and CH₃CO radicals, or a C₂ methyl ester with an aldehyde function and ethyl radicals. Ethyl radicals are a source of ethylene and H-atoms. Finally, the

Chapter II Oxidation of small saturated and unsaturated ethyl and methyl esters at high temperature and moderate pressure

last channel to be considered is unimolecular initiations (3% of the ester consumption) to give acetylene, methyl radicals and radicals, which can decompose to give carbon dioxide and methyl radicals.

- The lower reactivity of crotonates compared to acrylates, which leads to a lower global radicals concentration, explains the much larger importance of molecular reactions in the case of ethyl crotonate (see Figure II.13) than for ethyl acrylate. 45% of ethyl crotonate is consumed to give ethylene and crotonic acid and additions of H-atoms only account for 8% of this reactant. Like for methyl crotonate, initiation reactions from ethyl crotonate are also a source of methyl radicals.

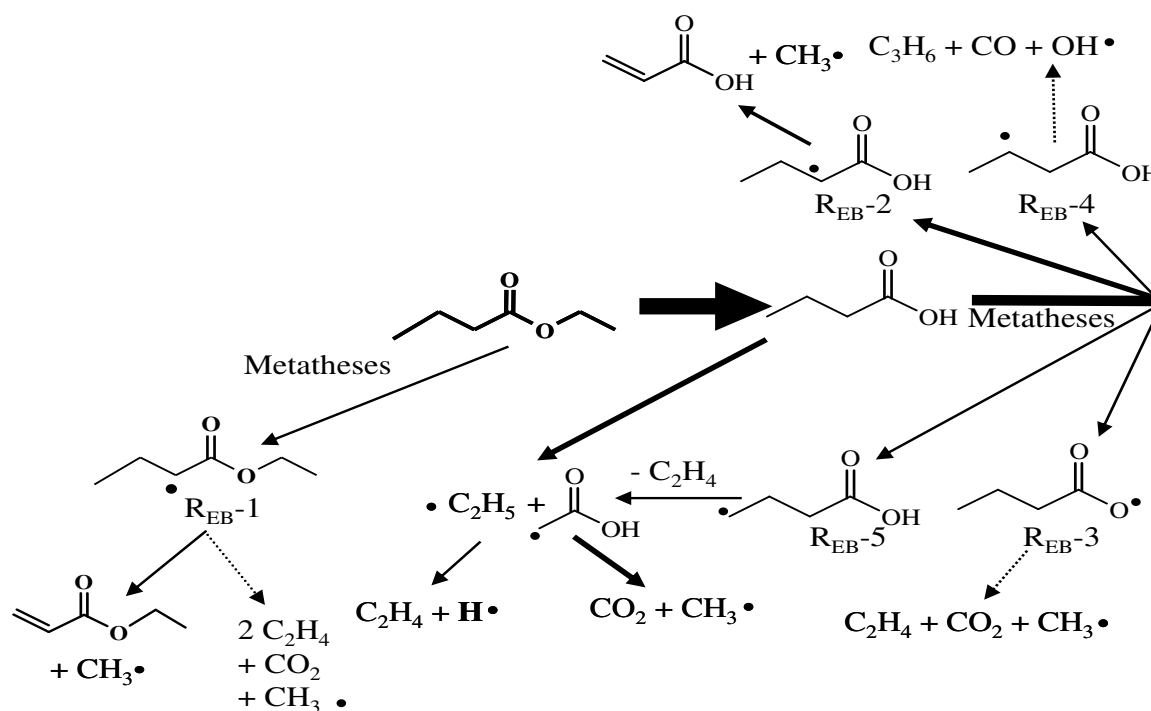


Figure II.9: Flow rate analysis for ethyl butanoate oxidation performed at 1370K for 50% conversion of ester, an equivalence ratio of 1 and 0.5% initial ester concentration. The size of the arrows is proportional to the relative flow rate. The channels involving a consumption of the esters below 5% are not shown. Broken arrows represent several successive elementary reactions.

Chapter II Oxidation of small saturated and unsaturated ethyl and methyl esters at high temperature and moderate pressure

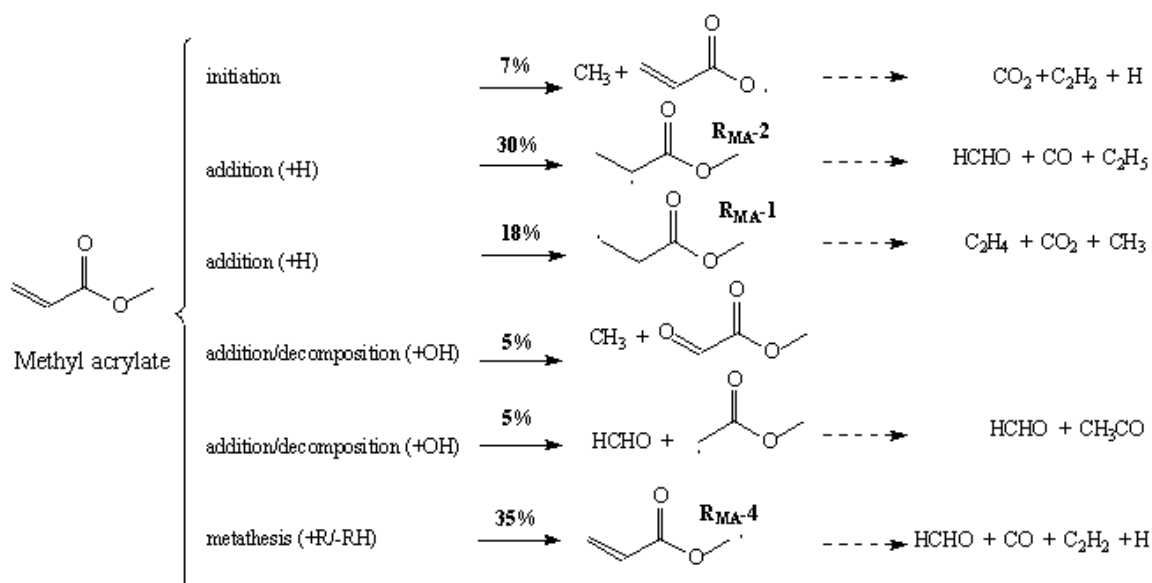


Figure II.10: Flow rate analysis performed for 50% conversion of ester at a temperature around 1440 K (pressure around 8 bar), for an equivalence ratio of 1 and 0.5% initial concentration of methyl acrylate. The channels involving a consumption of the ester below 5% are not shown. Broken arrows represent several successive elementary reactions.

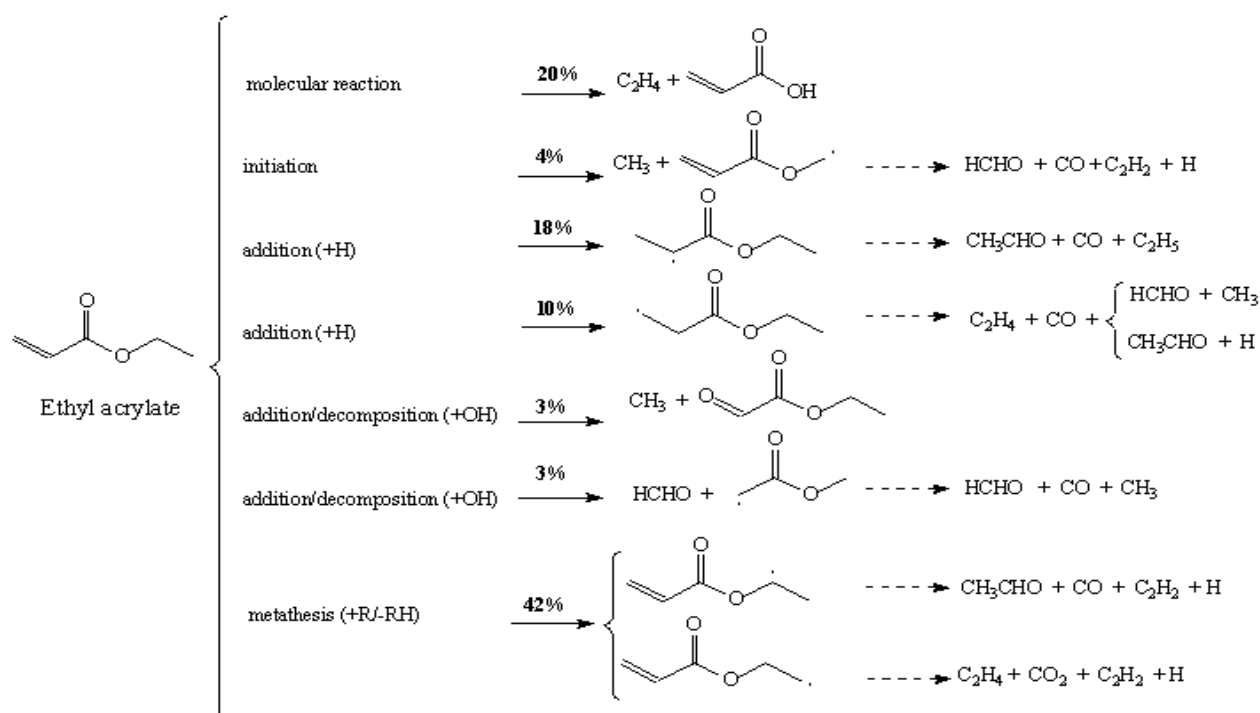


Figure II.11: Flow rate analysis performed for 50% conversion of ester at a temperature around 1440 K (pressure around 8 bar), for an equivalence ratio of 1 and 0.5% initial concentration of ethyl acrylate. The channels involving a consumption of the ester below 5% are not shown. Broken arrows represent several successive elementary reactions.

Chapter II Oxidation of small saturated and unsaturated ethyl and methyl esters at high temperature and moderate pressure

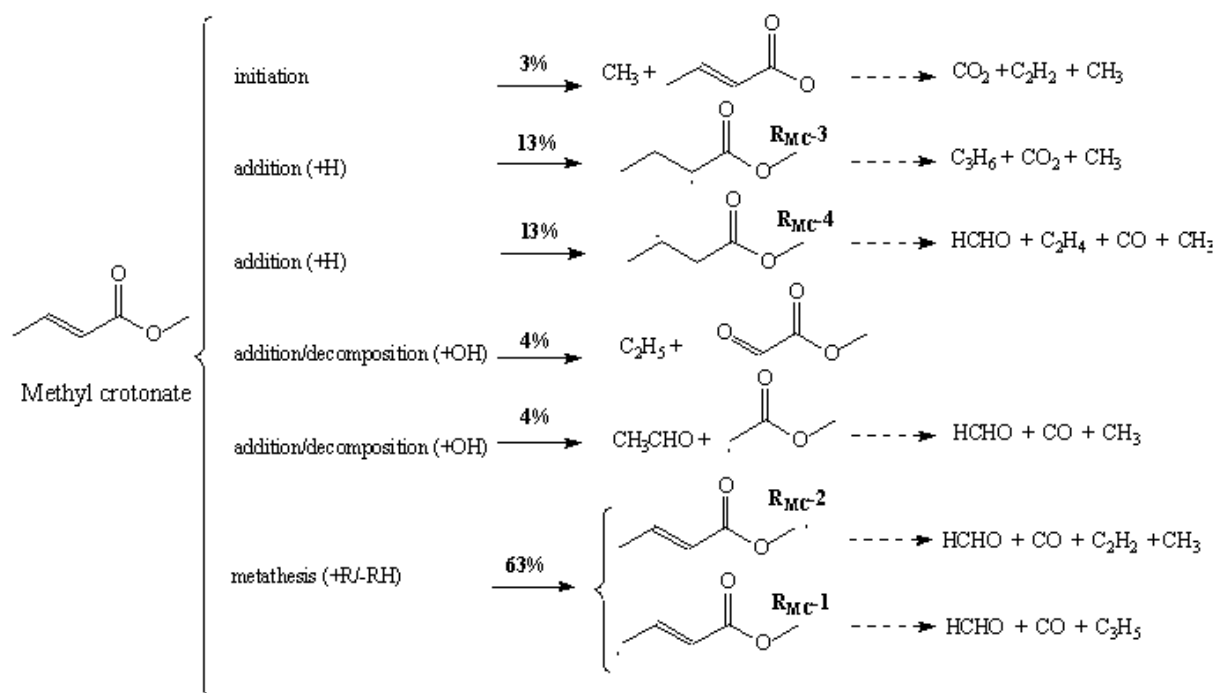


Figure II.12: Flow rate analysis performed for 50% conversion of ester at a temperature around 1440 K (pressure around 8 bar), for an equivalence ratio of 1 and 0.5% initial concentration of methyl crotonate. The channels involving a consumption of the ester below 5% are not shown. Broken arrows represent several successive elementary reactions.

Chapter II Oxidation of small saturated and unsaturated ethyl and methyl esters at high temperature and moderate pressure

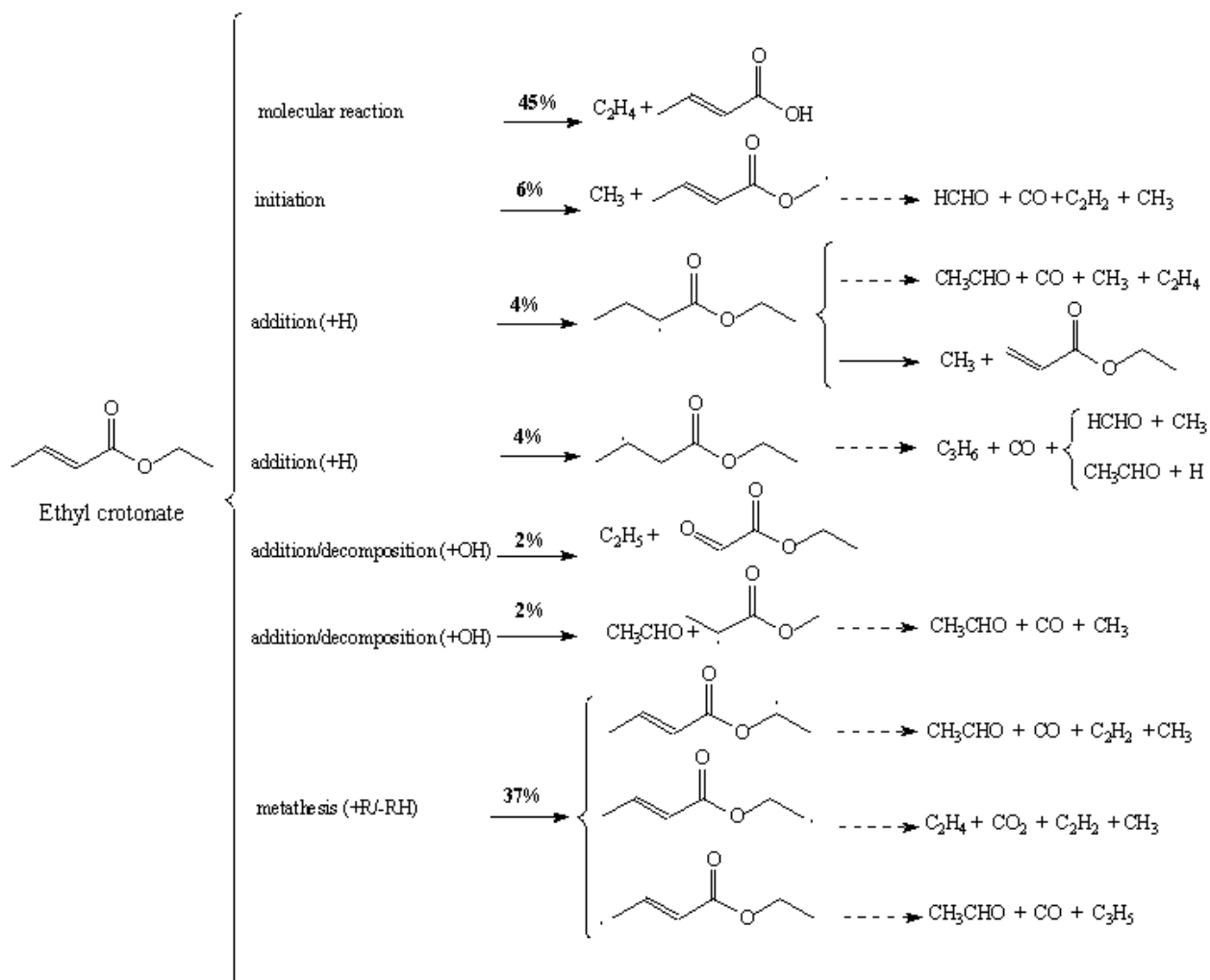


Figure II.13: Flow rate analysis performed for 50% conversion of ester at a temperature around 1440 K (pressure around 8 bar), for an equivalence ratio of 1 and 0.5% initial concentration of ethyl crotonate. The channels involving a consumption of the ester below 5% are not shown. Broken arrows represent several successive elementary reactions.

Figure II.14 below presents the computed temporal evolution of the initial organic reactant, the main products and $\cdot OH$ radicals. This figure has been depicted for the five modelled esters: ethyl butanoate, methyl acrylate, ethyl acrylate, methyl crotonate and ethyl crotonate under the same conditions as in Figures II.9 to II.13 respectively. It can be observed in Figures II.14a, II.14c and II.14e that contrary to the case of methyl acrylate (Figure II.14b) and methyl crotonate (Figure II.14d), the ignition of ethyl esters does not occur at the end of the consumption of ester, but when carboxylic acid is consumed.

Chapter II Oxidation of small saturated and unsaturated ethyl and methyl esters at high temperature and moderate pressure

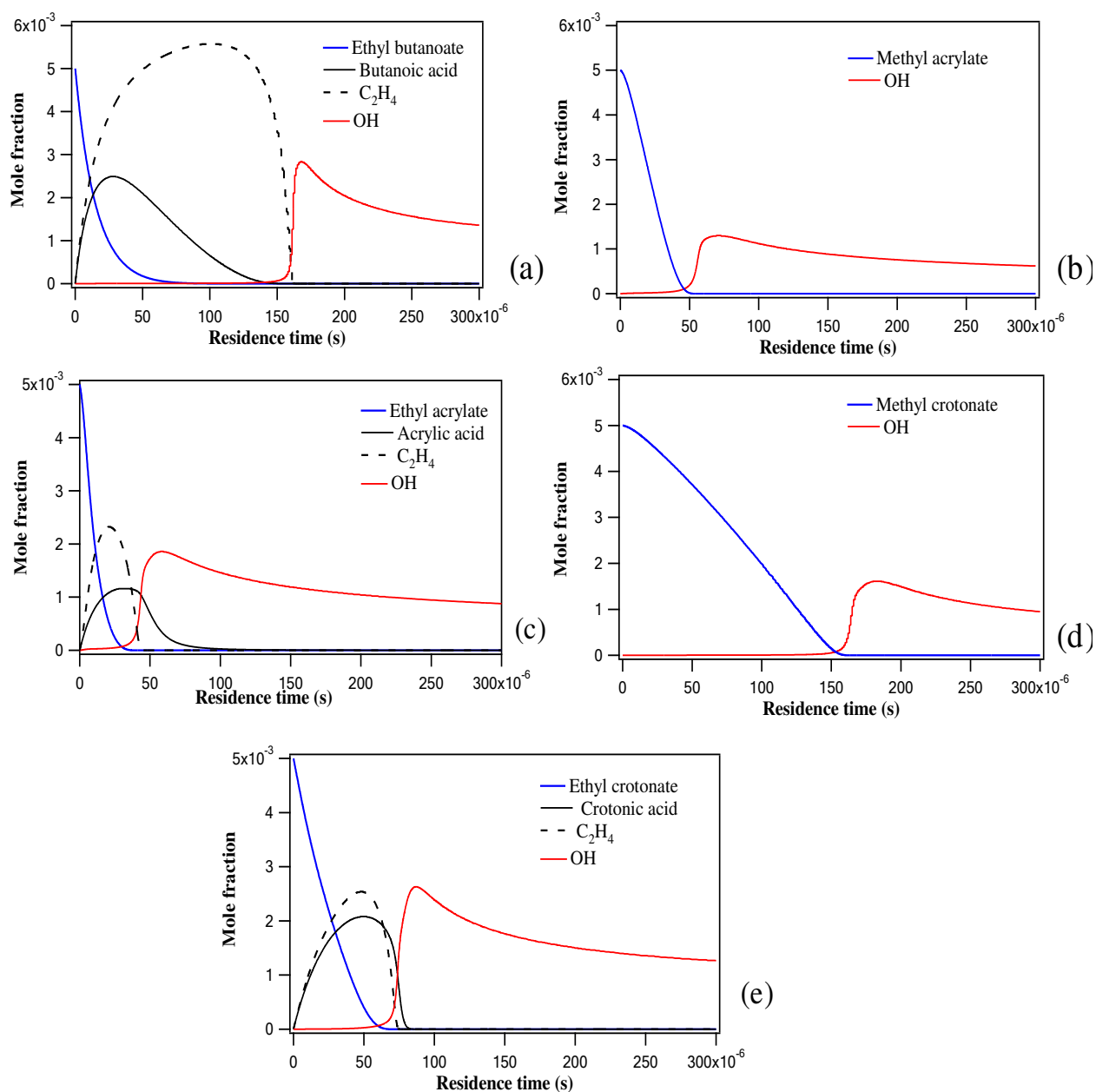


Figure II.14: Temporal decomposition of the initial ester, the main products, and OH radicals under the same conditions as in Figures 9 to 13 in the case of (a) ethyl butanoate (b) methyl acrylate (c) ethyl acrylate (d) methyl crotonate, and (e) ethyl crotonate respectively.

II.5.3 Sensitivity analysis

Figure II.15 displays first-order sensitivity analysis performed under the same conditions as the flux analysis, at a pressure of 8 bar and a temperature around 1400 K corresponding to an ignition delay time of approximately 48, 58, 77, 144, and 166 μs for respectively ethyl acrylate, methyl acrylate, ethyl crotonate, methyl crotonate, and ethyl butanoate. This sensitivity analysis has been performed on the kinetic models to elucidate the important channels of reaction for the studied esters. The brute force technique [38] was employed by multiplying by a factor of ten the forward rate constants of the main reactions consuming the esters and then calculating the percent change in ignition delay time relative to the baseline simulation. We define the sensitivity coefficient, $\sigma(\%)$ as:

$$\sigma(\%) = \left(\frac{\tau - \tau_0}{\tau_0} \right) \times 100 / \tau_0 \quad (\text{eqII.2})$$

where τ_0 is the original delay time and τ is the delay time calculated using the adjusted rate constant. For example, a ten-fold increase in the rate constant for the reaction of methyl crotonate with OH yielding $\text{R}_{\text{MC-1}}$ and H_2O results in a 40% increase in ignition delay time.

Thus, a positive sensitivity coefficient represents a longer ignition time, indicating that this reaction impedes reactivity, whereas a negative coefficient indicates a shorter ignition time, indicating that this reaction promotes reactivity.

Figure II.15 shows that the reactions consuming esters with the highest promoting influence on the reactivity are unimolecular initiations. The fact that these reactions are a source of branching agents, H-atoms, in the case of acrylates and of mildly reactive methyl and ethyl radicals for crotonates and ethyl butanoate certainly partly explains the difference of reactivity observed between the compounds. On the contrary reactions consuming H-atoms by addition to the double bond have the largest inhibiting influence. It is also interesting to note that metatheses have an inhibiting effect for the crotonates and ethyl butanoate whereas these reactions have a promoting effect for the acrylates. This is principally due to the possibility of formation of resonance stabilized radicals from crotonates which does not exist from acrylates. The additions of OH radicals have a more pronounced impact in the case of acrylates which are less easily consumed by H-abstractions. The formation of crotonic acid has a large inhibiting effect, because this species is a source of resonance stabilized radicals through H-abstractions.

Chapter II Oxidation of small saturated and unsaturated ethyl and methyl esters at high temperature and moderate pressure

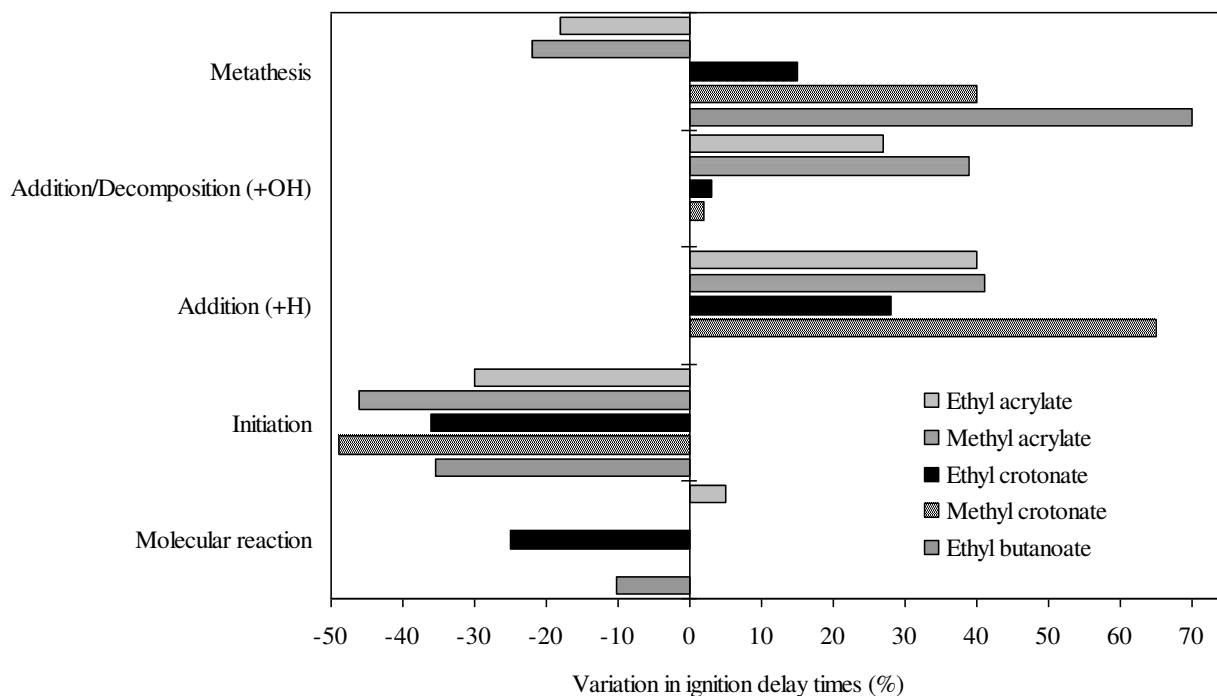


Figure II.15: Sensitivity analysis results for the ignition of the five investigated ester, for $\phi = 1.0$ and a 0.5% initial concentration, at around 1400 K and 8 bar. Sensitivity values represent the increase or decrease in ignition delay time for a 10 increase in rate constant(s) of the given reaction(s).

II.6 Conclusion

This chapter presents new measurements of ignition delay times concerning five esters: ethyl acrylate, methyl acrylate, ethyl crotonate, methyl crotonate, and ethyl butanoate, at high temperatures and high pressure from shock tube device using optical diagnostic from excited OH^* emission at 306 nm. For each fuel, a global correlation for ignition delay time applicable over a wide experimental range has been proposed. Experimental results show that a similar reactivity is observed for methyl and ethyl esters, but that acrylates auto-ignite more easily than crotonates.

In addition, detailed mechanisms for the combustion of the five esters have been automatically generated using the version of EXGAS software recently improved to take into account these oxygenated reactants. Overall, simulations were in good agreement with the experimental data generated, indicating that most of the reaction pathways and accompanying reaction rates are described reasonably well. A flow rate and sensitivity analyses were carried out for the five esters in an attempt to gain an understanding of the important reactions

Chapter II Oxidation of small saturated and unsaturated ethyl and methyl esters at high temperature and moderate pressure

controlling their reactions. These reaction flux and sensitivity analyses let us think that the difference of reactivity between C₃ and C₄ unsaturated esters would be mainly due to easier unimolecular initiations involving the production of branching agents, H-atoms in the case of the acrylates.

II.7 References

- [1] M. Canakci, A. Necati Ozsezen, E. Arcaklioglu, A. Erdil, Prediction of performance and exhaust emissions of a diesel engine fueled with biodiesel produced from waste frying palm oil, *Expert Systems with Applications* 36 (2009) 9268-9280.
- [2] A.K. Agarwal, Biofuels (alcohols and biodiesel) applications as fuels for internal combustion engines, *Progress in Energy and Combustion Science* 33 (2007) 233-271.
- [3] J.M. Marchetti, V.U. Miguel, A.F. Errazu, Possible methods production biodiesel, *Renewable and Sustainable Energy Reviews* 11 (2007) 1300-1311.
- [4] Y.F. Lin, Y.P. Greg Wu, C.T. Chang, Combustion characteristics of waste-oil produced biodiesel/diesel fuel blends, *Fuel* 86 (2007) 1772-1780.
- [5] J. Krahl, G.H. Knothe, A. Munack, Y. Ruschel, O. Schröder, E. Hallier, G. Westphal, J. Bünger, Comparison of exhaust emissions and their mutagenicity from the combustion of biodiesel, vegetable oil, gas-to-liquid and petrodiesel fuels, *Fuel* 88 (2009) 1064-1069.
- [6] C.K. Westbrook, W.J. Pitz, H.J. Curran, A chemical kinetic modeling study of the effects of oxygenated hydrocarbons on soot emissions from diesel engines, *Journal of Physical Chemistry A* 110, 6912-6922.
- [7] P. Pepiot-Desjardin, H. Pitsch, R. Malhotra, S.R. Kirby, A.L. Boehman, Structural group analysis for soot reduction tendency of oxygenated fuels, *Combustion and Flame* 154 (2008) 191-205.
- [8] M.S. Grabowski and R.L. McCormick, Combustion of fat and vegetable oil derived fuels in diesel engines, *Progress in Energy and Combustion Science* 24 (1998) 125-164.
- [9] A. Demirbas, Biodiesel production from vegetable oils via catalytic and non-catalytic supercritical methanol transesterification methods, *Progress in Energy and Combustion Science* 31 (2005) 466-487.
- [10] B.I Parsons, C.J. Danby, The oxidation of hydrocarbons and their derivatives, Parts I. The observation of the progress of the reaction by pressure change and by analysis, *Journal of Chemical Society* (1956) 1795-1798.
- [11] E.M. Fisher, W.J. Pitz, H.J. Curran, C.K. Westbrook, Detailed chemical kinetic mechanisms for combustion of oxygenated fuels, *Proceedings of the Combustion Institute* 28 (2000) 1579-1586.

Chapter II Oxidation of small saturated and unsaturated ethyl and methyl esters at high temperature and moderate pressure

- [12] S. Gail, M. Thomson, S.M. Sarathy, S.A. Syed, P. Dagaut, P. Diévert, A.J. Marchese, F.L.Dryer, A wide-ranging kinetic modeling study of methyl butanoate combustion, Proceedings of the Combustion Institute 31 (2007) 305-311.
- [13] W.K. Metcalfe, S. Dooley, H. J. Curran, J. M. Simmie, A. M. El-Nahas, M. V. Navarro, Experimental and modeling study of C₅H₁₀O₂ ethyl and methyl esters, Journal of Physical Chemistry A 111 (2007) 4001-4014.
- [14] W.K. Metcalfe, C. Togbé, P. Dagaut, H.J. Curran, J.M. Simmie, A jet-stirred reactor and kinetic modeling study of ethyl propanoate oxidation, Combustion and Flame 156 (2009) 250-260.
- [15] S. Dooley, H.J. Curran, J.M. Simmie, Autoignition measurements and a validated kinetic model for the biodiesel surrogate, methyl butanoate, Combustion and Flame 153 (2008) 2-32.
- [16] S.M. Walton, M.S. Woolridge, C.K. Westbrook, An experimental investigation of structural effects on the autoignition properties of two C₅ esters, Proceeding of the Combustion Institute 32 (2009) 255-262.
- [17] L.K. Huynh, A. Violi, Thermal decomposition of methyl butanoate: an Ab Initio study of a biodiesel fuel surrogate, Journal of organic Chemistry 73 (2008) 94-101.
- [18] A. Farooq, D. F. Davidson, R. K. Hanson, L. K. Huynh, A. Violi, An experimental and computational study of methyl ester decomposition pathways using shock tubes, Proceedings of the Combustion Institute 32 (2009) 247-253.
- [19] C.J. Hayes, D.R. Burgess Jr., Exploring the oxidative decompositions of methyl esters: Methyl butanoate and methyl pentanoate as model compounds for biodiesel, Proceedings of the Combustion Institute 32 (2009) 263-270.
- [20] M.H. Hakka, H. Bennadji, J. Biet, M. Yahyaoui, B. Sirjean, V. Warth, L.Coniglio, O. Herbinet, P.A. Glaude, F. Billaud, F. Battin-Leclerc, Oxidation of Methyl and Ethyl Butanoates, International Journal of Chemical Kinetics 42 (2010) 226-252.
- [21] G. Knothe, A.C. Matheaus, T.W. Ryan III, Cetane numbers of branched and straight chain fatty esters determined in an ignition quality tester, Fuel 82 (2003) 971-975.
- [22] S.M. Sarathy, S. Gail, S.A. Syed, M.J. Thomson, P. Dagaut, A comparison of saturated and unsaturated C₄ fatty acid methyl esters in an opposed flow diffusion flame and a jet stirred reactor, Proceedings of the Combustion Institute 31 (2007) 1015-1022.
- [23] S. Gail, S.M. Sarathy, M.J. Thomson, P. Diévert, P. Dagaut, Experimental and chemical kinetic modeling study of small methyl esters oxidation: Methyl (E)-2-butaenoate and methyl butanoate, Combustion and Flame 155 (2008) 635-650.

Chapter II Oxidation of small saturated and unsaturated ethyl and methyl esters at high temperature and moderate pressure

- [24] S. Bax, M.H. Hakka, P.A. Glaude, O. Herbinet, F. Battin-Leclerc, Experimental study of the oxidation of methyl oleate in a jet-stirred reactor, *Combustion and Flame* 157 (2010) 1220-1229.
- [25] R. Fournet, J.C Baugé, F. Battin-Leclerc, Experimental and modeling of oxidation of acetylene, propyne, allene and 1,3-butadiene, *International Journal of Chemical Kinetics* 31 (1999) 361-379.
- [26] N. Belmekki, P.A. Glaude, I. Da Costa, R. Fournet, F. Battin-Leclerc, Experimental and modeling study of the oxidation of 1-butyne and 2-butyne, *International Journal of Chemical Kinetics* 34 (2002) 172-183.
- [27] G. Dayma, P.A. Glaude, R. Fournet, F. Battin-Leclerc, Experimental and modeling study of the oxidation of cyclohexene, *International Journal of Chemical Kinetics* 35 (2003) 273-285.
- [28] C. Muller, V. Michel, G. Scacchi, G.M. Côme, A computer program for the evaluation of thermochemical data of molecules and free radicals in the gas phase, *Journal of Chemical Physics* 92 (1995) 1154-1177.
- [29] S.W. Benson, *Thermochemical Kinetics*, Edition John Wiley, 2nd edition (1976), New York.
- [30] A. Lifshitz, K. Scheller, A. Burcat, G.B. Skinner, Shock-tube investigation of ignition in methane-oxygen-argon mixtures, *Combustion and Flame* 16 (1971), 311-321.
- [31] V. Warth, N. Stef, P.A. Glaude, F. Battin-Leclerc, G. Scacchi, G.M. Côme, Computer-aided derivation of gas-phase oxidation mechanism: application to the modeling of the oxidation of n-butane, *Combustion and Flame* 114 (1998) 81-102.
- [32] F. Buda, R. Bounaceur, V. Warth, P.A. Glaude, R. Fournet, F. Battin-Leclerc, Progress toward a unified detailed kinetic model for the autoignition of alkanes from C₄ to C₁₀ between 600 et 1200 K, *Combustion and Flame* 142 (2005) 170-186.
- [33] J. Biet, M.H. Hakka, V. Warth, P.A. Glaude, F. Battin-Leclerc, Experimental and modeling study of the low-temperature oxidation of large alkanes *Energy and Fuel* 22 (2008) 2258-2269.
- [34] S. Touchard, F. Buda, G. Dayma, P.A. Glaude, R. Fournet, F. Battin-Leclerc, Experimental and modeling study of the oxidation of 1-pentene at high temperature, *International Journal of Chemical Kinetics* 37 (2005) 451-463.
- [35] R. Bounaceur, V. Warth, B. Sirjean, P.A. Glaude, R. Fournet, F. Battin-Leclerc, Influence of the position of the double bond on the autoignition of linear alkenes at low temperature, *Proceedings of the Combustion Institute* 32 (2009) 387-394.

Chapter II Oxidation of small saturated and unsaturated ethyl and methyl esters at high temperature and moderate pressure

- [36] H.J. Curran, Rate constant estimation for C₁ to C₄ alkyl and alkoxy radical decomposition, *International Journal of Chemical Kinetics* 38 (2006) 250-275.
- [37] J. Troe, Fall-off curves of unimolecular reaction, *Ber Buns Phys Chem* 78 (1974) 478-485.
- [38] R.J. Kee, F.M. Rupley, J.A. Miller, Chemkin II: A fortran chemical kinetics package for the analysis of gas phase chemical kinetics, Sandia Laboratories Report (1993), SAND 89-8009B.
- [39] J.M. Hall, M.J.A. Rickard, and E.L. Petersen, Comparison of Characteristic Time Diagnostics for Ignition and Oxidation of Fuel/Oxidizer Mixtures Behind Reflected Shock Waves, *Combustion Science and Technology* 177 (2005) 455-483.
- [40] M. Frenklach, in: W.C. Gardiner Jr. (Ed.), *Combustion Chemistry*, Springer-Verlag, New York, 1984, p. 440.

Appendix AII Shock tube measurements

Table AII.1: mixture compositions, shock conditions and ignition delay times for ethyl acrylate.

P ₁ (kPa)	P ₅ (atm)	V (m/s)	τ (μs)	T ₅ (K)	P ₁ (kPa)	P ₅ (atm)	V (m/s)	τ (μs)	T ₅ (K)
<i>φ = 1 ; X_{C₅H₈O₂}=1% ; X_{O₂}=6% ; X_{Ar}=93%</i>					<i>φ = 1 ; X_{C₅H₈O₂}=0.5% ; X_{O₂}=3% ; X_{Ar}=96.5%</i>				
29.5	8.6	782	60.7	1328	29.6	8.5	791	41.5	1415
28.6	8.4	784	76.6	1335	29.3	8.4	791	43.5	1416
27.9	8.4	790	50.4	1353	28	8.4	802	41.4	1452
29.3	9.1	800	40.7	1381	27.3	8.2	804	29.6	1456
28	9	806	33.3	1399	30	9.2	808	26.9	1469
28.6	9.3	812	20.2	1416	28.6	8.9	814	31.7	1488
26.6	8.8	817	15.4	1431	25.3	8.1	821	19.8	1512
25.3	8.7	826	18.5	1458	25.9	8.6	829	16.9	1538
25.6	8.9	831	12.4	1471	23.4	7.8	833	17.9	1552
21.9	7.8	838	15.2	1484	25.3	8.6	864	17.7	1570
23.3	8.4	840	10	1499	23.3	8.1	842	14	1581
24.6	8.9	814	7.6	1501	24.6	8.5	844	16.5	1586
21.3	8.3	865	5.2	1575	22	7.7	848	9.9	1601
-	-	-	-	-	22.4	8.3	864	7.5	1655
-	-	-	-	-	21.9	8.2	868	9.1	1669
-	-	-	-	-	22.6	8.6	874	7.7	1688
<i>φ = 1 ; X_{C₅H₈O₂}=0.4% ; X_{O₂}=2.4% ; X_{Ar}=97.2%</i>					<i>φ = 0.25 ; X_{C₅H₈O₂}=0.5% ; X_{O₂}=12% ; X_{Ar}=87.5%</i>				
27.9	7.8	783	68.2	1404	27.3	8.2	799	17.1	1367
29.3	8.2	785	58.7	1411	29.3	8.8	800	17.1	1371
27.1	7.9	798	29.8	1451	27.3	8.3	802	13.1	1379
27.4	8.1	801	28.5	1462	28.6	8.7	804	19.6	1382
27.3	8.2	804	30.4	1473	28	8.7	808	14.2	1395
28.2	8.7	813	35.4	1500	28	9	818	12.3	1425
27.7	8.7	817	28	1515	26.6	8.6	820	8	1430
26.6	8.6	826	25	1545	26	8.8	833	7.6	1471
25.3	8.3	831	15	1559	24.6	8.4	833	9.2	1471
24.6	8.1	833	13.3	1567	24	8.2	835	4.6	1476
25.9	8.6	835	17.7	1572	22.3	7.8	840	6	1493
24.1	8.0	836	12.6	1576	23.3	8.3	848	4.2	1517
25.5	8.6	838	14.2	1583	-	-	-	-	-
23.3	8.1	849	10.5	1620	-	-	-	-	-
22.6	8.0	852	10.9	1632	-	-	-	-	-
21.6	7.9	864	10.2	1673	-	-	-	-	-
<i>φ = 2 ; X_{C₅H₈O₂}=0.5% ; X_{O₂}=1.5% ; X_{Ar}=98%</i>									
23.2	7.7	831	38.3	1558	21.9	7.9	856	24	1641
24.7	8.3	835	41	1570	21.3	7.7	857	31.6	1648
23.3	7.8	836	38.3	1575	20.2	7.5	866	24.3	1675
21.8	7.5	840	36.8	1589	18.8	7.4	886	19.1	1744
22.9	7.9	844	30.6	1601	20.0	8.1	895	15.8	1777
21.6	7.6	851	33.9	1625	18.6	7.6	896	15.3	1783

Note: P₁ is the pressure of the mixture before the shock, V the velocity of the incident wave, P₅ and T₅ are pressure and temperature behind the reflected shock wave, τ is the ignition delay time.

Chapter II Oxidation of small saturated and unsaturated ethyl and methyl esters at high temperature and moderate pressure

Table AII.2: mixture compositions, shock conditions and ignition delay times for methyl acrylate.

P₁ (kPa)	P₅ (atm)	V (m/s)	τ (μs)	T₅ (K)	P₁ (kPa)	P₅ (atm)	V (m/s)	τ (μs)	T₅ (K)
<i>φ = 1 ; X_{C₄H₆O₂}=1% ; X_{O₂}=4.5% ; X_{Ar}=94.5%</i>					<i>φ = 1 ; X_{C₄H₆O₂}=0.5% ; X_{O₂}=2.25% ; X_{Ar}=97.25%</i>				
30.5	8.6	777	205.4	1341	26.6	7.6	791	75.4	1434
30	9.6	779	176.3	1347	27.3	7.9	794	52.3	1443
28.6	8.3	784	147.8	1363	27.9	8.2	799	46.1	1459
27.9	8.4	794	56.3	1391	27.3	8.2	804	55.4	1474
27.1	8.1	794	64.8	1392	26.6	8	807	31.6	1483
25.5	8	808	24.4	1434	25.9	7.9	807	28	1485
26.3	8.3	809	28.6	1437	26.6	8.1	808	37.3	1488
25.3	8.2	815	20.4	1454	23.9	7.5	816	25.7	1512
24.4	8	821	10.3	1474	24.9	7.9	820	15.6	1527
22	7.3	821	12.3	1475	24.6	7.9	825	17.2	1543
24.8	8.2	822	11.3	1476	25.3	8.3	830	15.3	1560
23.3	7.8	828	11.8	1494	22.7	7.5	831	11	1563
22.3	7.7	833	10.6	1510	23.9	7.9	831	16.5	1563
-	-	-	-	-	21.9	7.1	846	7.1	1615
-	-	-	-	-	22.6	7.9	849	8.3	1624
<i>φ = 0.25 ; X_{C₄H₆O₂}=0.5% ; X_{O₂}=9% ; X_{Ar}=90.5%</i>					<i>φ = 2 ; X_{C₄H₆O₂}=0.5% ; X_{O₂}=1.125% ; X_{Ar}=98.375%</i>				
26	7.7	799	46.3	1401	27.3	8.2	807	95	1494
25.9	7.8	804	43.9	1415	25.9	8	812	89.6	1510
27.3	8.4	808	17.7	1428	23.5	7.3	816	81.8	1523
24.7	7.6	808	19.5	1428	25.3	7.9	816	72.3	1525
26.6	8.3	812	13.9	1442	25.3	7.9	816	77.3	1526
27.9	8.7	813	21.5	1445	24.8	7.7	817	79.1	1529
25.9	8.3	818	8.7	1460	24.7	7.9	822	76.2	1545
25.6	8.2	819	11.3	1464	23.9	7.8	828	48.3	1566
25.3	8.1	819	9.8	1464	22.6	7.5	833	31.4	1580
24.7	8.1	829	6.9	1493	22.4	7.5	839	29.8	1602
23.9	8.0	832	4.8	1503	23.9	8.1	840	40.5	1607
23.3	7.9	836	4.1	1515	21.2	7.5	853	19	1648
22.6	7.6	836	4.4	1517	21.8	8.2	871	16.9	1714

Note: P₁ (1 Torr = 0,133 kPa) is the pressure of the mixture before the shock, V the velocity of the incident wave, P₅ and T₅ are pressure and temperature behind the reflected shock wave, τ is the ignition delay

Chapter II Oxidation of small saturated and unsaturated ethyl and methyl esters at high temperature and moderate pressure

Table AII.3: mixture compositions, shock conditions and ignition delay times for ethyl crotonate.

P_1 (kPa)	P_5 (atm)	V (m/s)	τ (μ s)	T_5 (K)	P_1 (kPa)	P_5 (atm)	V (m/s)	τ (μ s)	T_5 (K)
$\phi = 1 ; X_{C_6H_{10}O_2} = 1\% ; X_{O_2} = 7.5\% ; X_{Ar} = 91.5\%$					$\phi = 1 ; X_{C_6H_{10}O_2} = 0.5\% ; X_{O_2} = 3.75\% ; X_{Ar} = 95.75\%$				
30.6	9	780	137.9	1300	28.5	8.1	785	242.1	1384
28.6	8.7	786	137.9	1317	29.3	8.4	787	157.6	1391
29.9	9.2	789	101.9	1327	26.6	7.8	791	179	1402
26.1	8	790	70	1330	24.6	8	806	88.5	1449
29.7	9.3	794	58.9	1341	26.3	8.1	806	88.5	1449
28	8.8	796	102.6	1345	25.5	8.1	813	79.4	1472
25.1	8.2	798	55	1353	26.1	8.3	815	73.8	1477
23.9	7.8	807	35.2	1377	24.9	7.9	815	80.9	1477
26.6	8.8	811	50.4	1389	25.9	8.5	824	42.6	1507
24.7	8.5	823	27.1	1422	25.3	8.4	826	65.5	1512
26.7	9.3	826	20	1432	24.2	8.1	831	52.1	1528
26.3	8.6	843	8.5	1481	23.3	8.1	843	30.5	1566
23.3	8.8	850	10.2	1502	22.0	7.9	851	33.3	1593
22	8.5	857	4.7	1524	20.6	7.8	869	22.1	1653
$\phi = 1 ; X_{C_6H_{10}O_2} = 0.417\% ; X_{O_2} = 3.128\% ; X_{Ar} = 96.455\%$					$\phi = 0.25 ; X_{C_6H_{10}O_2} = 0.5\% ; X_{O_2} = 15\% ; X_{Ar} = 84.5\%$				
27.9	8.6	808	66	1469	27.1	8.5	805	69.5	1357
26.6	7.6	789	176.4	1411	25.3	8.4	824	18	1411
24.6	7.6	810	71.6	1476	24.6	8.4	831	17.6	1431
24.6	8.1	830	28.7	1540	29.3	9	802	66	1350
22.6	8.5	870	10.5	1674	28.0	8.8	808	54	1367
25.3	8.2	824	30.9	1522	25.0	8	810	38.5	1372
24.6	8.4	837	23.1	1564	24.8	8	815	40.1	1384
22	7.6	844	19.3	1586	22.7	7.5	822	16.6	1405
23.9	7.7	821	44.9	1511	24.8	8	815	40.1	1384
21.3	7.8	862	10.2	1648	-	-	-	-	-
20.6	7.4	854	13.4	1620	-	-	-	-	-
25.2	8.1	823	45.5	1517	-	-	-	-	-
$\phi = 2 ; X_{C_6H_{10}O_2} = 0.5\% ; X_{O_2} = 1.875\% ; X_{Ar} = 97.625\%$									
26.7	7.9	794	242	1427	21.9	7.9	854	52.3	1621
25.3	7.5	796	210	1435	20.6	8.1	881	29.8	1713
23.9	7.3	806	211	1464	19.3	7.8	891	38.7	1748
25.9	8.1	813	126.2	1487	17.3	7.3	904	24.9	1796
23.3	7.8	833	95.9	1553	16.6	7.4	921	21.7	1854
21.5	7.7	854	56.6	1621	-	-	-	-	-

Note: P_1 is the pressure of the mixture before the shock, V the velocity of the incident wave, P_5 and T_5 are pressure and temperature behind the reflected shock wave, τ is the ignition delay time.

Chapter II Oxidation of small saturated and unsaturated ethyl and methyl esters at high temperature and moderate pressure

Table AII.4: Mixture compositions, shock conditions and ignition delay times for methyl crotonate.

P₁ (kPa)	P₅ (atm)	V (m/s)	τ (μs)	T₅ (K)	P₁ (kPa)	P₅ (atm)	V (m/s)	τ (μs)	T₅ (K)
<i>φ = 1 ; X_{C₅H₈O₂}=1% ; X_{O₂}=6% ; X_{Ar}=93%</i>					<i>φ = 1 ; X_{C₅H₈O₂}=0.5% ; X_{O₂}=3% ; X_{Ar}=96.5%</i>				
28	8.1	779	177.9	1322	26.7	8.0	802	91.1	1453
28.6	8.6	788	91.6	1351	26.5	8.2	812	56.2	1487
27.3	8.5	799	98	1381	26.4	8.4	817	55.3	1501
25.9	8.2	803	57.3	1394	25.3	8.1	819	55.9	1509
25.3	8.2	811	54.1	1418	25.4	8.1	820	47.3	1511
26.6	8.8	817	44	1434	26.3	8.4	821	40.1	1515
24.1	8.1	820	42.2	1443	24.9	8.2	827	29.6	1535
25.3	8.5	821	38.8	1448	23.9	7.9	827	39.3	1535
23.9	8.3	831	29.4	1479	24.7	8.2	831	30.5	1548
21.9	7.9	839	26.6	1501	22.2	7.6	840	21.3	1578
22	8.3	854	17.3	1546	23.3	8.0	842	18.3	1583*
-	-	-	-	-	22.7	7.9	845	20.2	1593
<i>φ = 0.25 ; X_{C₅H₈O₂}=0.5% ; X_{O₂}=12% ; X_{Ar}=87.5%</i>					<i>φ = 2 ; X_{C₅H₈O₂}=0.5% ; X_{O₂}=1.5% ; X_{Ar}98%</i>				
27	8.1	798	79.4	1367	24.6	7.4	805	168.2	1476
27.5	8.3	799	74.2	1369	25.9	8	811	176.1	1497
26.5	8.1	803	40.6	1383	23.5	8	838	67.5	1584
25.5	7.8	804	35.4	1384	22.5	7.8	844	77.4	1605
25.1	7.8	807	32.5	1396	20.6	7.4	848	48	1619
25	7.8	808	30.7	1397	23.2	8.5	860	42.9	1662
25.9	8.2	812	29.6	1409	20.2	7.7	875	28.6	1714
26.2	8.4	815	37.9	1417	21	8.1	877	39	1720
25.8	8.3	816	29.2	1420	18.2	7.1	884	20.9	1743
24.3	7.8	818	23.2	1428	17.8	7.3	900	18.9	1800
23.4	7.8	826	17.5	1450	-	-	-	-	-
22.1	7.4	831	10.7	1466	-	-	-	-	-
24.5	8.3	833	11.9	1472	-	-	-	-	-
22.6	7.8	837	11.6	1484	-	-	-	-	-
21.5	7.5	842	8.5	1500	-	-	-	-	-

Note: P₁ is the pressure of the mixture before the shock, V the velocity of the incident wave, P₅ and T₅ are pressure and temperature behind the reflected shock wave, τ is the ignition delay time.

* Conditions of the signals displayed in Figure II.2.

Chapter II Oxidation of small saturated and unsaturated ethyl and methyl esters at high temperature and moderate pressure

Table AII.5: Mixture compositions, shock conditions and ignition delay times for ethyl butanoate.

P₁ (kPa)	P₅ (atm)	V (m/s)	τ (μs)	T₅ (K)	P₁ (kPa)	P₅ (atm)	V (m/s)	τ (μs)	T₅ (K)
<i>φ = 1 ; X_{EB}=1% ; X_{O2}=8% ; X_{Ar}=91%</i>					<i>φ = 1 ; X_{EB}=0.5% ; X_{O2}=4% ; X_{Ar}=95.5%</i>				
27	8.2	784	321.5	1296	29.3	8.5	788	111.7	1385
29.3	7.8	784	259	1301	27.9	8.2	790	97	1390
28.6	8.9	790	311	1313	27.3	8.2	797	71.3	1411
28	9.2	804	114	1352	26.6	8.3	807	37.8	1442
25.3	8.3	806	84.3	1358	25.9	8.2	813	36.5	1459
23.3	7.9	814	34.4	1378	24.6	7.9	815	25.5	1468
24.6	8.4	816	56.4	1384	25.3	8.5	831	26.7	1516
26	9	822	42.3	1401	22.6	7.8	835	15.5	1530
24	8.5	826	15.2	1412	23.9	8.2	836	13.3	1533
22.6	8.3	837	16.6	1443	23.3	8.2	843	12.4	1555
23	8.7	848	11	1474	-	-	-	-	-
<i>φ = 1 ; X_{EB}=0.42% ; X_{O2}=3.33% ; X_{Ar}=96.25%</i>					<i>φ = 0.25 ; X_{EB}=0.5% ; X_{O2}=16% ; X_{Ar}=83.5%</i>				
9.6	8.5	758	1485	1307	29.9	8.7	783	188.6	1282
2	8.7	785	123.4	1388	29.3	8.5	785	101.4	1288
42.8	8.9	786	153.7	1393	28	8.4	794	106.7	1311
2.2	9.2	788	191.1	1398	27.7	8.5	799	75.6	1325
15.2	8.7	798	87.2	1429	27.4	8.7	810	36	1356
12.6	8.4	802	59.4	1441	26.6	8.8	820	20.3	1386
5.6	7.9	813	31.9	1475	23.4	7.8	821	13.2	1386
4.6	8.4	820	23	1498	25.3	8.4	823	14.5	1393
34.4	8.6	822	22.3	1505	24.6	8.5	833	11.4	1422
11.2	8.1	834	10.7	1543	23.9	8.3	833	6.8	1423
41.4	7.8	840	10	1562	22.6	8.1	842	5.3	1448
7.5	8.1	843	5.5	1573	-	-	-	-	-
15	8.6	843	9.8	1574	-	-	-	-	-
<i>φ = 2 ; X_{EB}=0.5% ; X_{O2}=2% ; X_{Ar}=97.5%</i>									
25.5	8.6	830	88.3	1532	21.3	7.9	859	47.1	1628
24.4	8.4	837	58	1555	19.3	7.9	894	14.9	1743
22.3	7.7	840	40.4	1563	16.6	7.3	914	10.8	1814
22.3	7.8	840	65.5	1566	17.3	7.6	915	9.7	1816
22.6	7.9	841	39.4	1569	16.4	7.6	935	6.6	1888
23.3	8.1	842	47.3	1571	-	-	-	-	-

Note: P₁ is the pressure of the mixture before the shock, V the velocity of the incident wave, P₅ and T₅ are pressure and temperature behind the reflected shock wave, τ is the ignition delay time. Points in italic characters correspond to ignition delay times below 10 μs and then to a larger uncertainty.

CHAPTER III

**EXPERIMENTAL AND KINETIC MODELING
STUDY OF ETHYL BUTANOATE OXIDATION IN
A TUBULAR PLUG FLOW REACTOR - FROM
LOW TO HIGH TEMPERATURE UNDER
ATMOSPHERIC PRESSURE**

Chapter III

Experimental and Kinetic Modeling Study of Ethyl butanoate Oxidation in a Tubular Plug Flow Reactor – From Low to High Temperature under Atmospheric Pressure

This chapter has been the subject of a paper [H. Bennadji, P.A. Glaude, L. Coniglio, F. Billaud. “Experimental and kinetic modeling study of ethyl butanoate oxidation in a plug flow reactor”] submitted for publication in Fuel.

The work related to the experimental study of ethyl butanoate oxidation, together with the discussion of the performance of the model used via reaction flux and sensitivity analyses, have been carried out by the author, H. Bennadji, of the present PhD dissertation, whereas the model development was achieved by the co-author of the submitted paper, P.A. Glaude and his collaborators.

Abstract

This investigation examines the experimental and the kinetic modeling of the oxidation of ethyl butanoate (EB) selected as model molecule for fatty acid ethyl esters (FAEE). New experimental information of EB oxidation was generated from a tubular plug flow reactor (PFR) operating at atmospheric pressure, under dilute conditions, over the temperature range 500-1200 K, with various equivalence ratios ranging from 0.5 to 1.6, and at residence times varying between 0.25 and 0.55 s. Concentration profiles of the reactants, stable intermediates, and final products, identified by GC/MS, were measured by infrared ray absorption and GC/TCD-FID analyses. Experiments of EB oxidation carried out in the tubular PFR were simulated using a detailed chemical kinetic oxidation mechanism (117 species and 1035 reactions) proposed in a previous work [Hakka et al., Int. J. Chem. Kin. 42 (2010) 226] and automatically generated from an improved version of EXGAS software. Globally, good agreement was observed between experimental and simulated results, confirming the validity of the proposed model for EB oxidation. Reaction flux and sensitivity analyses allowed to determine the main reaction pathways involved the investigated conditions of EB oxidation.

Keywords: oxidation, chemical kinetics, biodiesel, FAEE, ethyl butanoate, plug flow reactor.

Chapter III Experimental and Kinetic Modeling Study of Ethyl butanoate Oxidation in a Tubular Plug Flow Reactor - From Low to High Temperature under Atmospheric Pressure

Nomenclature

N_{ePSR}	Number of ePSRs used for performing simulations of the actual PFR
P	Pressure
Pe_{RTP}	Péclet number relative to the actual PFR under a given operating condition
P_{R}	Tubular reactor pressure
Q_{RTP}^t	Total volumetric flow rate of the feed material (fresh reactants in helium) under T_{R} and P_{R}
T	Temperature
T_{R}	Tubular reactor temperature
V_{R}	Tubular reactor volume
x_{k}	Molar fraction of species k ($k = \text{ester}, \text{O}_2, \text{ or He}$)
z	axial coordinate of the tubular plug flow reactor

Greek symbols

ϕ	Equivalence ratio, i.e. for the reaction $C_nH_m + (n + m/4) O_2 \rightarrow n CO_2 + m/2 H_2O$, $\phi = \frac{\%C_nH_m / \%O_2}{(\%C_nH_m / \%O_2)_{\text{stoichiometric}}} = \frac{\%C_nH_m / \%O_2}{1/(n + m/4)}$
τ_{ePSR}	Residence time of the feed material (fresh reactants in helium) along an ePSR
τ_{RTP}	“Physical residence time” of the feed material (fresh reactants in helium) along the actual tubular PFR (defined according to T_{R} and P_{R})
τ_{STP}	“Theoretical residence time” of the feed material (fresh reactants in helium) along the actual tubular PFR (defined according to the STP conditions)

Abbreviations

BA	Butanoic acid
CFR	Cooperative federation research
CV	Coefficient of variation
EB	Ethyl butanoate
EP	Ethyl propanoate
ePSR	Equivalent continuous perfectly stirred tank reactor
FAEE	Fatty acid ethyl ester
FAME	Fatty acid methyl ester
GC	Gas chromatography
LTHR	Low temperature heat release
MB	Methyl butanoate
MS	Mass spectrometry
NTC	Negative temperature coefficient
PFR	Plug flow reactor
PSR	Continuous perfectly stirred tank reactor
RCM	Rapid compression machine
RME	Rapeseed methyl ester
STP	Standard conditions of temperature and pressure ($T=273.15 \text{ K}$ and $P=1 \text{ atm}$)
FID	Flame ionisation detector
TCD	Thermal conductivity detector

III.1 Introduction

Fast depletion of fossil fuels and worldwide worry about the protection of environment are demanding an urgent need to carry out research works for finding out viable alternative fuels. Among the most used fuels, the diesel oils of automotive industry are the most important. The alternatives to petrodiesel fuel must be technical feasible, economically competitive, environmentally acceptable, readily available, and renewable. Many of these requisites are satisfied by biodiesel fuel that can be manufactured from various lipid sources (enclosing both edible and non-edible vegetable oils, animal fats, and waste cooking oils) via transesterification reaction by addition of an alcohol (methanol or ethanol). Moreover, biodiesel has many advantages over petroleum diesel such as being renewable with greater energy efficiency, nontoxic, sulfur-free, and biodegradable; also, it generally produces a cleaner burning and helps to reduce global greenhouse gas emissions from the combustion in diesel engines [1]. Biodiesel can be used in blends with petrodiesel or as a neat fuel. Just like petrodiesel fuel, biodiesel operates in compression ignition engine and essentially requires very little or no engine modifications thanks to its very similar properties [2]. Thus, the use of biodiesel is being promoted by EU countries to partly replace petrodiesel fuel consumption in order to reduce greenhouse gas emissions and dependency on foreign oil. Meeting the targets established by the European Parliament for 2010 and 2020 would lead to a biodiesel market share of 5.75% and 10%, respectively. In a wide majority of cases, biodiesel production plants currently use methanol as alcohol during the transesterification process because of its low cost, which yields consequently biodiesel mainly composed by fatty acid methyl esters (FAME), only 90% wt renewable. By the contrary, the use in the transesterification process of bioethanol produced from agricultural resources should provide a fully renewable fuel consisting of fatty acid ethyl esters (FAEE), which would further contribute to reduce the life-cycle of greenhouse gas from vehicle emissions [3]. Furthermore, as ethanol is being recommended as fuel for transportation sector in some countries, it is expected that ethanol production will be enhanced. Under such circumstances, developing biodiesel from ethanol route seems to be justified. Baiju et al. [4] reported that the transesterification reaction can proceed faster if methanol is used instead of ethanol, which is due to methanol superior reactivity. On the other hand, ethanol possesses higher solubility and reduces the effect of the mass transfer limitation encountered during the transesterification process. In general, the physical and chemical properties of ethyl esters are comparable to those of the methyl esters [4]. The impact of biodiesels consisting of FAME or FAEE on engine performance and emissions has been extensively investigated by

Chapter III Experimental and Kinetic Modeling Study of Ethyl butanoate Oxidation in a Tubular Plug Flow Reactor - From Low to High Temperature under Atmospheric Pressure

researchers in recent years [5-13]. Overall, methyl and ethyl esters of the same fatty acids did not cause significant exhaust emission differences [6]. Besides, a better understanding of the oxidation kinetics for the FAME or FAEE-based biodiesels used as fuel in diesel engines is still requisite.

Due to the complexity of biodiesel components, much research has been conducted in the oxidation study of the small methyl esters. Methyl butanoate (MB) is the model molecule of FAME-based biodiesel the most commonly studied. Fisher et al. [14] developed the first detailed chemical kinetic model for MB oxidation and used it to simulate the limited oxidation data available in the literature at this time. These were conducted in closed vessels, under low temperature (520 – 750 K) and subatmospheric (13 – 54 kPa) conditions [15 – 18]. Fisher et al. found good agreement between simulated and experimental results, under nearly-stoichiometric conditions. Gail et al. [19] modified the mechanism by Fisher et al. in order to extend its applicability over a wide range of operating conditions, by using results obtained in various types of reactors: a jet stirred reactor (from 800 to 1350 K), an opposed flow diffusion flame, and a variable pressure flow reactor (from 500 to 900 K). Dooley et al. [20] investigated the low temperature ignition of MB in rapid compression machine (RCM) over the temperature range 640-949 K. The authors significantly modified the detailed chemical kinetic mechanism proposed by Fisher et al., leading to a reasonable agreement between simulated and experimental ignition delays in RCM.

Nevertheless, very little experimental and kinetic data are available in the literature about the oxidation of ethyl esters at low temperature and especially under tubular flow reactor conditions. Schwartz et al. [21] studied the effect of doping a methane/air non premixed flame with 5000 ppm of ethyl propanoate (EP, $C_5H_{10}O_2$) with chemical structure $CH_3CH_2C(O)OCH_2CH_3$. The authors found that the main decomposition pathway for EP was a unimolecular six-centered elimination reaction leading to the corresponding carboxylic acid (propanoic acid) and ethylene. Metcalfe et al. [22] examined EP oxidation behind reflected shock waves over the temperature range 1100-1670 K (at 1 and 4 atm for various equivalence ratios: 0.25, 0.5, 1.0, and 1.5). The authors developed a detailed chemical kinetic mechanism for EP oxidation from which the achieved simulations revealed to be in good agreement with the experimental data. Following this work, Metcalfe et al. [23] reported experimental jet-stirred reactor studies of EP at 10 atm over a temperature range from 750-1100 K. The authors also observed that ethylene and propanoic acid were the most abundant products formed, confirming the existence of the six-centered unimolecular elimination from EP. These results were used to further validate successfully the model that the authors had previously published

Chapter III Experimental and Kinetic Modeling Study of Ethyl butanoate Oxidation in a Tubular Plug Flow Reactor - From Low to High Temperature under Atmospheric Pressure

[22]. Moreover, some studies were conducted to compare the reactivity of methyl and ethyl esters, in order to examine in more details the impact of the functional group methyl and ethyl ester on fuel combustion. Metcalfe et al. [22] compared the reactivity of EP to that of MB and found that EP was more reactive than MB under the studied conditions. This feature was attributed to the higher reactivity of the two major intermediates, namely ethylene and propanoic acid. The same results were reported by Walton et al. [24] which studied the ignition of MB and EP using a RCM at temperature range of 935-1117 K. Hakka et al. [25] investigated the autoignition of EB and MB behind reflected shock waves over the temperature range of 1250-2000 K. The detailed chemical kinetic mechanism of MB and EB were automatically generated by EXGAS software [25]. The authors reported also that EB was slightly more reactive than MB above 1600 K, attributing this feature to the conversion of EB into ethylene and butanoic acid. Very recently, Zhang and Boehman [26] investigated the oxidation of ethyl hexanoate and methyl heptanoate in a motored CFR engine. Low temperature heat release (LTHR) was observed for both esters exhibiting evident cool flame behavior. Also, the authors found that at the same compression ratio, methyl heptanoate had both an earlier onset and a higher magnitude of LTHR than ethyl hexanoate, indicating that methyl heptanoate would be more reactive in the low temperature region than ethyl hexanoate. Furthermore, GC/MS analyses carried out by Zhang and Boehman [26] for the intermediate species formed in exhaust engine under LTHR conditions showed that the two fatty acid alkyl esters (with alkyl = ethyl or methyl) experienced the typical paraffin-like low temperature oxidation sequence with formation of unsaturated alkyl esters, epoxy alkyl esters, oxo-alkyl esters, aldehydes, and carboxylic acids. Additionally, hexanoic acid and ethylene formed from the six-centered unimolecular elimination from ethyl hexanoate were also observed. On the basis of these results, the authors finally proposed major low temperature oxidation pathways for ethyl hexanoate.

The aim of this work is to provide more information about the combustion characteristics of EB in order to extend the range of the previously published detailed chemical kinetic mechanism [25] and getting a better knowledge of ethyl ester function oxidation. Also, most of the comparative studies related to methyl- and ethyl esters oxidation concern molecules with the same number of carbon atoms but different aliphatic main chains. However, actual biodiesels based on FAME or FAEE comprise fatty acid esters with the same aliphatic main chains but different number of carbon atoms due to the different alcohol moiety (methyl or ethyl). Therefore, the present work related to EB oxidation should bring useful information for comparing the reactivity of EB and MB, as two potential surrogates for biodiesel. In

Chapter III Experimental and Kinetic Modeling Study of Ethyl butanoate Oxidation in a Tubular Plug Flow Reactor - From Low to High Temperature under Atmospheric Pressure

addition, another objective of this work is to examine in further details the effect of the ethyl ester function on combustion in diesel engine in terms of pollutant emissions (CO, CO₂, hydrocarbons...). The obtained information will still be significant even if EB is supposed to be not a suitable surrogate for FAEE-based biodiesel, particularly concerning the low temperature kinetic features (early production of CO₂ and cool flame behavior).

III.2 Experimental setup and materials

Oxidation of ethyl butanoate (EB, Figure III.1) selected in this work as model molecule for FAEE was carried out at pressure close to 1 atm using a quartz tubular plug flow reactor (PFR).

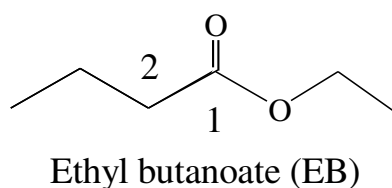


Figure III.1: Molecular structure of ethyl butanoate (EB).

The carbon atom of the carbonyl group is no.1 and the α -carbon of the carbonyl group is carbon no.2.

Gas chromatography (GC) and infrared analyses were used to determine the mole fractions of major and intermediate stable species formed, together with those of unreacted reagents. Identification of the species, and more particularly of the oxygenated intermediates, was primarily realized by coupling GC with mass spectrometry (GC/MS). Concentration profiles of the species were determined by coupling GC with classical thermal conductivity and flame ionization detectors (respectively, TCD and FID). For GC/FID analyses, the widely used internal standard method was applied with previous calibration conducted by evaluating a carbon response factor for each product relatively to a chosen internal standard (n-octane). The set-up of these complementary techniques was requisite to achieve a satisfactory characterization of EB oxidation.

The bench-scale experimental setup used in this study with the reactor and the measurement devices set-up is shown in Figure III.2. Primarily designed for kinetic pyrolysis studies of vegetable oils and carboxylic acids [27, 28], significant changes were brought for carrying out ester oxidation experiments. Therefore, a short description of the resulting bench-scale setup is given in the following.

Chapter III Experimental and Kinetic Modeling Study of Ethyl butanoate Oxidation in a Tubular Plug Flow Reactor - From Low to High Temperature under Atmospheric Pressure

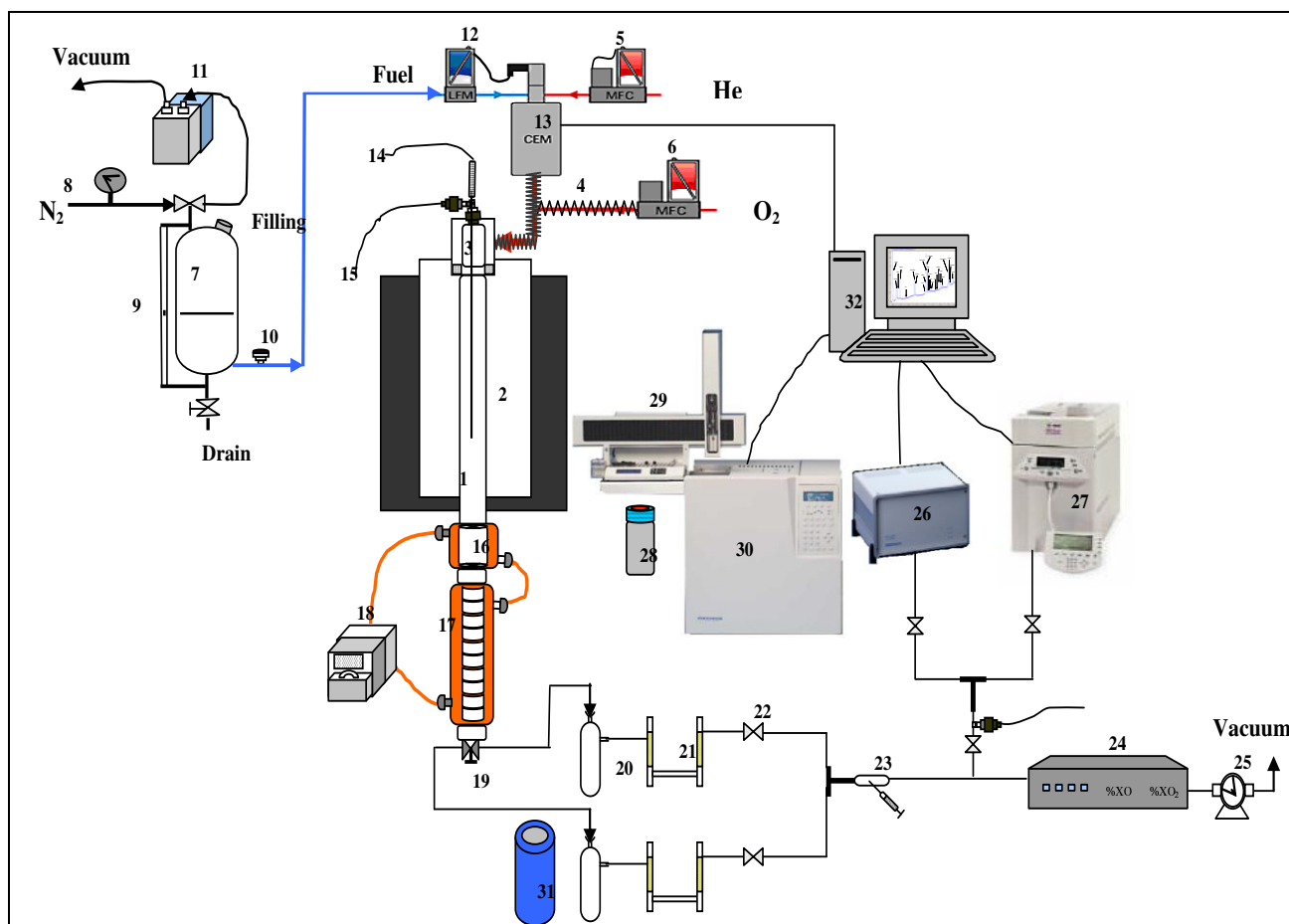


Figure III.2: Synoptic of the experimental set-up.

- | | |
|--|--|
| 1. Plug flow reactor (quartz) | 17. Column for separation |
| 2. Furnace (Thermolyne) | 18. Cryostat |
| 3. Preheating and mixing unit | 19. Three-way valve |
| 4. Heating resistances (Thermocoax) | 20. Glass trap |
| 5. Mass Flow Gas controller for He (MFG) | 21. Cartridge + cotton |
| 6. Mass Flow Gas controller for O ₂ (MFG) | 22. Valve |
| 7. Fuel tank | 23. Gas sampling bulb + Syringe (GC/MS) |
| 8. Manometer | 24. IR analyzer (CO and CO ₂ analysis) |
| 9. Level tank | 25. Flow meter |
| 10. Fuel feed valve | 26. GC-thermal conductivity detector TCD (O ₂ analysis) |
| 11. Pump | 27. GC-FID (light compounds analysis) |
| 12. Mass Flow Liquid controller (MFL) | 28. Vial for liquid phase analysis |
| 13. Controller Evaporator Mixer (CEM) | 29. Auto-sampler (ALS 104 type) |
| 14. Thermocouple (K-type) | 30. GC-FID (liquid compounds analysis) |
| 15. Pressure transducer | 31. Liquid nitrogen Dewar |
| 16. Annular quenching | 32. Computer for acquisition |

Chapter III Experimental and Kinetic Modeling Study of Ethyl butanoate Oxidation in a Tubular Plug Flow Reactor - From Low to High Temperature under Atmospheric Pressure

The reactor used in this work is a tube 8 mm in inner diameter and 55 cm in length, made of quartz to prevent wall catalytic reactions [27, 28] and housed in a thermostatically controlled electric resistance furnace (F 79300-type Thermolyne). The furnace ensures a quasi-isothermal section (± 0.6 K) within 150 mm around its middle. For a given set point temperature of the oven, the reactor temperature profile is measured with a K-type thermocouple of 1000 mm length that can be moved along the central axis of the reactor. Besides, the reactor is equipped upstream of a quartz unit for mixing/preheating, having an annular geometry (outer and inner diameters: 30 and 10 mm respectively; length: 20 cm), all surrounded by a roll of heating resistors of Thermocoax type. In order to ensure homogeneous gas-gas mixing, this heat exchanger was packed with quartz chips. Also, the reactants were preheated in this unit at 400 K to prevent any thermal cracking before entering to the reactor. A pressure transducer, located at the entrance of the reactor, gives the pressure measurement.

Upstream of the reactor, the liquid fuel EB (normal boiling point: 121°C) was contained in a stainless steel tank (1 L) pressurized with helium. After each load of the tank, helium bubbling and vacuum pumping were performed to remove oxygen traces dissolved in the liquid fuel. EB with a flow rate controlled by using a liquid mass flow controller (Bronkhorst CORIFLOW) was mixed to the carrier gas (helium), and then evaporated by passing through a single pass heat exchanger (Bronkhorst Controlled Evaporator Mixer) where temperature is set above the dew point of the mixture [fuel (EB) - carrier gas (helium)]. Helium (He) and oxygen flow rates were adjusted by computer-regulated mass flow controllers (RDM 280 Alphagaz and Bronkhorst El-Flow, respectively). The flow lines from the evaporator to the mixing/preheating unit were heated to prevent any inside condensation.

Downstream of the reaction unit, the gaseous flow leaving the reactor passes through a quartz quenching with annular geometry which allows a fast cooling of the reacting mixture and the stopping of any reactions. Thereafter, the condensable (liquid) and non-condensable (gases) products were separated efficiently. Wherefore, the outlet flow was directed toward a trap maintained at liquid nitrogen temperature (under atmospheric pressure) during the time of experiment (10 minutes). The use of helium instead of nitrogen as diluent prevents trapping of the carrier gas and has a negligible effect on the obtained results compared to the use of nitrogen. At the end of this period, the trap was removed after addition of the solvent (acetone) and of an internal standard with a known amount (n-octane), and then progressively heated up around 273 K.

Chapter III Experimental and Kinetic Modeling Study of Ethyl butanoate Oxidation in a Tubular Plug Flow Reactor - From Low to High Temperature under Atmospheric Pressure

Next, a sample of the reacting mixture from the trap was poured into a small vial and then injected by an auto-sampler (ALS104) in an off-line GC/FID (PERICHRON PR2100) for quantification. The column used for the separation was a SGE BP 21 capillary column with nitrogen as carrier gas. The integration of the chromatograms was carried out by the Winilab III 4.6 software that allows slice integration. Calibrations were performed duly by analyzing known mixtures of compounds of the same family and atomic composition as those of the products that were expected to be formed. However, carbon monoxide (CO) and carbon dioxide (CO₂) were measured online by a non-dispersive IR analyzer (Cosma Crystal 300); the measurement ranges were 10%, with an accuracy of 0.01%. The light hydrocarbon (C₁-C₄) were also analyzed online by a GC/FID (Agilent 6850) equipped with a HP-PLOT Q capillary column with helium as carrier gas. The integration of the chromatograms was carried out by the Chem-Station software. Furthermore, oxygen was measured online by GC/TCD equipped with molecular Sieve-5A (PERICHRON PR1250). Calibration was realized by injection of gaseous standard mixtures provided by Air Liquide. Ranges of repeatability (in terms of coefficient of variation), linearity (in terms of R-square of the regression line) and detection limit were 0.1-0.5%, 0.990-0.998, and 1-2 ppm, respectively. Conditions of gas chromatography analyses are detailed in Table AIII.1 (Appendix AIII).

All gases, helium (grade 99.999%) and oxygen (research grade 99.99%) were supplied from Messer France. Ethyl butanoate (purity > 98%), acetone (purity ≥ 99.8%), and n-octane (purity ≥ 98%) were provided by Sigma-Aldrich. All these chemicals were used without further purification.

III.3 Experimental results

Any device used to generate experimental data transmits its specific features to measurements it generates. These features are described in this section, before presenting experimental results in detail.

III.3.1 Theoretical and physical references used for residence time definitions

Two references were used to determine the residence time depending on the way selected for comparing results. This option has been adopted for decoupling the two operating variables, reaction temperature and residence time, despite the existence of a temperature profile within the tubular reactor.

- When the purpose is to achieve a qualitative comparison between the experiments conducted for various operating conditions (reaction temperature, residence time,

Chapter III Experimental and Kinetic Modeling Study of Ethyl butanoate Oxidation in a Tubular Plug Flow Reactor - From Low to High Temperature under Atmospheric Pressure

equivalence ratio, dilution), the standard conditions of temperature and pressure (STP with $T = 273.15$ K and $P = 1$ atm), invariant from one experiment to another, were selected as reference.

- When the purpose is to achieve a quantitative comparison between experimental and simulated results (the latter being obtained through combination of both kinetic and reactor models as described in the following section), a reference close to the actual operating conditions of the reactor was adopted. It corresponds to the reactor pressure (P_R) recorded during measurement of the temperature profile along the tubular reactor and to the mean temperature related to this profile (T_R). It is worth noting that the value experimentally determined for P_R at the inlet of the reactor is assumed to be constant until the outlet.

The reference based on the actual temperature and pressure of the reactor was designated "physical reference" and was used to define a "physical residence time" (τ_{RTP}). In contrast, the reference based on the STP conditions was designated "theoretical reference" and was used to define a "theoretical residence time" (τ_{STP}). Hence, $\tau_{STP} = V_R / Q_{STP}^t$ (similarly $\tau_{RTP} = V_R / Q_{RTP}^t$), where V_R is the reactor volume and Q_{STP}^t (similarly Q_{RTP}^t) is the inlet total volumetric flow rate of fresh reactants in He at STP (similarly at T_R and P_R) conditions. In this work, τ_{STP} was considered as an independent variable taken as reference to compare either experimental results between them or experiments and simulations.

III.3.2 Experimental design features

Two sets of experiments related to ethyl butanoate (EB) oxidation at the steady state were performed. A first set of experiments was conducted at "theoretical residence time" of the fresh gas feed fixed to 0.93 s (STP), with set point temperatures of the oven ranging from 500 to 1200 K, and for various equivalence ratios 0.5, 1.1, and 1.6 in order to investigate fuel-lean, stoichiometric, and fuel-rich mixtures; this was achieved by varying the oxygen initial concentration while maintaining constant the fuel initial concentration to 1.3 mol %. The second set of experiments was conducted for nearly-stoichiometric mixtures (equivalence ratio fixed to 1) at "theoretical residence times" of the fresh gas feed ranging from 0.6 to 1.4 s (STP), and for three set point temperatures of the oven 700 K, 800 K, and 1000 K. The high degree of dilution used (1.3 mol. % of fuel) was selected for limiting temperature gradients inside the tubular reactor and also heat release (no evident flame occurred in the reactor). The operating conditions related to the conducted experiments are summarized in Table III.1.

Chapter III Experimental and Kinetic Modeling Study of Ethyl butanoate Oxidation in a Tubular Plug Flow Reactor - From Low to High Temperature under Atmospheric Pressure

Table III.1: Operating conditions applied for ethyl butanoate oxidation in a tubular plug flow reactor

	Set point T (K) ^a	P (Torr)	ϕ	τ_{STP} (s) ^b	X_{ester}	X_{O_2}	X_{He}	Dilution $\frac{X_{He}}{(X_{O_2} + X_{He})}$
Runs at	450 - 1150	787-986	0.52 ± 0.03	0.93	0.0130	0.2000	0.7870	78.72%
constant	500 - 1200	809-985	1.12 ± 0.03	0.93	0.0130	0.0925	0.8945	89.46%
τ_{STP}	500 - 1200	800-985	1.59 ± 0.03	0.93	0.0130	0.0655	0.9215	92.60%
Runs at	700	845-1010	1.00 ± 0.03	0.65-1.40	0.0130	0.104	0.883	89.46%
constant	800	800-1015	1.00 ± 0.03	0.65-1.40	0.0130	0.104	0.883	89.46%
ϕ	1000	845-1025	1.00 ± 0.03	0.65-1.40	0.0130	0.104	0.883	89.46%

Notes: ^a The set point temperature of the oven is considered here as a reference parameter used for comparing experimental results between them. In contrast, the corresponding temperature profile measured along the tubular reactor was considered for comparing experimental and simulated results. ^b τ_{STP} is the “theoretical residence time” of the feed fresh reactants calculated under standard conditions of temperature and pressure (STP, with T=273 K and P=1 atm).

The detailed experimental data generated in this work for the oxidation of EB in a tubular PFR are reported in Tables AIII.3 and AIII.4 (Appendix AIII). Among the numerous experiments performed, only experiments with satisfactory errors in overall material balance (< 3 % in mass) were selected. Overall, the corresponding carbon balance was found to be better than ± 10 % (hydrogen and oxygen balance could not be evaluated because some species containing hydrogen and oxygen atoms, such as water, were not quantified). As illustration, Table III.2 shows the material balance obtained for two typical operating conditions related to EB oxidation experiments. Concerning the evaluation of the repeatability in the results, it was unfortunately impossible to repeat systematically two or three times all experiments. However, for those made indicate a good reproducibility in the results as shown in Tables AIII.2- AIII.4 through the performed statistical analyses (evaluation of averages, relative errors, and standard deviations).

Chapter III Experimental and Kinetic Modeling Study of Ethyl butanoate Oxidation in a Tubular Plug Flow Reactor - From Low to High Temperature under Atmospheric Pressure

Table III.2: Material Balance given as illustration for two typical operating conditions related to EB oxidation in a tubular PFE (each test condition were duplicated)

$x_{EB}= 0.013, \varphi = 0.52, \tau_{STP} = 0.93 \text{ s, T} = 900 \text{ K}$							
	Inlet of the reactor			Outlet of the reactor			Relative error
	\bar{F}_{EB}^i (g.min ⁻¹)	\bar{F}_{He}^i (g.min ⁻¹)	$\bar{F}_{O_2}^i$ (g.min ⁻¹)	^a \bar{F}^o (g.min ⁻¹)	\bar{F}_{He}^o (g.min ⁻¹)	$\bar{F}_{O_2}^o$ (g.min ⁻¹)	%
Run 1	0.1204	0.2510	0.5103	0.156	0.2510	0.486	1.26
Run 2	0.1204	0.2510	0.5103	0.166	0.2510	0.486	2.36
$x_{EB}= 0.013, \varphi = 0.52, \tau_{STP} = 0.93 \text{ s, T}=1000 \text{ K}$							
	Inlet of the reactor			Outlet of the reactor			Relative error
	\bar{F}_{EB}^i (g.min ⁻¹)	\bar{F}_{He}^i (g.min ⁻¹)	$\bar{F}_{O_2}^i$ (g.min ⁻¹)	^a \bar{F}^o (g.min ⁻¹)	\bar{F}_{He}^o (g.min ⁻¹)	$\bar{F}_{O_2}^o$ (g.min ⁻¹)	%
Run 1	0.1204	0.2510	0.5103	0.461	0.2510	0.200	3.30
Run 2	0.1204	0.2510	0.5103	0.454	0.2510	0.195	2.03

^a \bar{F}^o designates the mass flow rate relative to the liquid and gas products leaving the reactor with the exception of H₂ and O₂.

III.3.3 Temperature profiles along the tubular reactor under the investigated conditions

In order to avoid any wall catalytic reactions between the gas-phase medium and the thermocouple surface (type K, i.e. chromel/alumel), the temperature profiles along the longitudinal axis of the tubular reactor were established with a gas stream of helium where the molar flow was close to that applied during oxidation experiments. Therefore, temperature profiles along the tubular reactor, corresponding to given set points of the oven temperatures, were measured during separate experiments specifically devoted to this purpose. Also, it is noted that due to this procedure, the reactor temperature profiles depend only on the set points of the oven (which is in agreement with some verification tests conducted previously under various operating conditions and having shown that the most significant parameter in temperature profile experimental determination is the set point of the oven). Table AIII.5 gives the experimental temperature profiles obtained (without conducting oxidation) for each set point temperature ranging from 500 to 1200 K. As it can be observed, a temperature measurement was performed along the tubular reactor every centimeter from the inlet to the outlet, representing a total of 56 measuring temperature points. According to previous remarks, these temperature profiles were used for simulations without any modification, whatever the composition of the gas inlet.

III.3.4 Nature of the observed reaction products

Different classes of species were identified during ethyl butanoate (EB) oxidation conducted in the current work: hydrocarbons (C₁-C₄), aldehydes, alcohols, carboxylic acids, together with CO and CO₂. The results of quantification by GC/FID showed that the major intermediate species were ethylene (C₂H₄), butanoic acid (C₃H₇C(O)OH, BA), CO, CO₂, methane (CH₄), acetylene (C₂H₂), and propene (C₃H₆). Unfortunately, water (H₂O), formaldehyde (HCHO), and hydrogen (H₂) which are also supposed to be counted among the major species were not analyzed. The minors species were ethane (C₂H₆), allene (aC₃H₄), propyne (pC₃H₄), 1-butene (1-C₄H₈), 2-butene (2-C₄H₈), 1,3-butadiene (1,3-C₄H₆), acetaldehyde (CH₃CHO), propanal (C₂H₅CHO), acrolein (C₂H₃CHO), and acrylic acid (C₂H₃C(O)OH). Lower amounts of methanol (CH₄OH), ethanol (C₂H₅OH), formic acid (HC(O)OH), propanoic acid (C₂H₅C(O)OH), butanal (C₃H₇CHO), and ethylene oxide (the smallest cyclic ether) were detected by GC/MS analysis. Based on GC/FID and GC/MS analyses, no unsaturated ethyl esters were observed.

Figures III.3-III.5 display the mole fractions of the fuel, intermediate and product species as a function of the set point temperature of the oven considered here as a reference parameter for comparing experimental results between them (and later for comparing experimental and simulated results) at a fixed “theoretical residence time” (0.93 s STP).

As it can be observed (Figures III.3b-III.5b), the formation of ethylene and BA during the low temperature oxidation of EB occurs very early. This unique observation provides evidence for the existence, under the test conditions of this study, of the six-centered unimolecular elimination reaction that was previously suggested for various ethyl ester oxidation (ethyl propanoate [21-23] and EB [25]), in which EB decomposes into BA and ethylene (Figure III.6).

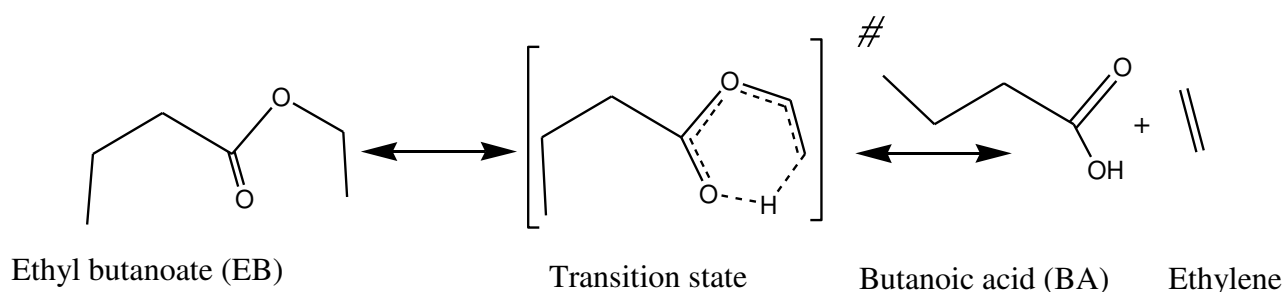


Figure III.6: Six-centered unimolecular elimination reaction for ethyl butanoate.

Chapter III Experimental and Kinetic Modeling Study of Ethyl butanoate Oxidation in a Tubular Plug Flow Reactor - From Low to High Temperature under Atmospheric Pressure

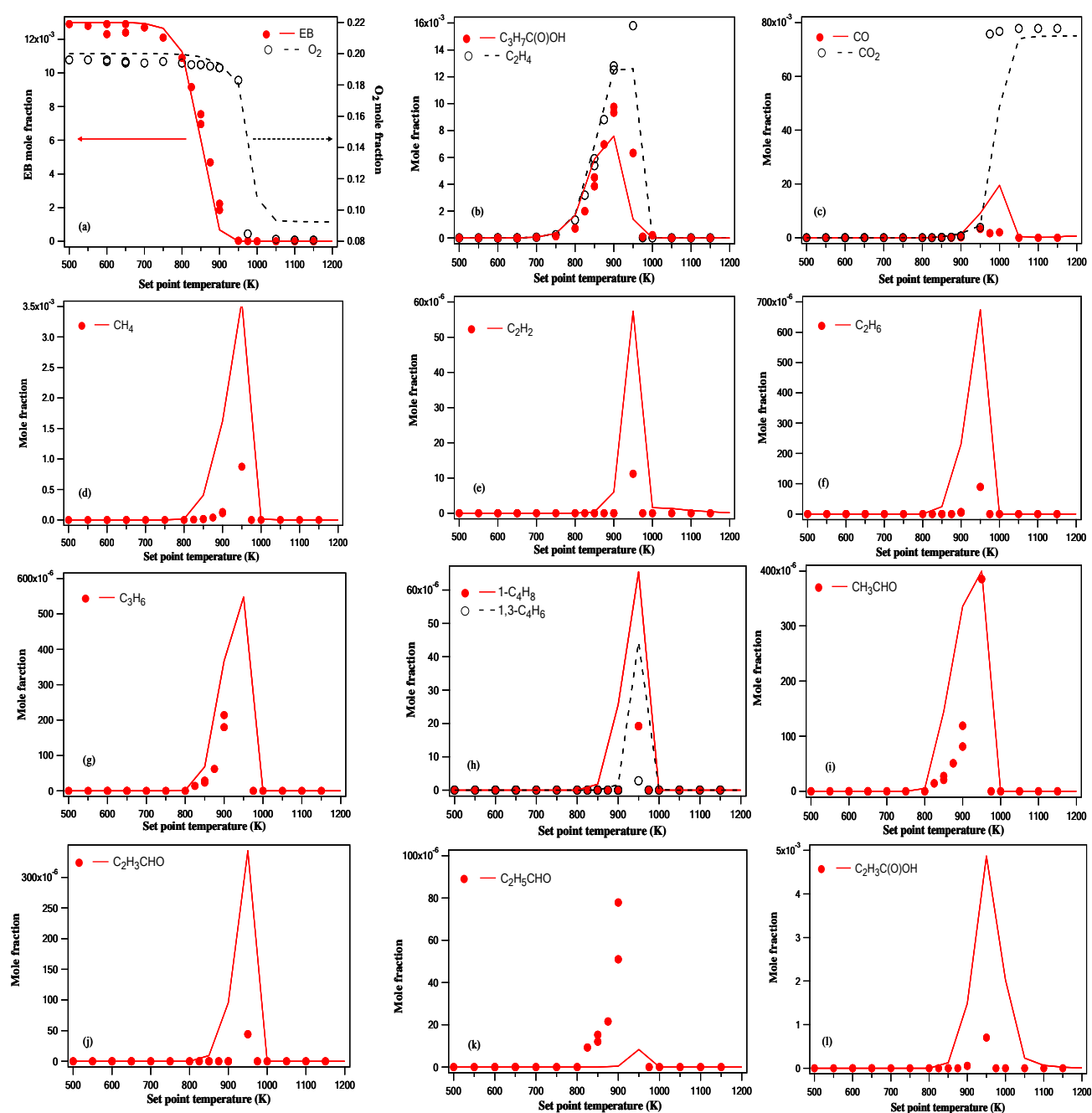


Figure III.3: Oxidation in a tubular plug flow reactor of a 1.3% mixture of ethyl butanoate in helium at 1 atm, $\phi = 0.5$, and $\tau_{STP} = 0.93$ s. Symbols are experimental data and solid lines represent modeling results for (a) EB and O₂, (b) C₂H₄ and C₃H₇C(O)OH, (c) CO and CO₂, (d) CH₄, (e) C₂H₂, (f) C₂H₆, (g) C₃H₆, (h) 1-C₄H₈ and 1,3-C₄H₆, (i) CH₃CHO, (j) C₂H₃CHO, (k) C₂H₅CHO, and (l) C₂H₃C(O)OH.

Chapter III Experimental and Kinetic Modeling Study of Ethyl butanoate Oxidation in a Tubular Plug Flow Reactor - From Low to High Temperature under Atmospheric Pressure

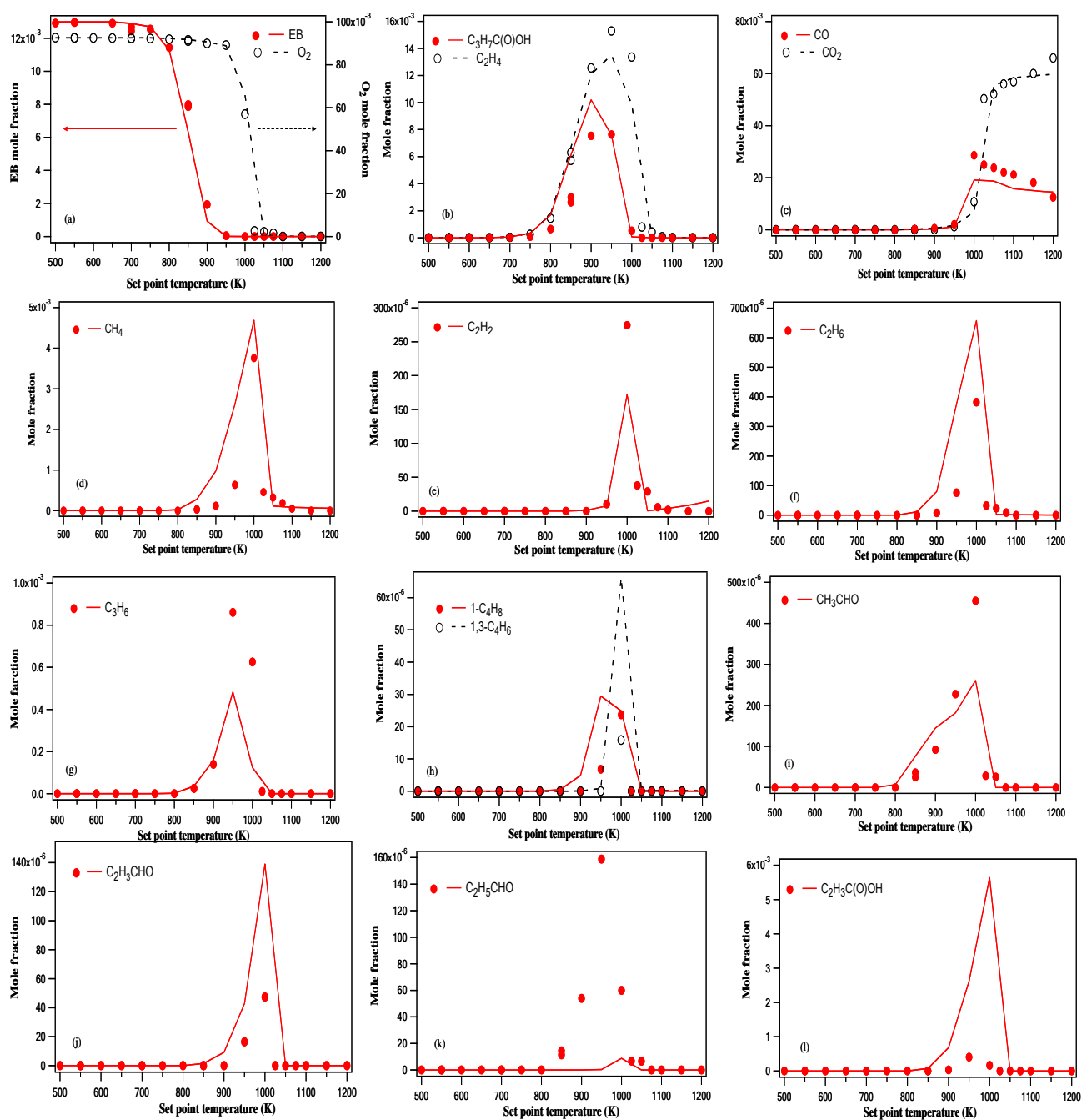


Figure III.4: Oxidation EB in a tubular plug flow reactor of a 1.3% mixture of ethyl butanoate in helium at 1 atm, $\varphi = 1.1$, and $\tau_{STP} = 0.93$ s. Symbols are experimental data and solid lines represent modeling results for (a) EB and O₂, (b) C₂H₄ and C₃H₇C(O)OH, (c) CO and CO₂, (d) CH₄, (e) C₂H₂, (f) C₂H₆, (g) C₃H₆, (h) 1-C₄H₈ and 1,3-C₄H₆, (i) CH₃CHO, (j) C₂H₃CHO, (k) C₂H₅CHO, and (l) C₂H₃C(O)OH.

Chapter III Experimental and Kinetic Modeling Study of Ethyl butanoate Oxidation in a Tubular Plug Flow Reactor - From Low to High Temperature under Atmospheric Pressure

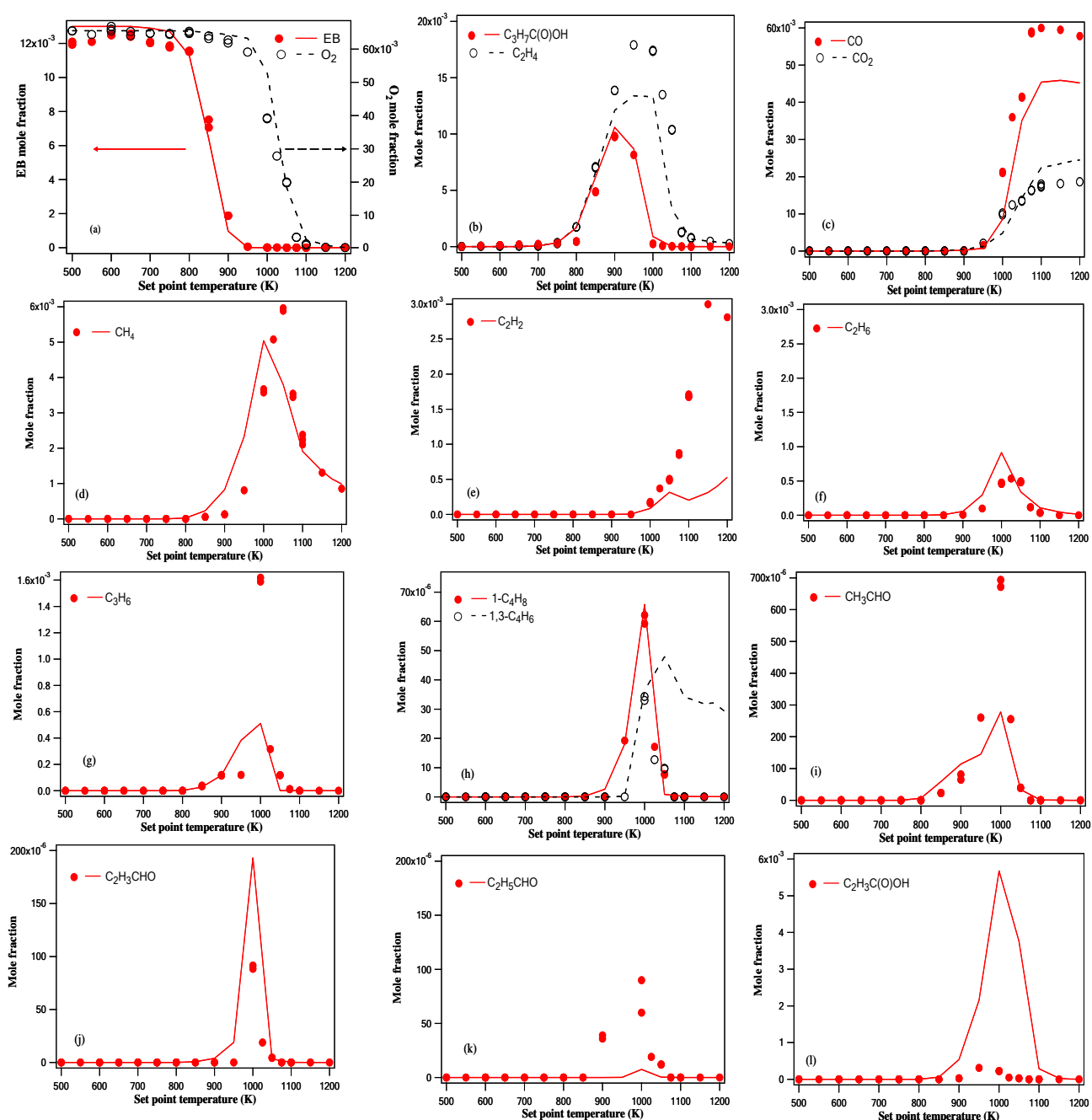


Figure III.5: Oxidation in a tubular plug flow reactor of a 1.3% mixture of ethyl butanoate in helium at 1 atm, $\phi = 1.6$ and $\tau_{STP} = 0.93$ s. Symbols are experimental data and solid lines represent modeling results for (a) EB and O₂, (b) C₂H₄ and C₃H₇C(O)OH, (c) CO and CO₂, (d) CH₄, (e) C₂H₂, (f) C₂H₆, (g) C₃H₆, (h) 1-C₄H₈ and 1,3-C₄H₆, (i) CH₃CHO, (j) C₂H₃CHO, (k) C₂H₅CHO, and (l) C₂H₃C(O)OH.

Chapter III Experimental and Kinetic Modeling Study of Ethyl butanoate Oxidation in a Tubular Plug Flow Reactor - From Low to High Temperature under Atmospheric Pressure

Under the investigated equivalence ratios ($\phi = 0.5, 1.1, \text{ and } 1.6$) EB reactivity reveals to be significant from 800 K, with a complete consumption of EB beyond 950 K. The sharp reactivity of EB in a narrow temperature range is probably due to the occurrence of a thermal runaway further increasing with temperature and thus promoting the highly exothermic oxidation reaction of CO to CO₂. Also, EB oxidation starts at 800 K as well for a fuel-lean mixture (Figure III.3a) as for a fuel-rich mixture (Figure III.5a). Furthermore, high concentration of CO coupled with low concentration of CO₂ was observed at the fuel-rich condition (Figure III.5c) whereas the reverse situation was obtained at the fuel-lean condition (Figure III.3c). As CO is a product of incomplete combustion, this phenomenon is due to O₂ deficit. The fraction of CO₂ resulting from CO oxidation is added to the CO₂ formed by decarboxylation of BA occurring from about 950 K in test conditions (Figure III.4c-III.5c). Also, this result, together with the almost complete consumption of BA at around 1000 K, suggests that decarboxylation of BA should not occur until its aliphatic chain has been largely consumed incorporating the contribution of oxygen in the molecule. Moreover, the increase in equivalence ratio induced no evident effect on the formation of oxygenated intermediate species (such as aldehydes) which are considered as potential pollutants.

Species profiles obtained from the oxidation of stoichiometric mixtures were plotted against “physical residence time” (τ_{RTP}) in Figures III.7-III.8. The graphs were divided into two series according to the temperature range covered. Results obtained at low set point temperatures of the oven (700 and 800 K) are displayed in Figure III.7 whereas those obtained at high set point temperature (1000 K) are displayed in Figure III.8. As can be observed between 700 and 800 K (Figure III.7a), EB conversion increases very slightly with “physical residence time”, in the range investigated (0.3 – 0.8 s). Negligible at 700 K, oxygen consumption starts to become significant only from 800 K, as well as formation of ethylene and BA resulting from the six-centered elimination reaction of EB. In addition, ethylene and BA were the most abundant products observed in the test conditions, which explains that only these two species were represented in this figure. In contrast, for the high set point temperature (1000 K), EB was almost completely consumed at the earliest residence times investigated (0.27 s, Figure III.8a). With the exception of CO and CO₂, formation of most species (both majors, like butyric acid, ethylene, methane, propylene or acrylic acid as minors, like 1-butene, 1,3-butadiene or acetaldehyde) decreased beyond a limit value of the physical residence time located approximately at 0.38 s (Figure III.8b-1) and tended towards zero for some (like BA or acrylic acid, Figure III.8b and III.8l).

Chapter III Experimental and Kinetic Modeling Study of Ethyl butanoate Oxidation in a Tubular Plug Flow Reactor - From Low to High Temperature under Atmospheric Pressure

Summarizing this section, under the conditions studied, no low-temperature reactivity (i.e. NTC behavior) was observed for EB, similarly to MB [22 - 23]. From the results, the main reaction pathway of EB consumption would be the unimolecular decomposition, leading to ethylene and BA, even for fuel-lean mixtures. In addition, BA and ethylene were the major products observed. No ethyl acrylate has been found among the products formed, indicating that few H-abstractions would occur on EB aliphatic main chain. These results show that the main pathway of EB oxidation should rather be of a molecular type than of a radicalar type.

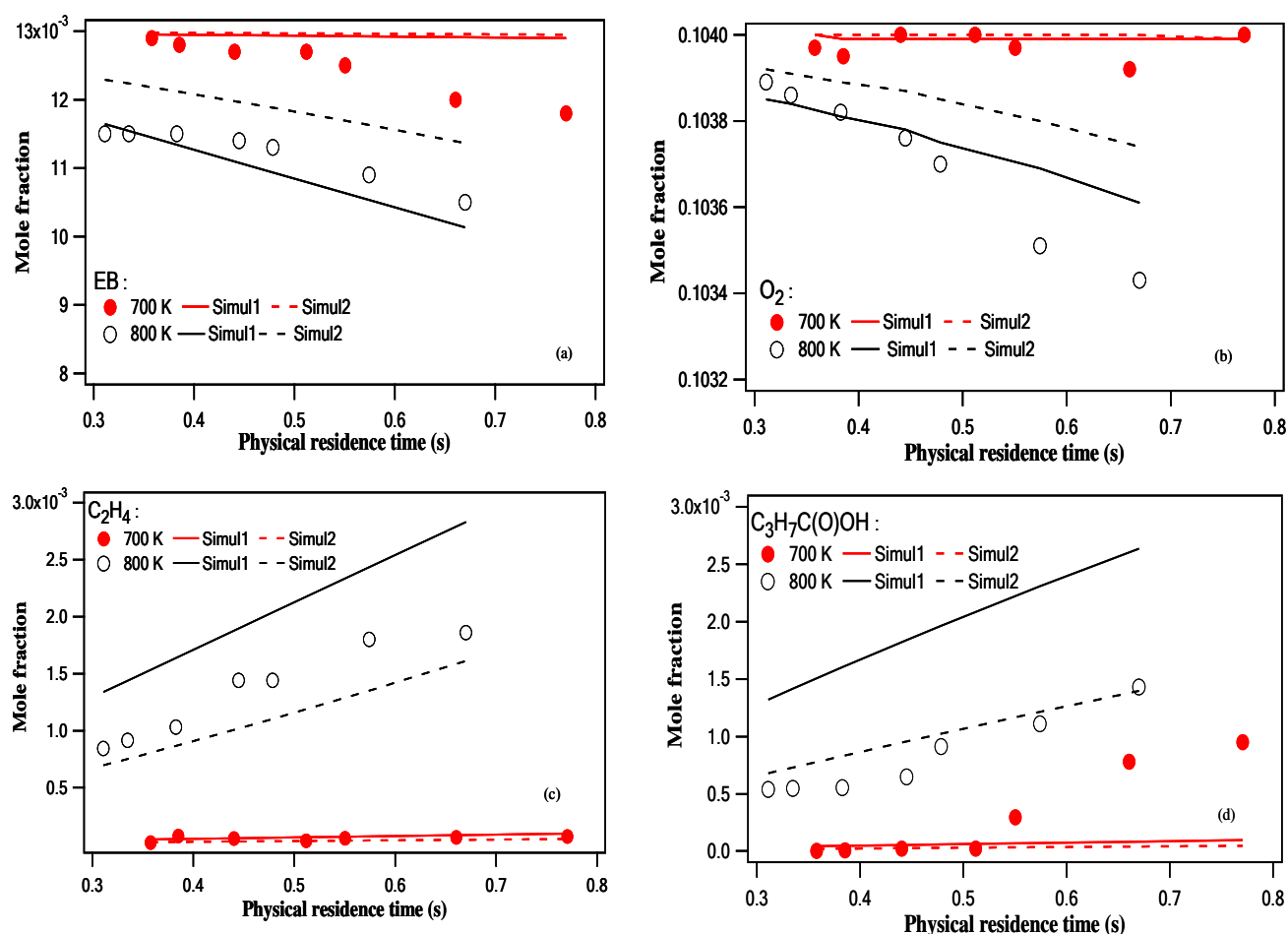


Figure III.7: Oxidation in a tubular plug flow reactor of a 1.3% mixture of ethyl butanoate in helium, at 1 atm, $\phi = 1.0$ and for the set point temperatures 700 and 800 K. Symbols are experimental data whereas the solid lines represent the simulation results obtained without modification of the mechanism [25] (Simul1) and the dotted lines the calculations resulting from multiplying the constant rate of the six-centered unimolecular elimination reaction producing ethylene and butanoic acid from ethyl butanoate by a factor 0.5 (Simul2). (a) EB, (b) O₂, (c) C₂H₄, and (d) C₃H₇C(O)OH.

Chapter III Experimental and Kinetic Modeling Study of Ethyl butanoate Oxidation in a Tubular Plug Flow Reactor - From Low to High Temperature under Atmospheric Pressure

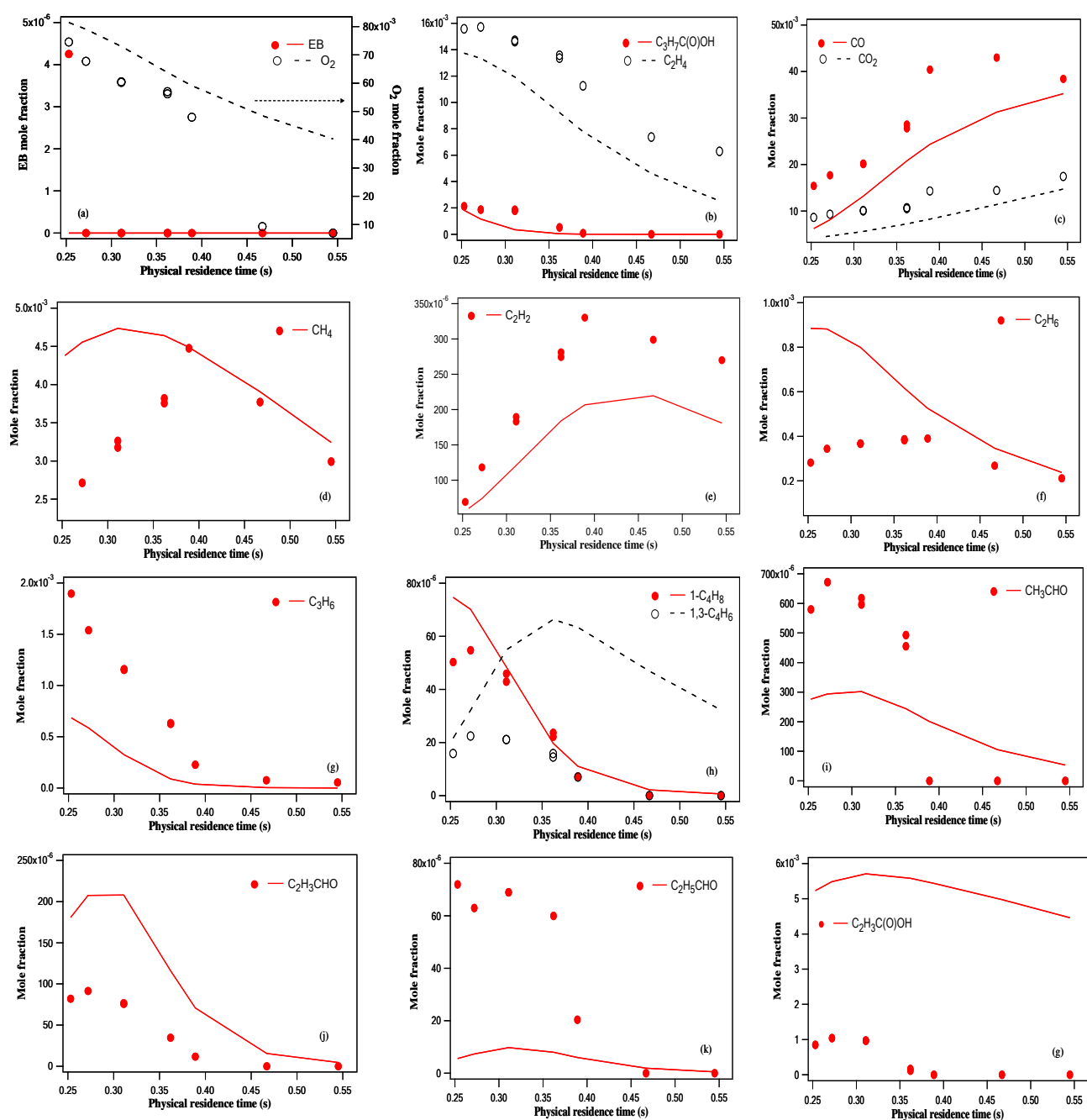


Figure III.8: Oxidation in the plug flow tubular reactor of a 1.3% mixture of ethyl butanoate in He at 1 atm, $\phi = 1.0$, and for the set point temperature 1000 K. Symbols are experimental data and solid lines represent modeling results for (a) EB and O_2 , (b) C_2H_4 and $C_3H_7C(O)OH$, (c) CO and CO_2 , (d) CH_4 , (e) C_2H_2 , (f) C_2H_6 , (g) C_3H_6 , (h) $1-C_4H_8$ and $1,3-C_4H_6$, (i) CH_3CHO , (j) C_2H_3CHO , (k) C_2H_5CHO , and (l) $C_2H_3C(O)OH$.

III.4 Kinetic model

The detailed chemical kinetic mechanism used in this work consists of 117 species and 1035 reactions and was generated from a version of EXGAS software [29] improved for taking into account oxygenated reactants [25, 30-31].

Since the model was described in outline in a previous paper [25], only the primary mechanism, which was not listed in detail, is given here in appendix AIII (Table AIII.6).

The thermodynamic properties for the molecules and radicals were obtained from THERGAS software [32] based on Benson's group additivity method [33] and were stored in the form of NASA polynomial with 14 coefficients, according to the CHEMKIN II formalism [34]. The kinetic data of isomerizations, combinations, and unimolecular decompositions were calculated from KINGAS software [35] based on the thermochemical kinetic methods using the transition state theory or the modified collision theory [33]. The kinetic data, for which the calculation was not possible from KINGAS software [35], were estimated either from correlations based on quantitative structure-reactivity relationships or from quantum calculations.

Overall, the primary and secondary mechanisms for the oxidation of ethyl butanoate (EB) were generated using rules very similar to those described in the case of methyl butanoate (MB) [25]. Since no reactivity was observed below 700 K, the low-temperature chemistry describing the isomerization of alkylperoxyl radicals to hydroperoxyl alkyl radicals was not included. The only significant differences that are characteristic of the mechanism of EB compared to that of MB are two in number: (i) first, the inclusion of the unimolecular elimination reaction leading to the formation of ethylene and butanoic acid (BA) from EB and (ii) second, the secondary reactions of BA for which new rules of generation had to be considered. Concerning the unimolecular elimination specific to ethyl esters, this reaction is favored thanks to the six-membered ring transition state it occurs through (Figure III.6). Blades and Gilderson [36] determined the rate constant of the six-centered unimolecular elimination for ethyl propanoate (EP) producing propanoic acid and ethylene, over the temperature range 780-875 K with the expression $5.20\text{E}+12 \cdot \exp(-48500 \pm 350/RT) \text{ s}^{-1}$. Also, for the same reaction, O'Neal and Benson [37] calculated an activation energy of $48.1 \text{ kcal} \cdot \text{mol}^{-1}$ using the transition state theory and recommended an A-factor of $4.00\text{E}+12 \text{ s}^{-1}$, whereas El Nahas et al. [38] recently proposed an estimation for the activation energy of $50.0 \text{ kcal mol}^{-1}$ on the basis of quantum calculations. Concerning EB six-centered unimolecular decomposition, Kairaitis and Stimson [39] measured an A-factor of $2.00\text{E}+12 \text{ s}^{-1}$ with an activation energy of

Chapter III Experimental and Kinetic Modeling Study of Ethyl butanoate Oxidation in a Tubular Plug Flow Reactor - From Low to High Temperature under Atmospheric Pressure

47.3 kcal·mol⁻¹. These values were adopted in the present mechanism, since they are in agreement with the average rate parameters listed for lighter ethyl esters.

Regarding the secondary reactions of BA, these were automatically generated by considering this intermediate product as an initial reactant and developing a new detailed chemical kinetic sub-mechanism for BA oxidation. The rules of generation of the primary mechanism for the high-temperature oxidation of carboxylic acids are the same as in the case of esters. The unimolecular initiation involving the breaking of the O-H bond was taken into account. Also, only the rate constants used for the abstraction of the H-atom linked to an O-atom by bimolecular oxidation and metatheses were taken equal to those proposed for a tertiary alkylic H-atom [40]. The primary reactions of BA lead to the formation of unsaturated acids (butenoic acids), globalized into a single species (C₄H₆O₂ZB, with Z and B designating occurrences of C=C and COOH in the molecule, respectively) which can react by H-abstractions with small radicals R[•] (H[•], OH[•], HO₂[•], CH₃[•], CH₃OO[•] and C₂H₅[•]) to give RH, CO₂ and allyl radicals.

III.5 Computational simulation results and discussion

The kinetic model used in the computational part of the work was validated against shock tube data performed under high temperatures ranging from 1250 to 2000 K and at moderate pressure (8 atm) [25].

III.5.1 Simulation model of the tubular PFR

The PSR module of CHEMKIN II computer package [34] was used to handle the simulations. Hence, the tubular PFR was modeled by a number of equivalent continuous perfectly stirred tank reactors (ePSR) in series, each uniform in composition, pressure and temperature. While composition of each ePSR is a derived variable (internally computed by CHEMKIN II from the input partial flow rates in each species and their net rate of consumption/production resulting by chemical reactions), pressure and temperature are instead input data to provide. Assuming reasonably that no pressure drop occurred inside the tubular reactor, each ePSR was considered to operate under the same pressure equal to the inlet tubular reactor pressure P_R (measured for each experience). Temperature of each ePSR was attributed according to the temperature profile along the tubular reactor (experimentally determined during specific experiments and considered to be only dependent on the given set point temperature of the oven, Table AIII.5). Moreover, it should be noted that as the temperature profile along the tubular reactor was experimentally determined, the energy balance equations

Chapter III Experimental and Kinetic Modeling Study of Ethyl butanoate Oxidation in a Tubular Plug Flow Reactor - From Low to High Temperature under Atmospheric Pressure

did not need to be solved during simulation of ePSRs-in-series. The walls of the tubular reactor made in quartz were considered non-catalytic and the residence time of the feed material (fresh reactants in He) along each ePSR (τ_{ePSR}) was calculated by: $\tau_{ePSR} = \tau_{RTP} / N_{ePSR}$, where τ_{RTP} is the “physical residence time” of the feed material along the actual tubular PFR (section III.3.1) and N_{ePSR} is the number of ePSRs used for performing simulation. It should be mentioned that an error margin of 5 K was accepted in the calculations, since this temperature change was observed to be too low for inducing significant changes in the rate constant of the reactions. A constant value $N_{ePSR} = 56$ was chosen according to the number of measurement points used to describe each of the temperature profiles (Table AIII.5). Also, $N_{ePSR} = 56$ corresponds to the lower limit value of the Péclet number evaluated under the operating conditions of each experiment $Pe_{RTP} = 2(N_{ePSR} - 1) = 110$.

III.5.2 Evaluation of the kinetic model performance

Performances of the kinetic model developed for ethyl butanoate (EB) oxidation [25] are displayed in Figures III.3-III.5 and III.7-III.8. Hence, comparison between experiments and simulations relating to EB oxidation in a PFR are displayed, for the three equivalence ratios investigated here ($\phi = 0.5, 1.1, \text{ and } 1.6$), versus the set point temperature of the oven in Figures III.3-III.5 (for a fixed $\tau_{STP} = 0.93$ s), but versus the “physical residence time” in Figures III.7-III.8 (for the set point temperatures 700 and 800 K in Figure III.7, and 1000 K in Figure III.8). As can be seen on Figures III.3-III.5, the model captures overall the main features of EB oxidation chemistry. The main trends vs. temperature are satisfactorily predicted, both in relation to EB reactivity and O_2 consumption than for the formation of the most abundant species, such as the primary products, ethylene, BA, or other products like CO, CO_2 , and methane (Figures III.3a-d to III.5a-d). It is only for the oxidation of fuel-rich mixtures conducted at the highest temperatures (>1000 K) that the model slightly overestimates the molar fraction of CO_2 and underestimates the molar fraction of CO. In addition, it can be observed in the case of the fuel-lean mixture (Figure III.3c) that the formation of CO_2 seems to occur according to calculations under higher temperatures than observed experimentally. However, this phenomenon is actually model-independent and is likely due to deviations between the temperature profile experimentally determined in this work in inert gas medium (i.e. with helium, section III.3.3) and the temperature profile actually occurring along the tubular reactor when conducting oxidation. Probably the helium dilution applied to the reaction mixture is not high enough to compensate for the exothermicity of the reaction which increases

Chapter III Experimental and Kinetic Modeling Study of Ethyl butanoate Oxidation in a Tubular Plug Flow Reactor - From Low to High Temperature under Atmospheric Pressure

further by increasing the concentration of O₂ to operate under fuel-lean conditions. As a result, the input data of the temperature profile required for simulating the tubular reactor by CHEMKIN II [34] might be, for these fuel-lean conditions, under-evaluated because of the procedure used for its experimental determination. Nevertheless, discrepancies exist for some products which are for most of them minor species (1,3-butadiene, propanal, acrolein, and acrylic acid) with the exception of acetylene and propene. Figures III.3e-1 to III.5e-1 show that concentration profiles of acrylic acid, acrolein, and 1,3-butadiene are over-predicted by the kinetic model, whereas those of propanal, propene, and acetylene are under-predicted (for propanal, this occurs for the three equivalence ratios while for acetylene, this occurs at temperatures higher than 1000 K and at fuel-rich conditions, and for propene at temperatures higher than 900 K and at nearly-stoichiometric and fuel-rich conditions).

As can be seen in Figure III.7, the kinetic model predicts satisfactorily the consumption of EB and slightly less the one of O₂ over the entire range of residence time, for both temperatures 700 and 800 K. However, ethylene and BA concentrations are over-predicted, especially at 800 K. As mentioned previously, these products are formed from EB unimolecular elimination reaction via a six-centered transition state (Figure III.6) for which a single experimental determination of the rate constant was found in the literature [39] (section III.4). In addition, it was observed that decreasing this rate constant by a factor two (A-factor value changed from 2.0E+12 [39] to 1.0E+12, which is of the order of magnitude of the experimental accuracy for this variable) led to improve the model performances, particularly for stoichiometric conditions, with low set point temperature (700-800 K) and “physical residence times” ranging from 0.3 to 0.75 s. Specifically, this change leads to a decrease of the predicted concentrations of ethylene and butanoic acid by approximately a factor two (curves in dotted lines on Figures III.7c-d). The results obtained at higher temperature (set point temperature of the oven: 1000 K, Figure III.8) show that the concentration profiles of the major species (EB, O₂, BA, C₂H₄, CO, CO₂, and CH₄) are predicted with significant accuracy, the main discrepancy in agreement between model and experiment occurring for the minor species at the lowest “physical residence times”.

Results displayed in figures III.3-III.5 and III.7-III.8, and those reported in a previous work [25], indicate that the kinetic model used in this work is appropriate for the simulation of EB oxidation over a wide temperature range (800-2000 K). Consequently, it can be used with some confidence to assess formation of pollutants for various engine operating conditions and inlet gas compositions.

III.5.3 Reaction flux analysis

In an attempt to better understand the oxidation of ethyl butanoate (EB) under tubular PFR conditions, a reaction flux analysis, based on the computation of consumption rate of species, was carried out using both fuel-rich ($\varphi=1.6$) and nearly-stoichiometric ($\varphi=1.1$) mixtures of 1.3% EB, at 1 atm, for a 0.93 s (STP) residence time, and at a set point temperature of the oven of 900 K. For these conditions, the corresponding conversions of EB computed along the tubular PFR are displayed in Figure III.9 in terms of the axial coordinate of the tubular PFR. The experimental temperature profile measured for the set point of the oven 900 K was also plotted on the illustration. As it can be observed, very similar conversions of EB are computed for all equivalence ratios of study. This result shows that the model predicts a consumption of EB occurring mainly through a molecular reaction path than through a radicalar reaction path, which is in agreement with experimental observations previously commented (section III.3.4).

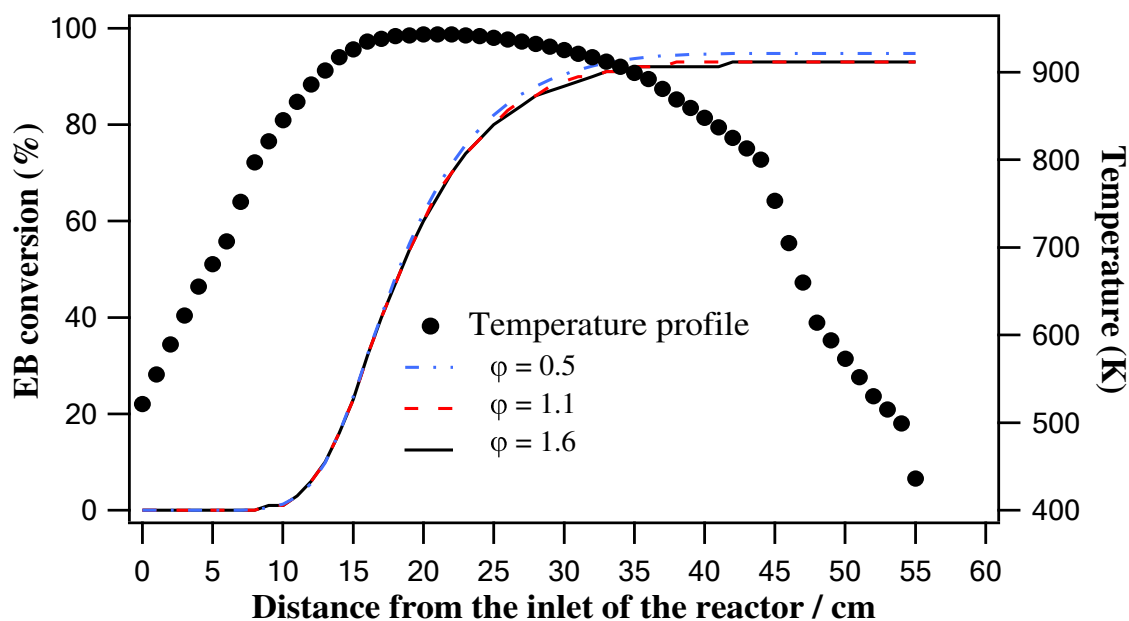


Figure III.9: Conversion of ethyl butanoate (EB) computed during oxidation of a 1.3% mixture of EB in helium and various equivalence ratios ($\varphi = 0.5, 1.1, \text{ and } 1.6$) versus axial coordinate of the tubular plug flow reactor (oven set point temperature: 900 K).

The decomposition pathways of EB, resulting from the reaction flux analysis, was depicted for two pre-defined axial coordinates z of the tubular PFR, i.e. $z_1/\text{cm} = 21$ and $z_2/\text{cm} = 44$ (distances from the inlet of the tubular reactor). These PFR coordinates were chosen

Chapter III Experimental and Kinetic Modeling Study of Ethyl butanoate Oxidation in a Tubular Plug Flow Reactor - From Low to High Temperature under Atmospheric Pressure

because their corresponding temperatures, respectively 943 and 800 K, enclose the set point temperature of the oven, 900 K, selected for performing the reaction flux analysis.

Figure III.10 shows the decomposition pathways of EB in the PFR fed under nearly-stoichiometric conditions ($\varphi = 1.1$), on Figure III.10a for the axial coordinate z_1 (thus at high temperature and for a moderate conversion of EB, i.e. 943 K and 65% conversion) and on Figure III.10b for the axial coordinate z_2 (thus at moderate temperature and for a high conversion of EB, i.e. 800 K and 93% conversion). The values over the arrows indicate the percentage of the parent species forming the daughter species.

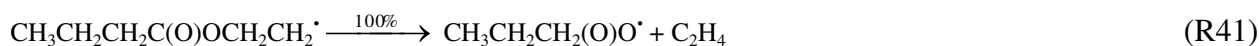
Also, in the equations below, only those related to reactions belonging to the primary mechanism were referenced according to Table AIII.6.

Moreover, “oxidation” designates in the following addition reaction of O_2 yielding HO_2^\bullet and the conjugated alkene.

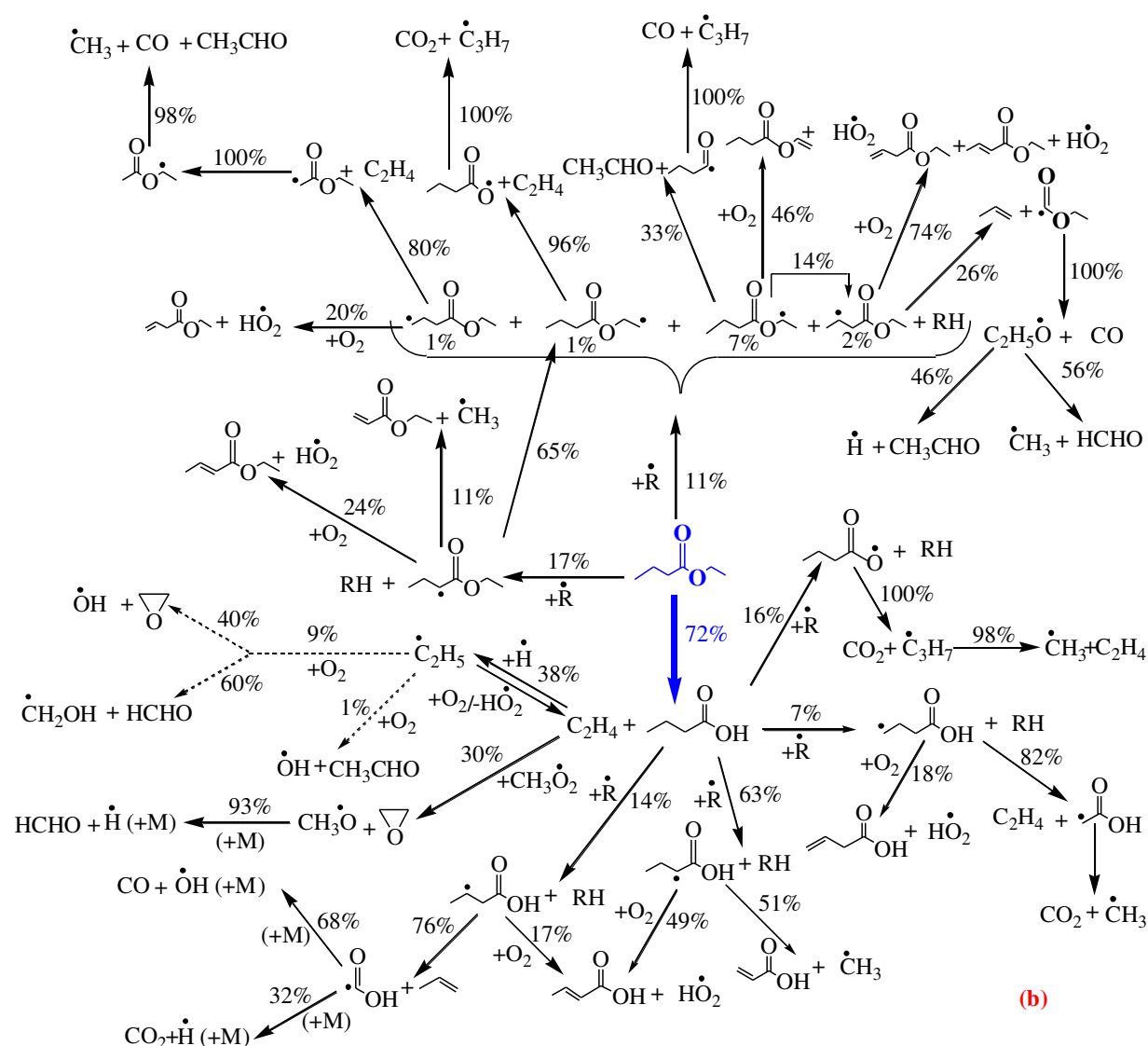
At 943 K and for 65% conversion of EB (Figure III.10a), nearly all of EB reacts through a six-centered unimolecular elimination channel (98%) to form the two major intermediates, ethylene (C_2H_4) and butanoic acid (BA, $C_3H_7C(O)OH$) (R1). The remainder of the fuel undergoes H-abstraction with $^\bullet CH_3$ from the C-H bond in position α to the carbonyl group (the weakest C-H bond in the molecule, Figure III.1) to form the fuel-radical species $CH_3CH_2^\bullet CHC(O)OC_2H_5$ (R123).



Then, the larger amount of this fuel-radical species undergoes isomerization through an internal 1,5-H-atom transfer (83%) to form another EB-radical species $CH_3CH_2CH_2C(O)OCH_2CH_2^\bullet$ (-R26) which in turn decomposes to produce $CH_3CH_2CH_2(O)O^\bullet$ and C_2H_4 (R41):



Chapter III Experimental and Kinetic Modeling Study of Ethyl butanoate Oxidation in a Tubular Plug Flow Reactor - From Low to High Temperature under Atmospheric Pressure



The remaining amount of the fuel-radical species $CH_3CH_2\dot{C}HC(O)OC_2H_5$ is then consumed by β -scission (15%) leading to \dot{C}_2H_5 radical and ethyl acrylate (R47) and by oxidation (2%) to form \dot{H}_2O_2 and ethyl crotonate (ethyl 2-butenoate) (R77):



Butanoic acid (BA) is almost entirely consumed by H-abstraction with \dot{H} , \dot{OH} , \dot{HO}_2 and \dot{C}_2H_5 radicals producing the four BA-radicals $CH_3CH_2\dot{C}HC(O)OH$, $\dot{C}_2H_5\dot{C}HC(O)OH$, $\dot{C}_2H_4CH_2C(O)OH$, and $\dot{C}_2H_3CH_2C(O)OH$:



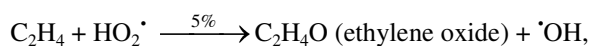
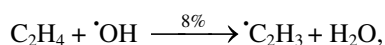
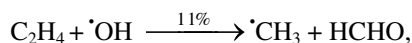
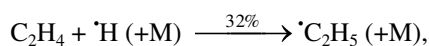
Chapter III Experimental and Kinetic Modeling Study of Ethyl butanoate Oxidation in a Tubular Plug Flow Reactor - From Low to High Temperature under Atmospheric Pressure



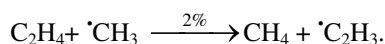
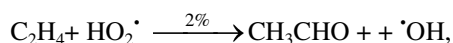
The remaining 2% of BA undergoes a thermal decomposition reaction leading to the formation of $\cdot\text{CH}_2\text{C}(\text{O})\text{OH}$ and $\cdot\text{C}_2\text{H}_5$ radicals. $\cdot\text{CH}_2\text{C}(\text{O})\text{OH}$ radical decomposes completely to form CO_2 and $\cdot\text{CH}_3$ radical.

Regarding now BA-radicals, these are mainly converted through β -scissions. $\text{CH}_3\text{CH}_2\text{CH}_2(\text{O})\text{O}\cdot$ is completely decomposed to give CO_2 and $\cdot\text{C}_3\text{H}_7$ radical which contributes to ethylene formation. $\text{C}_2\text{H}_5\cdot\text{CHC}(\text{O})\text{OH}$ (which is a resonance stabilized radical as it can be written in the form $\text{CH}_3\text{CH}=\text{CO}\cdot\text{OH}$) contributes for 88% to the acrylic acid (propenoic acid) formation. This radical also allows the formation of crotonic acid (2-butenic acid) via oxidation or β -scission of a C-H bond. The importance of these two reactions is 9% and 3%, respectively. The other two BA-radical species, i.e. $\cdot\text{CH}_2\text{C}_2\text{H}_4\text{C}(\text{O})\text{OH}$ and $\text{CH}_3\cdot\text{CHCH}_2\text{C}(\text{O})\text{OH}$, decompose by β -scission (96%) to give respectively, ethylene plus $\cdot\text{CH}_2\text{C}(\text{O})\text{OH}$ radical, and propene plus $\cdot\text{C}(\text{O})\text{OH}$ radical. The radicals in turn produce carbon monoxide and carbon dioxide, plus $\cdot\text{OH}$, $\cdot\text{H}$ and $\cdot\text{CH}_3$ radicals.

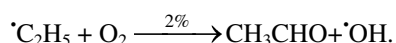
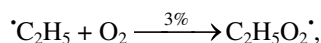
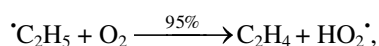
Formation of ethylene, occurring partly from BA-radicals but mainly through the six-centered unimolecular elimination from EB, enhances the C_2 oxidation channels. Ethylene is mostly consumed by additions according to:



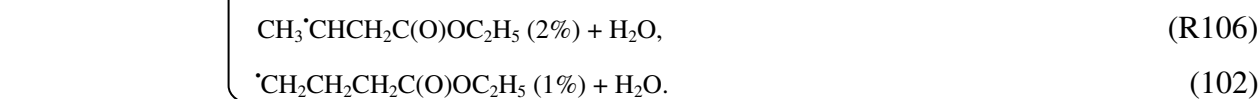
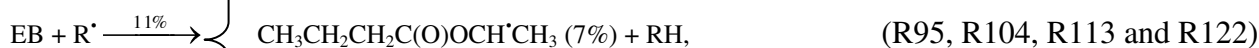
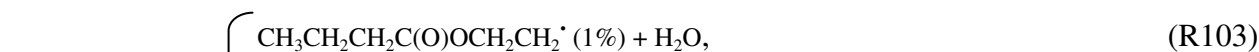
Chapter III Experimental and Kinetic Modeling Study of Ethyl butanoate Oxidation in a Tubular Plug Flow Reactor - From Low to High Temperature under Atmospheric Pressure



Ethyl radical formed from ethylene oxidation decomposes often at high temperature (1370 K) [25] by β -scission giving ethylene and $\cdot\text{H}$ radical, but under the present conditions it reacts entirely with molecular oxygen to form again ethylene (95%), acetaldehyde (2%), formaldehyde (2%), and ethylene oxide (1%).



At 800 K and for 93% conversion of EB ($\varphi = 1.1$, Figure 10b), the main consumption pathway of EB is still the six-centered unimolecular elimination producing BA and ethylene. However, this molecular reaction has now a smaller contribution (72% of EB consumption against 98% at 943 K) to the benefit of H-abstractions by small radicals ($\cdot\text{OH}$, $\cdot\text{H}$, $\cdot\text{CH}_3$, and HO_2^\cdot) producing thus the five possible EB-radical species:



with $\text{R}^\cdot = \cdot\text{H}$, $\cdot\text{OH}$, $\cdot\text{CH}_3$, or HO_2^\cdot .

The EB-radical species formed predominantly, i.e. $\text{CH}_3\text{CH}_2\cdot\text{CHC}(\text{O})\text{OC}_2\text{H}_5$ with the active site on the α -carbon of the carbonyl group (17%), undergoes then three very different reaction pathways. The most dominant channel is an isomerization into another EB-radical species $\text{C}_3\text{H}_7\text{C}(\text{O})\text{OCH}_2\text{CH}_2^\cdot$ via internal 1,5-H-atom transfer (65%). The second rank channel is an oxidation yielding HO_2^\cdot and ethyl crotonate (24%) whereas the third and last channel is a β -scission leading to the formation of ethyl acrylate and $\cdot\text{CH}_3$ radical (11%). Regarding the EB-radical $\text{C}_3\text{H}_7\text{C}(\text{O})\text{OCH}_2\text{CH}_2^\cdot$, this species almost entirely undergoes β -scission to produce ethylene and $\text{C}_3\text{H}_7\text{C}(\text{O})\text{O}^\cdot$ radical which in turn decomposes for yielding ultimately CO_2 and $\text{C}_3\text{H}_7^\cdot$ radical. Concerning the EB-radical $\cdot\text{CH}_2\text{C}_2\text{H}_5\text{C}(\text{O})\text{OC}_2\text{H}_5$, this species partially undergoes oxidation (20%) yielding HO_2^\cdot and ethyl 3-butenate, while the main channel of consumption is β -scission (80%) yielding ethylene and $\cdot\text{CH}_2\text{C}(\text{O})\text{OC}_2\text{H}_5$ radical which

Chapter III Experimental and Kinetic Modeling Study of Ethyl butanoate Oxidation in a Tubular Plug Flow Reactor - From Low to High Temperature under Atmospheric Pressure

isomerizes into $\text{CH}_3\text{C}(\text{O})\text{OCH}^*\text{CH}_3$ and in turn decomposes to form acetaldehyde, CO and $^*\text{CH}_3$ radical. The two last EB-radicals not yet described, i.e. $\text{C}_3\text{H}_7\text{C}(\text{O})\text{OCH}^*\text{CH}_3$ and $\text{CH}_3\text{CH}^*\text{CH}_2\text{C}(\text{O})\text{OC}_2\text{H}_5$, are linked together. Indeed, the first radical $\text{C}_3\text{H}_7\text{C}(\text{O})\text{OCH}^*\text{CH}_3$ isomerizes into the second $\text{CH}_3\text{CH}^*\text{CH}_2\text{C}(\text{O})\text{OC}_2\text{H}_5$, via 1,5-H-atom transfer. This one in turn undergoes mainly an oxidation (74%) to produce HO_2^* and again ethyl 3-butenate and 2-butenate, and to a lesser extent a β -scission (26%) to produce ultimately propene, CO, acetaldehyde, and formaldehyde as molecules, $^*\text{H}$ and $^*\text{CH}_3$ as radical species. Finally, 33% of the radical $\text{C}_3\text{H}_7\text{C}(\text{O})\text{OCH}^*\text{CH}_3$ yields acetaldehyde and butionyl radical ($\text{C}_3\text{H}_7\text{C}^*(\text{O})$) which in turn decomposes to give ultimately CO and propyl radical while 46% undergoes oxidation to produce HO_2^* and the vinyl butanoate $\text{C}_3\text{H}_7\text{C}(\text{O})\text{OCH}=\text{CH}_2$. On the other hand, BA, ethylene and their products follow almost similar channels of consumption as previously at higher temperature (943 K, $z_1/\text{cm} = 21$, Figure 10a); the only difference lies in the relative contributions of the reaction paths.

Reaction flux analysis performed under fuel-rich conditions ($\varphi = 1.6$), for both temperatures 943 K (65% conversion of EB, $z_1/\text{cm} = 21$) and 800 K (93% conversion of EB, $z_2/\text{cm} = 44$) produced very similar consumption pathways to those obtained under nearly-stoichiometric conditions ($\varphi = 1.1$). While, for both equivalence ratios ($\varphi = 1.6$ or 1.1), the relative contributions of the reaction paths were strictly identical at the highest temperature 943 K ($z_1/\text{cm} = 21$), small differences were observed at 800 K ($z_2/\text{cm} = 44$) for the rates of consumption of EB. Particularly, at 800 K from $\varphi = 1.1$ to $\varphi = 1.6$, the importance of the channel related to the six-centered elimination leading to the formation of BA and ethylene increased from 72 to 77%, whereas the rate of H-abstractions by small radicals ($^*\text{H}$, $^*\text{OH}$, $^*\text{CH}_3$, and HO_2^*) decreased by almost a factor 2, from 11 to 6%. This observation is in agreement with the results obtained by Hakka et al. [25] according to which importance of EB elimination reaction into BA and ethylene slightly increases when equivalence ratio increases.

III.5.4 Sensitivity analysis

A sensitivity analysis was performed on the kinetic model to elucidate the important reaction pathways for ethyl butanoate (EB) under tubular PFR conditions. The first order sensitivity coefficients of the EB mole fractions were computed with respect to reaction rates. A negative sensitivity coefficient indicates that an increase in the forward reaction rate will decrease the EB concentration implying that this reaction promotes reactivity. However, a positive sensitivity coefficient implies an increase of EB concentration indicating a decrease in

Chapter III Experimental and Kinetic Modeling Study of Ethyl butanoate Oxidation in a Tubular Plug Flow Reactor - From Low to High Temperature under Atmospheric Pressure

reactivity. The sensitivity analysis was carried out at 943 K and 800 K (corresponding to the PFR axial coordinates $z_1/\text{cm} = 21$ and $z_2/\text{cm} = 44$, respectively, and a set point temperature of 900 K) using fuel-lean, nearly-stoichiometric, and fuel-rich mixtures ($\varphi = 0.5, 1.1, \text{ and } 1.6$, respectively). As it is going to be seen, under these conditions, concentration of EB is actually globally sensitive to a limited number of reactions which involve in addition simple intermediates.

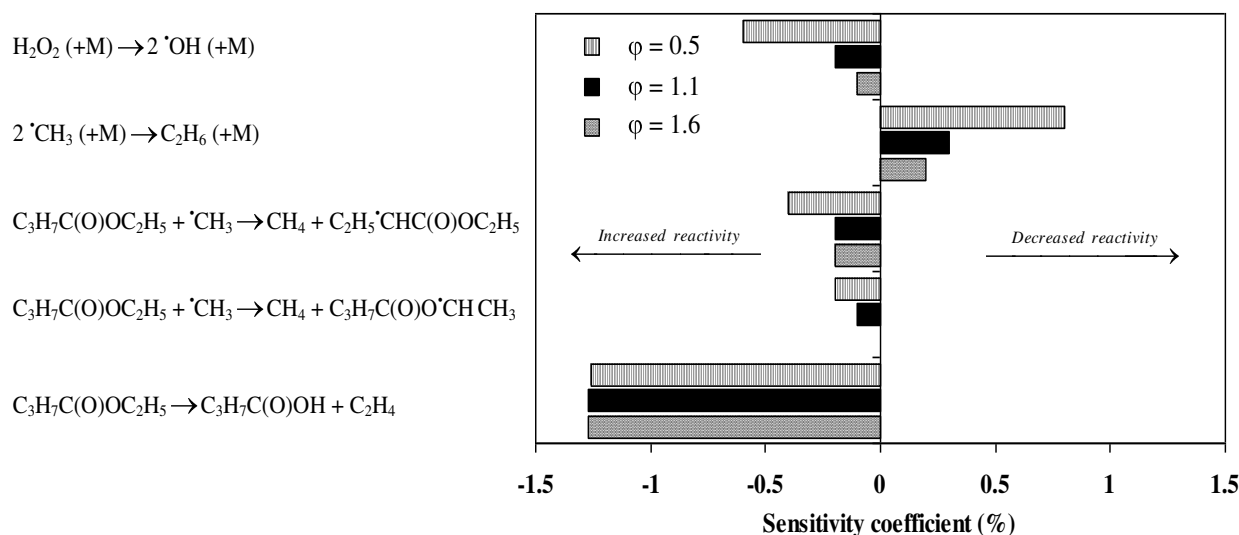
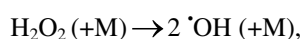


Figure III.11: First order normalized sensitivity coefficient computed for a 1.3% mixture of ethyl butanoate (EB) in helium at three equivalence ratios ($\varphi = 0.5, 1, \text{ and } 1.4$) and $P = 1$ atm. Results are shown for a single axial coordinate (z) of the tubular reactor and for the temperature profile related to set point of the oven 900 K, thus at 943 K ($z_1/\text{cm} = 21$) corresponding to 65% conversion of EB. For a clearer graphical representation, the sensitivity coefficient of the six-centered unimolecular decomposition has been divided by a factor ten.

Results depicted in Figure III.11 show that at 943 K and for the three equivalence ratios, concentration of EB is mainly sensitive to the six-centered unimolecular elimination involving ethylene and BA. Increasing the rate constants of this reaction will accelerate EB consumption, and thus, will involve an overall increase in reactivity. This result is in agreement with the observation made previously when decreasing the rate constant of EB elimination reaction by a factor 2, which had the effect of diminishing EB consumption and thus BA and ethylene production too (Figure III.7). The computed EB conversions reported vs. the axial coordinate of the tubular reactor for the three equivalence ratios of study ($\varphi = 0.5, 1.1, \text{ and } 1.6$) also

Chapter III Experimental and Kinetic Modeling Study of Ethyl butanoate Oxidation in a Tubular Plug Flow Reactor - From Low to High Temperature under Atmospheric Pressure

confirm this result by showing three curves almost identical (Figure III.9). Hence, under these conditions, EB concentration is much less sensitive to H-abstraction by $\cdot\text{CH}_3$, although this channel leads to the formation of the predominant EB-radical species, i.e. $\text{C}_2\text{H}_5\cdot\text{CHC}(\text{O})\text{OC}_2\text{H}_5$. Nevertheless, this reaction becomes a little more important under fuel-lean conditions ($\varphi = 0.5$) because of the slight global increase of EB consumption via radical channels when increasing O_2 concentration in the medium under high temperature. In addition, still at fuel-lean conditions, EB concentration becomes sensitive to other processes involving hydroxyl radicals, like:



which increases thus the global reactivity of the system by producing two very reactive radicals (here $\cdot\text{OH}$ species). On the other hand, the combination of the reactive methyl radical $\cdot\text{CH}_3$ yielding ethane has the largest positive sensitivity coefficient, which decreases the global reactivity of the system.

Results of the sensitivity analysis performed at 800 K led to the observation that the six-centered unimolecular elimination from EB producing BA and ethylene is the single important reaction controlling EB consumption. This result is probably due to the fact that under these conditions the reaction mixture which reaches the last quarter of the reactor ($z_2/\text{cm} = 44$) has accumulated a large population of radical species and has now a fuel almost entirely consumed (93% conversion of EB). In such circumstances, sensitivity analysis does not provide meaningful information.

III.6 Conclusion

Oxidation of ethyl butanoate (EB), with a molecular formula of $\text{C}_6\text{H}_{12}\text{O}_2$, was studied in a tubular plug flow reactor (PFR) at atmospheric pressure, temperature conditions below than 1300 K, and varying fuel/oxygen equivalence ratios. Molecular species concentration profiles were obtained by gas chromatography (GC/TCD-FID) and IR analysis. The temperature profiles were established using a type-K thermocouple. To reproduce these results by simulations using the PSR module of CHEMKIN II computer package [34], a recently improved version of EXGAS software was first used for generating the oxidation model of ethyl butanoate (EB) [25]. The parametric study indicated that a significant conversion of EB occur in the 900-1000 K range, promoted by the six-centered unimolecular elimination reaction leading to ethylene and butanoic acid formations. In addition, the variables involving significant changes in mole fractions of the species formed during EB oxidation in tubular PFR are: primarily the ester/ O_2 ratio in the feed material, together with the residence time and the

Chapter III Experimental and Kinetic Modeling Study of Ethyl butanoate Oxidation in a Tubular Plug Flow Reactor - From Low to High Temperature under Atmospheric Pressure

temperature profile of the tubular PFR. The obtained results also show that EB does not exhibit NTC behavior. Therefore, EB is not an ideal surrogate molecule for a detailed study of biodiesel combustion, but should rather be regarded as a suitable model molecule for gaining insight into the oxidation chemistry of the ethyl ester functional group.

Overall, the proposed detailed chemical kinetic model [25] is in good agreement with experiments, which provides additional arguments to suggest that most resulting reaction pathways, together with kinetic and thermochemical data selected are reliable. This kinetic model of EB oxidation predicts accurately the pollutant emissions (CO, CO₂, HC...) and leads to a better knowledge of the effect of the ethyl ester functional group on combustion in diesel engine.

III.7 References

- [1] S.A. Basha, K.R. Gopal, S. Jebaraj, A review on biodiesel production, combustion, emissions and performance, *Renewable and Sustainable Energy Reviews* 13 (2009) 1628-1634.
- [2] A.K. Agarwal, Biofuels (alcohols and biodiesel) applications as fuels for internal combustion engines, *Progress in Energy and Combustion Science* 33 (2007) 233-271.
- [3] M. Lapuerta, J.M. Herreros, L.L. Lyons, R. García-Contreras, Y. Briceño, Effect of the alcohol type used in the production of waste cooking oil biodiesel on diesel performance and emissions, *Fuel* 87 (2008) 3161-3169.
- [4] B. Baiju, M.K. Naik, L.M. Das, A comparative evaluation of compression ignition engine characteristics using methyl and ethyl esters of Karanja oil, *Renewable Energy* 34 (2009) 1616-1621.
- [5] M.S. Grabowski and R.L. McCormick, Combustion of fat and vegetable oil derived fuels in diesel engines, *Progress in Energy and Combustion Science* 24 (1998) 125-164.
- [6] R.L. McCormick, T.L. Alleman, M.S. Graboski, A.M. Herring, K.S. Tyson, Impact of biodiesel source material and chemical structure on emissions of criteria pollutants from a heavy-duty engine, *Environmental Science and Technology*, 35 (2001) 1742-1747.
- [7] J.P. Szybist, S.R. Kirby, A.L. Boehman, NO_x Emissions of Alternative Diesel Fuels: A Comparative Analysis of Biodiesel and FT Diesel, *Energy Fuels* 19 (2005) 1484–1492.
- [8] Y. Zhang, A.L. Boehman, Impact of biodiesel on NO_x emissions in a common rail direct injection diesel engine, *Energy & Fuels* 21 (2007) 2003-2012.
- [9] G. Knothe, C.A. Sharp, T.W. Ryan, Exhaust emissions of biodiesel, petrodiesel, neat methyl esters, and alkanes in a new technology engine, *Energy & Fuels* 20 (2006) 403-408
- [10] C.L. Peterson, D.L. Reece, J.C. Thompson, S. M. Beck, C. Chase, Ethyl ester of rapeseed used as a biodiesel fuel-a case study, *Biomass and Bioenergy* 10 (1996) 331-336.
- [11] V. Makareviciene, P. Janulis, Environmental effect of rapeseed oil ethyl ester, *Renewable Energy* 28 (2003) 2395-2403.
- [12] Sukumar Puhan, N. Vedaraman, G. Sankaranarayanan, Boppana V. Bharat Ram, Performance and emission study of Mahua oil (madhuca indica oil) ethyl ester in a 4-stroke natural aspirated direct injection diesel engine, *Renewable Energy* 30 (2005) 1269-1278.
- [13] M.I. Al-Widyan, G.Tashtoush, M. Abu-Qudais, Utilization of ethyl ester of waste vegetable oils as fuel in diesel engines, *Fuel Processing Technology* 76 (2002) 91-103.

Chapter III Experimental and Kinetic Modeling Study of Ethyl butanoate Oxidation in a Tubular Plug Flow Reactor - From Low to High Temperature under Atmospheric Pressure

- [14] E.M. Fisher, W.J. Pitz, H.J. Curran, C.K. Westbrook, Detailed chemical kinetic mechanisms for combustion of oxygenated fuels, *Proceedings of the Combustion Institute* 28 (2000) 1579-1586.
- [15] B.I. Parsons, C.J. Dandy, The oxidation of hydrocarbons and their derivatives. Part I. The observation of the progress of the reaction by pressure change and by analysis, *Journal of the Chemical Society* (1956) 1795-1798.
- [16] B.I. Parson, C. Hinshelwood, The oxidation of hydrocarbons and their derivatives. Part II. Structural effects in the ester series, *Journal of the Chemical Society* (1956) 1799-1803.
- [17] B.I. Parson, The oxidation of hydrocarbons and their derivatives. Part III. The role of intermediates, *Journal of the Chemical Society* (1956) 1804-1809.
- [18] D.E. Hoare, T.M. Li, A.D. Walsh, Cool flames and molecular structure, *Proceedings of the Combustion Institute* 11 (1967) 879-887.
- [19] S. Gail, M. Thomson, S.M. Sarathy, S.A. Syed, P. Dagaut, P. Diévert, A.J. Marchese, F.L. Dryer, A wide-ranging kinetic modeling study of methyl butanoate combustion, *Proceedings of the Combustion Institute* 31 (2007) 305-311.
- [20] S. Dooley, H.J. Curran, J.M. Simmie, Autoignition measurements and a validated kinetic model for the biodiesel surrogate, methyl butanoate, *Combustion and Flame* 153 (2008) 2-32.
- [21] W.R. Schwartz, C.S. McEnally, L.D. Pfefferle, Decomposition and hydrocarbon growth process for esters in non-premixed flames, *Journal of Physical Chemistry A* 110 (2006) 6643-6648.
- [22] W.K. Metcalfe, S. Dooley, H. J. Curran, J. M. Simmie, A.M. El-Nahas, M.V. Navarro, Experimental and modeling study of C₅H₁₀O₂ ethyl and methyl esters, *Journal of Physical Chemistry A* 111 (2007) 4001-4014.
- [23] W.K. Metcalfe, C. Togbé, P. Dagaut, H.J. Curran, J.M. Simmie, A jet-stirred reactor and kinetic modeling study of ethyl propanoate oxidation, *Combustion and Flame* 156 (2009) 250-260.
- [24] S.M. Walton, M.S. Wooldridge, C.K. Westbrook, An experimental investigation of structural effects on the autoignition properties of two C₅ esters, *Proceeding of the Combustion Institute* 32 (2009) 255-262.
- [25] M.H. Hakka, H. Bennadji, J. Biet, M. Yahyaoui, B. Sirjean, V. Warth, L. Coniglio, O. Herbinet, P.A. Glaude, F. Billaud, F. Battin-Leclerc, Oxidation of Methyl and Ethyl Butanoates, *International Journal of Chemical Kinetics* 42 (2010) 226-252.
- [26] Y. Zhang, A.L. Boehman, Experimental study of the autoignition of C₈H₁₆O₂ ethyl and methyl esters in a motored engine, *Combustion and Flame* 157 (2010) 546-555.

Chapter III Experimental and Kinetic Modeling Study of Ethyl butanoate Oxidation in a Tubular Plug Flow Reactor - From Low to High Temperature under Atmospheric Pressure

- [27] J. Gornay, L. Coniglio, F. Billaud, G. Wild, Octanoic acid pyrolysis in a stainless-steel tube: What is the role of the coke formed on the wall? *Journal of Analytical and Applied Pyrolysis* 87 (2010) 78-84.
- [28] J. Gornay, L. Coniglio, F. Billaud, G. Wild, Steam Cracking and Steam Reforming of Waste Cooking Oil in a Tubular Stainless Steel Reactor with Wall Effects, *Energy Fuels* 23 (2009) 5663-5676.
- [29] S. Touchard, R. Fournet, P.A. Glaude, V. Warth, F. Battin-Leclerc, G. Vanhove, M. Ribaucour, R. Minetti. *Proc. Combust. Inst.* 30 (2005) 1073-1081.
- [30] J. Biet, M.H. Hakka, V. Warth, P.A. Glaude, F. Battin-Leclerc, *Energy and Fuel* 22 (2008) 2258-2269.
- [31] P.A. Glaude, O. Herbinet, S. Bax, J. Biet, V. Warth, F. Battin-Leclerc, Modeling of the oxidation of methyl esters – Validation for methyl hexanoate, methyl heptanoate, and methyl decanoate in a jet-stirred reactor, *combustion and Flame* (2010) in press.
- [32] C. Muller, V. Michel, G. Scacchi, G.M. Côme, A computer program for the evaluation of thermochemical data of molecules and free radicals in the gas phase, *Journal of Chemical Physics* 92 (1995) 1154-1177.
- [33] S.W. Benson, *Thermochemical Kinetics*, Edition John Wiley, 2nd edition (1976), New York.
- [34] R.J. Kee, F.M. Rupley, J.A. Miller, Chemkin II: A fortran chemical kinetics package for the analysis of gas phase chemical kinetics, Sandia Laboratories Report (1993), SAND 89-8009B.
- [35] V. Warth, N. Stef, P.A. Glaude, F. Battin-Leclerc, G. Scacchi, G.M. Côme, Computer-aided derivation of gas-phase oxidation mechanism: application to the modelling of the oxidation of n-butane, *Combustion and Flame* 114 (1998) 81-102.
- [36] A.T. Blades and P.W. Gilderson, Kinetics of the thermal decomposition of ethyl propionate, *Canadian Journal of Chemistry* 38 (1960) 1412-1415.
- [37] H.E. O'Neal and S.W. Benson, Method for estimating the Arrhenius a factors for four- and six- center unimolecular reactions *Journal of Physical Chemistry* 71 (1967) 2903-2921.
- [38] A.M. El-Nahas, M.V. Navarro, J.M. Simmie, J.W. Bozzelli, H. J. Curran, S. Dooley and W. Metcalfe, Enthalpies of formation, bond dissociation energies and reaction paths for the decomposition of model biofuels: ethyl propanoate and methyl butanoate, *Journal of Physical Chemistry A* 111 (2007) 3727-3739.
- [39] D.A. Kairaitis and V.R. Stimson, The thermal decompositions of ethyl trans-crotonate and ethyl n-butyrate, *Australian Journal of Chemistry* 21 (1968) 1349-1354.

Chapter III Experimental and Kinetic Modeling Study of Ethyl butanoate Oxidation in a Tubular Plug Flow Reactor - From Low to High Temperature under Atmospheric Pressure

[40] F. Buda, R. Bounaceur, V. Warth, P.A. Glaude, R. Fournet, F. Battin-Leclerc, Progress toward a unified detailed kinetic model for the autoignition of alkanes from C₄ to C₁₀ between 600 et 1200 K, Combustion and Flame 142 (2005) 170-186.

Chapter III Experimental and Kinetic Modeling Study of Ethyl butanoate Oxidation in a Tubular Plug Flow Reactor - From Low to High Temperature under Atmospheric Pressure

Appendix AIII Experimental oxidation of ethyl butanoate in a plug flow reactor

This part gives details related to the experimental work conducted for ethyl butanoate (EB) oxidation in a tubular plug flow reactor: reproducibility of GC/FID analyses for EB and butanoic acid (BA) which is a key intermediate species of EB oxidation process and exhaustive results obtained for all experiments (mole fractions in reactants, intermediate species, and final products formed).

Table AIII.1: Main features of gas chromatography analyses

1. PERICHROM PR1250 (PROGRAM O₂ analysis)			
Oven	Injector	Detector	Column
Oven security temperature: 85°C Initial temperature: 40 °C Isothermal time: 10 min	Classic Temperature: Room T Carriers gas: N ₂ , He Carrier gas pressure: 190 KPa Sampling loop: 3ml	TCD Temperature: Room T Gain: 10 Current: 80 mA	Molecular sieve column 5A°, Length 2.5 m
2. PERICHROM PR2100 (PROGRAM liquid compounds analysis)			
Oven Security temperature: 250 °C Initial temperature: 50°C Isothermal Time: 20 min Ramp 1 Rate: 5°C/min Final temperature: 240°C Isothermal Time: 40 min	Spl/Spls Temperature: 200°C Carriers gas: N ₂ Carrier gas pressure: 30 kPa Split: 150 ml/m Auto sampler ALS104 Syringe SGE 0.5µl needle length 5cm	FID Temperature: 260°C Gain: 11 Pressure of FID combustion gas Air pressure: 50 Kpa H ₂ pressure: 50 Kpa	Column polar SGE BP 21 polyethylene glycol GC capillary column Length 30m Inner diameter 0.53 mm Thickness film 1µm
3. Agilent 6850 (PROGRAM gas compounds analysis)			
Oven Security temperature: 255 °C Initial temperature: 60°C Isothermal Time: 10 min Ramp 1 Rate: 5°C/min Final temperature: 250°C Isothermal Time: 15 min	Spl/Spls Temperature: 250°C Carriers gas: He Carrier gas pressure: 103 kPa Split: 1/100 (200 ml/min) Splitless: No Sampling loop: 0.25ml Loop temperature: 180°C	FID Temperature: 300°C Flow rate of FID combustion gas Air: 400 ml/min H ₂ : 30 ml/min Makeup flow + column flow = 25 ml/min	Column apolar HP- PLOT Q polystyrene- divinylbenzene capillary column Length 30m Inner diameter 320 µm Thickness film 20µm

Note: Synthetic mixtures of representative pure reference compounds were analyzed under the same conditions in order to calculate their relative response factors in comparison to the internal standard (*n*-octane). The internal standard was assigned a value of 1.0. The reproducibility of the areas was better than 1%. The corresponding mass of all reacting mixture components were then calculated by comparison with the internal standard and corrected by the relative response factors.

Chapter III Experimental and Kinetic Modeling Study of Ethyl butanoate Oxidation in a Tubular Plug Flow Reactor - From Low to High Temperature under Atmospheric Pressure

Table AIII.2: Reproducibility of GC/FID analysis illustrated for one typical experiment related to ethyl butanoate (EB) oxidation ($x_{EB} = 0.013$, $\phi = 1.0$, $\tau_{STP} = 1.4$ s, and $T = 800$ K)^a

<i>(a) GC/FID experimental information</i>						
Species	T_r (min)	Area 1	Area 2	Area 3		
n-Octane (internal standard)	1.7	21.83	20.15	21.7		
Acetone (solvent)	1.87	2187.54	2011.88	2196.57		
EB	4.48	132.63	123.26	133.54		
BA	36.53	10.31	9.64	10.22		

<i>(b) Mass calculation</i>						
Mass species	Mean area 1	Mean area 2	Mean area 3	Average	Standard deviation	CV % ^b
m_{EB} (g)	0.733	0.738	0.743	0.738	0.005	0.67
M_{BA} (g)	0.071	0.072	0.071	0.072	0.0006	0.81

Notes: ^a Samples for GC/FID analyses were achieved with acetone as solvent, by using internal standard method with n-octane as internal standard. EB is ethyl butanoate and BA butanoic acid. ^b Coefficient of variation (CV) % = (Standard deviation*100)/Average.

Table AIII.3: Experimental results related to EB oxidation in a tubular plug flow reactor – Effect of temperature and residence time for given EB molar fraction and equivalence ratio ($x_{EB} = 0.013$ and $\phi = 1.0$)

Residence time τ_{STP} (s)	0.65	0.70	0.80	0.93	1.00	1.20	1.40
Pressure (torr)	1007	950	900	880	867	846	890
Compounds	Mole Fraction						
(a) T = 700K ($x_{EB} = 0.013$, $\phi = 1.0$)							
O ₂	1.04E-01	1.04E-01	1.04E-01	1.04E-01	1.04E-01	1.04E-01	1.04E-01
C ₂ H ₄	1.84E-05	7.50E-05	5.43E-05	3.36E-05	5.69E-05	6.46E-05	7.24E-05
CH ₃ CH ₂ CH ₂ C(O)OH	5.78E-06	9.02E-06	2.43E-05	2.46E-05	2.97E-04	7.80E-04	9.51E-04
CH ₃ CH ₂ CH ₂ C(O)OC ₂ H ₅	1.29E-02	1.28E-02	1.27E-02	1.27E-02	1.25E-02	1.20E-02	1.18E-02
(b) T = 800K ($x_{EB} = 0.013$, $\phi = 1.0$)							
O ₂	1.04E-01	1.04E-01	1.04E-01	1.04E-01	1.04E-01	1.04E-01	1.03E-01
C ₂ H ₄	8.43E-04	9.15E-04	1.03E-03	1.44E-03	1.44E-03	1.80E-03	1.86E-03
CH ₃ CH ₂ CH ₂ C(O)OH	5.38E-04	5.48E-04	5.54E-04	6.47E-04	9.11E-04	1.11E-03	1.43E-03
CH ₃ CH ₂ CH ₂ C(O)OC ₂ H ₅	1.15E-02	1.15E-02	1.15E-02	1.14E-02	1.13E-02	1.09E-02	1.05E-02

Chapter III Experimental and Kinetic Modeling Study of Ethyl butanoate Oxidation in a Tubular Plug Flow Reactor - From Low to High Temperature under Atmospheric Pressure

Table AIII.3 (Continued)

(c) T= 1000 K ($x_{EB} = 0.013$, $\varphi = 1.0$)									
Residence time τ_{STP} (s)	0.65	0.70	0.80 ^a			0.93	1.00	1.20	1.40
Pressure (torr)	1024	981	940			888	878	859	846
Compounds	Mole Fraction								
O ₂	7.46E-02	6.77E-02	6.02E-02	6.05E-02	6.04E-02 ± 2E-04 ^b	5.62E-02	5.70E-02	4.80E-02	9.30E-03
CO	1.54E-02	1.77E-02	2.02E-02	2.01E-02	2.02E-02 ± 7E-05	2.78E-02	2.86E-02	4.04E-02	4.30E-02
CO ₂	8.60E-03	9.30E-03	1.00E-02	1.01E-02	1.01E-02 ± 7E-05	1.05E-02	1.07E-02	1.43E-02	1.44E-02
CH ₄	2.18E-03	2.71E-03	3.18E-03	3.26E-03	3.22E-03 ± 6E-05	3.82E-03	3.76E-03	4.47E-03	3.77E-03
C ₂ H ₂	6.91E-05	1.18E-04	1.90E-04	1.83E-04	1.86E-04 ± 5E-06	2.81E-04	2.74E-04	3.30E-04	2.99E-04
C ₂ H ₄	1.56E-02	1.57E-02	1.47E-02	1.46E-02	1.47E-02 ± 8E-05	1.36E-02	1.34E-02	1.13E-02	7.37E-03
C ₂ H ₆	2.82E-04	3.44E-04	3.69E-04	3.66E-04	3.67E-04 ± 2E-06	3.87E-04	3.82E-04	3.90E-04	2.68E-04
C ₃ H ₆	1.90E-03	1.54E-03	1.16E-03	1.15E-03	1.16E-03 ± 6E-06	6.33E-04	6.26E-04	2.28E-04	7.53E-05
C ₃ H ₈	0	3.29E-05	2.93E-05	3.11E-05	3.02E-05 ± 2E-06	2.19E-05	4.39E-05	2.01E-05	1.83E-05
aC ₃ H ₄	0	2.82E-06	0	0	0E+00 ± 0E+00	0	0	0	0
pC ₃ H ₄	0	8.14E-06	9.31E-06	9.11E-06	9.21E-06 ± 2E-07	-	5.43E-06	3.68E-06	0
1C ₄ H ₈	5.03E-05	5.48E-05	4.59E-05	4.29E-05	4.44E-05 ± 2E-06	2.37E-05	2.22E-05	7.25E-06	0
1,3-C ₄ H ₆	1.58E-05	2.24E-05	2.11E-05	2.11E-05	2.11E-05 ± 0E+00	1.58E-05	1.45E-05	7.00E-06	0
nC ₄ H ₁₀	0	0	3.65E-06	3.80E-06	3.72E-06 ± 1E-07	0	0	0	0
CH ₃ CHO	5.80E-04	6.72E-04	5.96E-04	6.18E-04	6.07E-04 ± 2E-05	4.93E-04	4.55E-04	0	0
CH ₃ OH	0	0	2.74E-05	2.87E-05	2.81E-05 ± 9E-07	0	0	0	0
CH ₃ CH ₂ OH	2.75E-05	2.48E-05	1.55E-05	1.59E-05	1.57E-05 ± 3E-07	0	0	0	0
CH ₂ =CHCHO	8.20E-05	9.15E-05	7.57E-05	7.67E-05	7.62E-05 ± 7E-07	-	3.47E-05	1.17E-05	0
C ₂ H ₅ CHO	7.19E-05	6.30E-05	6.89E-05	6.89E-05	6.89E-05 ± 0E+00	6.00E-05	8.69E-05	2.04E-05	0
CH ₃ CH ₂ CH ₂ C(O)OH	2.13E-03	1.87E-03	1.86E-03	1.78E-03	1.82E-03 ± 5E-05	8.43E-04	5.23E-04	8.40E-05	0
CH ₂ =CHC(O)OH	8.52E-04	1.04E-03	9.71E-04	9.68E-04	9.70E-04 ± 3E-06	1.18E-04	1.65E-04	0	0
CH ₃ CH ₂ CH ₂ C(O)OC ₂ H ₅	4.25E-06	0	0	0	0E+00 ± 0E+00	0	0	0	0

Chapter III Experimental and Kinetic Modeling Study of Ethyl butanoate Oxidation in a Tubular Plug Flow Reactor - From Low to High Temperature under Atmospheric Pressure

Table AIII.4: Experimental results related to EB oxidation in a tubular plug flow reactor - Effect of temperature and equivalence ratio for given EB molar fraction and residence time ($x_{EB} = 0.013$ and $\tau_{STP} = 0.93$ s)

(a) $\varphi = 1.12$ ($x_{EB} = 0.013$, $\tau_{STP} = 0.93$ s)												
Temperature (K)	500	550 ^b				600	650	700			750	800
Pressure (torr)	809	810				815	826	835			841	857
Compounds	Mole Fraction											
O ₂	9.26E-02	9.24E-02	9.25E-02	9.25E-02±5E-05	9.25E-02	9.24E-02	9.23E-02	9.22E-02	9.23E-02±4E-05	9.22E-02	9.19E-02	
CO	0	0	0	0±0	0	0	0	0	0±0	0	0	
CO ₂	0	0	0	0±0	0	0	0	0	0±0	0	0	
CH ₄	0	0	0	0±0	0	0	0	0	0±0	0	0	
C ₂ H ₂	0	0	0	0±0	0	0	0	0	0±0	0	0	
C ₂ H ₄	0	0	0	0±0	0	0	3.36E-05	3.36E-05	3.36E-05±0E+00	2.59E-04	1.44E-03	
C ₂ H ₆	0	0	0	0±0	0	0	0	0	0±0	0	0	
C ₃ H ₆	0	0	0	0±0	0	0	0	0	0±0	0	0	
C ₃ H ₈	0	0	0	0±0	0	0	0	0	0±0	0	0	
1C ₄ H ₈	0	0	0	0±0	0	0	0	0	0±0	0	0	
C ₄ H ₁₀	0	0	0	0±0	0	0	0	0	0±0	0	0	
CH ₃ CHO	0	0	0	0±0	0	0	0	0	0±0	0	0	
CH ₃ CH ₂ OH	0	0	0	0±0	0	0	0	0	0±0	0	0	
CH ₂ =CHCHO	0	0	0	0±0	0	0	0	0	0±0	0	0	
C ₂ H ₅ CHO	0	0	0	0±0	0	0	0	0	0±0	0	0	
CH ₃ CH ₂ CH ₂ C(O)OH	0	0	0	0±0	0	0	3.02E-05	2.46E-05	2.74E-05±4E-06	7.38E-05	6.47E-04	
CH ₂ =CHC(O)OH	0	0	0	0±0	0	0	0	0	0±0	0	0	
CH ₃ CH ₂ CH ₂ C(O)OC ₂ H ₅	1.29E-02	1.30E-02	1.30E-02	1.30E-02±3E-06	1.31E-02	1.29E-02	1.25E-02	1.27E-02	1.26E-02±1E-04	1.26E-02	1.14E-02	

Chapter III Experimental and Kinetic Modeling Study of Ethyl butanoate Oxidation in a Tubular Plug Flow Reactor - From Low to High Temperature under Atmospheric Pressure

Table AIII.4 (Continued)

(a) $\phi = 1.12$ ($x_{EB} = 0.013$, $\tau_{STP} = 0.93$ s)												
Temperature (K)	850 ^b			900	950	1000	1025	1050	1075	1100	1150	1200
Pressure (torr)	880			890	896	910	915	927	937	952	971	985
Compounds	Mole Fraction											
O ₂	9.16E-02	9.10E-02	9.13E-02±4E-04	8.99E-02	8.91E-02	5.70E-02	2.54E-03	2.14E-03	1.48E-03	0	0	0
CO	2.00E-04	3.00E-04	2.50E-04±7E-05	6.00E-04	2.10E-03	2.86E-02	2.50E-02	2.38E-02	2.20E-02	2.12E-02	1.81E-02	1.24E-02
CO ₂	0	0	0±0	0	1.20E-03	1.07E-02	5.03E-02	5.21E-02	5.60E-02	5.68E-02	6.00E-02	6.60E-02
CH ₄	2.14E-05	3.34E-05	2.74E-05±8E-06	1.20E-04	6.33E-04	3.76E-03	4.54E-04	3.24E-04	1.85E-04	4.74E-05	0	0
C ₂ H ₂	0	0	0±0	0	1.03E-05	2.74E-04	3.79E-05	2.90E-05	5.80E-06	1.85E-06	0	0
C ₂ H ₄	5.72E-03	6.30E-03	6.01E-03±4E-04	1.26E-02	1.53E-02	1.34E-02	7.91E-04	4.32E-04	7.50E-05	1.22E-05	0	0
C ₂ H ₆	0	0	0±0	7.86E-06	7.59E-05	3.82E-04	3.25E-05	2.33E-05	8.40E-06	0	0	0
C ₃ H ₆	2.51E-05	2.51E-05	2.51E-05±0E+00	1.39E-04	8.61E-04	6.26E-04	1.02E-05	0	0	0	0	0
C ₃ H ₈	0	0	0±0	0	0	2.40E-05	0	0	0	0	0	0
1C ₄ H ₈	0	0	0±0	0	6.81E-06	2.37E-05	0	0	0	0	0	0
1,3-C ₄ H ₆	0	0	0±0	0	0	1.58E-05	0	0	0	0	0	0
CH ₃ CHO	2.49E-05	3.63E-05	3.06E-05±8.05E-06	9.21E-05	2.28E-04	4.55E-04	2.87E-05	2.60E-05	0	0	0	0
CH ₃ CH ₂ OH	3.52E-05	2.44E-05	2.98E-05±7.66E-06	2.40E-05	0	0	0	0	0	0	0	0
CH ₂ =CHCHO	0	0	0±0	0	1.64E-05	4.73E-05	0	0	0	0	0	0
C ₂ H ₅ CHO	1.44E-05	1.14E-05	1.29E-05±2.12E-06	5.40E-05	1.59E-04	6.00E-05	6.6E-06	6.59E-06	0	0	0	0
CH ₃ CH ₂ CH ₂ C(O)OH	2.62E-03	2.99E-03	2.81E-03±2.62E-04	7.54E-03	7.63E-03	5.23E-04	0	0	0	0	0	0
CH ₂ =CHC(O)OH	0	0	0±0	3.33E-05	4.06E-04	1.65E-04	0	0	0	0	0	0
CH ₃ CH ₂ CH ₂ C(O)OC ₂ H ₅	7.99E-03	7.87E-03	7.93E-03±8.09E-05	1.94E-03	4.78E-05	0	0	0	0	0	0	0

Chapter III Experimental and Kinetic Modeling Study of Ethyl butanoate Oxidation in a Tubular Plug Flow Reactor - From Low to High Temperature under Atmospheric Pressure

Table AIII.4 (Continued)

(b) $\phi = 0.52$ ($x_{EB} = 0.013$, and $\tau_{STP} = 0.93$ s)													
Temperature (K)	450	500	550	600 ^b			650 ^b			700	750	800	825
Pressure (torr)	787	800	814	820			832			843	851	865	879
Compounds	Mole Fraction												
O ₂	1.96E-01	1.96E-01	1.96E-01	1.95E-01	1.96E-01	1.95E-01±5E-04	1.95E-01	1.94E-01	1.95E-01±1E-04	1.95E-01	1.95E-01	1.94E-01	1.94E-01
CO	0	0	0	0	0	0±0	0	0	0±0	0	0	0	0
CO ₂	0	0	0	0	0	0±0	0	0	0±0	0	0	0	0
CH ₄	0	0	0	0	0	0±0	0	0	0±0	0	0	0	5.99E-06
C ₂ H ₂	0	0	0	0	0	0±0	0	0	0±0	0	0	0	0
C ₂ H ₄	0	0	0	0	0	0±0	0	0	0±0	4.65E-05	2.35E-04	1.33E-03	3.18E-03
C ₂ H ₆	0	0	0	0	0	0±0	0	0	0±0	0	0	0	0
C ₃ H ₆	0	0	0	0	0	0±0	0	0	0±0	0	0	0	1.39E-05
1-C ₄ H ₈	0	0	0	0	0	0±0	0	0	0±0	0	0	0	0
1,3-C ₄ H ₆	0	0	0	0	0	0±0	0	0	0±0	0	0	0	0
CH ₃ CHO	0	0	0	0	0	0±0	0	0	0±0	0	0	0	1.46E-05
CH ₃ CH ₂ OH	0	0	0	0	0	0±0	0	0	0±0	0	2.55E-05	2.21E-05	2.83E-05
CH ₂ =CHCHO	0	0	0	0	0	0±0	0	0	0±0	0	0	0	0
C ₂ H ₅ CHO	0	0	0	0	0	0±0	0	0	0±0	0	0	0	9.29E-06
CH ₃ CH ₂ CH ₂ C(O)OH	0	0	0	0	0	0±0	0	0	0±0	4.62E-05	1.41E-04	7.08E-04	2.00E-03
CH ₂ =CHC(O)OH	0	0	0	0	0	0±0	0	0	0±0	0	0	0	0
CH ₃ CH ₂ CH ₂ C(O)OC ₂ H ₅	1.30E-02	1.29E-02	1.28E-02	1.23E-02	1.29E-02	1.26E-02±4E-04	1.29E-02	1.24E-02	1.27E-02±4E-04	1.27E-02	1.21E-02	1.09E-02	9.16E-03

Chapter III Experimental and Kinetic Modeling Study of Ethyl butanoate Oxidation in a Tubular Plug Flow Reactor - From Low to High Temperature under Atmospheric Pressure

Table AIII.4 (Continued)

(b) $\phi = 0.52$ ($x_{EB} = 0.013$ and $\tau_{STP} = 0.93$ s)													
Temperature (K)	850 ^b			875	900 ^{a,b}			950	975	1000 ^a	1050	1100	1150
Pressure (torr)	885			915	930			939	941	953	964	977	986
Compounds	Mole Fraction												
O ₂	1.93E-01	1.93E-01	1.93E-01±1E-04	1.92E-01	1.91E-01	1.91E-01	1.91E-01±5E-05	1.83E-01	8.47E-02	7.78E-02	8.12E-02	8.07E-02	8.07E-02
CO	0	0	0±0	0	2.00E-04	2.00E-04	2.00E-04±0E+00	3.30E-03	1.70E-03	2.00E-03	0	0	0
CO ₂	1.00E-04	1.00E-04	1.00E-04±0E+00	2.00E-04	6.00E-04	6.00E-04	6.00E-04±0E+00	3.80E-03	7.57E-02	7.67E-02	7.78E-02	7.78E-02	7.78E-02
CH ₄	1.25E-05	1.80E-05	1.52E-05±4E-06	3.94E-05	1.10E-04	1.30E-04	1.20E-04±1E-05	8.73E-04	0	0	0	0	0
C ₂ H ₂	0	0	0±0	0	0	0	0±0	1.12E-05	0	0	0	0	0
C ₂ H ₄	5.38E-03	5.90E-03	5.64E-03±3E-04	8.81E-03	1.25E-02	1.28E-02	1.26E-02±2E-04	1.58E-02	2.38E-05	6.46E-06	0	0	0
C ₂ H ₆	0	0	0±0	0	4.34E-06	6.77E-06	5.55E-06±1E-06	8.94E-05	0	0	0	0	0
C ₃ H ₆	2.32E-05	2.90E-05	2.61E-05±4E-06	6.18E-05	1.80E-04	2.14E-04	1.97E-04±2E-05	1.46E-03	0	0	0	0	0
1-C ₄ H ₈	0	0	0±0	0	0	0	0±0	1.92E-05	0	0	0	0	0
1,3-C ₄ H ₆	0	0	0±0	0	0	0	0±0	2.77E-06	0	0	0	0	0
CH ₃ CHO	2.09E-05	2.76E-05	2.43E-05±4E-06	5.09E-05	8.13E-05	1.19E-04	1.00E-04±2E-05	3.85E-04	0	0	0	0	0
CH ₃ CH ₂ OH	2.09E-05	2.86E-05	2.48E-05±5E-06	2.28E-05	2.17E-05	2.36E-05	2.26E-05±1E-06	2.13E-05	0	0	0	0	0
CH ₂ =CHCHO	0	0	0±0	0	0	0	0±0	4.42E-05	0	0	0	0	0
C ₂ H ₅ CHO	1.20E-05	1.53E-05	1.36E-05±2E-06	2.16E-05	5.10E-05	7.79E-05	6.44E-05±2E-05	2.19E-04	0	0	0	0	0
CH ₃ CH ₂ CH ₂ C(O)OH	3.85E-03	4.51E-03	4.18E-03±4E-04	6.96E-03	9.33E-03	9.75E-03	9.54E-03±3E-04	6.33E-03	9.16E-05	2.04E-04	0	0	0
CH ₂ =CHC(O)OH	0	0	0±0	0	5.79E-05	5.30E-05	5.55E-05±3E-06	7.02E-04	0	0	0	0	0
CH ₃ CH ₂ CH ₂ C(O)OC ₂ H ₅	7.55E-03	6.96E-03	7.25E-03±4E-04	4.69E-03	2.23E-03	1.86E-03	2.05E-03±2E-04	3.14E-05	1.79E-05	0	0	0	0

Chapter III Experimental and Kinetic Modeling Study of Ethyl butanoate Oxidation in a Tubular Plug Flow Reactor - From Low to High Temperature under Atmospheric Pressure

Table AIII.4 (Continued)

(c) $\phi = 1.59$ ($x_{EB} = 0.013$, and $\tau_{STP} = 0.93$ s)														
Temperature (K)	500 ^b			550	600 ^b				650 ^b			700 ^b		
Pressure (torr)	800			801	804				810			815		
Compounds	Mole Fraction													
O ₂	6.55E-02	6.54E-02	6.55E-02±7.91E-05	6.43E-02	6.68E-02	6.59E-02	6.54E-02	6.60E-02±7E-04	6.40E-02	6.52E-02	6.46E-02±8E-04	6.48E-02	6.47E-02	6.47E-02±2E-05
CO	0	0	0±0	0	0	0	0	0±0	0	0	0±0	0	0	0±0
CO ₂	0	0	0±0	0	0	0	0	0±0	0	0	0±0	0	0	0±0
CH ₄	0	0	0±0	0	0	0	0	0±0	0	0	0±0	0	0	0±0
C ₂ H ₂	0	0	0±0	0	0	0	0	0±0	0	0	0±0	0	0	0±0
C ₂ H ₄	0	0	0±0	2.82E-05	4.10E-05	4.35E-05	4.23E-05	4.23E-05±1E-06	4.61E-05	4.50E-05	4.55E-05±7E-07	4.99E-05	5.12E-05	5.06E-05±9E-07
C ₂ H ₆	0	0	0±0	0	0	0	0	0±0	0	0	0±0	0	0	0±0
C ₃ H ₆	0	0	0±0	0	0	0	0	0±0	0	0	0±0	0	0	0±0
C ₃ H ₈	0	0	0±0	0	0	0	0	0±0	0	0	0±0	0	0	0±0
1-C ₄ H ₈	0	0	0±0	0	0	0	0	0±0	0	0	0±0	0	0	0±0
1,3-C ₄ H ₆	0	0	0±0	0	0	0	0	0±0	0	0	0±0	0	0	0±0
CH ₃ CHO	0	0	0±0	0	0	0	0	0±0	0	0	0±0	0	0	0±0
CH ₂ =CHCHO	0	0	0±0	0	0	0	0	0±0	0	0	0±0	0	0	0±0
C ₂ H ₅ CHO	0	0	0±0	0	0	0	0	0±0	0	0	0±0	0	0	0±0
CH ₃ CH ₂ CH ₂ C(O)OH	0	0	0±0	7.57E-05	1.13E-04	1.12E-04	1.13E-04	1.13E-04±2E-07	1.77E-04	1.75E-04	1.76E-04±1E-06	2.29E-04	1.30E-04	1.80E-04±7E-05
CH ₂ =CHC(O)OH	0	0	0±0	0	0	0	0	0±0	0	0	0±0	0	0	0±0
CH ₃ CH ₂ CH ₂ C(O)OC ₂ H ₅	1.19E-02	1.21E-02	1.20E-02±1.19E-04	1.21E-02	1.25E-02	1.25E-02	1.25E-02	1.20E-02±1E-05	1.24E-02	1.26E-02	1.25E-02±1E-04	1.21E-02	1.20E-02	1.21E-02±4E-05

Chapter III Experimental and Kinetic Modeling Study of Ethyl butanoate Oxidation in a Tubular Plug Flow Reactor - From Low to High Temperature under Atmospheric Pressure

Table AIII.4 (Continued)

(c) $\phi = 1.59$ ($x_{EB} = 0.013$ and $\tau_{STP} = 0.93$ s)														
Temperature (K)	750 ^b				800 ^b				850 ^b			900 ^b		
Pressure (torr)	835				860				880			885		
Compounds	Mole Fraction													
O ₂	6.47E-02	6.44E-02	6.45E-02	6.45E-02±1E-04	6.53E-02	6.49E-02	6.46E-02	6.49E-02±3E-04	6.31E-02	6.39E-02	6.35E-02±5E-04	6.18E-02	6.27E-02	6.23E-02±6E-04
CO	0	0	0	0±0	0±0				0	0	0±0	2.00E-04	2.00E-04	2.00E-04±0E+00
CO ₂	0	0	0	0±0	0	0	0	0±0	0	0	0±0	0	0	0±0
CH ₄	0	0	0	0±0	0	0	0	0±0	5.49E-05	5.59E-05	5.54E-05±7E-07	1.30E-04	1.25E-04	1.27E-04±3E-06
C ₂ H ₂	0	0	0	0±0	0	0	0	0±0	0	0	0±0	0	0	0±0
C ₂ H ₄	2.61E-04	3.12E-04	3.38E-04	3.04E-04±4E-05	1.74E-03	1.73E-03	1.75E-03	1.74E-03±8E-06	7.08E-03	7.00E-03	7.04E-03±6E-05	1.39E-02	1.39E-02	1.39E-02±1E-05
C ₂ H ₆	0	0	0	0±0	0	0	0	0±0	0	0	0±0	6.50E-06	6.50E-06	6.50E-06±0E+00
C ₃ H ₆	0	0	0	0±0	0	0	0	0±0	3.28E-05	3.86E-05	3.57E-05±4E-06	1.14E-04	1.20E-04	1.17E-04±4E-06
C ₃ H ₈	0	0	0	0±0	0	0	0	0±0	0	0	0±0	0	0	0±0
1-C ₄ H ₈	0	0	0	0±0	0	0	0	0±0	0	0	0±0	0	0	0±0
1,3-C ₄ H ₆	0	0	0	0±0	0	0	0	0±0	0	0	0±0	0	0	0±0
CH ₃ CHO	0	0	0	0±0	0	0	0	0±0	2.27E-05	2.32E-05	2.30E-05±3E-07	8.13E-05	6.50E-05	7.31E-05±1E-05
CH ₂ =CHCHO	0	0	0	0±0	0	0	0	0±0	0	0	0±0	0	0	0±0
C ₂ H ₅ CHO	0	0	0	0±0	0	0	0	0±0	0	0	0±0	3.90E-05	3.60E-05	3.75E-05±2E-06
CH ₃ CH ₂ CH ₂ C(O)OH	2.90E-04	2.89E-04	2.87E-04	2.89E-04±2E-06	4.50E-04	4.56E-04	4.52E-04	4.53E-04±2E-06	4.90E-03	4.83E-03	4.87E-03±4E-05	9.82E-03	9.74E-03	9.78E-03±5E-05
CH ₂ =CHC(O)OH	0	0	0	0±0	0	0	0	0±0	0	0	0±0	2.70E-05	2.70E-05	2.70E-05±0E+00
CH ₃ CH ₂ CH ₂ C(O)OC ₂ H ₅	1.19E-02	1.18E-02	1.18E-02	1.18E-02±5E-05	1.15E-02	1.16E-02	1.15E-02	1.15E-02±3E-05	7.06E-03	7.52E-03	7.29E-03±3E-04	1.88E-03	1.88E-03	1.88E-03±0E+00

Chapter III Experimental and Kinetic Modeling Study of Ethyl butanoate Oxidation in a Tubular Plug Flow Reactor - From Low to High Temperature under Atmospheric Pressure

Table AIII.4 (Continued)

(c) $\phi = 1.59$ ($x_{EB} = 0.013$ and $\tau_{STP} = 0.93$ s)											
Temperature (K)	950	1000 ^b			1025	1050 ^b			1075 ^b		
Pressure (torr)	890	900			911	920			930		
Compounds	Mole Fraction										
O ₂	5.91E-02	3.90E-02	3.93E-02	3.91E-02±1E-04	2.78E-02	2.00E-02	1.97E-02	1.99E-02±1E-04	3.35E-03	3.40E-03	3.37E-03±3E-05
CO	1.60E-03	2.13E-02	2.10E-02	2.12E-02±2E-04	3.60E-02	4.15E-02	4.13E-02	4.14E-02±1E-04	5.86E-02	5.90E-02	5.88E-02±2E-04
CO ₂	2.10E-03	9.70E-03	1.02E-02	9.95E-03±3E-04	1.24E-02	1.36E-02	1.34E-02	1.35E-02±1E-04	1.62E-02	1.64E-02	1.63E-02±1E-04
CH ₄	8.08E-04	3.67E-03	3.58E-03	3.62E-03±6E-05	5.08E-03	5.89E-03	5.96E-03	5.92E-03±5E-05	3.45E-03	3.54E-03	3.49E-03±6E-05
C ₂ H ₂	0	1.78E-04	1.58E-04	1.68E-04±1E-05	3.69E-04	4.83E-04	5.07E-04	4.95E-04±1E-05	8.48E-04	8.74E-04	8.61E-04±2E-05
C ₂ H ₄	1.79E-02	1.74E-02	1.73E-02	1.74E-02±6E-05	1.35E-02	1.03E-02	1.04E-02	1.04E-02±3E-05	1.24E-03	1.29E-03	1.27E-03±3E-05
C ₂ H ₆	9.75E-05	4.77E-04	4.55E-04	4.66E-04±1E-05	5.35E-04	4.77E-04	4.98E-04	4.88E-04±1E-05	1.14E-04	1.19E-04	1.17E-04±3E-06
C ₃ H ₆	9.73E-04	1.62E-03	1.59E-03	1.60E-03±2E-05	3.16E-04	1.19E-04	1.17E-04	1.18E-04±1E-06	1.16E-05	1.27E-05	1.22E-05±8E-07
C ₃ H ₈	0	4.4E-05	4.57E-05	4.48 0E-05±1E-06	5.28E-05	6.7E-05	6.7E-05	6.7E-05±0E+00	6.58E-06	7.32E-06	6.95E-06±5E-07
1-C ₄ H ₈	1.92E-05	6.22E-05	5.92E-05	6.07E-05±2E-06	1.71E-05	7.83E-06	7.55E-06	7.7E-06±2E-07	0	0	0±0
1,3-C ₄ H ₆	0	3.30E-05	3.43E-05	3.36E-05±9E-07	1.27E-05	9.52E-06	9.77E-06	9.65E-06±2E-07	0	0	0±0
CH ₃ CHO	2.60E-04	6.94E-04	6.72E-04	6.83E-04±1E-05	2.56E-04	3.96E-05	3.86E-05	3.91E-05±7E-07	0	0	0±0
CH ₂ =CHCHO	0	8.84E-05	9.15E-05	8.99E-05±2E-06	1.88E-05	4.25E-06	4.56E-06	4.40E-06±2E-07	0	0	0±0
C ₂ H ₃ CHO	2.04E-04	8.99E-05	6.00E-05	7.49E-05±2E-05	1.90E-05	1.18E-05	1.21E-05	1.20E-05±2E-07	0	0	0±0
CH ₃ CH ₂ CH ₂ C(O)OH	8.14E-03	2.45E-04	2.45E-04	2.45E-04±2E-07	7.62E-05	2.09E-05	2.06E-05	2.08E-05±1E-07	0	0	0±0
CH ₂ =CHC(O)OH	3.10E-04	2.19E-04	2.30E-04	2.25E-04±7E-06	4.68E-05	2.60E-05	2.68E-05	2.64E-05±5E-07	0	0	0±0
CH ₃ CH ₂ CH ₂ C(O)OC ₂ H ₅	5.63E-05	1.04E-05	1.00E-05	1.02E-05±2E-07	5.08E-06	2.38E-06	2.30E-06	2.34E-06±5E-08	5.50E-07	6.15E-07	5.82E-07±4E-08

Chapter III Experimental and Kinetic Modeling Study of Ethyl butanoate Oxidation in a Tubular Plug Flow Reactor - From Low to High Temperature under Atmospheric Pressure

Table AIII.4 (Continued)

(c) $\phi = 1.59$ ($x_{EB} = 0.013$ and $\tau_{STP} = 0.93$ s)							
Temperature (K)	1100 ^b				1150	1200	
Pressure (torr)	955				976	983	
Compounds	Mole Fraction						
O ₂	9.59E-04	1.28E-03	1.31E-03	1.18E-03±2E-04	3.44E-04	2.72E-04	
CO	6.00E-02	6.07E-02	6.10E-02	6.06E-02±5E-04	5.95E-02	5.78E-02	
CO ₂	1.80E-02	1.72E-02	1.75E-02	1.76E-02±4E-04	1.81E-02	1.86E-02	
CH ₄	2.10E-03	2.38E-03	2.24E-03	2.24E-03±1E-04	1.31E-03	8.53E-04	
C ₂ H ₂	1.71E-03	1.67E-03	1.68E-03	1.69E-03±2E-05	3.00E-03	2.81E-03	
C ₂ H ₄	7.34E-04	7.65E-04	7.86E-04	7.62E-04±2E-05	4.58E-04	2.43E-04	
C ₂ H ₆	3.52E-05	4.06E-05	3.25E-05	3.61E-05±4E-06	0	0	
C ₃ H ₆	0	0	0	0±0	0	0	
C ₃ H ₈	0	0	0	0±0	0	0	
1-C ₄ H ₈	0	0	0	0±0	0	0	
1,3-C ₄ H ₆	0	0	0	0±0	0	0	
CH ₃ CHO	0	0	0	0±0	0	0	
CH ₂ =CHCHO	0	0	0	0±0	0	0	
C ₂ H ₅ CHO	0	0	0	0±0	0	0	
CH ₃ CH ₂ CH ₂ C(O)OH	0	0	0	0±0	0	0	
CH ₂ =CHC(O)OH	0	0	0	0±0	0	0	
CH ₃ CH ₂ CH ₂ C(O)OC ₂ H ₅	0	0	0	0±0	0	0	

Notes: ^a Material balances were illustrated in Table 2 for these experiments. ^b Experiments for which the composition analysis by GC/FID was repeated two or three times.

Chapter III Experimental and Kinetic Modeling Study of Ethyl butanoate Oxidation in a Tubular Plug Flow Reactor - From Low to High Temperature under Atmospheric Pressure

Table AIII.5: Experimental temperature profiles measured along the tubular reactor without conducting oxidation reaction for different set point temperatures of the oven

Axial coordinate (z/cm)	Oven set point temperature (K)															
	500	550	600	650	700	750	800	850	900	950	1000	1050	1100	1150	1175	1200
0	480	484	487	491	492	508	506	513	521	531	544	557	581	585	587	593
1	481	486	490	497	497	520	524	555	555	563	570	580	614	630	629	631
2	482	487	493	503	501	531	542	597	589	595	595	603	647	675	676	669
3	485	492	498	511	510	547	560	616	622	625	632	641	683	700	720	721
4	487	496	503	519	518	562	577	635	655	655	669	679	719	724	770	773
5	492	503	512	531	535	576	597	661	681	681	715	717	760	766	808	812
6	497	509	520	543	551	590	616	686	707	708	760	755	801	807	845	851
7	500	515	530	556	565	611	638	719	752	760	811	797	861	871	893	900
8	503	520	540	568	578	632	659	751	797	814	862	839	921	935	941	948
9	507	530	552	586	603	657	687	776	821	850	874	878	957	980	985	1002
10	511	540	563	603	628	681	715	800	845	885	885	916	993	1025	1029	1055
11	517	555	576	625	655	704	741	818	866	906	911	942	1021	1040	1062	1097
12	523	569	588	647	682	727	767	835	886	927	936	967	1049	1054	1095	1139
13	529	576	607	659	696	740	783	856	902	945	956	991	1078	1085	1125	1151
14	535	582	626	670	710	753	798	876	917	963	976	1015	1106	1115	1154	1162
15	539	588	632	678	723	767	811	884	926	971	988	1036	1118	1125	1171	1187
16	543	593	638	686	736	780	824	891	935	979	1000	1057	1130	1134	1188	1211
17	546	597	643	692	744	788	834	894	938	984	1015	1068	1134	1149	1193	1212
18	549	600	647	698	751	796	844	896	941	988	1030	1078	1137	1163	1198	1213
19	550	601	650	700	754	799	846	897	942	989	1035	1081	1139	1168	1199	1217
20	550	602	652	702	756	802	847	898	943	990	1040	1084	1140	1173	1200	1220
21	549	602	652	702	757	802	848	897	943	990	1041	1085	1140	1175	1201	1222
22	548	601	651	701	757	802	848	896	943	990	1042	1086	1140	1177	1201	1224
23	547	600	650	700	756	801	848	895	942	989	1042	1086	1140	1178	1201	1225
24	545	598	648	699	754	800	847	894	941	988	1042	1086	1139	1178	1200	1225
25	543	595	646	697	752	798	846	892	939	987	1041	1084	1138	1178	1200	1225
26	540	591	644	694	749	796	844	889	937	985	1039	1082	1137	1177	1199	1224
27	537	587	642	691	746	794	842	887	935	983	1038	1080	1134	1176	1197	1223
28	533	583	640	688	743	792	839	884	932	980	1036	1077	1131	1174	1195	1222
29	530	580	635	684	739	788	835	880	929	977	1033	1075	1129	1173	1193	1221
30	526	576	629	679	735	783	830	876	925	974	1029	1072	1126	1171	1191	1219
31	521	571	618	673	729	779	825	871	921	971	1028	1069	1122	1168	1189	1217
32	515	565	607	667	723	774	820	866	917	967	1027	1066	1118	1165	1186	1214
33	507	557	599	661	716	767	815	860	912	963	1020	1061	1113	1161	1183	1211
34	499	548	591	654	708	760	809	853	906	959	1012	1056	1107	1157	1179	1208
35	494	540	580	647	699	752	802	845	899	952	1006	1049	1101	1153	1174	1204
36	488	531	568	639	690	744	794	836	892	944	999	1041	1094	1148	1168	1200

Chapter III Experimental and Kinetic Modeling Study of Ethyl butanoate Oxidation in a Tubular Plug Flow Reactor - From Low to High Temperature under Atmospheric Pressure

Table AIII.5 (Continued)

Axial coordinate (z/cm)	Oven set point temperature (K)															
	500	550	600	650	700	750	800	850	900	950	1000	1050	1100	1150	1175	1200
37	478	521	556	629	674	731	782	823	881	935	989	1034	1086	1141	1162	1194
38	468	510	543	619	658	718	769	810	869	926	978	1026	1077	1134	1156	1187
39	458	497	536	608	643	703	755	802	859	918	971	1020	1068	1130	1149	1183
40	448	484	529	597	627	688	741	793	848	910	963	1013	1058	1126	1142	1179
41	441	475	515	585	613	678	731	783	837	898	948	1000	1047	1114	1136	1170
42	433	465	500	573	599	668	720	773	825	886	933	987	1036	1102	1129	1161
43	426	459	486	561	582	652	711	751	813	874	921	965	1018	1092	1113	1152
44	419	453	471	549	564	635	702	728	800	861	908	943	999	1081	1097	1143
45	407	437	454	533	534	612	671	696	753	802	859	865	920	1029	1044	1093
46	394	421	436	516	504	589	640	664	705	743	810	787	841	976	990	1042
47	387	406	420	485	469	548	592	608	660	706	736	727	779	920	918	986
48	379	390	403	453	434	506	544	552	614	669	661	667	717	863	845	930
49	375	387	393	435	419	490	523	538	594	654	630	633	685	818	818	876
50	370	383	383	417	403	474	501	523	573	638	598	599	653	773	790	821
51	367	380	381	415	394	465	491	515	552	606	571	586	607	732	737	772
52	363	377	379	412	385	456	480	506	530	573	543	573	561	691	683	723
53	360	375	377	408	377	447	467	491	515	551	517	534	532	650	636	677
54	357	373	374	403	368	437	454	476	499	528	491	494	503	609	589	631
55	353	354	369	376	356	403	415	426	436	448	453	459	467	494	532	559

Chapter III Experimental and Kinetic Modeling Study of Ethyl butanoate Oxidation in a Tubular Plug Flow Reactor - From Low to High Temperature under Atmospheric Pressure

Table AIII.6: Primary mechanism for the oxidation of ethyl butanoate

n°	Reactions	A	b	E
<i>Unimolecular decomposition</i>				
1	$C_6H_{12}O_2S \Rightarrow C_4H_8O_2B + C_2H_4Z$	2.00E+12	0	47290
<i>Unimolecular initiation</i>				
2	$C_6H_{12}O_2S \Rightarrow \cdot CH_2CH_2C(=O)OC_2H_5 + \cdot CH_3$	1.70E+17	0	86910.5
3	$C_6H_{12}O_2S \Rightarrow \cdot CH_2C(=O)OC_2H_5 + \cdot C_2H_5$	4.50E+15	0	81275.1
4	$C_6H_{12}O_2S \Rightarrow \cdot C(=O)OCH_2CH_3 + nC_3H_7\cdot$	7.50E+16	0	91443
5	$C_6H_{12}O_2S \Rightarrow C_2H_5O\cdot + C_3H_7\cdot C(=O)$	1.30E+16	0	96618.7
6	$C_6H_{12}O_2S \Rightarrow \cdot C_2H_5 + C_3H_7C(=O)O\cdot$	1.10E+15	0	86283.5
7	$C_6H_{12}O_2S \Rightarrow \cdot CH_3 + C_3H_7C(=O)OCH_2\cdot$	1.00E+17	0	88727.2
8	$C_4H_8O_2B \Rightarrow \cdot OH + C_3H_7\cdot C(=O)$	1.40E+17	0	105815.7
9	$C_4H_8O_2B \Rightarrow \cdot H + C_3H_7C(=O)O\cdot$	2.30E+14	0	106345.3
10	$C_4H_8O_2B \Rightarrow nC_3H_7\cdot + \cdot C(=O)OH$	8.20E+16	0	88817
11	$C_4H_8O_2B \Rightarrow \cdot C_2H_5 + \cdot CH_2C(=O)OH$	2.90E+16	0	78917.1
12	$C_4H_8O_2B \Rightarrow \cdot CH_3 + \cdot CH_2CH_2C(=O)OH$	1.70E+17	0	87662.1
<i>Bimolecular initiation</i>				
13	$C_6H_{12}O_2S + O_2 \Rightarrow HO_2\cdot + \cdot CH_2C_2H_4C(=O)OC_2H_5$	2.10E+13	0	53029.5
14	$C_6H_{12}O_2S + O_2 \Rightarrow HO_2\cdot + C_3H_7C(=O)OCH_2CH_2\cdot$	2.10E+13	0	53029.5
15	$C_6H_{12}O_2S + O_2 \Rightarrow HO_2\cdot + C_3H_7C(=O)OCH\cdot CH_3$	1.40E+13	0	48666.7
16	$C_6H_{12}O_2S + O_2 \Rightarrow HO_2\cdot + C_2H_5\cdot CHC(=O)OC_2H_5$	1.40E+13	0	46508.9
17	$C_6H_{12}O_2S + O_2 \Rightarrow HO_2\cdot + CH_3\cdot CHCH_2C(=O)OC_2H_5$	1.40E+13	0	50585.5
18	$C_4H_8O_2B + O_2 \Rightarrow HO_2\cdot + C_3H_7C(=O)O\cdot$	7.00E+12	0	57766.2
19	$C_4H_8O_2B + O_2 \Rightarrow HO_2\cdot + \cdot CH_2C_2H_4C(=O)OH$	2.10E+13	0	53029.5
20	$C_4H_8O_2B + O_2 \Rightarrow HO_2\cdot + CH_3\cdot CHCH_2C(=O)OH$	1.40E+13	0	50585.5
21	$C_4H_8O_2B + O_2 \Rightarrow HO_2\cdot + C_2H_5\cdot CHC(=O)OH$	1.40E+13	0	46507.3
<i>Isomerizations</i>				
22	$nC_4H_9\cdot = CH_3\cdot CHC_2H_5$	3.30E+09	1	37000
23	$\cdot CH_2C_2H_4C(=O)OC_2H_5 = C_2H_5\cdot CHC(=O)OC_2H_5$	3.30E+09	1	35000
24	$\cdot CH_2C_2H_4C(=O)OC_2H_5 = C_3H_7C(=O)OCH\cdot CH_3$	1.70E+07	1	15400
25	$\cdot CH_2C_2H_4C(=O)OC_2H_5 = C_3H_7C(=O)OCH_2CH_2\cdot$	4.40E+06	1	23400
26	$C_3H_7C(=O)OCH_2CH_2\cdot = C_2H_5\cdot CHC(=O)OC_2H_5$	9.90E+07	1	12000
27	$C_3H_7C(=O)OCH_2CH_2\cdot = CH_3\cdot CHCH_2C(=O)OC_2H_5$	1.70E+07	1	17400
28	$C_3H_7C(=O)OCH\cdot CH_3 = C_2H_5\cdot CHC(=O)OC_2H_5$	5.70E+08	1	21300
29	$C_3H_7C(=O)OCH\cdot CH_3 = CH_3\cdot CHCH_2C(=O)OC_2H_5$	9.90E+07	1	18000
30	$\cdot CH_2C_2H_4C(=O)OH = C_2H_5\cdot CHC(=O)OH$	3.3E+09	1	37000
31	$\cdot CH_2C(=O)OC_2H_5 = CH_3(=O)OCH\cdot CH_3$	5.70E+08	1	15300

Chapter III Experimental and Kinetic Modeling Study of Ethyl butanoate Oxidation in a Tubular Plug Flow Reactor - From Low to High Temperature under Atmospheric Pressure

Table AIII.6 (Continued)

n°	Reactions	A	b	E
<i>Isomerizations (continued)</i>				
32	$\cdot\text{CH}_2\text{C}(=\text{O})\text{OC}_2\text{H}_5 = \text{CH}_3(=\text{O})\text{OCH}_2\text{CH}_2\cdot$	1.50E+08	1	14500
33	$\cdot\text{CH}_2\text{C}_2\text{H}_4\text{C}(=\text{O})\text{OH} = \text{C}_2\text{H}_5\cdot\text{CHC}(=\text{O})\text{OH}$	3.30E+09	1	37000
33	$\cdot\text{CH}_2\text{C}(=\text{O})\text{OC}_2\text{H}_5 = \text{CH}_3\text{C}(=\text{O})\text{O}\cdot\text{CHCH}_3$	5.70E+08	1	15300
34	$\cdot\text{CH}_2\text{C}(=\text{O})\text{OC}_2\text{H}_5 = \text{CH}_3\text{C}(=\text{O})\text{OCH}_2\text{CH}_2\cdot$	1.50E+08	1	14500
<i>β-scissions</i>				
35	$n\text{C}_3\text{H}_7\cdot \Rightarrow \cdot\text{CH}_3 + \text{C}_2\text{H}_4\text{Z}$	2.00E+13	0	31000
36	$n\text{C}_3\text{H}_7\cdot \Rightarrow \cdot\text{H} + \text{C}_3\text{H}_6$	3.00E+13	0	38000
37	$n\text{C}_4\text{H}_9\cdot \Rightarrow \cdot\text{C}_2\text{H}_5 + \text{C}_2\text{H}_4\text{Z}$	2.00E+13	0	28700
38	$n\text{C}_4\text{H}_9\cdot \Rightarrow \cdot\text{H} + \text{C}_4\text{H}_8\text{Y}$	3.00E+13	0	38000
39	$\cdot\text{CH}_2\text{C}_2\text{H}_4\text{C}(=\text{O})\text{OC}_2\text{H}_5 \Rightarrow \cdot\text{CH}_2\text{C}(=\text{O})\text{OC}_2\text{H}_5 + \text{C}_2\text{H}_4\text{Z}$	2.10E+13	0	27800
40	$\cdot\text{CH}_2\text{C}_2\text{H}_4\text{C}(=\text{O})\text{OC}_2\text{H}_5 \Rightarrow \cdot\text{H} + \text{C}_6\text{H}_{10}\text{O}_2\text{ZS}$	3.00E+13	0	38000
41	$\text{C}_3\text{H}_7\text{C}(=\text{O})\text{OCH}_2\text{CH}_2\cdot \Rightarrow \text{C}_3\text{H}_7\text{C}(=\text{O})\text{O}\cdot + \text{C}_2\text{H}_4\text{Z}$	2.10E+13	0	25100
42	$\text{C}_3\text{H}_7\text{C}(=\text{O})\text{OCH}_2\text{CH}_2\cdot \Rightarrow \cdot\text{H} + \text{C}_6\text{H}_{10}\text{O}_2\text{ZS}$	3.00E+13	0	38000
43	$\text{C}_3\text{H}_7\text{C}(=\text{O})\text{OCH}\cdot\text{CH}_3 \Rightarrow \text{C}_3\text{H}_7\cdot\text{C}(=\text{O}) + \text{CH}_3\text{CHO}$	2.10E+13	0	31900
44	$\text{C}_3\text{H}_7\text{C}(=\text{O})\text{OCH}\cdot\text{CH}_3 \Rightarrow \cdot\text{H} + \text{C}_6\text{H}_{10}\text{O}_2\text{ZS}$	3.0E+13	0	39000
45	$\text{C}_2\text{H}_5\cdot\text{CHC}(=\text{O})\text{OC}_2\text{H}_5 \Rightarrow \cdot\text{H} + \text{C}_6\text{H}_{10}\text{O}_2\text{ZS}$	3.00E+13	0	38000
46	$\text{C}_2\text{H}_5\cdot\text{CHC}(=\text{O})\text{OC}_2\text{H}_5 \Rightarrow \text{C}_2\text{H}_5\text{O}\cdot + \text{C}_4\text{H}_6\text{OKZ}$	2.10E+13	0	49000
47	$\text{C}_2\text{H}_5\cdot\text{CHC}(=\text{O})\text{OC}_2\text{H}_5 \Rightarrow \cdot\text{CH}_3 + \text{C}_5\text{H}_8\text{O}_2\text{ZS}$	2.00E+13	0	31300
48	$\text{CH}_3\cdot\text{CHCH}_2\text{C}(=\text{O})\text{OC}_2\text{H}_5 \Rightarrow \cdot\text{C}(=\text{O})\text{OCH}_2\text{CH}_3 + \text{C}_3\text{H}_6$	2.10E+13	0	31200
49	$\text{CH}_3\cdot\text{CHCH}_2\text{C}(=\text{O})\text{OC}_2\text{H}_5 \Rightarrow \cdot\text{H} + \text{C}_6\text{H}_{10}\text{O}_2\text{ZS}$	3.00E+13	0	38000
50	$\text{CH}_3\cdot\text{CHCH}_2\text{C}(=\text{O})\text{OC}_2\text{H}_5 \Rightarrow \cdot\text{H} + \text{C}_6\text{H}_{10}\text{O}_2\text{ZS}$	3.00E+13	0	39000
51	$\text{C}_3\text{H}_7\text{C}(=\text{O})\text{O}\cdot \Rightarrow n\text{C}_3\text{H}_7\cdot + \text{CO}_2$	2.00E+13	0	5100
52	$\cdot\text{CH}_2\text{C}_2\text{H}_4\text{C}(=\text{O})\text{OH} \Rightarrow \cdot\text{CH}_2\text{C}(=\text{O})\text{OH} + \text{C}_2\text{H}_4\text{Z}$	2.00E+13	0	28700
53	$\cdot\text{CH}_2\text{C}_2\text{H}_4\text{C}(=\text{O})\text{OH} \Rightarrow \cdot\text{H} + \text{C}_4\text{H}_6\text{O}_2\text{ZB}$	3.00E+13	0	38000
54	$\text{CH}_3\cdot\text{CHCH}_2\text{C}(=\text{O})\text{OH} \Rightarrow \cdot\text{C}(=\text{O})\text{OH} + \text{C}_3\text{H}_6$	2.00E+13	0	28700
55	$\text{CH}_3\cdot\text{CHCH}_2\text{C}(=\text{O})\text{OH} \Rightarrow \cdot\text{H} + \text{C}_4\text{H}_6\text{O}_2\text{ZB}$	3.00E+13	0	38000
56	$\text{CH}_3\cdot\text{CHCH}_2\text{C}(=\text{O})\text{OH} \Rightarrow \cdot\text{H} + \text{C}_4\text{H}_6\text{O}_2\text{ZB}$	3.00E+13	0	39000
57	$\text{C}_2\text{H}_5\cdot\text{CHC}(=\text{O})\text{OH} \Rightarrow \cdot\text{OH} + \text{C}_4\text{H}_6\text{OKZ}$	2.00E+13	0	49000
58	$\text{C}_2\text{H}_5\cdot\text{CHC}(=\text{O})\text{OH} \Rightarrow \cdot\text{H} + \text{C}_4\text{H}_6\text{O}_2\text{ZB}$	3.00E+13	0	38000
59	$\text{C}_2\text{H}_5\cdot\text{CHC}(=\text{O})\text{OH} \Rightarrow \cdot\text{CH}_3 + \text{C}_3\text{H}_4\text{O}_2\text{ZB}$	2.00E+13	0	31000
60	$\text{CH}_3\cdot\text{CHC}_2\text{H}_5 \Rightarrow \cdot\text{CH}_3 + \text{C}_3\text{H}_6$	2.00E+13	0	31000
61	$\text{CH}_3\cdot\text{CHC}_2\text{H}_5 \Rightarrow \cdot\text{H} + \text{C}_4\text{H}_8\text{Y}$	3.00E+13	0	38000
62	$\text{CH}_3\cdot\text{CHC}_2\text{H}_5 \Rightarrow \cdot\text{H} + \text{C}_4\text{H}_8\text{Y}$	3.00E+13	0	39000
63	$\cdot\text{CH}_2\text{C}(=\text{O})\text{OC}_2\text{H}_5 \Rightarrow \text{C}_2\text{H}_5\text{O}\cdot + \text{CH}_2\text{COZ}$	2.00E+13	0	49000

Chapter III Experimental and Kinetic Modeling Study of Ethyl butanoate Oxidation in a Tubular Plug Flow Reactor - From Low to High Temperature under Atmospheric Pressure

Table AIII.6 (Continued)

n°	Reactions	A	b	E
<i>β -scissions (continued)</i>				
64	$\text{CH}_3\text{C}(=\text{O})\text{O}^*\text{CHCH}_3 \Rightarrow \text{CH}_3^*\text{C}(=\text{O}) + \text{CH}_3\text{CHO}$	2.00E+13	0	31900
65	$\text{CH}_3\text{C}(=\text{O})\text{O}^*\text{CHCH}_3 \Rightarrow ^*\text{H} + \text{C}_4\text{H}_6\text{O}_2\text{ZS}$	3.00E+13	0	39000
66	$\text{CH}_3\text{C}(=\text{O})\text{OCH}_2\text{CH}_2^* \Rightarrow ^*\text{H} + \text{C}_4\text{H}_6\text{O}_2\text{ZS}$	3.00E+13	0	38000
67	$^*\text{CH}_2\text{CH}_2\text{C}(=\text{O})\text{OC}_2\text{H}_5 \Rightarrow ^*\text{C}(=\text{O})\text{OCH}_2\text{CH}_3 + \text{C}_2\text{H}_4\text{Z}$	2.10E+13	0	31200
68	$^*\text{CH}_2\text{CH}_2\text{C}(=\text{O})\text{OC}_2\text{H}_5 \Rightarrow ^*\text{H} + \text{C}_5\text{H}_8\text{O}_2\text{ZS}$	3.00E+13	0	38000
69	$\text{C}_3\text{H}_7\text{C}(=\text{O})\text{OCH}_2^* \Rightarrow \text{C}_3\text{H}_7^*\text{C}(=\text{O}) + \text{HCHO}$	2.10E+13	0	31900
70	$^*\text{CH}_2\text{CH}_2\text{C}(=\text{O})\text{OH} \Rightarrow ^*\text{C}(=\text{O})\text{OH} + \text{C}_2\text{H}_4\text{Z}$	2.00E+13	0	28700
71	$^*\text{CH}_2\text{CH}_2\text{C}(=\text{O})\text{OH} \Rightarrow ^*\text{H} + \text{C}_3\text{H}_4\text{O}_2\text{ZB}$	3.00E+13	0	38000
72	$\text{C}_3\text{H}_7^*\text{C}(=\text{O}) \Rightarrow n\text{C}_3\text{H}_7^* + ^*\text{C}^*\text{O}$	2.80E+13	0	17150
73	$^*\text{C}(=\text{O})\text{OCH}_2\text{CH}_3 \Rightarrow \text{C}_2\text{H}_5\text{O}^* + ^*\text{C}^*\text{O}$	2.80E+13	0	17150
<i>Oxidations</i>				
74	$^*\text{CH}_2\text{C}_2\text{H}_4\text{C}(=\text{O})\text{OC}_2\text{H}_5 + \text{O}_2 \Rightarrow \text{C}_6\text{H}_{10}\text{O}_2\text{ZS} + \text{HO}_2^*$	1.90E+12	0	5000
75	$\text{C}_3\text{H}_7\text{C}(=\text{O})\text{OCH}_2\text{CH}_2^* + \text{O}_2 \Rightarrow \text{C}_6\text{H}_{10}\text{O}_2\text{ZS} + \text{HO}_2^*$	1.90E+12	0	5000
76	$\text{C}_3\text{H}_7\text{C}(=\text{O})\text{OCH}^*\text{CH}_3 + \text{O}_2 \Rightarrow \text{C}_6\text{H}_{10}\text{O}_2\text{ZS} + \text{HO}_2^*$	8.10E+11	0	5000
77	$\text{C}_2\text{H}_5^*\text{CHC}(=\text{O})\text{OC}_2\text{H}_5 + \text{O}_2 \Rightarrow \text{C}_6\text{H}_{10}\text{O}_2\text{ZS} + \text{HO}_2^*$	1.90E+12	0	5000
78	$\text{CH}_3^*\text{CHCH}_2\text{C}(=\text{O})\text{OC}_2\text{H}_5 + \text{O}_2 \Rightarrow \text{C}_6\text{H}_{10}\text{O}_2\text{ZS} + \text{HO}_2^*$	1.90E+12	0	5000
79	$\text{CH}_3^*\text{CHCH}_2\text{C}(=\text{O})\text{OC}_2\text{H}_5 + \text{O}_2 \Rightarrow \text{C}_6\text{H}_{10}\text{O}_2\text{ZS} + \text{HO}_2^*$	8.10E+11	0	5000
80	$^*\text{CH}_2\text{C}_2\text{H}_4\text{C}(=\text{O})\text{OH} + \text{O}_2 \Rightarrow \text{C}_4\text{H}_6\text{O}_2\text{ZB} + \text{HO}_2^*$	1.30E+12	0	5000
81	$\text{CH}_3^*\text{CHCH}_2\text{C}(=\text{O})\text{OH} + \text{O}_2 \Rightarrow \text{C}_4\text{H}_6\text{O}_2\text{ZB} + \text{HO}_2^*$	1.30E+12	0	5000
82	$\text{CH}_3^*\text{CHCH}_2\text{C}(=\text{O})\text{OH} + \text{O}_2 \Rightarrow \text{C}_4\text{H}_6\text{O}_2\text{ZB} + \text{HO}_2^*$	5.30E+11	0	5000
83	$\text{C}_2\text{H}_5^*\text{CHC}(=\text{O})\text{OH} + \text{O}_2 \Rightarrow \text{C}_4\text{H}_6\text{O}_2\text{ZB} + \text{HO}_2^*$	1.30E+12	0	5000
<i>Metathesis</i>				
84	$^*\text{O} + \text{C}_6\text{H}_{12}\text{O}_2\text{S} \Rightarrow ^*\text{OH} + ^*\text{CH}_2\text{C}_2\text{H}_4\text{C}(=\text{O})\text{OC}_2\text{H}_5$	5.10E+13	0	7850
85	$^*\text{O} + \text{C}_6\text{H}_{12}\text{O}_2\text{S} \Rightarrow ^*\text{OH} + \text{C}_3\text{H}_7\text{C}(=\text{O})\text{OCH}_2\text{CH}_2^*$	5.10E+08	0	7850
86	$^*\text{O} + \text{C}_6\text{H}_{12}\text{O}_2\text{S} \Rightarrow ^*\text{OH} + \text{C}_3\text{H}_7\text{C}(=\text{O})\text{OCH}^*\text{CH}_3$	3.40E+13	1.5	2500
87	$^*\text{O} + \text{C}_6\text{H}_{12}\text{O}_2\text{S} \Rightarrow ^*\text{OH} + \text{C}_2\text{H}_5^*\text{CHC}(=\text{O})\text{OC}_2\text{H}_5$	3.40E+08	1.5	620
88	$^*\text{O} + \text{C}_6\text{H}_{12}\text{O}_2\text{S} \Rightarrow ^*\text{OH} + \text{CH}_3^*\text{CHCH}_2\text{C}(=\text{O})\text{OC}_2\text{H}_5$	2.60E+13	0	5200
89	$^*\text{O} + \text{C}_4\text{H}_8\text{O}_2\text{B} \Rightarrow ^*\text{OH} + \text{C}_3\text{H}_7\text{C}(=\text{O})\text{O}^*$	1.00E+13	0	3280
90	$^*\text{O} + \text{C}_4\text{H}_8\text{O}_2\text{B} \Rightarrow ^*\text{OH} + ^*\text{CH}_2\text{C}_2\text{H}_4\text{C}(=\text{O})\text{OH}$	5.10E+13	0	7850
91	$^*\text{O} + \text{C}_4\text{H}_8\text{O}_2\text{B} \Rightarrow ^*\text{OH} + \text{CH}_3^*\text{CHCH}_2\text{C}(=\text{O})\text{OH}$	2.60E+13	0	5200
92	$^*\text{O} + \text{C}_4\text{H}_8\text{O}_2\text{B} \Rightarrow ^*\text{OH} + \text{C}_2\text{H}_5^*\text{CHC}(=\text{O})\text{OH}$	3.4E+08	1.5	620
93	$\text{C}_6\text{H}_{12}\text{O}_2\text{S} + ^*\text{H} \Rightarrow \text{H}_2 + ^*\text{CH}_2\text{C}_2\text{H}_4\text{C}(=\text{O})\text{OC}_2\text{H}_5$	2.90E+07	2	7700
94	$\text{C}_6\text{H}_{12}\text{O}_2\text{S} + ^*\text{H} \Rightarrow \text{H}_2 + \text{C}_3\text{H}_7\text{C}(=\text{O})\text{OCH}_2\text{CH}_2^*$	2.90E+07	2	7700
95	$\text{C}_6\text{H}_{12}\text{O}_2\text{S} + ^*\text{H} \Rightarrow \text{H}_2 + \text{C}_3\text{H}_7\text{C}(=\text{O})\text{OCH}^*\text{CH}_3$	9.00E+06	1.5	4610

Chapter III Experimental and Kinetic Modeling Study of Ethyl butanoate Oxidation in a Tubular Plug Flow Reactor - From Low to High Temperature under Atmospheric Pressure

Table AIII.6 (Continued)

n°	Reactions	A	b	E
<i>Metathesis (continued)</i>				
96	$C_6H_{12}O_2S + \cdot H \Rightarrow H_2 + C_2H_5 \cdot CHC(=O)OC_2H_5$	4.80E+08	1.5	2980
97	$C_6H_{12}O_2S + \cdot H \Rightarrow H_2 + CH_3 \cdot CHCH_2C(=O)OC_2H_5$	9.00E+06	2	5000
98	$C_4H_8O_2B + \cdot H \Rightarrow H_2 + C_3H_7C(=O)O \cdot$	4.20E+06	2	2400
99	$C_4H_8O_2B + \cdot H \Rightarrow H_2 + \cdot CH_2C_2H_4C(=O)OH$	2.90E+07	2	7700
100	$C_4H_8O_2B + \cdot H \Rightarrow H_2 + CH_3 \cdot CHCH_2C(=O)OH$	9.00E+06	2	5000
101	$C_4H_8O_2B + \cdot H \Rightarrow H_2 + C_2H_5 \cdot CHC(=O)OH$	4.80E+08	1.5	2980
102	$C_6H_{12}O_2S + \cdot OH \Rightarrow H_2O + \cdot CH_2C_2H_4C(=O)OC_2H_5$	2.70E+06	2	450
103	$C_6H_{12}O_2S + \cdot OH \Rightarrow H_2O + C_3H_7C(=O)OCH_2CH_2 \cdot$	2.70E+06	2	450
104	$C_6H_{12}O_2S + \cdot OH \Rightarrow H_2O + C_3H_7C(=O)OCH \cdot CH_3$	2.40E+06	2	-1200
105	$C_6H_{12}O_2S + \cdot OH \Rightarrow H_2O + C_2H_5 \cdot CHC(=O)OC_2H_5$	2.40E+06	2	-2450
106	$C_6H_{12}O_2S + \cdot OH \Rightarrow H_2O + CH_3 \cdot CHCH_2C(=O)OC_2H_5$	2.60E+06	2	-765
107	$C_4H_8O_2B + \cdot OH \Rightarrow H_2O + C_3H_7C(=O)O \cdot$	1.10E+06	2	-1865
108	$C_4H_8O_2B + \cdot OH \Rightarrow H_2O + \cdot CH_2C_2H_4C(=O)OH$	2.70E+06	2	450
109	$C_4H_8O_2B + \cdot OH \Rightarrow H_2O + CH_3 \cdot CHCH_2C(=O)OH$	2.60E+06	2	-765
110	$C_4H_8O_2B + \cdot OH \Rightarrow H_2O + C_2H_5 \cdot CHC(=O)OH$	2.40E+06	2	-2450
111	$C_6H_{12}O_2S + HO_2 \cdot \Rightarrow H_2O_2 + \cdot CH_2C_2H_4C(=O)OC_2H_5$	6.00E+11	0	17000
112	$C_6H_{12}O_2S + HO_2 \cdot \Rightarrow H_2O_2 + C_3H_7C(=O)OCH_2CH_2 \cdot$	6.00E+11	0	17000
113	$C_6H_{12}O_2S + HO_2 \cdot \Rightarrow H_2O_2 + C_3H_7C(=O)OCH \cdot CH_3$	2.80E+04	2.7	16500
114	$C_6H_{12}O_2S + HO_2 \cdot \Rightarrow H_2O_2 + C_2H_5 \cdot CHC(=O)OC_2H_5$	2.80E+04	2.7	15000
115	$C_6H_{12}O_2S + HO_2 \cdot \Rightarrow H_2O_2 + CH_3 \cdot CHCH_2C(=O)OC_2H_5$	4.00E+11	0	15500
116	$C_4H_8O_2B + HO_2 \cdot \Rightarrow H_2O_2 + C_3H_7C(=O)O \cdot$	2.00E+11	0	14000
117	$C_4H_8O_2B + HO_2 \cdot \Rightarrow H_2O_2 + \cdot CH_2C_2H_4C(=O)OH$	6.00E+11	0	17000
118	$C_4H_8O_2B + HO_2 \cdot \Rightarrow H_2O_2 + CH_3 \cdot CHCH_2C(=O)OH$	4.00E+11	0	15500
119	$C_4H_8O_2B + HO_2 \cdot \Rightarrow H_2O_2 + C_2H_5 \cdot CHC(=O)OH$	2.80E+04	2.7	15000
120	$C_6H_{12}O_2S + \cdot CH_3 \Rightarrow CH_4 + \cdot CH_2C_2H_4C(=O)OC_2H_5$	3.00E-01	4	8200
121	$C_6H_{12}O_2S + \cdot CH_3 \Rightarrow CH_4 + C_3H_7C(=O)OCH_2CH_2 \cdot$	3.00E-01	4	8200
122	$C_6H_{12}O_2S + \cdot CH_3 \Rightarrow CH_4 + C_3H_7C(=O)OCH \cdot CH_3$	1.60E+06	1.9	8140
123	$C_6H_{12}O_2S + \cdot CH_3 \Rightarrow CH_4 + C_2H_5 \cdot CHC(=O)OC_2H_5$	1.60E+06	1.9	6510
124	$C_6H_{12}O_2S + \cdot CH_3 \Rightarrow CH_4 + CH_3 \cdot CHCH_2C(=O)OC_2H_5$	2.00E+11	0	9600
125	$C_4H_8O_2B + \cdot CH_3 \Rightarrow CH_4 + C_3H_7C(=O)O \cdot$	1.00E+11	0	7900
126	$C_4H_8O_2B + \cdot CH_3 \Rightarrow CH_4 + \cdot CH_2C_2H_4C(=O)OH$	3.00E-01	4	8200
127	$C_4H_8O_2B + \cdot CH_3 \Rightarrow CH_4 + CH_3 \cdot CHCH_2C(=O)OH$	2.00E+11	0	9600
128	$C_4H_8O_2B + \cdot CH_3 \Rightarrow CH_4 + C_2H_5 \cdot CHC(=O)OH$	1.60E+06	1.9	6510
129	$C_6H_{12}O_2S + \cdot CHO \Rightarrow HCHO + \cdot CH_2C_2H_4C(=O)OC_2H_5$	1.00E+05	2.5	18500

Chapter III Experimental and Kinetic Modeling Study of Ethyl butanoate Oxidation in a Tubular Plug Flow Reactor - From Low to High Temperature under Atmospheric Pressure

Table AIII.6 (Continued)

n°	Reactions	A	b	E
<i>Metathesis (continued)</i>				
130	$C_6H_{12}O_2S + \dot{C}HO \Rightarrow HCHO + C_3H_7C(=O)OCH_2CH_2\dot{C}$	1.00E+05	2.5	18500
131	$C_6H_{12}O_2S + \dot{C}HO \Rightarrow HCHO + C_3H_7C(=O)OCH\dot{C}H_3$	6.80E+04	2.5	13500
132	$C_6H_{12}O_2S + \dot{C}HO \Rightarrow HCHO + C_2H_5\dot{C}HC(=O)OC_2H_5$	6.80E+04	2.5	13500
133	$C_6H_{12}O_2S + \dot{C}HO \Rightarrow HCHO + CH_3\dot{C}HCH_2C(=O)OC_2H_5$	1.00E+07	1.9	17000
134	$C_4H_8O_2B + \dot{C}HO \Rightarrow HCHO + C_3H_7C(=O)O\dot{C}$	3.40E+04	2.5	13500
135	$C_4H_8O_2B + \dot{C}HO \Rightarrow HCHO + \dot{C}H_2C_2H_4C(=O)OH$	1.00E+05	2.5	18500
136	$C_4H_8O_2B + \dot{C}HO \Rightarrow HCHO + CH_3\dot{C}HCH_2C(=O)OH$	1.00E+07	1.9	17000
137	$C_4H_8O_2B + \dot{C}HO \Rightarrow HCHO + C_2H_5\dot{C}HC(=O)OH$	6.80E+04	2.5	13500
138	$C_6H_{12}O_2S + \dot{C}H_2OH \Rightarrow CH_3OH + \dot{C}H_2C_2H_4C(=O)OC_2H_5$	9.90E+01	2.95	14000
139	$C_6H_{12}O_2S + \dot{C}H_2OH \Rightarrow CH_3OH + C_3H_7C(=O)OCH_2CH_2\dot{C}$	9.90E+01	2.95	14000
140	$C_6H_{12}O_2S + \dot{C}H_2OH \Rightarrow CH_3OH + C_3H_7C(=O)OCH\dot{C}H_3$	2.40E+02	2.8	10800
141	$C_6H_{12}O_2S + \dot{C}H_2OH \Rightarrow CH_3OH + C_2H_5\dot{C}HC(=O)OC_2H_5$	2.40E+02	2.8	10800
142	$C_6H_{12}O_2S + \dot{C}H_2OH \Rightarrow CH_3OH + CH_3\dot{C}HCH_2C(=O)OC_2H_5$	6.00E+01	2.95	12000
143	$C_4H_8O_2B + \dot{C}H_2OH \Rightarrow CH_3OH + C_3H_7C(=O)O\dot{C}$	1.20E+02	2.8	10800
144	$C_4H_8O_2B + \dot{C}H_2OH \Rightarrow CH_3OH + \dot{C}H_2C_2H_4C(=O)OH$	9.90E+01	2.95	14000
145	$C_4H_8O_2B + \dot{C}H_2OH \Rightarrow CH_3OH + CH_3\dot{C}HCH_2C(=O)OH$	6.00E+01	2.95	12000
146	$C_4H_8O_2B + \dot{C}H_2OH \Rightarrow CH_3OH + C_2H_5\dot{C}HC(=O)OH$	2.40E+02	2.8	10800
147	$C_6H_{12}O_2S + CH_3O\dot{C} \Rightarrow CH_3OH + \dot{C}H_2C_2H_4C(=O)OC_2H_5$	1.60E+11	0	7300
148	$C_6H_{12}O_2S + CH_3O\dot{C} \Rightarrow CH_3OH + C_3H_7C(=O)OCH_2CH_2\dot{C}$	1.60E+11	0	7300
149	$C_6H_{12}O_2S + CH_3O\dot{C} \Rightarrow CH_3OH + C_3H_7C(=O)OCH\dot{C}H_3$	4.60E+01	0	2900
150	$C_6H_{12}O_2S + CH_3O\dot{C} \Rightarrow CH_3OH + C_2H_5\dot{C}HC(=O)OC_2H_5$	4.60E+10	0	2900
151	$C_6H_{12}O_2S + CH_3O\dot{C} \Rightarrow CH_3OH + CH_3\dot{C}HCH_2C(=O)OC_2H_5$	1.50E+11	0	4500
152	$C_4H_8O_2B + CH_3O\dot{C} \Rightarrow CH_3OH + C_3H_7C(=O)O\dot{C}$	2.30E+10	0	2900
153	$C_4H_8O_2B + CH_3O\dot{C} \Rightarrow CH_3OH + \dot{C}H_2C_2H_4C(=O)OH$	1.60E+11	0	7300
154	$C_4H_8O_2B + CH_3O\dot{C} \Rightarrow CH_3OH + CH_3\dot{C}HCH_2C(=O)OH$	1.50E+11	0	4500
155	$C_4H_8O_2B + CH_3O\dot{C} \Rightarrow CH_3OH + C_2H_5\dot{C}HC(=O)OH$	4.60E+01	0	2900
156	$C_6H_{12}O_2S + CH_3OO\dot{C} \Rightarrow CH_3OOH + \dot{C}H_2C_2H_4C(=O)OC_2H_5$	6.00E+12	0	20000
157	$C_6H_{12}O_2S + CH_3OO\dot{C} \Rightarrow CH_3OOH + C_3H_7C(=O)OCH_2CH_2\dot{C}$	6.00E+12	0	20000
158	$C_6H_{12}O_2S + CH_3OO\dot{C} \Rightarrow CH_3OOH + C_3H_7C(=O)OCH\dot{C}H_3$	3.00E+12	0	15000
159	$C_6H_{12}O_2S + CH_3OO\dot{C} \Rightarrow CH_3OOH + C_2H_5\dot{C}HC(=O)OC_2H_5$	3.00E+12	0	15000
160	$C_6H_{12}O_2S + CH_3OO\dot{C} \Rightarrow CH_3OOH + CH_3\dot{C}HCH_2C(=O)OC_2H_5$	3.00E+12	0	17500
161	$C_4H_8O_2B + CH_3OO\dot{C} \Rightarrow CH_3OOH + C_3H_7C(=O)O\dot{C}$	1.50E+12	0	15000
162	$C_4H_8O_2B + CH_3OO\dot{C} \Rightarrow CH_3OOH + \dot{C}H_2C_2H_4C(=O)OH$	6.00E+12	0	20000
163	$C_4H_8O_2B + CH_3OO\dot{C} \Rightarrow CH_3OOH + CH_3\dot{C}HCH_2C(=O)OH$	3.00E+12	0	17500

Chapter III Experimental and Kinetic Modeling Study of Ethyl butanoate Oxidation in a Tubular Plug Flow Reactor - From Low to High Temperature under Atmospheric Pressure

Table AIII.6 (Continued)

n°	Reactions	A	b	E
<i>Metathesis (continued)</i>				
164	$C_4H_8O_2B + CH_3OO\cdot \Rightarrow CH_3OOH + C_2H_5\cdot CHC(=O)OH$	3.00E+12	0	15000
165	$C_6H_{12}O_2S + \cdot C_2H_5 \Rightarrow C_2H_6 + \cdot CH_2C_2H_4C(=O)OC_2H_5$	3.00E+11	0	13500
166	$C_6H_{12}O_2S + \cdot C_2H_5 \Rightarrow C_2H_6 + C_3H_7C(=O)OCH_2CH_2\cdot$	3.00E+11	0	13500
167	$C_6H_{12}O_2S + \cdot C_2H_5 \Rightarrow C_2H_6 + C_3H_7C(=O)OCH\cdot CH_3$	2.00E+11	0	9200
168	$C_6H_{12}O_2S + \cdot C_2H_5 \Rightarrow C_2H_6 + C_2H_5\cdot CHC(=O)OC_2H_5$	2.00E+11	0	9200
169	$C_6H_{12}O_2S + \cdot C_2H_5 \Rightarrow C_2H_6 + CH_3\cdot CHCH_2C(=O)OC_2H_5$	2.00E+11	0	11000
170	$C_4H_8O_2B + \cdot C_2H_5 \Rightarrow C_2H_6 + C_3H_7C(=O)O\cdot$	1.00E+11	0	9200
171	$C_4H_8O_2B + \cdot C_2H_5 \Rightarrow C_2H_6 + \cdot CH_2C_2H_4C(=O)OH$	3.00E+11	0	13500
172	$C_4H_8O_2B + \cdot C_2H_5 \Rightarrow C_2H_6 + CH_3\cdot CHCH_2C(=O)OH$	2.00E+11	0	11000
173	$C_4H_8O_2B + \cdot C_2H_5 \Rightarrow C_2H_6 + C_2H_5\cdot CHC(=O)OH$	2.00E+11	0	9200

Notes: ^a The rate constants are given at 1 atm ($k=A T^b \exp(-E_a/RT)$) in cm^3 , mol, s, cal units and have been estimated as detailed in a previous paper by Hakka et al. [25]. ^b The letters indicate the chemical functions carried by the molecules. B: acid carboxylic function (-C(=O)OH), K: ketone function (-C(=O)-), S: ester function (-C(=O)-O-R), Z: unsaturation (C=C). Several reactions are written in duplicate with different rate parameters as they correspond to distinct channels.

CONCLUSIONS & ROSPECTS

Conclusions & Prospects

As expressed in introduction, the aim of this PhD work was to provide more information on the combustion characteristics of biodiesel which is a renewable and environmental friendly alternative fuel for diesel engine. Indeed, this biofuel can be produced from various bio-lipid raw materials (i.e. food grade vegetable oils, nonfood grade vegetable oils, animal fats or waste cooking oils) and alcohol (mainly methanol or ethanol) by transesterification in the presence of a catalyst. The main products of the reaction, i.e. fatty acid alkyl (methyl or ethyl) esters are the biodiesel components, while glycerol which is simultaneously formed is the by-product,

This work has been especially focused on the oxidation kinetics of ethyl esters as biodiesel surrogates for a better knowledge on the combustion in diesel engine of this class of compounds in terms of the pollutant emissions (CO, CO₂, hydrocarbons...). Therefore, to accomplish this objective, experiments were carried out in two types of reactors.

A shock tube study was carried out for five methyl or ethyl esters with a saturated or unsaturated aliphatic main chain: ethyl butanoate, ethyl crotonate, ethyl acrylate, methyl crotonate, and methyl acrylate, as model components of biodiesel. The delay times were measured for temperatures from 1280 to 1930 K, pressures from 7 to 9.65 atm, fuel molar concentrations of 0.4, 0.5, and 1%, and equivalence ratios equal to 0.25, 1.0, and 2.0. Ignition delay times were recorded behind the reflected shock wave using chemiluminescence emission from OH* at 306 nm and piezoelectric pressure measurements made at the shock tube sidewall. Furthermore, the reactivity of ethyl esters was compared to that of methyl esters under shock tube conditions of $\varphi=1.0$. It was found that under these conditions, no important difference of reactivity was observed between methyl and ethyl unsaturated esters, methyl and ethyl crotonate having the same reactivity as methyl butanoate. The reactivity of acrylates is more important than that of crotonates especially at the lowest investigated temperatures. Moreover, detailed chemical kinetic mechanisms of these esters were automatically generated using the version of EXGAS software recently improved to take into account the ester chemical function. These mechanisms including only the high temperature oxidation chemistry consist of:

- 885 reactions and 111 species for ethyl acrylate,
- 826 reactions and 103 species for methyl acrylate,
- 954 reactions and 128 species for ethyl crotonate,
- 885 reactions and 119 species for methyl crotonate and,
- 1035 reactions and 117 species for ethyl butanoate.

The mechanisms were then validated through satisfactory comparison of simulated and experimental ignition delay times where the effects of changes in reflected-shock temperature and of varying ester and oxygen concentrations were all well reproduced. The main reaction pathways were derived from flow rate and sensitivity analyses. The ways of consumption of both classes of esters (ethyl and methyl esters) were slightly different due to the considerable importance of the molecular reaction yielding ethylene and carboxylic acid in the case of ethyl esters.

Additionally, experimental and kinetic modeling of oxidation of ethyl butanoate (EB) selected as model compound for fatty acid ethyl esters (FAEE) was also examined. New experimental results were obtained in tubular plug flow reactor at atmospheric pressure, under dilute conditions, over the temperature range 500-1200 K, with an equivalence ratio ranging from $\varphi = 0.5$ to $\varphi = 1.6$, and a theoretical residence time of the fresh gas feed ranging from 0.6 to 1.4 s (under standard conditions of temperature and pressure, i.e. $T = 273.15$ K and $P = 1$ atm). The results consist of concentration profiles of the reactants, stable intermediates, and final products. These species were identified by gas chromatography coupled to mass spectrometry (GC/MS) and quantified by off-line and on-line non dispersive infrared ray absorption analyzer and gas chromatography coupled with thermal conductivity or flame ionization detector (GC/TCD/FID). Oxidation of EB under tubular plug flow reactor conditions was modeled using the detailed chemical kinetic reaction mechanism previously developed on the basis of shock tube experimental information and including thus only the high temperature chemical reactions. The comparison between computed results and the experimental data provided under the plug flow reactor conditions has shown satisfactory agreement, especially for the reactants (ethyl butanoate, O_2) and for the major species (CO, CO_2 , ethylene and butanoic acid). This evaluation was a good test of validation for the model since the latter had previously been tested only against ignition delay times, a measure of global reactivity. Flow rate and sensitivity analyses reinforced the results obtained from the shock tube study, once again highlighting the importance of the unimolecular reaction leading to the formation of ethylene and butanoic acid.

Nevertheless, it should be noted that during this PhD work much part was devoted to the development and the improvement of the experimental setup for the esters oxidation in a tubular plug flow reactor together with the analytical methods used for obtaining the concentrations profiles of the stable species.

Regarding the prospects of this work, development of further analytical methods to quantify other products of oxidation such as formaldehyde, water and hydrogen should help to improve the performances of the model. Particular attention should be also given to improve the reliable measurement of the temperature profile along the tubular plug flow reactor during oxidation reactions by taking care of involving no catalytic effects.

Moreover, the present work may be considered as the beginning of a further investigation which can be supplemented by studying the oxidation of the five esters investigated in other physical environments than shock tube or plug flow reactor (such as premixed flames, jet-stirred reactor, or internal combustion engines) in which experiments could be conducted in various ranges of temperature, pressure, and biodiesel/oxygen equivalence ratios. Regarding the mechanisms describing the oxidation of the unsaturated esters, it would be interesting to improve the kinetic models by including the low temperature oxidation pathways and their validation under various experimental conditions (generated by various physical environments).

It would also be interesting to extend the study to the oxidation of ethyl decanoate which should be a good surrogate of “ethylic” biodiesel (as it was shown regarding methyl decanoate for “methylic” biodiesel). Of course, oxidation of ethyl oleate which is the main component of FAEE-based biodiesel produced from virgin or waste rapeseed oil should be investigated afterwards. Additionally, further work might be useful to achieve a better understanding of the chemistry of carboxylic acids oxidation which are the major intermediate compounds of the ethyl ester oxidation.

AUTORISATION DE SOUTENANCE DE THESE
DU DOCTORAT DE L'INSTITUT NATIONAL
POLYTECHNIQUE DE LORRAINE

o0o

VU LES RAPPORTS ETABLIS PAR :

Madame Nabiha CHAUMEIX, Directeur de Recherche, ICARE, CNRS, Orléans

Monsieur Edward BLUROCK, Professeur Associé, Lund University, Sweden

Le Président de l'Institut National Polytechnique de Lorraine, autorise :

Madame BENNADJI Hayet

à soutenir devant un jury de l'INSTITUT NATIONAL POLYTECHNIQUE DE LORRAINE,
une thèse intitulée :

**"Biodiesel : combustion des esters éthyliques d'huiles végétales comme additifs au
pétrodiesel"**

en vue de l'obtention du titre de :

DOCTEUR DE L'INSTITUT NATIONAL POLYTECHNIQUE DE LORRAINE

Spécialité : « **Génie des Procédés et des Produits** »

Fait à Vandoeuvre, le 23 septembre 2010

Le Président de l'I.N.P.L.,

F. LAURENT



NANCY BRABOIS
2, AVENUE DE LA
FORET-DE-HAYE
BOITE POSTALE 3
F - 5 4 5 0 1
VANDŒUVRE CEDEX

Biodiesel: Combustion des esters éthyliques d'huiles végétales comme additifs au pétrodiesel

Le biodiesel est un biocarburant, composé d'un mélange de mono-esters d'acide gras saturés et insaturés avec une longue chaîne carbonée. Ce travail de thèse présente les données de la littérature sur l'origine du biodiesel et son procédé de fabrication ; sont présentées aussi les performances et les émissions des moteurs diesel fonctionnant au biodiesel et la cinétique d'oxydation du biodiesel. Des efforts ont été faits pour mettre en évidence les principales différences entre les esters méthyliques et éthyliques tout en montrant que d'autres recherches sont encore à développer. Pour ces raisons, les délais d'auto-inflammation de cinq esters méthyliques et éthyliques ont été mesurés dans un tube à onde de choc : l'acrylate d'éthyle, l'acrylate de méthyle, le crotonate d'éthyle, le crotonate de méthyle et le butanoate d'éthyle. Les mécanismes cinétiques détaillés d'oxydation des cinq esters étudiés ont été générés automatiquement en utilisant le logiciel EXGAS. L'oxydation du butanoate d'éthyle, molécule modèle d'esters éthyliques d'huiles végétales (EEHV) a été étudiée dans un réacteur piston à pression atmosphérique pour une gamme de température allant de 500 à 1200 K. Les résultats représentent les profils de concentration des réactifs, les intermédiaires stables et les produits finaux. Le modèle cinétique a été validé de façon satisfaisante par une comparaison entre les résultats simulés et expérimentaux.

Mots clés : biodiesel, esters méthyliques et éthyliques, transestérification, oxydation, tube à onde de choc, réacteur piston, modèle cinétique, EXGAS

Biodiesel: Combustion of fatty acid ethyl esters as additives to petrodiesel

An increasingly popular biofuel is biodiesel, composed of a mixture of saturated and unsaturated fatty acid methyl or ethyl esters, with a long aliphatic main chain. This PhD dissertation provides a literature review concerning the origin of biodiesel, its manufacturing process, performance and emissions of diesel engines fueled with biodiesel, and the kinetics of oxidation of biodiesel. Efforts were made to highlight the main differences between methyl and ethyl esters while showing where further research needs to be developed or pursued. For these reasons, the autoignition of five esters were measured behind reflected shock tube: ethyl acrylate, methyl acrylate, ethyl crotonate, methyl crotonate, and ethyl butanoate. Detailed mechanisms for the oxidation of the five studied esters were automatically generated using the version of EXGAS software. In addition, the oxidation of ethyl butanoate as a model compound for Fatty Acid Ethyl Esters (FAEE) has been investigated in tubular plug flow reactor at atmospheric pressure over wide range of temperature (500-1200 K). The results consist of concentration profiles of the reactants, stable intermediates, and final products. The model was again validated satisfactorily by comparison between computed results and the generated experimental data.

Keywords: biodiesel, methyl esters, ethyl esters, transesterification, oxidation, shock tube plug flow reactor, kinetics model, EXGAS